

**CLINICALLY RELEVANT MECHANISMS OF SPINAL CORD INJURY:
CONTUSION, DISLOCATION, AND DISTRACTION**

by

ANTHONY MIN-TE CHOO

B.A.Sc, The University of Toronto, 1998
M.A.Sc, The University of British Columbia, 2001

A THESIS SUBMITTED IN PARTIAL FULFILLMENT OF
THE REQUIREMENTS FOR THE DEGREE OF

DOCTOR OF PHILOSOPHY

in

THE FACULTY OF GRADUATE STUDIES

(Mechanical Engineering)

THE UNIVERSITY OF BRITISH COLUMBIA

August 2007

© Anthony Min-Te Choo 2007

Abstract

There remains no cure for traumatic spinal cord injury (SCI). Pre-clinical research typically models spinal cord transection, contusion, and compression, although in humans, other injury mechanisms such as cord shearing from vertebral dislocation, and stretching from distraction occur frequently. This creates a potentially important disparity between experimental paradigms and clinical injuries. The objective of this thesis was to develop and compare three biomechanically distinct, yet clinically relevant SCI animal models.

A multi-mechanism SCI system was developed to deliver high-speed (~100cm/s) injuries along any direction vector. A new vertebral clamping strategy with enhanced clamping strength ($64.7 \pm 10.2\text{N}$) and stiffness ($83.6 \pm 18.9\text{N/mm}$) was designed for modelling cervical vertebral dislocation (2.5mm), distraction (4.1mm), as well as contusion (1.1mm) injuries.

The pattern of primary mechanical injury ($n = 36$ rats) was found to differ between the three injury models. Contusion and dislocation produced intramedullary hemorrhage whereas overt vascular damage was not detected following distraction injury. Vertebral dislocation consistently sheared axons in the lateral columns. Plasma membrane disruption was detected by assessing the intracellular penetration of 10kDa dextran. Following contusion, membrane compromise of neuronal somata and axons was localized near the lesion epicentre whereas following dislocation and distraction, membrane damage extended several vertebral segments rostrally.

At 3 hours post-trauma ($n = 39$ rats), damaged cell membranes were found to reseal especially in the white matter. In spite of this recovery, extensive loss of neurofilaments and accumulation of β -amyloid precursor protein was observed following dislocation injury. In the gray matter, staining for cytochrome *c* and the oxidative stress marker 3-nitrotyrosine was similar following contusion and dislocation but less pronounced after distraction. Reactive astrocytes and activated microglia extended over a greater rostro-caudal zone only in the dislocation model.

These rostro-caudal patterns demarcate disparate populations of primary and secondary injury suggesting that therapies developed in contusion paradigms may not translate to other SCIs. Neuroprotection and repair strategies might favour contusion and distraction injuries, whereas axonal regeneration across a lengthy lesion may inevitably be required for restoring function following dislocation. This interaction between the primary mechanism of injury and secondary neuropathology suggests treatment paradigms may be guided in a mechanism-specific manner.

TABLE OF CONTENTS

Abstract	ii
Table of Contents	iii
List of Tables	vi
List of Figures	vii
Acknowledgements	ix
Dedication	x
Co-Authorship Statement	xi
Chapter 1 Introduction	1
1.1 Overview	1
1.2 Spine and Spinal Cord Anatomy	2
1.2.1 Orientation	2
1.2.2 Spinal Column	2
1.2.3 Spinal Cord	4
1.2.4 Neurons and Glia	6
1.2.5 Cytoskeleton	10
1.3 Human Spinal Cord Injuries	11
1.3.1 Epidemiology	11
1.3.2 Vertebral Column Injuries	13
1.3.2.1 Burst Fractures	15
1.3.2.2 Dislocations & Fracture-Dislocations	16
1.3.2.3 Distraction	17
1.3.2.4 Other Vertebral Column Injuries	18
1.3.3 Spinal Cord Injury Mechanisms	18
1.3.4 Pathology of Human Spinal Cord Injury	19
1.3.5 Clinical Spinal Cord Treatment	21
1.3.5.1 Decompression	21
1.3.5.2 Pharmacotherapy	22
1.3.6 Summary of Human Injuries	23
1.4 Biomechanics of Neurotrauma	24
1.4.1 Mechanical Properties of Neural Tissue	24
1.4.2 Constitutive Models	28
1.4.3 Primary Mechanical Injury	29
1.4.3.1 Tissue Failure	30
1.4.3.2 Vascular Damage	31
1.4.3.3 Electrophysiological Deficits	32
1.4.3.4 Cellular Injury	33
1.4.3.5 Plasma Membrane Compromise	34
1.4.4 Spinal Cord Injury Models	36
1.4.4.1 Allen's Weight-Drop	36
1.4.4.2 Controlled Displacement	37
1.4.4.3 Controlled Force	39
1.4.4.4 Residual Compression	40
1.4.4.5 Transection	40

1.4.4.6	Cervical Injury Models	40
1.4.4.7	Vertebral Fracture-Dislocation	41
1.4.4.8	Vertebral Distraction	41
1.4.4.9	Comparison of Models	42
1.4.5	Summary of Biomechanics	43
1.5	Neurobiology of Spinal Cord Injury	43
1.5.1	Secondary Injury & Neuroprotection	43
1.5.1.1	Hemorrhage & Ischemia	44
1.5.1.2	Inflammation	44
1.5.1.3	Oxidative Stress	45
1.5.1.4	Calcium & Excitotoxicity	46
1.5.1.5	Apoptosis	47
1.5.2	Repair & Regeneration	48
1.5.2.1	The Inhibitory Environment	49
1.5.2.2	Growth Factors	50
1.5.2.3	Axonal Repair	50
1.5.3	Summary of Neurobiology	51
1.6	Thesis Objectives and Hypotheses	52
1.6.1	Scope	52
1.7	References	54
Chapter 2	A Novel SCI Device	69
2.1	Introduction	69
2.2	Materials and Methods	71
2.2.1	Multi-Mechanism Injury System	71
2.2.2	Part 1: Vertebral Clamps	73
2.2.3	Part 2: Injury Models	75
2.2.4	Hemorrhage Analysis	78
2.2.5	White Matter Immunohistochemistry	79
2.3	Results	79
2.3.1	Part 1: Vertebral Clamps	79
2.3.2	Part 2: Injury Models	81
2.4	Discussion	88
2.5	References	92
Chapter 3	Distribution of Primary Injury	97
3.1	Introduction	97
3.2	Materials and Methods	98
3.3	Results	103
3.4	Discussion	110
3.5	References	116
Chapter 4	Initiation of Secondary Injury	121
4.1	Introduction	121
4.2	Materials and Methods	122
4.2.1	Animal Models	122
4.2.2	Immunohistochemistry	125

4.2.3	General Image Acquisition & Analysis	127
4.2.4	Changes in Membrane Permeability	128
4.2.5	Cell Bodies in the Gray Matter	128
4.2.6	Axons in the White Matter	129
4.2.7	Reactive Astrocytes	130
4.2.8	Microglial Activation	130
4.3	Results	133
4.3.1	Changes in Membrane Permeability	133
4.3.2	Cell Bodies in the Gray Matter	137
4.3.3	Axons in the White Matter	139
4.3.4	Reactive Astrocytes	144
4.3.5	Microglial Activation	146
4.4	Discussion	148
4.5	References	153
Chapter 5 Discussion & Conclusion		159
5.1	Overview	159
5.2	Modelling Considerations	159
5.3	Biomechanics of Primary Injury Patterns	162
5.3.1	Contusion	162
5.3.2	Dislocation	165
5.3.3	Distraction	169
5.4	Association of Primary and Secondary Injury	171
5.4.1	Contusion	171
5.4.2	Dislocation	173
5.4.3	Distraction	174
5.4.4	Summary of Primary and Secondary Injury	174
5.5	Clinical Relevance	176
5.6	Limitations	177
5.7	Recommendations	178
5.8	Contributions	180
5.9	Conclusion	181
5.10	References	182
Appendix A SCI Test System		187
5.11	Test System Assembly	188
5.12	Test System Drawings	189
5.13	Sensors	190
Appendix B Image Analysis		192
5.14	Image Analysis Tools	193
Appendix C ANOVA Tables		194
Appendix D Ethics Board Certificates of Approval		199

LIST OF TABLES

Number	Page
Table 2.1: Vertebral clamping characteristics _____	80
Table 2.2: Mechanical parameters for graded injuries _____	81
Table 3.1: Injury parameters for primary injury study _____	103
Table 4.1: Immunohistochemical markers for secondary injury _____	126
Table 4.2: Mechanical injury parameters in secondary injury study _____	133
Table C.1: ANOVA summary – Acute dextran penetration into axons _____	195
Table C.2: ANOVA summary – Acute dextran penetration into neuronal somata _____	195
Table C.3: ANOVA summary – Evolution of dextran penetration at 3 hours post-trauma _____	196
Table C.4: ANOVA summary – 3NT-positive cells _____	197
Table C.5: ANOVA summary – Neurofilament degradation in ventro-medial white matter _____	197
Table C.6: ANOVA summary – β APP accumulation in axons _____	197
Table C.7: ANOVA summary – Reactive astrocytes _____	197
Table C.8: ANOVA summary – Microglial activation _____	198

LIST OF FIGURES

Number	Page
Figure 1.1: Orientation in humans and quadrupeds _____	2
Figure 1.2: The spinal column _____	3
Figure 1.3: Anatomy of a vertebra _____	3
Figure 1.4: Spinal cord anatomy _____	4
Figure 1.5: Spinal cord gray and white matter _____	5
Figure 1.6: Segments of Neurologic Deficits _____	6
Figure 1.7: The neuron _____	7
Figure 1.8: Synapse _____	7
Figure 1.9: Micrographs and illustrations of glia cells _____	9
Figure 1.10: Cytoskeletal proteins _____	11
Figure 1.11: SCI epidemiology _____	12
Figure 1.12: Denis's three column spine _____	14
Figure 1.13: Vertebral column fractures _____	15
Figure 1.14: Spinal cord injury mechanisms _____	19
Figure 1.15: Anisotropy of neural tissue _____	27
Figure 1.16: Thesis scope _____	53
Figure 2.1: Multi-mechanism injury system _____	72
Figure 2.2: Cervical vertebral clamps and dimensions _____	74
Figure 2.3: Illustrations and photos of experimental injury configurations _____	76
Figure 2.4: Failure and stiffness of Allis clamps and novel vertebral clamps _____	80
Figure 2.5: Representative curves for graded injuries _____	83
Figure 2.6: Mortality rates for dislocation and distraction injuries _____	84
Figure 2.7: Morphology stained with H&E _____	85
Figure 2.8: Regression curves for hemorrhage versus injury displacement and force _____	86
Figure 2.9: White matter damage following three injury mechanisms _____	87
Figure 3.1: Classification of membrane permeability into neuronal somata _____	101
Figure 3.2: Dextran accumulation at nodes of Ranvier _____	102
Figure 3.3: Representative mechanical injury curves _____	104
Figure 3.4: Primary hemorrhage volumes following three injury mechanisms _____	105
Figure 3.5: Axonal membrane compromise detected with fluorescein-dextran _____	106
Figure 3.6: Quantitative measurements of dextran-positive axons _____	108
Figure 3.7: Quantitative measurements dextran-positive cell bodies _____	109
Figure 4.1: Illustration of three injury mechanisms _____	124
Figure 4.2: Novel microglial ramification index _____	132
Figure 4.3: Representative micrographs showing evolution of membrane permeability _____	134
Figure 4.4: Quantitative analysis of dextran penetration into somata and axons _____	136
Figure 4.5: Photomicrographs and quantitative counts of 3-NT immunostaining _____	137
Figure 4.6: Cytochrome <i>c</i> immunostaining _____	139
Figure 4.7: Neurofilament degradation in the ventro-medial white matter _____	141
Figure 4.8: β APP accumulation in white matter _____	143
Figure 4.9: Distribution of reactive astrocytes _____	145

Figure 4.10: Microglial activation _____	147
Figure 5.1: Central damage pattern in contusion injuries _____	163
Figure 5.2: Injury patterns following fracture-dislocation _____	167
Figure 5.3: Ventro-medial axolemma compromise following dislocation injury _____	169
Figure 5.4: Dorsal axolemma compromise following distraction injury _____	170
Figure 5.5: Parallel patterns of primary and secondary injury _____	172
Figure A.1: Test system assembly sequence _____	188
Figure A.2: Accelerometer housing _____	189
Figure A.3: Rotary detent _____	189
Figure A.4: Load cell calibration model 31: 22.5N _____	190
Figure A.5: Load cell calibration model 31: 225N _____	190
Figure A.6: Load cell calibration model 208C02: 444N _____	191
Figure B.1: StereolTools interface and screen images _____	193

ACKNOWLEDGEMENTS

I would not be here without the support of Drs. Thomas Oxland and Wolfram Tetzlaff. Tom has given me an opportunity to venture into a new and inspiring field while Wolf has welcomed me—a naïve engineer—into his neuroscience laboratory. I am forever indebted to them for their mentorship.

I owe heartfelt thanks to Hanspeter Frei, Ward Plunet, Clarrie Lam, Jie Liu, Derek Wilson, David Tsai, Joey Doherty, Lin-P'ing Choo-Smith, and my parents for their perpetual encouragement. Thanks also to Bryan Sniderman and Raymond Li at ATI Technologies for enabling me and my wife to keep our family together in Vancouver.

Most importantly, I am forever grateful to my wife, Ngoc Luu, for all her patience and love during this long journey, and to my children, Cianna and Braeden, for always reminding me of what is most precious in life—I owe many thanks to God for blessing me with this family.

Many others have contributed in some way to my growth over these years.

Sincere thanks to,

DOUGLAS BOURNE, EDWARD CHEUNG, ELIZABETH CLARKE, PETER CRIPTON, MARCEL DVORAK,
CORINA FREI, JOHNSON GO, CAROLYN GREAVES, ZHUOWEI LIU, LINA MADILAO,
CAROLYN SPARREY, JUAY SENG TAN, QINGAN ZHU

This work was supported by the Canadian Institutes of Health Research, Canada Foundation of Innovation, the Canada Research Chairs Program, the British Columbia Neurotrauma Fund, the Rix Family Leading Edge Endowment Fund, and the George W. Bagby Research Fund.

DEDICATION

*for my ever supportive parents Lip Kung and Keow Geen
&
Ngoc and the children, my Cianna and little Braeden*

CO-AUTHORSHIP STATEMENT

The research contained within this thesis draws on the expertise from the biomedical engineering laboratory of Dr. Thomas R. Oxland and the neuroscience laboratory of Dr. Wolfram Tetzlaff. The doctoral candidate designed the experiments and their outcome measures under the combined mentorship of Drs. Oxland and Tetzlaff. The research was performed by the candidate. The candidate designed and built the novel spinal cord injury apparatus and the associated stereotatic devices. The candidate conducted the animal experiments with microsurgical assistance from Dr. Jie Liu. Tissue processing and immunohistochemistry were conducted by the candidate with advice, where necessary, from Ms. Clarrie Lam. The candidate wrote the image analysis software and analysed the data. The candidate led the preparation of the manuscripts with revisions from the senior co-authors Drs. Oxland, Tetzlaff, and Dvorak.

Chapter 1

INTRODUCTION

1.1 Overview

A clinically viable cure for traumatic spinal cord injury (SCI) remains elusive. Pre-clinical research has relied on spinal cord transection, contusion, and compression injury models, though they are representative of only some human SCI cases. Other types of vertebral column fracture result in different biomechanical injury mechanisms to the spinal cord. Comparisons between distinct injury mechanisms has received little attention because of the prevailing consensus that the pathophysiology of SCI is dominated by the myriad biochemical processes which are thought to be independent of the initial mechanical injury. Given that experimental therapies have met with only modest success in human clinical trials, this thesis examines the influence of distinct, yet clinically relevant biomechanical injury mechanisms on the characteristics of acute SCI.

This introductory chapter overviews the clinical, biomechanical, and neuropathological aspects of SCI. The chapter begins with an outline of human SCI pathology with a focus on the different types of vertebral column fractures which cause SCI by differing injury mechanisms. A review of biomechanical aspects of neurotrauma describes the behaviour of neural tissue, how biomechanical damage is characterized at the tissue and cellular levels, and how mechanically controlled injuries are currently modelled experimentally. Next, the main avenues of secondary degeneration that are initiated by primary mechanical injury are highlighted, along with a brief discussion of spinal cord regeneration. The chapter concludes by presenting the thesis objectives and hypotheses that are the focus of chapters 2 to 4. Chapter 5 discusses the role of biomechanical injury mechanisms in SCI and concludes with recommendations for future directions.

1.2 Spine and Spinal Cord Anatomy

1.2.1 Orientation

The position of anatomical structures discussed in this thesis depends on whether they refer to humans or animals. In humans (Figure 1.1A), superior and cranial refer to the direction of the head while inferior and caudal refer to the direction of the feet. Anterior refers to a direction towards the front of the body while posterior denotes the direction towards the back. In quadruped animals (Figure 1.1B), rostral and caudal refer to the direction of the head and tail respectively. Dorsal refers to the animal's back while ventral refers to the front. In both humans and quadrupeds, left and right are divided by a mid-sagittal plane from which lateral denotes a direction away from this plane while medial indicates a direction towards the mid-sagittal plane.

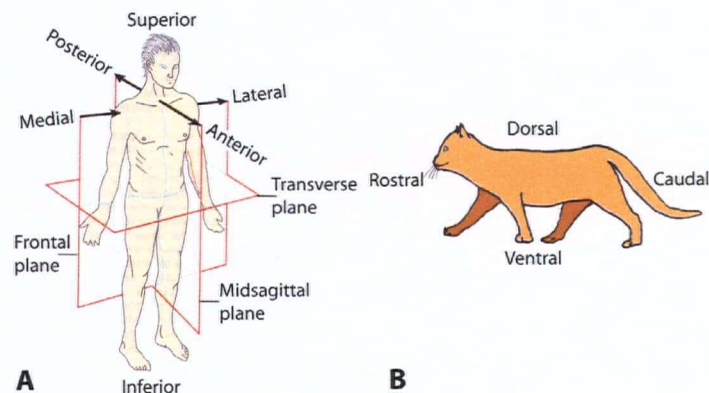


Figure 1.1: Orientation in humans and quadrupeds

Cardinal planes and direction vectors used to describe anatomical positions in humans and quadrupeds. (Graphics from: Swanson LW, 2003. The architecture of nervous systems. In: Fundamental Neuroscience, 2nd Edition [Squire LR et al. eds], p.24. San Diego, CA: Academic Press. © Elsevier Science [USA], 2003, adapted by permission.)

1.2.2 Spinal Column

The osteoligamentous vertebral column (Figure 1.2) encases the spinal cord and protects it from traumatic loads. In humans, the spinal column consists of a series of vertebrae that can be divided into cervical, thoracic, lumbar, sacral and coccygeal regions. Intervertebral discs separate the vertebral bodies to cushion loads and to allow for intersegmental motion between vertebrae. A typical vertebra (Figure 1.3A & B) consists of a vertebral body, which supports the majority of the axial loads applied to the spinal column, and posterior elements that are attached to the vertebral body via the pedicles to form an arch that encloses the vertebral foramen through which the spinal cord courses. Intervertebral discs separate the vertebral bodies (Figure 1.3B) to cushion loads and allow for intersegmental motion.

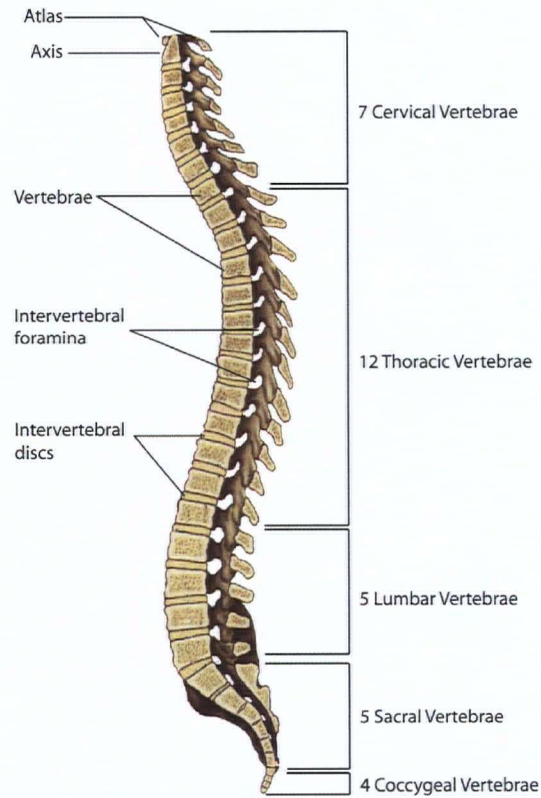


Figure 1.2: The spinal column

Lateral view of the spinal column and its sub-divisions: cervical, thoracic, lumbar, sacral, coccygeal. Each vertebral body is separated by an intervertebral disc that cushions loads and allows for intersegmental motion. Illustration adapted from Moore KL and Dalley AF, 1999. Clinically oriented anatomy, 4th Edition. p.433. Philadelphia, PA: Lippincott Williams & Wilkins.)

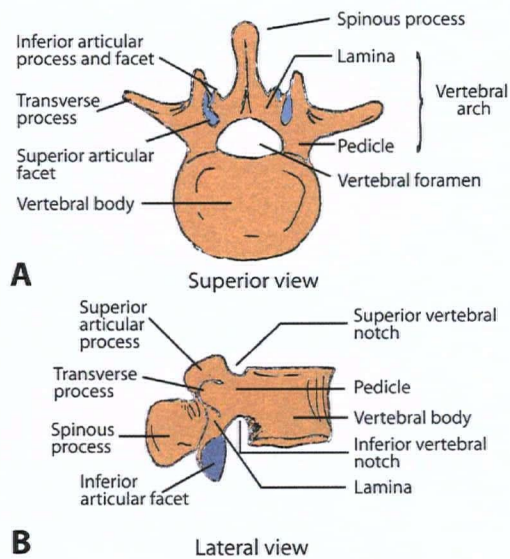


Figure 1.3: Anatomy of a vertebra

Superior (A) and lateral (B) view of a vertebra with anatomical features labeled. The spinal cord travels through the vertebral foramen visible in A.

1.2.3 Spinal Cord

The spinal cord is covered by several membrane layers (Figure 1.4). The outermost membrane that is in direct contact with the vertebral foramen is the dura mater. The arachnoid mater lines the inner surface of the dura. Beneath the arachnoid mater, the subarachnoid space contains the cerebrospinal fluid that circulates through both this space and the cerebral ventricles in the brain. The innermost membrane is the pia mater which directly covers the spinal cord. The spinal cord is suspended within the dural sac via the denticulate ligaments which extend laterally from the pia to dura.

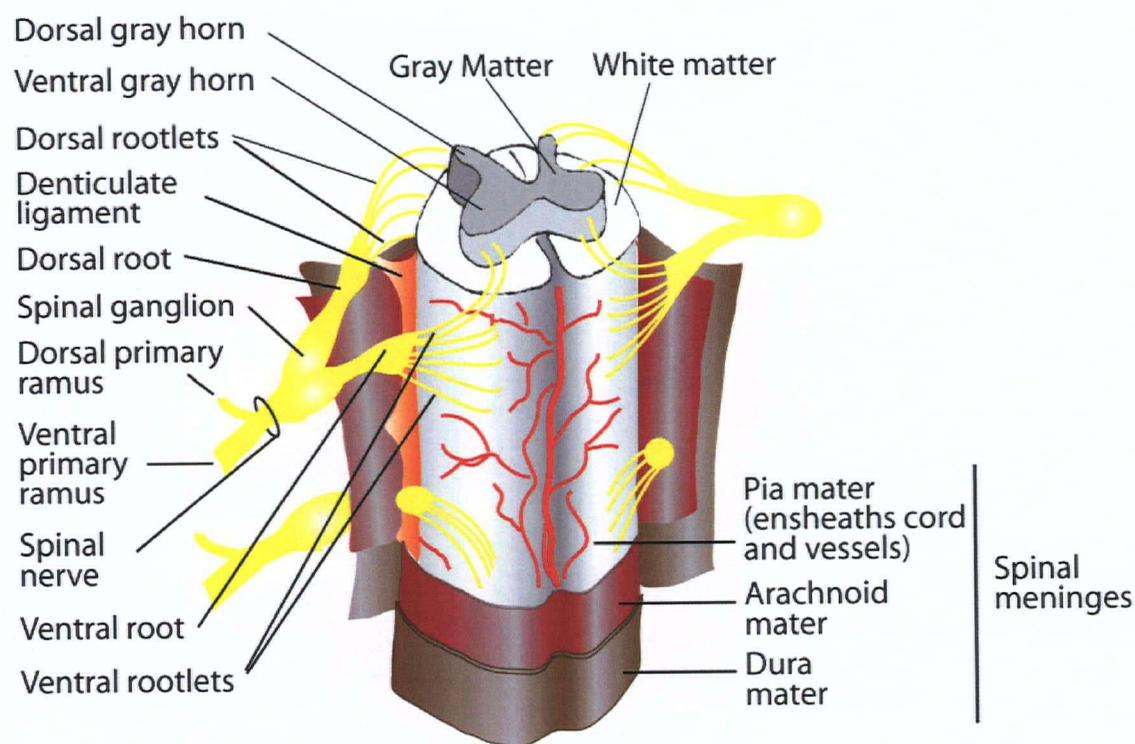


Figure 1.4: Spinal cord anatomy

Illustration of the spinal cord shows the gray and white matter with sensory fibers entering the cord dorsally and motor fibers exiting the cord ventrally. The spinal cord is covered in three membrane layers: pia mater, arachnoid mater, and dura mater. The cerebrospinal fluid lies between the pia and arachnoid.

Nerve roots enter and exit the spinal cord between each vertebral segment. Sensory fibers enter posteriorly (*dorsal rootlets* Figure 1.4) while motor fibers exit anteriorly (*ventral rootlets* Figure 1.4). The central region of the spinal cord is occupied by gray matter while the peripheral region contains ascending and descending axons that are ensheathed in myelin giving them a white appearance (Figure 1.5A). Gray matter is highly vascularized and contains neuronal cell bodies

(Figure 1.5B) as well as glial cells which support neuronal functions (described below). The white matter axons (Figure 1.5C) transmit signals between the neurons in the brain and brainstem, and the neurons in the spinal cord gray matter. The cells in the gray matter mediate motor and sensory functions primarily at the local segment in which they lie and hence damage to gray matter results in localized segmental deficits. In contrast, interruption of ascending and descending white matter tracts will compromise the transmission of signals between the brain and segments below the level of injury (Figure 1.6).

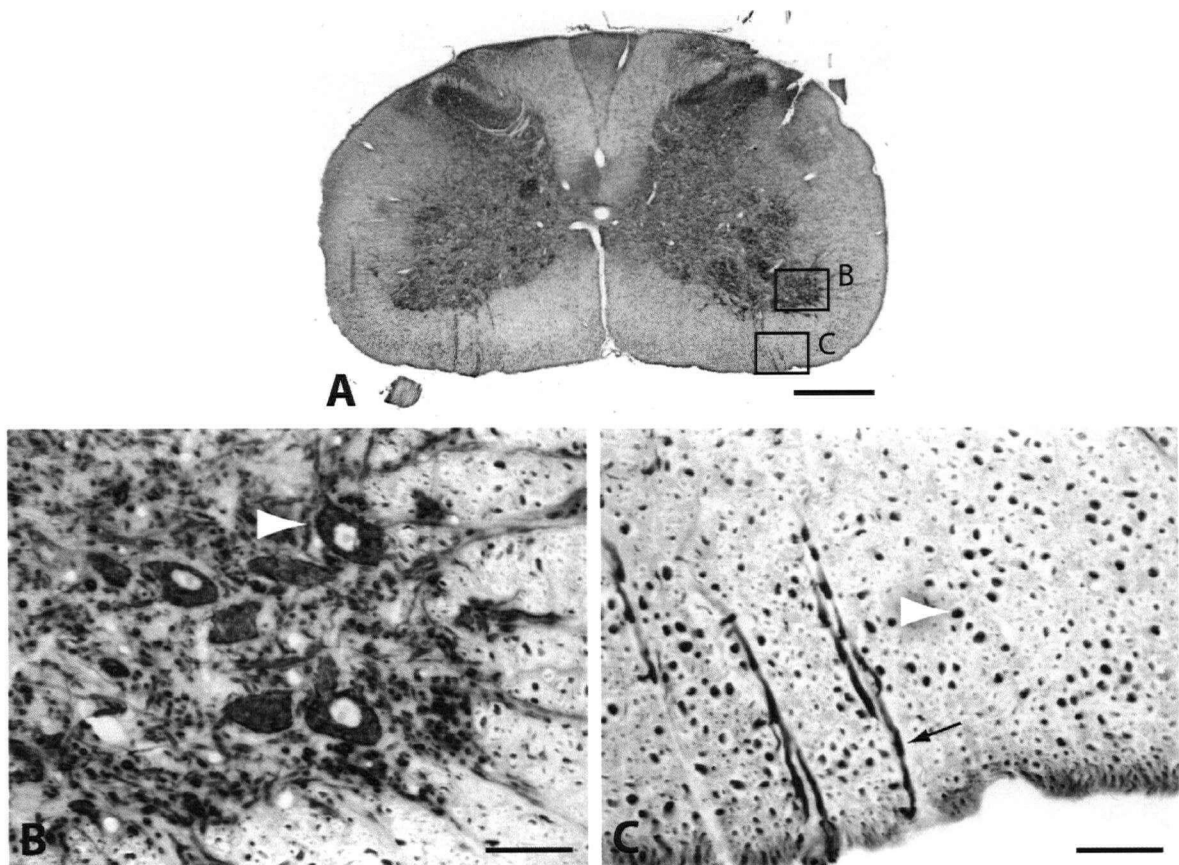


Figure 1.5: Spinal cord gray and white matter

Photomicrographs of rat cervical spinal cord cross-section immunostained for non-phosphorylated epitopes of heavy neurofilament (SMI-32, Sternberger Monoclonals). A. Gray matter is located in the central region of the spinal cord surrounded by ascending and descending white matter tracts. B. Higher magnification image of ventral gray matter in tile A. *Arrowhead* highlights an example of neuronal cell body with positive neurofilament staining in the cytoplasm. C. Higher magnification image of ventral white matter in tile A. *Arrowhead* marks example of large caliber axon whose cytoskeleton stains positive for heavy neurofilaments. *Arrow* marks ventral exit of an axon from a motoneuron. Scale bars 500 μ m in A, 50 μ m in B and C.

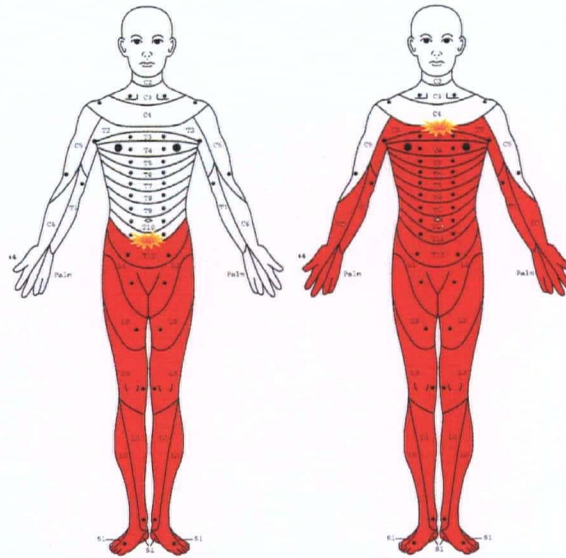


Figure 1.6: Segments of Neurologic Deficits

Illustration shows injury to the spinal cord (*star graphic*) can result in neurologic deficits at the segment of injury and segments below (shaded red) due to interruption of ascending and descending white matter fibres. (Illustration adapted from asia-spinalinjury.org by permission).

1.2.4 Neurons and Glia

Neurons possess a complex architecture (Figure 1.7) that stems from the specialized functions of its different components. Dendritic processes extend from the cell body to receive neurotransmitters at synaptic clefts (Figure 1.8A). These neurotransmitters open channels embedded in the cell's membrane, allowing the exchange of ions across the electrochemical gradient between the extracellular and intracellular space (Figure 1.8B). This exchange of ions can transiently raise (excitatory influx of positive charges) or lower (inhibitory influx of negative charges) the voltage across the cell membrane. The cell body integrates repeated signals over time and integrates spatially separate signals over space. If the membrane potential rises above an excitatory threshold, the cell body fires an action potential that propagates down its axonal process to the axon's terminal where neurotransmitters are released to the next target.

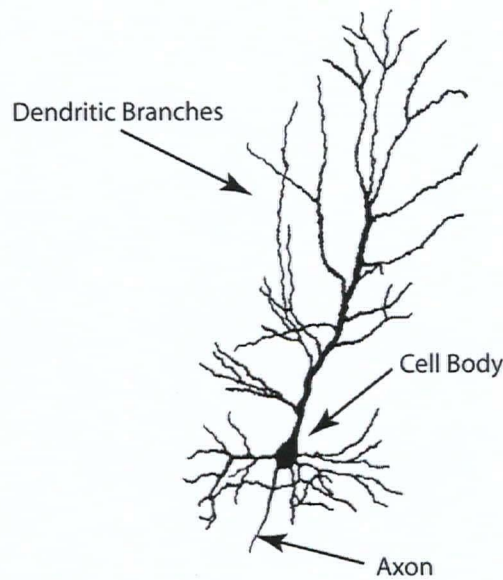


Figure 1.7: The neuron

Pyramidal neuron from the cerebral cortex demonstrates the specialized components of the nerve cell. Dendritic arborizations receive signals. The cell body transmits action potentials via the axon. (Graphics from: Hof PR et al., 2003. Cellular components of nervous tissue. In: Fundamental Neuroscience, 2nd Edition [Squire LR et al. eds], p.49. San Diego, CA: Academic Press. © Elsevier Science [USA], 2003, adapted by permission.)

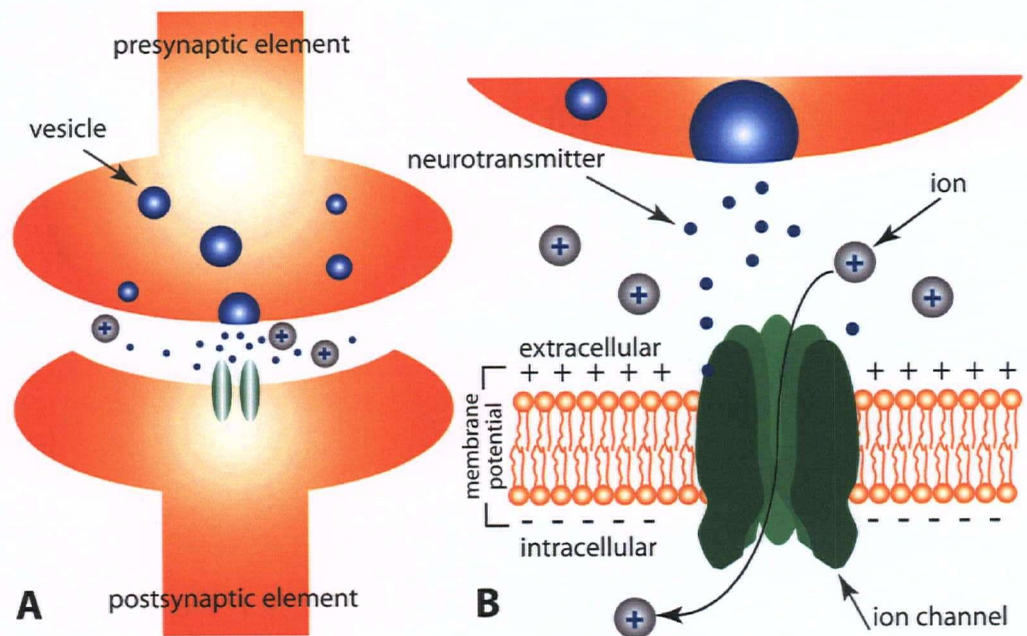


Figure 1.8: Synapse

Illustration of an excitatory synapse. A. Neurotransmitters released from vesicles in the pre-synaptic element stimulate channels on the post-synaptic element. B. Zoomed illustration of ion channel embedded in the plasma membrane. For an excitatory neurotransmitter, cation channels are opened allowing positively charged ions to enter the intracellular space resulting in a depolarization of the membrane potential.

Glial cells coexist with neurons and support their survival and function. Astrocytes are the most numerous cells in the central nervous system. Their stellate morphology (Figure 1.9A) is visualizable by immunostaining with antibodies directed against glial fibrillary acidic protein (GFAP) which is an intermediate filament of the astrocyte cytoskeleton. Astrocytes perform numerous supporting functions including buffering neurotransmitters such as glutamate and converting it to glutamine to be recycled by axon terminals. Following injury or disease, an increase in GFAP expression is a commonly used indicator of reactive astrocytes (Figure 1.9B).

Microglia are resident immune cells of the central nervous system. In their resting state, microglia have small cell bodies and a network of highly branched—ramified—processes (Figure 1.9C). Under pathological conditions, microglia become activated whereupon their processes thicken and retract (Figure 1.9D) as they evolve into phagocytes.

Oligodendrocytes (Figure 1.9E) extend their cell membranes to ensheath axons in compacted concentric layers of myelin (Figure 1.9F). Myelin electrically insulates the axon thereby allowing action potentials to travel more quickly between exposed segments of the axon called nodes of Ranvier (*arrowhead* Figure 1.9G and I). Nodes of Ranvier are identifiable by immunostaining for voltage-gated sodium and potassium channels which are highly organized in the nodal region (Figure 1.9H and I).

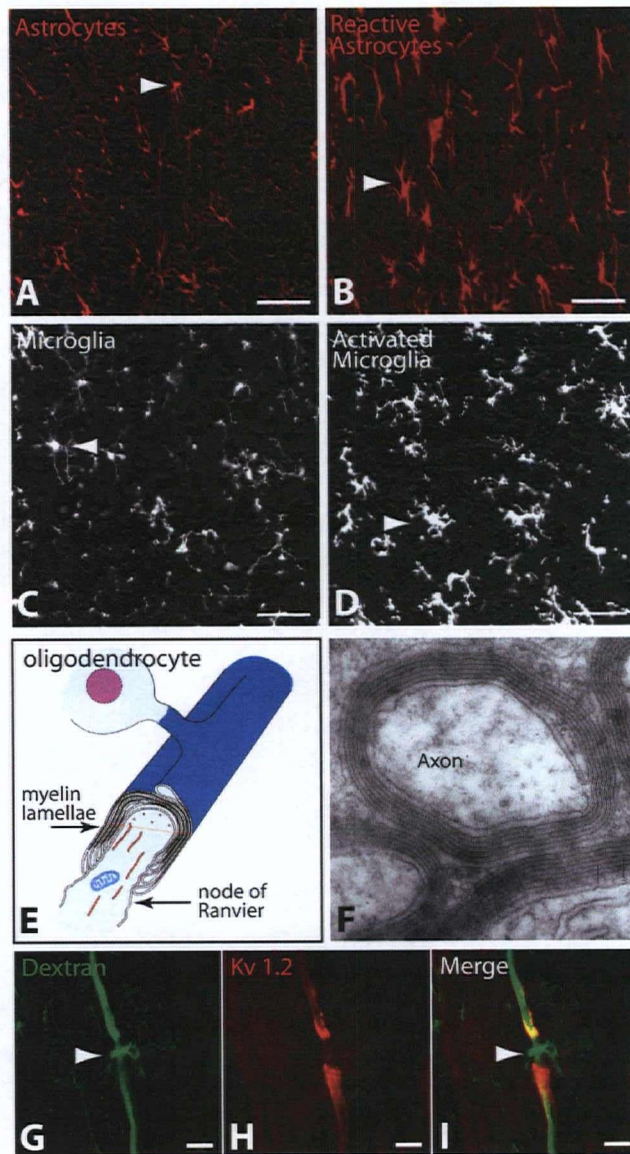


Figure 1.9: Micrographs and illustrations of glia cells

Immunostaining with anti-glial fibrillary acid protein (GFAP) reveals stellate morphology of astrocytes (*arrow* in A). Following neurotrauma, reactive astrocytes express greater GFAP (*arrow* in B). Immunostaining with anti-Iba1 shows the morphology of resting microglia which exhibit small cell bodies with highly ramified processes (*arrow* in C). Following activation, microglial processes thicken and retract (*arrow* in D) following disease or neurotrauma. E. Illustration of oligodendrocyte which ensheath the axon in myelin lamellae. The axon is exposed at periodic gaps in the myelin sheath called nodes of Ranvier. F. Electronmicrograph of axon shows electron-dense layers of myelin. G. An axon partially filled with a molecular tracer (dextran) which also accumulates at the axon's node of Ranvier (*arrow* in G) thereby highlighting this gap in the myelin sheath. H. Immunostaining for voltage-gated potassium channels (Kv1.2) highlights the juxtapanodal region. I. Merged image of G and H. Scale bars 50 μ m in A to D, 10 μ m in G to I. (Graphics in E from: Quarles RH et al. 2006. Myelin formation, structure and biochemistry. In: Basic Neurochemistry: Molecular, Cellular and Medical Aspects, 7th Edition [Siegel GJ et al. eds], p.53. Burlington, MA: Elsevier Academic Press. © American Society for Neurochemistry, 2006, adapted by permission. Electronmicrograph in F reproduced from Journal of Experimental Medicine, 1947, 86:175-184. © 1947 Rockefeller University Press, adapted by permission. Remaining micrographs were taken from thesis work.)

1.2.5 Cytoskeleton

Cytoskeletal proteins form the internal structure of cells which allows them to exhibit diverse morphologies such as those found in neural tissue. Microtubules, intermediate filaments, and microfilaments are the three basic classes of cytoskeletal proteins (Figure 1.10) in eukaryotic cells. Microtubules are hollow tubes approximately 25nm in diameter. Microtubules consist of alternating units of α - and β -tubulin and serve to provide structural stiffness to the cytoskeleton. In addition, microtubules serve as tracks for the transport of proteins and organelles to and from the cell body. An example of this cargo is β -amyloid precursor protein which is assessed later in this thesis.

Intermediate filaments are approximately 10nm in diameter. Glial fibrillary acidic protein is a specific intermediate filament of astrocytes while neurofilaments are specific to neurons. There are three subtypes of neurofilaments which are distinguished by molecular weight. The molecular weight of heavy neurofilaments (NF-H) is 200kDa while medium (NF-M) and light neurofilaments (NF-L) are approximately 160kDa and 68kDa respectively. Medium and heavy neurofilaments possess protein sidearms that project outward from a core domain (Hirokawa et al., 1984). These projections maintain the spacing between neurofilaments and this has been shown to be necessary for the development of large caliber axons (Elder et al., 1998).

Microfilaments are the smallest of the cytoskeletal proteins and they have a diameter of approximately 5nm. Microfilaments such as actin are highly labile structures which are found in areas such as the axonal growth cone and beneath the plasma membrane where they maintain the distribution of membrane bound proteins.

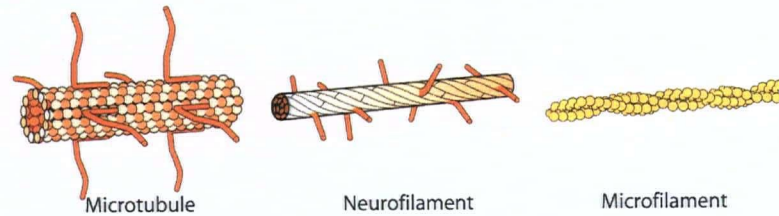


Figure 1.10: Cytoskeletal proteins

Cytoskeletal proteins form the internal structure of cells enabling them to exhibit a diverse range of morphologies. Microtubules consist of repeating units of α - and β -tubulin. Neurofilaments consist of a core domain with sidearm projections that are believed to maintain the separation distance between these intermediate filaments. Microfilaments such as actin are the smallest of the three basic cytoskeletal proteins. (Graphics from: Pignio G et al. 2006. The cytoskeleton of neurons and glia. In: Basic Neurochemistry: Molecular, Cellular and Medical Aspects, 7th Edition [Siegel GJ et al. eds], p.125. Burlington, MA: Elsevier Academic Press. © American Society for Neurochemistry, 2006, adapted by permission.)

This brief overview highlights some of the anatomical structures that arise later in this thesis. The structure and function of neural tissue and its cellular constituents are rather more intricate than can be covered in this introduction, though these additional details are readily available elsewhere (Squire et al., 2003; Siegel et al., 2006).

1.3 Human Spinal Cord Injuries

1.3.1 Epidemiology

The overall incidence of traumatic SCI has remained relatively unchanged over the last thirty years (Wyndaele and Wyndaele, 2006). In the developed world, the annual incidence rate has been reported between 11.5 and 53.4 per million (Sekhon and Fehlings, 2001). Within the United States, this rate translates to approximately 11,000 new SCI cases per year with an estimated prevalence of nearly 250,000 individuals currently living with SCI impairments. The mortality rate ranges between 48.3 and 79% prior to hospital admission and between 4.4 to 16.7% during hospital care. Complications are predominantly due to respiratory failure, pneumonia, pressure sores, urinary tract infections, and thrombosis.

Many of the injuries occur in a youthful adult population where individuals between the ages of 20-40 years of age account for approximately 40% of SCI cases (Pickett et al., 2006). The elderly (>65 years) account for approximately 10% of SCI cases with falls being the dominant cause in this group. Cases of SCI in males outnumber those in females by a ratio of 3:1. Overall, motor vehicle accidents consistently account for the majority of traumatic SCI with falls, work and sports related injuries, and violence accounting for 10-20% each (Figure 1.11A).

Traumatic SCI is frequently associated with vertebral column injuries (Figure 1.11B). Two of the most common vertebral fracture patterns are burst fractures and fracture-dislocations; each having a reported incidence rate of 30-40% in the human population (Sekhon and Fehlings, 2001; Pickett et al., 2006). SCI without radiographic abnormality (SCIWORA) and SCI without obvious radiographic evidence of trauma (SCIWORET) have also been reported though these cases have declined because the use of magnetic resonance imaging has improved the sensitivity of detecting cord injuries that were previously missed with x-ray radiography (Sekhon and Fehlings, 2001). Dislocations without fracture of the facets are also encountered clinically and it is hypothesized that a dynamic flexion-extension force cause these vertebrae to jump over each other resulting in dislocation with locked facets (Allen et al., 1982).

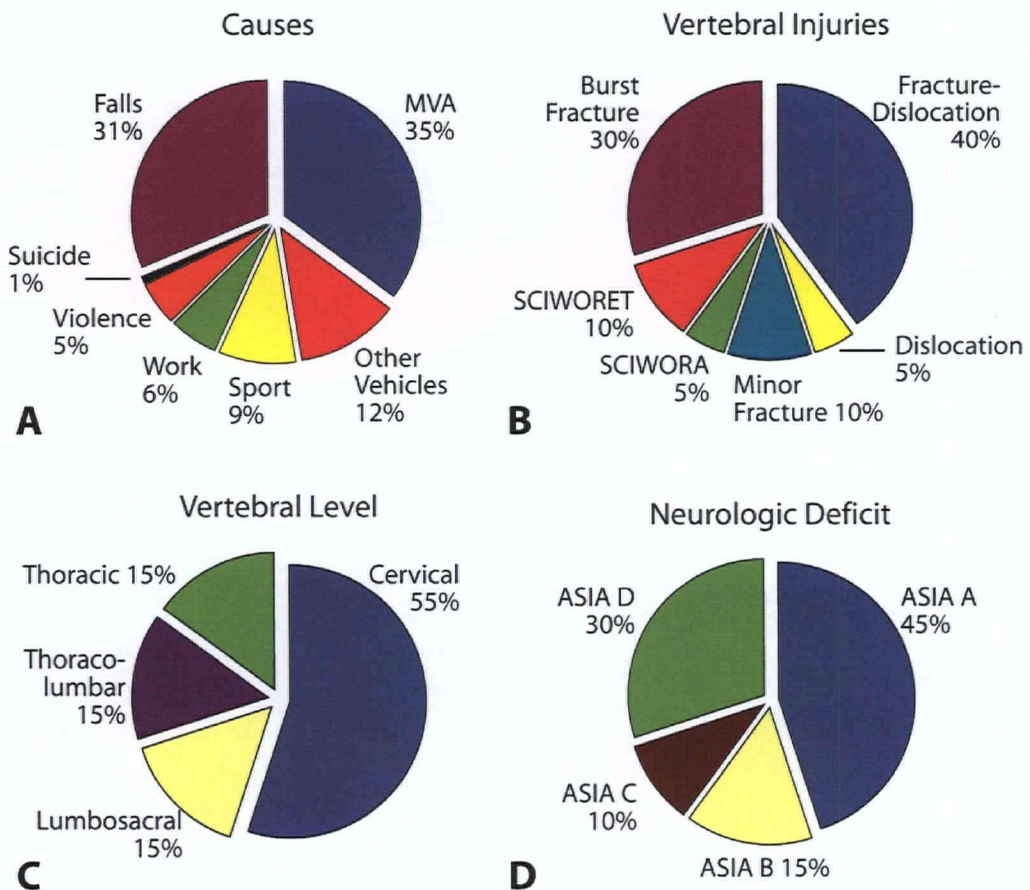


Figure 1.11: SCI epidemiology

Causes compiled from Pickett et al. 2006. Spine 31:799-805. Vertebral injuries, vertebral level, neurologic deficit compiled from Sekhon LH and Fehlings MG, 2001. Spine 26:S2-S12.

SCI is most common in the cervical region (55%) with the incidences in the thoracic, thoracolumbar, and lumbar spines estimated at 15% each (Figure 1.11C). The extent of neurological deficit is frequently assessed by the American Spinal Injury Association (ASIA) impairment scale. ASIA A denotes a complete loss of motor and sensory function in the sacral segments while ASIA E indicates normal motor and sensory function (Figure 1.11D). Between these two extremes, ASIA B represents the preservation of sensory function but no motor function below the level of injury (includes sacral segments S4-S5), ASIA C indicates the presence of motor function below the lesion with more than half of the key muscles exhibiting a grade less than 3/5 (where 0/5 denotes total muscle paralysis), while ASIA D denotes the presence of motor function with at least half of the key muscles exhibiting a grade of 3/5 or better. Almost half of all SCI patients (45%) are ASIA A while the remaining patients are distributed between ASIA B to ASIA D.

Several trends have been reported in SCI subpopulations. Incidences due to motor vehicle accidents have been decreasing due to improved seat belt usage. This decrease, however, has been offset by an increase in SCI in the elderly population. Thoracic injuries are more frequently (73%) associated with complete SCI (Tator, 1983). Vertebral dislocation has been also more frequently associated with complete injuries (Kiwerski, 1991). Isolated SCI only occurs in 20% of cases while other types of trauma such as brain and thoracic injuries are present in the remaining cases. SCI without fracture occurs more frequently in the cervical region (92%) in the older population (mean age 58) and is often associated with cervical spondylosis or spinal canal narrowing.

1.3.2 Vertebral Column Injuries

SCI in humans usually occurs when the osteoligamentous vertebral column dynamically traumatizes the spinal cord. Injuries due to progressive canal stenosis, tumor growth, and ischemia subsequent to vertebral artery occlusion will not be addressed here.

Different patterns of vertebral column injuries are readily visible on radiographs and magnetic resonance images (MRI). Numerous classification systems have been proposed for describing the different types of vertebral injuries in order to standardize terminology and assist in the development of treatment algorithms. Denis introduced the terminology of the three column spine (Denis, 1983) which is convenient for describing structural damage in spinal injuries (Figure 1.12A). The anterior column encompasses the anterior longitudinal ligament, the anterior vertebral

body and the anterior portion of the annulus fibrosus (Figure 1.12B). The middle column includes the posterior wall of the vertebral body, the posterior longitudinal ligament, and the posterior segment of the annulus fibrosus (Figure 1.12C). The posterior column is comprised of the posterior bony complex, ligamentum flavum, interspinous and supraspinous ligaments, and the joints capsules (Figure 1.12D). Note that Allen and Ferguson have proposed mechanistic classifications for cervical (Allen et al., 1982) and thoracolumbar (Ferguson and Allen, 1984) spine fractures, though these mechanisms refer to vertebral column injuries rather than spinal cord injuries. No classification system, however, has gained unanimous acceptance (Schweitzer et al., 2006). The following sections will focus on three stereotypical vertebral injuries—burst fractures, fracture-dislocations, and distractions—as these vertebral column injuries account for over 80% of the column injuries observed in humans (Sekhon and Fehlings, 2001; Pickett et al., 2006) and therefore, they will form the basis of the three idealized mechanisms of spinal cord injury compared in this thesis.

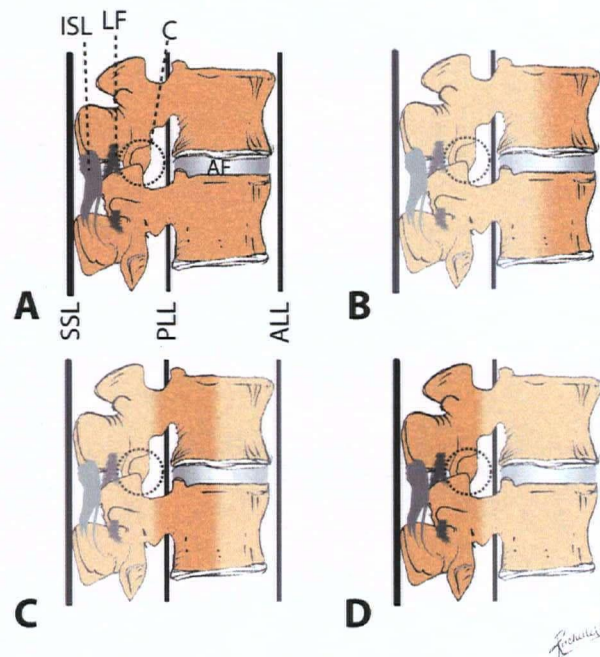


Figure 1.12: Denis's three column spine

A. Labels for structures of the three column spine. B. The anterior column is comprised of the anterior longitudinal ligament (ALL), the anterior half of the annulus fibrosus (AF), and the anterior wall of the vertebral body. C. The middle column which consists of the posterior longitudinal ligament (PLL), the posterior annulus fibrosus, and the posterior wall of the vertebral body. D. The posterior column consists of the posterior bony complex (posterior arch) and the posterior ligamentous complex (supraspinous ligament [SSL], interspinous ligament [ISL], ligamentum flavum [LF], capsule [C]).

1.3.2.1 Burst Fractures

The burst fracture (Figure 1.13A) is characterized by comminution of one, or sometimes both vertebral endplates, that results in the collapse of vertebral body height with retropulsion of bony fragments into the spinal canal (Denis, 1983; Magerl et al., 1994). In this type of vertebral fracture, the exploding bony fragments contuse the spinal cord from the anterior to posterior direction. After this dynamic contusion, the bone fragments may come to rest in a position that occludes the spinal canal and often results in residual compression of the cord. These fractures occur most often in the thoracolumbar spine where they account for approximately 50% to 80% of the spine fractures in this region (Petersilge and Emery, 1996; Bensch et al., 2006). In this region, the narrower spinal canal increases the likelihood of SCI (Bohlman, 1985).

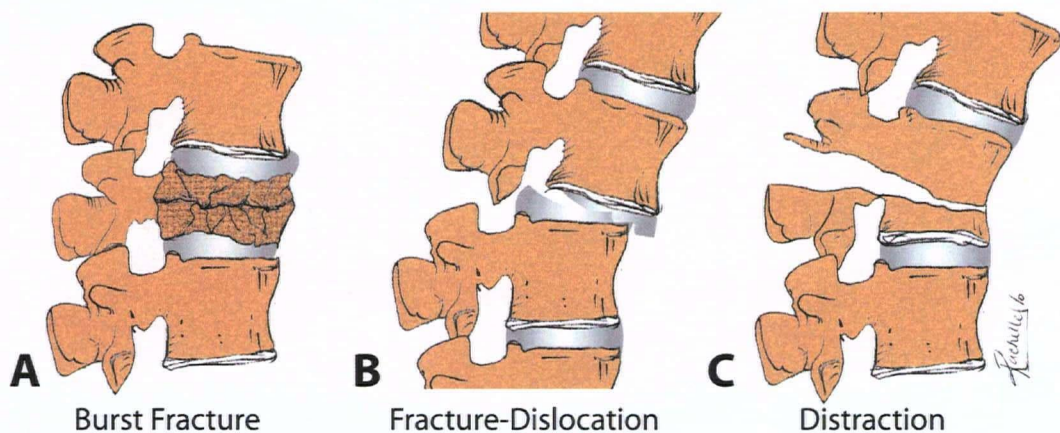


Figure 1.13: Vertebral column fractures

Three clinically relevant types of vertebral column injuries. A. Burst fracture is characterized by the retropulsion of bony fragment into the spinal canal. B. Fracture-dislocation is characterized by the translation of one vertebrae over another. C. Distraction injuries are characterized by a distractive tensile component that results in an increased intersegmental space between the vertebral bodies or posterior elements.

Biomechanically, burst fractures occur by axial compression to the vertebral bodies (Oxland, 1992). In the cervical and thoracolumbar spines, Allen and Ferguson classified these injuries as resulting from compressive flexion and vertical compression mechanisms. In compressive flexion, anterior vertebral wedging is observed with the posterior elements injured in tension. In contrast, vertical compression uniformly collapses the vertebral height without wedging and hence, no tensile loads are applied to the posterior elements.

Of prime importance in the acute assessment of the burst fracture is the extent of spinal column instability that may exacerbate neurologic damage. Vertical compression fractures, where

the posterior elements are intact, are generally thought to be clinically stable meaning that the neurologic status of the patient will not deteriorate. In severe wedge fractures, however, tensile rupture of the posterior ligamentous complex may render these injuries mechanically unstable and susceptible to progressive kyphosis that can further displace bone fragments into the spinal canal (Denis, 1984). A 50% reduction in the height of the anterior vertebral body suggests a risk of posterior element failure and instability (Ferguson and Allen, 1984). Stable burst fractures can be treated non-operatively and the retropulsed bone usually resorbs over time (Petersilge and Emery, 1996).

1.3.2.2 Dislocations & Fracture-Dislocations

Vertebral dislocations and fracture-dislocations (Figure 1.13B) are characterized by the relative displacement—subluxation—of one vertebral body over another (Denis, 1983). The post-traumatic misalignment of the adjacent vertebrae suggests the spinal cord is injured by a shearing mechanism; however, the precise trajectory of the vertebrae during the injury is uncertain. In some injuries, dislocation occurs with facet fracture whereas in other injuries, dislocation occurs with jumped facets indicating a dynamic distractive component during the dislocation.

In Allen and Ferguson's mechanistic classification of lower cervical fractures, dislocations with and without fracture may occur by three types of vertebral injury mechanisms – distractive flexion, compressive extension, and distractive extension (Allen et al., 1982). In distractive flexion, the posterior ligamentous complex is injured by distractive tensile forces enabling facet dislocation while the vertebral body rotates and translates in the anterior direction over the caudal vertebra. In a compressive extension mechanism, the posterior elements are loaded in compression which may result in fracture of the vertebral arches, lamina, and articular processes. In the distractive extension mechanism, the anterior column is placed under tension and there is excessive widening of the intervertebral disc space with possible displacement of the cephalad vertebrae posteriorly shearing the spinal cord between the inferior margin of the moving vertebral body and the lamina of the caudal vertebra. Dislocation injuries can also be caused by torsion (Magerl et al., 1994) or pure translations (Ferguson and Allen, 1984) and this highlights the broad range of injuries grouped under this type of vertebral injury.

Fracture-dislocation involves disruption of Denis's anterior, middle, and posterior columns rendering these vertebral injuries mechanically unstable (Denis, 1984). Anatomical repositioning

of dislocated vertebrae can be achieved with traction (Reindl et al., 2006). Posterior instrumentation, anterior plating, or both can be used to stabilize the fractured segments. Rapid reduction is likely favourable for neurologic recovery, however, anatomical reduction may cause retropulsion of a herniated disc into the spinal canal. The presence of a herniated disc can be ruled out with pre-operative MRI but the delay introduced (1-2 hrs) may compromise the potential for neurologic recovery afforded by the rapid vertebral reduction and decompression of the spinal cord (Hart, 2002).

1.3.2.3 Distraction

Distraction injuries are characterized by tensile forces acting on vertebral bodies, facet capsules, or posterior ligaments (Figure 1.13C). Although pure axial distraction of the vertebral column is routinely used clinically to restore vertebral alignment, this type of injury is not typically encountered in accidental trauma (Iencean, 2003). Rather, distraction between vertebrae usually accompanies other types of injury. In the mechanistic classification proposed by Allen and Ferguson (Allen et al., 1982), distractive tensile forces are present in mechanisms such as distractive flexion, compressive extension, and distractive extension. In the more recent classification proposed by Magerl et al. (Magerl et al., 1994), flexion-distraction and hyperextension-shear injuries both incorporate aspects of tensile distraction forces on the vertebral column. Due to these combinations, the role of distraction in traumatic SCI has been difficult to isolate and remains poorly understood.

In contrast to burst fractures and vertebral dislocations, vertebral distraction does not necessarily occlude the spinal canal. As such, the biomechanics of force transfer between the vertebral column and spinal cord is unclear. A distraction injury of 3cm between C5 and C6 has been associated with complete spinal cord rupture (Schauer and Sokolove, 2003). Spinal cord stretching has been proposed as the underlying cause of non-contiguous SCI that extends over several vertebral levels (Silberstein and McLean, 1994). In tethered cord syndrome, vertebral distraction does not occur but thickening of the filum terminalis results in stretching of the lumbosacral cord which causes motor and sensory deficits of the lower limbs (Yamada et al., 2004). In the cervical and thoracic region, tension may occur between the brain and nerve roots (Cusick et al., 1982). During surgical distraction, somatosensory evoked potentials are frequently monitored as an indication of spinal cord integrity. Excessive distraction results in the loss of these

evoked potentials due to a combination of ischemia and direct mechanical stretching of axons (Cusick et al., 1982).

The biomechanics of distraction injuries and their clinical treatment are similar to that already outlined above for dislocation injuries with a tensile component.

1.3.2.4 Other Vertebral Column Injuries

There are other types of spinal column injury than the three highlighted above. Vertebral compression fractures may occur without the retropulsion of bone into the spinal canal. Lateral flexion injuries are a distinct classification in both the cervical and thoracolumbar spines (Allen et al., 1982; Ferguson and Allen, 1984). Upper cervical injuries such as atlanto-occipital dislocations are also important, though they are usually lethal (Horn et al., 2007) and hence, less relevant for SCI treatment. A problem of utilizing the mechanism of injury to classify spinal fractures is that the mechanism needs to be inferred from post-traumatic imaging and some have advocated that a morphological classification may remove the need to make this inference (Schweitzer et al., 2006).

1.3.3 Spinal Cord Injury Mechanisms

The different types of vertebral column failure result in distinct spinal cord injury mechanisms. Vertebral burst fracture results in a *contusion injury mechanism* where the cord is transiently compressed in a direction that is transverse to its cranial-caudal axis (Figure 1.14A). Vertebral dislocations and fracture-dislocations shear the spinal cord between adjacent vertebral segments. The term *dislocation injury mechanism* will be used in this thesis to denote the spinal cord shear injury caused by the anterior-posterior subluxation of vertebrae (Figure 1.14B). The term shear has not been selected in this thesis as there will come a day when it is possible—indeed preferable—to discuss the local shear stress between gray and white matter, the shear strain near a blood vessel, or the shear strength of myelin lamellae; quantities that will be present in all types of injuries. Vertebral distraction results in a *distraction injury mechanism* that imparts tensile forces to the spinal cord (Figure 1.14C). Local tensile forces will also be present in other injury mechanisms hence the use of the term distraction. In this way, contusion, dislocation, and distraction, SCI mechanisms are defined here to tie-in with vertebral injuries that may be readily classified via radiographs and MRI.

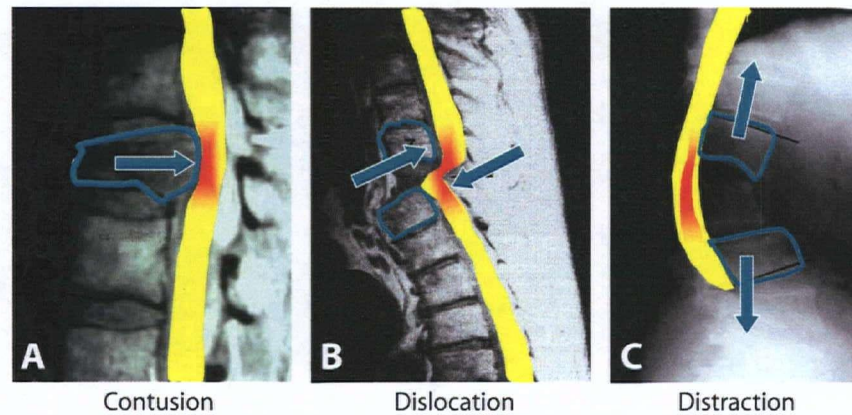


Figure 1.14: Spinal cord injury mechanisms

A. Vertebral burst fracture injures the cord by a transverse contusion mechanism. B. Fracture-dislocation injures the cord by a shearing dislocation mechanism. C. Vertebral distraction injures the cord by a tensile distraction mechanism.

1.3.4 Pathology of Human Spinal Cord Injury

Acute human SCI is typically characterized by hemorrhage, necrosis, and edema (Hayes and Kakulas, 1997) that is detectable with magnetic resonance imaging (MRI). On T2-weighted MRIs, hemorrhage appears dark while edema appears bright (Bondurant et al., 1990; Hackney et al., 1994). Blood-borne monocytes infiltrate the SCI lesion where they transform into phagocytic macrophages that have still been found at the lesion five months post-trauma where their cranial-caudal distribution follows the protracted course of Wallerian degeneration of disconnected axons (Croul and Flanders, 1997). Over time, necrosis evolves into a cystic cavity surrounded by a fibrous astrocytic scar (Croul and Flanders, 1997; Hayes and Kakulas, 1997) though the extent of astrogliosis has been reported to be milder in humans than animals (Norenberg et al., 2004). On occasion, a fluid filled syrinx may also form that requires drainage. Evidence of spared peripheral white matter has been consistently reported even in cases of complete neurological deficits (Hayes and Kakulas, 1997). These spared fibers are often demyelinated, and consequently dysfunctional, though remyelination from Schwann cells originating from the peripheral nervous system has been observed (Norenberg et al., 2004).

Functional recovery following SCI is frequently assessed using the American Spinal Injury Association (ASIA) impairment scale. Approximately half of all patients exhibit incomplete neurological damage with residual motor and sensory function (i.e. ASIA B-D). Intramedullary hemorrhage is predictive of greater neurologic deficits (Schaefer et al., 1989; Bondurant et al., 1990; Ramon et al., 1997). Spinal cord edema without concomitant hemorrhage has been

associated with better outcomes unless the edema spans more than one spinal segment (Schaefer et al., 1989). The cranial-caudal extent of the lesion holds greater functional significance in the cervical region (Hedel and Curt, 2006) where the gray matter contains the phrenic nuclei that control respiration and the motoneurons that innervate the upper limbs. Thoracic lesions between T1 and T12 result in similar ASIA motor scores (~50/100) whereas each ascension in lesion level from C8 (ASIA ~50/100) to C4 (ASIA ~10/100) results in a decline on 10 points per level (Hedel and Curt, 2006). In humans, some have reported the cranial-caudal extent of the lesion spans several vertebral segments (Hayes and Kakulas, 1997), while others have reported a relatively narrow lesion that would be more favourable for axonal regeneration (Tuszynski et al., 1999; Norenberg et al., 2004).

The influence of the mechanism of SCI on the ultimate functional outcome of patients remains unclear. In a series of 1687 cervical spine injuries, Kiwerski (Kiwerski, 1991) found that neurologically complete lesions were more strongly associated with a flexion mechanism (364/651 or 56% of complete injuries) which was partitioned into two groups: flexion with fracture ($n = 96$ complete injuries) and flexion with dislocation ($n = 268$ complete injuries). Within injury mechanisms, however, burst fractures (referred by Kiwerski as crushing compression) were more likely to result in neurologically complete injuries (149/195 or 76% of all burst fractures were complete). By comparison, flexion injuries (with fracture or dislocation) resulted in complete lesions in 364 of 817 (45%) patients.

In a post-mortem analysis of 20 sports related injuries, Hayes and Kakulas described two fracture-dislocation injuries that resulted in a lesion extending over several vertebral segments (Hayes and Kakulas, 1997). In one C3/4 fracture-dislocation, the patient died at 14 days post-trauma and the lesion was found to span approximately 10cm between C1 and C6. In a C4/5 fracture-dislocation where the patient died at 9 days post-trauma, a central hematoma was observed over 4 to 5 segments. In a more recent study, neurologic deterioration due to ascension of the SCI lesion was observed in 12 of 186 (6.0%) patients (Harrop et al., 2001). Nine of the patients had a subluxation or facet dislocation. The neurologic deterioration for these patients was attributed to traction and hypotension rather than the mechanism of injury.

1.3.5 Clinical Spinal Cord Treatment

An understanding of the characteristics of vertebral column injury has been used to specifically target treatment paradigms towards repairing the damaged osteoligamentous structures. Bone grafts, interbody cages, and anterior plates can be used to repair fractures of the vertebral body. Similarly, posterior instrumentation such as wires and rods can restore the stability that is lost by the rupture of posterior ligaments and the fracture of posterior elements (Pitzen et al., 2003; Kwon et al., 2006). Hence treatment for the vertebral column differs to accommodate the pattern of structural failure, however, regardless of the mechanism of spinal cord injury treatment for the cord remains essentially the same.

1.3.5.1 Decompression

Spinal cord injury in humans is frequently accompanied by persistent spinal canal occlusion from fractured or dislocated vertebral elements which can compress the spinal cord. Intuitively, this residual compression should exacerbate cord injury due to factors such as protracted ischemia and therefore should be rapidly relieved via anatomical reduction or decompressive surgery. Clinically, however, no definitive evidence exists to prove the benefit of early decompression (Fehlings et al., 2001). Some have argued the neurologic damage is caused by the initial mechanical insult and is thus irreversible regardless of the timing of decompression (Boerger et al., 2000). Indeed, the maximum dynamic spinal canal occlusion during a burst fracture has been reported to be 85% greater than that measured from post-traumatic radiographs (Panjabi et al., 1995) indicating that radiographs may vastly underestimate the extent of the initial mechanical injury.

In experimental animals, early decompression has consistently improved post-traumatic locomotor function (Dolan et al., 1980a; Guha et al., 1987; Delamarter et al., 1995; Dimar et al., 1999) and somatosensory evoked potentials (Delamarter et al., 1995; Carlson et al., 1997b; Carlson et al., 1997a). Delamarter et al. (1995) found recovery in dogs if decompression was performed within one hour, but no recovery if decompression was delayed until 6 hours after the onset of compression. Dimar et al. inserted spacers of different sizes into the spinal canal of Sprague-Dawley rats following a weight-drop contusion injury and found improved locomotor scores for decompression within 2 hours and poorer function for canal occlusions of 35% or greater.

The disparity between the experimental and clinical literature remains unresolved. The clinical definition of early decompression may be 24 hours whereas in the experimental setting, shorter time-periods have typically been analysed. In addition, it is possible that the current animal models do not reflect the high injury velocities and broader spectrum of injury mechanisms encountered clinically. In burst fractures that are stable, a canal encroachment greater than 50% may benefit from decompression whereas smaller intrusions may be treated conservatively (Agus et al., 2004). In bilateral facet dislocations, retrospective evidence suggests possible neurological improvements with early reduction (La Rosa et al., 2004).

1.3.5.2 Pharmacotherapy

To date, the only treatment that has been widely used clinically is high dose methylprednisolone (MP) though its application has declined amidst intense controversy regarding its efficacy (Hurlbert, 2000; Sayer et al., 2006). Hemorrhagic necrosis, inflammation, and oxidative stress had long been postulated to exacerbate the primary spinal cord lesion (Hall and Braughler, 1982). Several animal studies have demonstrated the effectiveness of MP in attenuating the secondary inflammatory response thought to exacerbate the primary SCI lesion (Means et al., 1981), however, the first National Acute Spinal Cord Injury Study (NASCIS) found no benefit of MP in a prospective series of patients (Bracken et al., 1984; Bracken et al., 1985). Further experimental work then suggested higher MP doses were necessary to achieve lasting benefits (Hall et al., 1984; Braughler et al., 1987). In 1992, NASCIS II reported a beneficial effect of MP if it was administered within 8 hours of acute SCI (Bracken et al., 1990; Bracken et al., 1992). NASCIS III refined the treatment protocol. Patients treated within 3 hours would receive one high dose bolus of MP, followed by MP over the next 24 hours (Bracken et al., 1997; Bracken et al., 1998). Patients treated between 3 and 8 hours would receive one high dose bolus followed by MP over the next 48 hours.

NASCIS II originally included patients admitted up to 12 hours post-trauma. The *post hoc* change to 8 hours has been criticized for its lack of statistical merit (Hurlbert, 2000; Sayer et al., 2006). Likewise, in NASCIS III the 3 hour versus 3 to 8 hour stratification seemed arbitrary and again lacked statistical rigor (Sayer et al., 2006). In both cases, however, the partitioning of patients emphasized the need for examining very early intervention within a few hours of trauma. This early therapeutic time-window is consistent with meta analyses of the clinical timing of

decompression (Fehlings et al., 2001; La Rosa et al., 2004). Moreover, many animal studies have shown the benefit of pharmacotherapies administered within minutes to a few hours following injury (Faden et al., 1988; Mu et al., 2000; Gris et al., 2004), while studies comparing both early and late drug administration have found the latter to be ineffective (Wrathall et al., 1996; Rosenberg and Wrathall, 2001).

Opponents of MP continue to argue that the neurological benefits are extremely modest while the increased risks of sepsis and pneumonia are unacceptable (Hurlbert, 2000; Sayer et al., 2006). Although Young and Bracken have argued that numerous alternative analyses show the same trends (Young and Bracken, 1992), the issue can likely only be settled with another prospective trial that identifies the optimal treatment population *a priori*. The amount of tissue available for pharmacological sparing is controlled by the extent of primary mechanical damage, the degree and duration of residual compression, and the timing of intervention.

Other therapies have also been tested. In addition to MP, NASCIS II tested the opiate antagonist naloxone which is thought to reduce edema and post-traumatic allodynia (Baptiste and Fehlings, 2006) but found no significant benefit (Bracken et al., 1990). In NASCIS III, MP was compared with Tirilazad—a 21-aminosteroid, which was hoped to reduce lipid peroxidation without the glucocorticoid side-effects of MP. Tirilazad did not show improved benefits over MP (Bracken et al., 1997). Gangliosides are thought to promote the growth of neurites and hence restore post-traumatic neurologic function (Geisler et al., 1991). A pilot clinical trial comparing monosialotetrahexosylganglioside (GM-1) to placebo showed a significant improvement of motor deficits in the lower limbs between 2 and 12 months after trauma (Geisler et al., 1991), but a larger trial failed to confirm the results (Geisler et al., 2001).

1.3.6 Summary of Human Injuries

Promising experimental therapies have yet to demonstrate clear benefits when applied to human SCI. In humans, the spinal cord is injured by differing mechanisms that result from various types of vertebral column trauma. As will be discussed later in this thesis, the current animal models do not reflect this broader range of injury mechanisms encountered in the human population. In addition, evidence from clinical trials suggests earlier pharmacological treatment improves neurological recovery, thus indicating the importance of the first few hours following mechanical injury.

1.4 Biomechanics of Neurotrauma

The rationale for comparing biomechanical mechanisms of injury stems, in part, on the understanding that most materials and structures exhibit different patterns of mechanical damage in response to the application of different forces. In neurotrauma, one of the most relevant measures is that of injury or damage. Injury, however, can manifest itself in different contexts. Damage can be defined as overt gross tissue tearing, though this only represents one extreme end of the injury continuum. Cells may be dysfunctional or die in the absence of overt mechanical tissue failure. Neural tissue is inhomogeneous and consists of an intricate architecture of cells such as neurons, astroglia, oligodendroglia, and microglia, embedded in an extracellular matrix that is interwoven with a network of capillaries. Neurons themselves are complex structures with dendritic arbors extending from neuronal somata (cell bodies) that transmit action potentials (nerve impulses) via their axonal processes, many of which are ensheathed in myelin lamellae that are punctuated by the unmyelinated nodes of Ranvier. Each cell's plasma membrane encapsulates a cytoskeleton of organized microtubules, intermediate filaments, and microfilaments. Hence, the following section outlines some of what is known about the gross mechanical response of neural tissue, then progresses to discuss the myriad injuries that occur at the tissue, cellular, and subcellular levels. The section concludes with an overview of existing methods used to model spinal cord injuries.

1.4.1 Mechanical Properties of Neural Tissue

The characterization of the macroscopic mechanical behaviour of neural tissue has long confounded the experimentalist. The inherent softness of the tissue complicates attempts to grip the tissue for tests such as tensile loading while post-mortem degradation potentially alters the material properties. Consequently, the mechanical properties that have been reported vary widely and is an ongoing limitation in the field (Prange and Margulies, 2002; Kohandel et al., 2006).

Neural tissue can be partitioned into gray and white matter components. The gray matter consists of neuronal cell bodies, their dendrites and axonal processes as well as supporting glia cells such as astrocytes and microglia. White matter consists of organized tracts of axons, as well as astrocytes, microglia and the oligodendrocytes which myelinate the axons and gives them their white appearance. A network of vasculature permeates neural tissue and these capillaries are more numerous in the gray matter.

In general, the modulus is a quantity that characterizes the material's response to force and deformation. The modulus is defined by the ratio of stress (force per unit area) to strain (ratio of the change in length to the original length). Hence, a tensile modulus characterizes the relation between force and deformation to tension. Likewise, the bulk modulus is measured under confined compression, and the shear modulus is the response under shear. The modulus is an intrinsic property of the material that is independent of its macroscopic geometry. Doubling the cross-sectional area of a rod will double its stiffness under axial tension, however, the modulus of the rod's material would remain the same. For neural tissue, the modulus has usually been measured grossly and hence these values represent some aggregate behaviour of the individual cellular components.

Neural tissue possesses fluid components, thereby rendering it viscoelastic. Consequently, the modulus, is characterized by an elastic component and a viscous component. Deformations imparted to the elastic component are recoverable (i.e. energy stored). In contrast, viscous deformations are not recoverable unless additional force is applied (i.e energy lost). The viscous property also exhibits a dependence on the rate of deformation. Higher rates usually result in greater losses in energy. To detect these properties of energy stored, energy lost, and the rate dependence, sinusoidal excitations at different frequencies are used to cyclically displace the material and measure the resultant forces which will be offset in sinusoidal phase due to viscous energy losses. This type of material test yields a complex modulus, $G = G' + iG''$, where G' is the storage modulus, G'' is the loss modulus, and i is the complex variable $\sqrt{-1}$. Complex numbers are a tool for representing the phase relationship of sinusoids.

The *in vivo* tensile properties of the spinal cord has been reported by Hung et al. (Hung and Chang, 1981). After removal of the canine dura, stainless steel rings were bonded with cyanoacrylate to the lumbar spinal cord and the rings were coupled to an actuator. At a loading rate of 0.021 mm/s, the *in vivo* Young's modulus of the spinal cord was found to range from 200 kPa to 300 kPa (where 1 Pascal = 1 Newton per m² per strain, where strain is the dimensionless ratio of the change in length to the initial length) and similar values were found by the same group in the cat lumbar spine (Chang et al., 1988). *In vitro* testing of human cervical spinal cords examined within 24 hours of death indicated a Young's modulus of 1020 kPa at a tensile loading rate of 0.068s⁻¹ that increased to 1370 kPa at a loading rate of 0.21s⁻¹ (Bilston and Thibault, 1996).

Ex vivo compressive tests of unconfined cylindrical specimens obtained from human brains exhibited a modulus of ~ 70 kPa at a sinusoidal displacement frequency of 34 Hz (Galford and McElhane, 1970). Neural tissue is usually considered to be incompressible with a bulk modulus that is much higher than either its tensile or shear modulus (Mendis et al., 1995b; Lippert et al., 2004).

To determine the shear moduli, Fallenstein et al. (Fallenstein et al., 1969) applied sinusoidal (9-10 Hz) shear to *in vitro* human brain white matter and found the storage modulus to be in the range of 0.6 kPa to 1.1 kPa while the loss modulus ranged between 0.3 to 0.6 kPa. In a higher frequency test (up to 350 Hz), the storage and loss moduli of gray and white matter in post-mortem brains were found to be on the order of 7 kPa and 2 kPa respectively. More recently, *in vitro* tests of porcine brainstems tested dynamically in shear showed the anisotropic behaviour of white matter (Arbogast and Margulies, 1998). The shear modulus transverse to the direction of axonal fibers ($G' \sim 2$ kPa, $G'' \sim 2.5$ kPa at 200Hz) was significantly greater than in the other two directions ($G' \sim 1.75$ kPa; $G'' \sim 2.2$ kPa at 200Hz) demonstrating the anisotropy of white matter tracts (Figure 1.15). This anisotropy is lost, however, in regions such as the corona radiata (in the brain) where the white matter tracts are not aligned along a single orientation (Prange and Margulies, 2002).

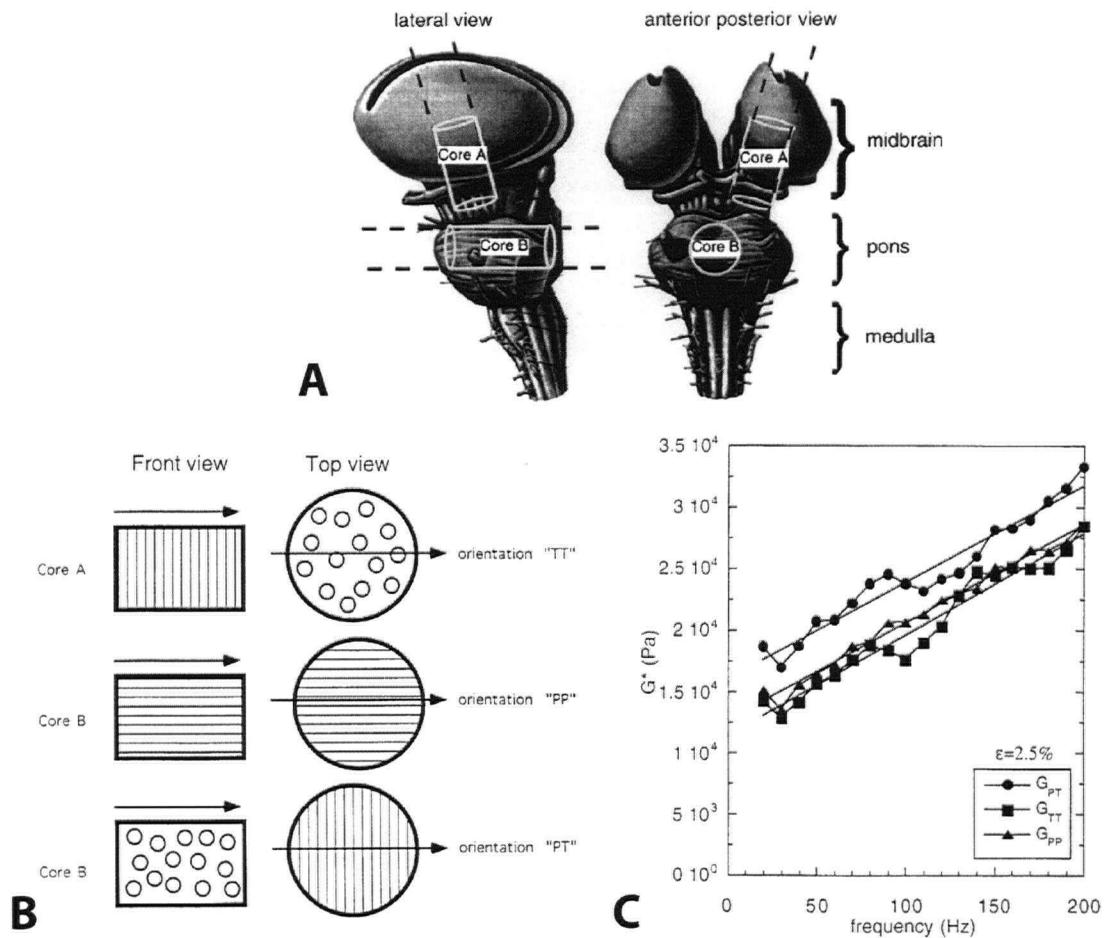


Figure 1.15: Anisotropy of neural tissue

Arbogast and Margulies examined the anisotropy of neural tissue using oscillatory shear tests. A. Illustration of core samples taken from the brainstem. B. Schematic of axonal fibre orientations in the directions tested. C. Magnitude of complex shear modulus (G^*) shows a greater modulus when shear is applied transverse to the parallel direction of the fibres (PT). (Graphics compiled from: Arbogast KB and Margulies SS, 1994. Material characterization of the brainstem from oscillatory shear tests. *J Biomech* 31:801-807. © Elsevier, 1994, adapted by permission.)

In addition to anisotropy, the heterogeneity of gray and white matter characteristics remains unresolved. In 2001, two studies addressed this issue using different techniques (Ichihara et al., 2001; Ozawa et al., 2001). Ichihara and colleagues applied tensile tests to 2.5mm diameter biopsy specimens obtained from bovine cervical spinal cords. Over a range of strains (5% to 55%), they reported a higher tangent modulus for gray matter (~ 100 kPa at 15% strain) compared to white matter (~ 38 kPa at 15% strain). In addition, their gray matter specimens failed at a lower strain level ($\sim 50\%$) compared to white matter ($\sim 126\%$). In contrast, Ozawa et al. utilized a pipette aspiration technique with rabbit spinal cords and found no difference in the elastic modulus of gray and white matter (~ 3.5 kPa).

The estimated material properties for neural tissue span a wide range due to the experimental differences such as *in vivo* testing versus *in vitro* testing and gray matter versus white matter. A shear modulus on the order of 1 to 10 kPa appears consistent between several reports (Fallenstein et al., 1969; Shuck and Advani, 1972; Arbogast and Margulies, 1998). In addition, the organized architecture of white matter results in transverse anisotropy (Arbogast and Margulies, 1998) in contrast to gray matter and regions of less organized white matter (Prange and Margulies, 2002).

1.4.2 Constitutive Models

Empirical determination of the material properties of neural tissue can ultimately be used to solve for the parameters of mathematical models that relate force and deformation—the constitutive model. These constitutive relations can then be used in computational models which predict the internal stresses and strains within the neural tissue under a more general range of conditions than the simple paradigms used to initially determine the material properties. For example, in a numerical simulation of traumatic brain injuries, high shear strains were detected in the corpus callosum—the white matter tract that bridges the two cerebral hemispheres—while high tensile strains were detected in some of the bridging veins which could lead to hemorrhage (Zhou et al., 1995). Although the quantitative values generated by numerical simulations are highly dependent on the validity of the material properties (shown above to be problematic), these simulations can still provide insight into the behaviour of the brain and spinal cord during trauma that would be difficult to obtain experimentally.

Several material models have been fit to experimental data of neural tissue. In linear viscoelastic models, the elastic component is proportional to the strain and the viscous component is proportional to the strain rate. Fung's quasilinear viscoelastic formulation proposes tensile experimental data can be fit to a linear elastic component that is multiplied by a relaxation function that is parameterized by exponentials (Fung, 1993). The model has been widely used (Bilston and Thibault, 1996; Darvish and Crandall, 2001). Hyperelastic models have also been used which utilize the experimental data to determine the exponents in a strain-energy equation (Mendis et al., 1995a; Meaney, 2003). More recently, biphasic models have also been applied to describe the flow of fluid out of a viscoelastic solid matrix for neural tissue under compression (Cheng and Bilston, 2007). Other modified formulations have also been reported (Mendis et al., 1995b; Davis

et al., 2006; Kohandel et al., 2006; Velardi et al., 2006), however, no single constitutive model has been agreed upon as the standard.

The constitutive equation provides a valuable mathematical tool to describe the gross behaviour of neural tissue, however, the formulations do not capture the underlying behaviour of the tissue's individual cellular components (Fung, 1993). Microstructural models have thus been developed to provide an anatomically more meaningful sense of the tissue's behaviour.

Arbogast and Margulies applied a fiber-reinforced composite formulation to model the brainstem (Arbogast and Margulies, 1999). Myelinated axons were treated as fibers in a gray matter matrix. Combining the known distribution of fibers and matrix in the brainstem (i.e. from histology) with mechanical data from shear tests (Arbogast and Margulies, 1998), they determined the relative complex moduli of myelinated axons and gray matter. The method was validated by empirically determining the mechanical properties of myelinated axons from the optic nerve which is devoid of gray matter. The innovative approach indicated a shear modulus on the order of 2kPa for fibers and <1kPa for the matrix at 20Hz. The myelinated axons were determined to be stiffer and more viscous (i.e. greater change in the loss modulus with increased frequency) than the matrix in shear. Microstructural models have also been proposed for modelling features such as the inherent undulations of axons in white matter axons (Meaney, 2003).

Possible future approaches might entail a further partition of the fibers into the myelin lamellae, the axonal plasma membrane, and the axonal cytoskeleton since physiologically, injury to each of these structures would require distinct interventions—remyelination, membrane resealing, cytoskeletal repair or regeneration respectively. Hence, the evolution of gross constitutive models towards microstructural formulations may potentially provide a more physiologically relevant meaning to the numerical predictions in terms of a greater specificity regarding the cellular structures damaged.

1.4.3 Primary Mechanical Injury

Traumatic SCI is routinely acknowledged to occur by a mechanical insult customarily referred to as the *primary injury* in order to distinguish the damage from the secondary tissue degeneration that is mediated by biochemical processes. Primary injury is thought to be irreversible and hence, few investigators have focused on this aspect in the context of treatment. Due to the range of clinically observed cord injury mechanisms, and the biomechanics of neural

tissue, it seems reasonable that our understanding of SCI could benefit from a broader consideration of the characteristics of primary damage at the tissue, cellular, and molecular levels. For example, although primary axotomy is irreversible, injury to collateral structures such as glia and capillaries as well as the rostro-caudal extent of damage along the axon's length may significantly influence important variables such as the extent of demyelination, the rate of axonal die-back, and the final distance required for regeneration. Moreover, a growing body of evidence suggests even molecular mechanisms are modulated to some extent by mechanical stimuli (Paoletti and Ascher, 1994; Eder et al., 1998; Jacques-Fricke et al., 2006). This section characterizes primary injury from the gross tissue scale down to the cellular level.

1.4.3.1 Tissue Failure

Overt mechanical tissue failure, particularly of white matter, is reported to be rare in SCI except in cases of lacerations due to stabbings or bullet wounds. In the only reports of *in vivo* tensile testing of canine and feline spinal cords, the cyano acrylate bond failed (~40% strain) between the testing device and the spinal cords before mechanical disruption of tissue was observed (Hung and Chang, 1981; Chang et al., 1988). *In vitro* tests at a strain rate of 0.05s^{-1} , estimated the tensile strength of gray matter to be $43.4 \pm 3.2\text{kPa}$ (SD, $1\text{ Pa} = 1\text{ Newton/m}^2$) at an elongation $48.6 \pm 8.0\%$ (SD) (Ichihara et al., 2001). In the same study, the white matter possessed a higher tensile strength and failed at $61.3 \pm 4.2\text{kPa}$ when deformed by $126.1 \pm 53.0\%$. If the lower tensile strength of gray matter found *in vitro* can be extended to the *in vivo* case, it would be consistent with the pattern of damage observed in experimental spinal cord contusions where primary injury initiates centrally in the gray matter and progressively extends to the surrounding white matter (Bresnahan et al., 1991).

In addition to the relative strength properties of gray and white matter, other factors, such as the internal strain distribution within the spinal cord likely also contribute to the centralized primary tissue failure pattern observed in contusion SCI models. Using a model of a gel filled cylinder, Blight and Decrescito reasoned that damage to the central region of the cord stemmed from the increased displacement of the central part of the cylinder under transverse compression (Blight and Decrescito, 1986; Blight, 1988). Similar arguments have been used to explain central cord syndrome where upper limb motor deficits result from dysfunction of centrally located lateral corticospinal fibers (Raynor and Koplik, 1985).

1.4.3.2 Vascular Damage

Mechanical failure of neural tissue is accompanied by damage to vascular structures. Overt intramedullary hemorrhage leads to immediate hemorrhagic necrosis. Gray matter is more highly vascularized than white matter (Banks et al., 1998) and this is also a contributing factor to the preferential damage to the central gray matter that is observed following contusion injuries. Even in the absence of visible hemorrhage, primary damage to the vasculature can result from compromise of the blood-brain barrier (BBB) or blood-spinal cord barrier (BSB). The BSB consists of endothelial cells that form tight junctions that restrict large molecules and immune cells from infiltrating the central nervous system (CNS). Compromise of the BSB allows fluids and proteins to cross into the CNS (i.e. vasogenic edema) and perhaps more importantly, the infiltration of immune cells whose actions can damage neural tissue (Popovich et al., 1996a).

Compromise of the BSB can be detected by measuring the extravasation of molecular markers into the spinal cord parenchyma (Noble and Wrathall, 1989; Popovich et al., 1996b; Yamauchi et al., 2004; Maikos and Shreiber, 2007). Intravenous infusion of radioactive tracers (molecular weight 107 Da) showed greater BSB compromise in the gray matter between 3 and 7 days post-trauma compared to white matter. Between 2 and 4 weeks after injury, the pattern had reversed, with white matter exhibiting greater barrier compromise (Popovich et al., 1996b). Thresholds for primary mechanical injury to the BSB has recently been reported for spinal cord contusion injuries (Maikos and Shreiber, 2007). The extravasation of markers with different sizes (730 Da hydrazide, 70 kDa bovine serum albumin, $\sim 5\mu\text{m}$ red blood cells) was used to show a graded extent of BSB damage where smaller markers occupied a greater volume of extravasation into the spinal cord. SCI was produced by dropping a weight onto the exposed dura of the spinal cord. At a drop-height of 25mm (moderate injury), hydrazide extravasation occupied approximately 10mm^3 while albumin and red blood cells filled 8mm^3 and 5mm^3 respectively. Extravasation across the barrier was significantly greater in the gray matter than in the white matter ($\sim 7\text{mm}^3$ vs $\sim 3\text{mm}^3$ for hydrazide at a moderate injury severity). In the weight-drop SCI model, adjusting the drop-height varies the impact velocity, the rate of compression, as well as the final magnitude of spinal cord compression. Linear regression indicated a critical threshold for albumin extravasation in the white matter at an impact velocity of 19cm/s, cord compression rate of 22cm/s, and cord compression of 0.8mm. In the gray matter, a non-zero threshold could not be determined indicating a greater sensitivity to primary BSB compromise in this tissue component.

The effect of velocity on BSB compromise extends to intramedullary hemorrhage. In the mid 1980's, Anderson demonstrated an interaction between the velocity of spinal cord contusion and the magnitude of the cord compression (Anderson, 1985). SCI was produced using a pneumatic impactor that enabled injuries to be produced over a wide range of velocities (0.6, 3.0, 10.0m/s) with physical stops used to independently control the degree of spinal cord compression (25, 50, 75%). The impact velocity demonstrated a higher correlation with hemorrhagic necrosis while latency in somatosensory evoked potentials was better correlated with the extent of cord compression. The product of the velocity and compression magnitude has been suggested as a more relevant criteria for predicting SCI severity (Kearney et al., 1988). At contusion impact velocities of 300mm/s, hemorrhage has been observed to extend into the peripheral white matter tracts whereas as at lower speeds (3mm/s) vascular damage was restricted to the gray matter (Sparrey et al., 2004). Hence, vascular damage is an important type of primary injury that is strongly tied to the speed of trauma.

1.4.3.3 Electrophysiological Deficits

In the absence of overt mechanical tissue failure, mechanical injury is also evident by the loss of action potential conduction. The electrophysiological integrity of white matter funiculi can be tested by stimulating sensory or motor tracts (i.e. somatosensory or motor evoked potentials). Under slow loading conditions, such as surgical distraction for vertebral realignment, mechanical stress on neural tissue results in conduction failure before mechanical failure. The loss of electrophysiologic function can be caused by the mechanical deformation of axons (Brodkey et al., 1972; Shi and Pryor, 2002) or the loss of vascular perfusion due to increased interstitial pressure (Kobrine et al., 1978; Dolan et al., 1980b; Jarzem et al., 1991; Naito et al., 1992).

Under transverse compression, the amplitude of evoked potentials begin to decline at a compression magnitude of 60% (Nacimiento et al., 1986). This amplitude reduction is reversible up to a maximum compression of 80% whereas 100% compression results in permanent deficits.

Optic nerve stretch models have also been used to determine mechanical thresholds for producing conduction deficits (Bain and Meaney, 2000). The optic nerve consists of a homogeneous population of myelinated central nervous system axons that is interspersed by astrocytic processes. A strain threshold of 28% results in complete loss of visual evoked potentials (sensitivity = 1.0). No functional compromise was detected below a strain of 13% (specificity =

1.0). An optimal injury threshold that balanced sensitivity and specificity was found to be 18% strain. Injury to the neurofilament cytoskeleton was only detected at higher strain thresholds where abnormal axonal morphology was consistently detected at strains above 34% while no apparent injury was detected below a strain of 14%. A threshold of 21% was found to optimally predict morphological damage. The results elucidated injury thresholds in the white matter and also demonstrated that functional failure precedes detectable cytoskeletal injury.

1.4.3.4 Cellular Injury

In vitro experiments have been used to study mechanical injury thresholds on isolated cells thereby removing confounding factors such as hemorrhage and the more complex load distributions found *in vivo*. Gallant analysed transverse compression of isolated squid giant axons with diameters ranging from 0.3mm to 1.0mm (Gallant, 1992). The unmyelinated squid axons could withstand 0.005N (0.5g) of compression, distributed over a 1mm length, resulting in a 10% strain, for a duration of 10 seconds without permanent deformation. When the compressive load was increased to 0.05N (5g), strain approached 100% and the axoplasm was displaced from the epicentre of applied force. Interestingly, when the compression was removed, action potentials rapidly recovered in spite of the displaced axoplasm. Over time, the axoplasm gradually returned to the compression epicentre, however, axonal transport of organelles was dysfunctional for at least 5 hours. A compressive load of 1N (100g) was found to be a critical threshold that caused changes in the refractive index of the axoplasm. Changes in refractive index were attenuated when the medium outside the axon was changed to match the ionic properties of the axoplasm. This demonstrated that the pathologic changes were due to the exchange of ions across the damaged cell membrane.

The squid giant axon has also been studied under axial tension (Galbraith et al., 1993). Tensile strains above 20%, produced at a loading rate of 27.5cm/s, resulted in irrecoverable loss of ionic homeostasis and abolition of action potential conduction. A strain of 25% resulted in axotomy. At low strains and strain rates, the membrane potentials could recover and the action potentials reappeared at 3 minutes post-injury. A higher tolerance to mechanical tensile stretching has been observed with *in vitro* axonal cultures (Smith et al., 1999). Axons with diameters ranging from 0.5 to 1.5 μ m were stretched up to 77% of their initial length at a rate of 26 to 35s⁻¹. Primary

axotomy occurred at strains greater than 65%. At lower stretch levels, axons exhibited an increase in undulations that recovered over a 45 minute period post-injury.

The effect of shear strains on isolated neuronal cell cultures has been extensively characterized by LaPlaca et al. (Laplaca et al., 1997; LaPlaca and Thibault, 1997, 1998; LaPlaca et al., 2005; Prado et al., 2005; Cullen and LaPlaca, 2006). In a parallel disk viscometer, a rotating disk is used to generate fluid shear stresses (1-4Pa) that can injure neurons cultured onto the stationary disk (LaPlaca and Thibault, 1997). Neuronal strains up to ~50% can be produced resulting in the efflux of lactate dehydrogenase, which is indicative of plasma membrane compromise, and the influx of calcium ions (Laplaca et al., 1997) which is known to initiate secondary degeneration. In another model, three-dimensional cell cultures sandwiched between two parallel plates are injured in shear by translating the plates relative to each other (LaPlaca et al., 2005). When compared to two-dimensional planar cultures, neurons cultured in the three-dimensional matrix exhibit higher cell death rates following comparable levels of mechanical trauma (Cullen and LaPlaca, 2006).

1.4.3.5 Plasma Membrane Compromise

The cell's plasma membrane is among the first structures damaged in the sequence of events that initiate cellular injury. In the absence of overt lysis of the cell body or transection of cellular processes, mechanical forces can still produce sub-lethal breaches in membrane integrity, sometimes referred to as mechanoporation. Membrane compromise allows free passage of ions between the intracellular and extracellular space resulting in the loss of normal ionic gradients and compromise of the generation and the conduction of action potentials (Shi et al., 2000). In addition, the influx of calcium ions across the damaged membrane is one of the main triggers of secondary deleterious processes (Young, 1992).

LaMotte developed a method to probe the integrity of axons following a weight-drop spinal cord injury by incubating horseradish peroxidase (HRP) soaked gelfoam near the lesion epicentre and demonstrated HRP penetration in all white matter tracts at the injury site (LaMotte, 1980). Since that time, similar strategies have been used to detect plasma membrane compromise *in vitro* (Geddes et al., 2003; Prado et al., 2005), *ex vivo* (Shi et al., 2000; Shi and Pryor, 2000), and *in vivo* (Pettus et al., 1994; Singleton and Povlishock, 2004; Stone et al., 2004).

In myelinated axons, membrane compromise initiates at the nodes of Ranvier (Maxwell et al., 1991) where the axolemma is unsupported by compact myelin and thus seems exposed to stress concentrations (Blight, 1988). Cytoskeletal microtubules in the nodal region are lost within 15 minutes of neurotrauma (Maxwell and Graham, 1997). This focal mechanical disruption at the nodes of Ranvier suggests axonal conduction failure is due to a combination of ionic dysregulation across the permeabilized membrane and the exposure of voltage-gated potassium channels normally covered by myelin in the juxtaparanodal region (Figure 1.9H). Consequently, conduction deficits can be improved by either membrane repair using surfactants such as polyethelene glycol (Shi and Borgens, 1999; Borgens and Shi, 2000) or lowering the conductance of exposed potassium channels with channel blockers such as 4-aminopyridine (Shi and Blight, 1997; Shi et al., 1997).

Even without treatment, membrane integrity can be restored by endogenous repair mechanisms. In *ex vivo* preparations, transected axons appear to reseal within approximately 30 minutes (Shi et al., 2000). However, membrane permeability persisted for at least 1 hour post-trauma for excised white matter subjected to transverse compression and axial stretching (Shi and Pryor, 2002; Shi and Whitebone, 2006). This phenomena is likely due to increased membrane compromise distributed throughout the axon's length (Shi and Whitebone, 2006).

Paradoxically, the removal of extracellular calcium—the influx of which is known to initiate cytoskeletal degradation via calcium activated neutral proteases—reduces the efficiency of endogenous membrane repair (Shi et al., 2000). Hypothermia also reduces axolemma resealing though it is unclear if this is due to a reduction in membrane fluidity or reduced enzyme kinetics at lower temperatures (Shi and Pryor, 2000; Shi et al., 2001).

Prado and LaPlaca have studied membrane repair processes using *in vitro* neuronal cultures (Prado and LaPlaca, 2004). Similar to reports in *ex vivo* white matter, cultured neuronal somata also require extracellular calcium in order to reseal the plasma membrane. In addition, the chelation of intracellular calcium appears to abolish membrane resealing suggesting the influx of extracellular calcium into the intracellular compartment is a necessary event in the repair process. However, the simultaneous removal of extracellular calcium and chelation of intracellular calcium restores membrane resealing properties. Depolymerization of the actin cytoskeleton with latrunculin-B was shown to enhance membrane repair and this was attributed to an increase in

fluidity of the plasma membrane. Counterintuitively, stabilization of the actin cytoskeleton with jasplakinolide also appears to enhance membrane resealing (Prado, 2004).

Membrane disruption is a pivotal event in neurotrauma that results in immediate, though perhaps transient, loss of action potential capabilities and the initiation of secondary pathomechanisms. This type of primary damage is reversible to some extent though much remains to be understood about this dynamic process.

1.4.4 Spinal Cord Injury Models

SCI research relies heavily on animal models for testing therapeutic strategies prior to human trials. Virtually all the animal models control one or more mechanical parameters in order to produce a consistent SCI lesion. Animal models based on the contusion and compression injury mechanisms have been widely adopted as they are thought to closely mimic human SCI (Wrathall, 1992; Stokes and Jakeman, 2002; Young, 2002). Spinal cord transection models are also widely employed to demonstrate the efficacy of axonal regeneration therapies (Kwon et al., 2002a). The following section reviews the current contusion injury models and highlights the few reports that model other SCI mechanisms.

1.4.4.1 Allen's Weight-Drop

The weight-drop method was pioneered by Allen in 1911 (Allen, 1911, 1914). Using a dog model, the spinal cord was exposed with a laminectomy and a known mass was then dropped onto the exposed dura from a controlled height. The injury was thus characterized by the product of the mass in grams and drop height in centimeters (g-cm); a quantity proportional to the initial potential energy of the mass. Allen observed progressive tissue destruction due to hemorrhage and conducted early experiments on dural incisions to relieve intramedullary pressure. He postulated the presence of biochemical processes which progressively destroys the spinal cord parenchyma—an insightful notion which today is called the secondary injury cascade.

The weight-drop contuses the animal's spinal cord in a dorso-ventral direction and hence bears close resemblance the anterior-posterior burst fracture mechanism frequently encountered clinically. This clinical significance has led to the widespread adoption of the weight-drop experimental model (Wrathall, 1992; Basso et al., 1995; Beattie et al., 1997; Kwon et al., 2002a; Young, 2002). The model was used as the standard in a Multicenter Animal Spinal Cord Injury Study (MASCIS) which led to the development of the Basso-Beattie-Breashan (BBB) locomotor

rating scale for assessing post-traumatic function following thoracic contusion injuries (Basso et al., 1995).

Although the weight-drop was intuitively similar to the dynamics of a vertebral bony fragment impinging on the spinal cord during an actual SCI event, there were some experimental issues. In early protocols, the vertebral column was not supported and hence, the column was able to deflect during impact, thus adding experimental variability. Measurements in a cat model indicated 4.6mm of cord/thorax deflection resulted in only 1.1mm of actual cord deformation (Dohrmann et al., 1978). The transfer of energy to the cord, column, and surrounding anatomy was difficult to quantify. In subsequent rodent models, direct support of the vertebral column was introduced in order to isolate the contusion impact to the spinal canal compartment (Noble and Wrathall, 1985; Gruner, 1992). Current versions of the weight-drop model directly measure vertebral column deflection to determine the actual spinal cord deformation (Maikos and Shreiber, 2007).

One advantage of the weight-drop method was its apparent simplicity and characterization by the single g-cm parameter. However, the g-cm product is an indeterminate quantity. Using a cat model, Dohrmann et al. varied combinations of mass (5 to 100 g) and drop heights (4 to 80 cm) to produce constant 400 g-cm injuries (Dohrmann et al., 1978). It was shown that the injury force varied from 5.1N for the 5g × 80cm to 16N for the 100g × 4cm product. Similarly, the resultant displacement also varied from 0.73mm for the 5g drop mass to 1.1mm for the 60g × 6.6cm injury. A consensus of using a 10g drop mass with a diameter of 2.5mm has been used to control this issue (Gruner, 1992; Young, 2002). For injury in rats, standard drop heights are 12.5, 25, and 50mm which achieve impact velocities of 48.9, 69.0, and 97.4cm/s respectively (Maikos and Shreiber, 2007).

Other standardizations have been introduced including the use of 77±1 day old rats, intraperitoneal injection of pentobarbital (45mg/kg for females, 65mg/kg for males) and injuries 60±5 minutes following induction of anaesthesia (Young, 2002). The presence of multiple bounces of the drop mass remains a limitation that has been assumed to be negligible.

1.4.4.2 *Controlled Displacement*

As an alternative to the weight-drop model, a controlled displacement device was developed at The Ohio State University (OSU) in the 1980's (Bresnahan et al., 1987; Noyes,

1987a, b; Somerson and Stokes, 1987). The device was used to examine the effect of physical parameters other than g-cm on contusion injuries.

As with the weight-drop, the spinal canal is exposed via a laminectomy and the vertebrae are stabilized to limit movement during impact. The rat vertebral column was originally stabilized with pins inserted into the vertebral body, though the vertebral stabilization has evolved to use Allis clamps to hold the spinous processes of the thoracic vertebrae. In thoracic contusion injuries, the animal is partially suspended by its spinous processes in order to reduce breathing artifacts. The injury device features a touch mode where a 60Hz, 30 μ m peak-to-peak oscillation of the 2mm impactor tip is used to probe the laminectomy for bony debris in order to ensure a clear impact. A 0.03N (3kdyn) pre-load is used to displace the cerebrospinal fluid between the dura and the spinal cord thereby establishing an initial contact position from which to apply the injury stroke. The choice of a 0.03N contact force evolved from a 0.01N (1 to 1.5kdyn) contact force originally used to mimic the 1g die that was placed on the dura in some weight-drop models (Somerson, 1986). The injury was produced using a computer controlled electromechanical impactor. In its initial version, the device utilized proportional feedback control of any one or combination of displacement, force, velocity, impulse-momentum (force integrated over time), power, or energy (Noyes, 1987a). In order to simplify the operation of the device, a physical stop was eventually incorporated into the device to control the depth of the contusion injury (Stokes et al., 1992). This reduced the variation of the peak displacement from 0.11 to 0.01 mm (Stokes et al., 1992). Three distinct levels of graded contusion injury can be produced with displacements of 0.8mm, 0.95mm, and 1.1mm with resultant forces of $2.6 \pm 0.08\text{N}$ (SD), $2.9 \pm 0.2\text{N}$ (SD) and $3.0 \pm 0.2\text{N}$ (SD) respectively (Behrmann et al., 1992). The device can achieve a peak impact velocity of 300mm/s though impact speeds have been rarely reported.

As with the weight-drop method, uncontrolled deflection of the underlying vertebral column introduces variability (Somerson, 1986). The deflection during a 1.53mm injury has been estimated at 10-20% (Stokes et al., 1992). In addition, the determination of the initial position based on a 0.03N contact force is also a source of variability. The spinal cord, cerebrospinal fluid and meninges form a viscoelastic structure. Consequently, the preload is sensitive to the rate of load application and the force magnitude decays over time due to fluid movement. These two factors may contribute to the disparity of impact forces reported in the literature. For example, a

1.0mm injury at the ninth or tenth thoracic level in Sprague-Dawley rats has been reported to result in peak forces of ~2.4N (Bresnahan et al., 1991), ~3.0N (Behrmann et al., 1992), ~4.0N (Kloos et al., 2005). In order to reduce the variability of the impact force, a window of ± 1.3 standard deviations of the mean force in each group has been suggested though this criteria can result in an exclusion rate of approximately 30% (Kloos et al., 2005).

Another displacement controlled model used pneumatic pistons to apply injuries at speeds up to 6m/s (Anderson, 1982; Kearney et al., 1988). In this model, the velocity was pre-calibrated and assumed constant while the magnitude of compression was controlled by a physical stop. The model has been able to produce injuries at velocities not possible with other devices although the lack of a force sensor was a limitation.

1.4.4.3 *Controlled Force*

More recently, a new device, has been developed that uses force feedback to control the severity of the contusion injury (Scheff et al., 2003). As with other contusion models, the injuries are produced through a laminectomy with the spinous processes of the rostral and caudal vertebrae clamped and stabilized to a frame. The actuator is a servo controlled rack and pinion system with a step resolution of 1/1200th inch. This mechanical drive system results in a slightly slower peak velocity of 13cm/s. Starting from 3 to 4mm above the spinal cord, the actuator is advanced in steps (smoothly) until the desired peak force is measured. The microcontroller then retracts the impactor.

Graded injuries have also been established for this device. In an initial series reported by Scheff et al., Sprague-Dawley rats were injured at 1.0, 1.5 and 2.0N with a variation of approximately ± 0.1 N. The resultant displacements were approximately 0.8, 1.0 and 1.2 mm respectively.

A potential advantage of force control over displacement control may be the ability to compensate for vertebral column movement. If the vertebral body were to deflect away from the impactor, the device would continue to increase the displacement until the desired impact force was achieved.

1.4.4.4 *Residual Compression*

The spinal cord clip compression model was pioneered by Rivlin and Tator and aimed to mimic the residual compression that is present in many human SCI cases (Rivlin and Tator, 1978; Fehlings and Tator, 1995). The method uses a calibrated aneurysm clip to apply a constant force to the spinal cord usually for 1 minute. The closing force of the clip is customarily reported in grams with 18g (0.18N), 30g (0.29N), and 50g (0.49N) producing mild, moderate, and severe injuries (Fehlings and Tator, 1995). Other residual compression models have used pistons (Carlson et al., 2003a), cables (Delamarter et al., 1995), and spacers (Dimar et al., 1999). The main limitation with this type of injury is the lack of velocity control that is known to influence injury (Anderson, 1985; Kearney et al., 1988). In addition, the lack of displacement data precludes immediate feedback as to the similarity of the lesions. In both the displacement and force controlled models, the response to force or displacement is used to prospectively eliminate outliers from injury groups (Stokes et al., 1992; Jakeman et al., 2000; Ghasemlou et al., 2005; Kloos et al., 2005).

1.4.4.5 *Transection*

Complete transection of the spinal cord is rarely observed clinically where motor vehicle accidents, falls, and sport injuries are the most common causes of SCI (Sekhon and Fehlings, 2001). Transection may occur in gunshot wounds or stabbings. In spite of this, transection and partial transection models have an important advantage particularly in assessing regeneration strategies (Bregman et al., 1997; Kwon et al., 2002a; Lu et al., 2004). By transecting all fibers in a specific tract, this type of model removes the ambiguity of whether axons crossing the lesion site are true regenerating fibers or collaterals branching from spared tracts. The main limitation with transection is that the local environment of the lesion is likely different from the clinical scenario. It is usually necessary to transect the dura in order to reduce the risk of spared fibers. In addition, the degree of vascular damage and resultant ischemia is likely more localized than that observed during blunt trauma with residual bony impingement on the cord.

1.4.4.6 *Cervical Injury Models*

Cervical contusion injury models have only recently been developed (Pearse et al., 2005; Baussart et al., 2006; Gensel et al., 2006). The morbidity and mortality in cervical contusion injuries is more severe than in the thoracic region (Pearse et al., 2005). The mortality rate of experimental rat cervical contusions has been reported at ~12% compared to ~1% for thoracic

injury models. Moreover, forelimb deficits increase the demands of post-operative care where hand feeding may be necessary (Pearse et al., 2005).

There are several advantages to cervical SCI models. The gray matter in the cervical region plays an essential role in forelimb function in contrast to the neuronal somata in the lower thoracic region. Consequently, cervical injuries are a more sensitive model for detecting functional improvements from therapies that enhance gray matter sparing. Improvements from gray matter sparing are difficult to detect in the thoracic region and hence treatment in this region has been focused on preserving subpial white matter. In addition, descending axons injured in the cervical region are closer to their cell bodies thereby increasing their regenerative capacity.

1.4.4.7 Vertebral Fracture-Dislocation

Although vertebral fracture-dislocation is one of the most common causes of SCI in humans, no standardized model has been reported in the literature. A review by Bunegin et al. in 1987 discussed the development, at the University of Pittsburgh, of fracture-dislocation models in cats and rats produced by lateral displacement of lumbar vertebrae (Bunegin et al., 1987). The Pittsburgh model was not found in the general literature. The first thoracolumbar dislocation model was reported in 2004 (Fiford et al., 2004). In this rat model, T12 was held stationary, T13 was unconstrained, and L1 was displaced laterally. Injury severities ranged from 3.2mm of displacement produced at a speed of 5.7cm/s, to 7.5mm of displacement produced at 12.7cm/s. Displacements of 7.5mm ruptured the spinal cord. At lower severities, the model reported diffuse hemorrhage in regions of the cord thought to be under tensile strain.

1.4.4.8 Vertebral Distraction

Many human spinal injuries involve distractive forces between vertebral segments (Breig, 1970; Yamada et al., 2004) but there have been few attempts to model this dynamic component experimentally. Early models applied quasi static and dynamic (~100cm/s) tensile loads to the head of primates while the torso or pelvis was restrained (Cusick et al., 1982; Myklebust et al., 1988). Distractive forces on the order of 445N (100lbs) resulted in a 50% reduction of evoked potentials indicating white matter conduction deficits. Vertebral column disruption usually occurred at approximately 2668N (600lbs) of traction with corresponding cervical displacements of 1.5 to 2cm. Measurement of blood flow indicated the initial loss of evoked potentials was due to mechanical compromise of the white matter rather than ischemia.

In a cat model of vertebral distraction injury, cellular injury was not evident until 24 hours post-trauma even in animals where evoked potentials were diminished by 50 to 95% (Myklebust et al., 1988). In addition, central hemorrhage in the gray matter was only observed at 3-4 hours post-injury and only in animals where distraction reduced evoked potentials by 95%.

Radio-opaque markers have been injected into the cat spinal cord to estimate the extent of coupling between the vertebral column and the spinal cord during cervical distraction (Maiman et al., 1989). The coupling between the spinal cord and cervical vertebrae differed between levels but the average coupling ranged from 0.52 at 5 kg, 0.78 at 10 kg, and 0.52 at 15 kg (Maiman et al., 1989). At low levels of distraction, inherent slack in the spinal cord reduced the extent of coupling while at high levels of distraction, the reduction in coupling was attributed to cord stiffening. The physical mechanism of load transfer between the vertebrae and spinal cord has not been established. Sectioning of the denticulate ligaments appears to increase the strain in the tethered spinal cord by ~2% suggesting intact ligaments partially support tensile loads (Tani et al., 1987). Computer-controlled models of thoracic vertebral distraction in rats have also been developed that use Harrington rods and laminar hooks to dynamically displace the vertebrae at speeds up to 0.9cm/s (Dabney et al., 2004). Mild, moderate, and severe injury severities were reported at 3, 5, and 7mm of distraction respectively. Comparisons between distraction models are difficult due to the sparsity of reports and differences in the animal species (i.e. monkey, cat, rat).

1.4.4.9 Comparison of Models

Each of the injury models has strengths and limitations. An important feature of both the controlled displacement and controlled force models is the measurement of the complementary biomechanical response variable (resultant force or resultant displacement) thereby providing an *a priori* method to exclude outliers. In displacement controlled injuries, an exclusion criteria has been proposed that eliminates animals from the study when the impact force lies outside ± 1.3 standard deviations of the group mean (Kloos et al., 2005). In force controlled contusion injuries, a similar criteria based on the resultant displacement has been proposed (Ghasemlou et al., 2005). Variability in the injuries will arise due to biological differences, as well as variability introduced by the experimentalist such as the consistency of surgical preparation.

Stabilization of the vertebral column in order to minimize movement during impact is an unresolved issue in all the current contusion injury models described above. Only the weight-drop

device explicitly measures the deflection of the vertebral column (Young, 2002). In addition, the injury velocities differ widely between models. The difficulty in establishing a consistent contact position is a drawback of the displacement controlled model.

Regardless of which mechanical parameter is controlled in a particular model, it is perhaps more important to recognize the model's limitations (Blight, 1988) and the scope of human injuries that the model represents. A repeatable model improves its statistical power to detect treatment effects. There is an inevitable tradeoff, however, as the model's consistency limits its ability to demonstrate the robustness of a treatment. The robustness of an SCI therapy can only be assessed by considering other injury paradigms that mimic the broad spectrum of human SCI.

1.4.5 Summary of Biomechanics

The spinal cord is a complex structure consisting of vascular and cellular components each of which can be damaged by primary mechanical injury. The gross mechanical behaviour of neural tissue requires further characterization and the sophistication of computational models continues to evolve from the gross tissue level to the microstructural scale. Animal models of SCI have predominately focused on biomechanically controlled contusion and compression injury paradigms. These are useful models, but they only mimic a narrow portion of spectrum of biomechanical injuries that occur in the human population.

1.5 Neurobiology of Spinal Cord Injury

The pathophysiology of SCI involves numerous, interdependent biochemical processes that evolve over time. Many factors continue to be identified that contribute to tissue degeneration following SCI or that regulate axonal regeneration. No single variable appears to dominate over any other factor and hence research efforts proceed in parallel. In cats, it has been reported that sparing of as little as 10% of the axons might be sufficient to enable locomotion (Blight, 1983). Thus, small therapeutic effects might some day be compounded to restore function. The primary mechanical injury is yet another variable—among many—that this thesis will examine to understand its interaction with other pathomechanisms which are outlined in this section.

1.5.1 Secondary Injury & Neuroprotection

The primary mechanical injuries, discussed in the previous sections, immediately trigger a cascade of secondary degenerative processes. Neuroprotective strategies aim to mitigate this

secondary injury and thereby spare sufficient neural tissue to enable function or minimize the extent of tissue damage that must be repaired or regenerated to restore function.

1.5.1.1 Hemorrhage & Ischemia

Intramedullary hemorrhage following SCI occurs following rupture of the capillary network within the spinal cord. Following experimental spinal cord contusion, hemorrhage of the dorsal vasculature is immediately visible through the laminectomy. The extravasation of blood results in immediate, irreversible necrosis of the neurons and glia in the vicinity of the hemorrhage. Hemorrhage volumes have been reported to remain constant over the initial hours following injury suggesting the majority of hemorrhage occurs near the time of primary injury (Rawe et al., 1978; Khan et al., 1985). The stability of hemorrhage volumes may stem from the reduction in spinal cord blood flow that results from the release of vasoconstrictive agents such as prostaglandin and thromboxane (Demediuk et al., 1985; Hall and Springer, 2004).

The depression in spinal cord blood flow subjects the cord parenchyma to ischemia that exacerbates necrosis (Balentine, 1978). Inducing systemic hypertension in order to improve blood flow has been shown experimentally to increase hemorrhage and edema rather than reduce ischemic injury (Guha et al., 1989). Moreover, once ischemia has occurred, reperfusion is accompanied by the generation of reactive oxygen species that further perpetuate secondary damage (Stys, 1998; Dumont et al., 2001).

Methylprednisolone sodium succinate has been shown to improve spinal cord blood flow and reduce ischemic damage following weight-drop contusion injuries that were produced in cats (Hall et al., 1984). The effects were most beneficial with early (30 minutes) intravenous injection. The effects were reduced if treatment was delayed until 1.5 hours post-trauma and completely lost if treatment was delayed until 4.5 hours after injury (Hall et al., 1984). In contrast, another study examined the effect of methylprednisolone in a dog model of SCI with residual compression on the spinal cord and found reduced reperfusion following decompression in animals treated with methylprednisolone (Carlson et al., 2003b). The differences may suggest a differential time-course of neuropathology in the cord under sustained compression.

1.5.1.2 Inflammation

Spinal cord trauma activates microglia (resident inflammatory cells of the CNS) and allows the infiltration of blood borne leukocytes across the compromised blood-spinal cord barrier.

Activated microglia and blood borne monocytes transform into phagocytic macrophages that, along with neutrophils, clear cellular debris from the lesion. In the process of phagocytosis, enzymes and free radicals are generated that can result in bystander damage of healthy tissue thereby expanding the SCI lesion (Schnell et al., 1999).

Anti-inflammatory treatments have long been shown to reduce bystander injury and improve post-traumatic function in animals (Popovich et al., 1999; Gris et al., 2004; Stirling et al., 2004; Teng et al., 2004). The inflammatory response varies over time. Neutrophils infiltrate into the tissue early after trauma and their numbers appear to peak by 24 hours (Carlson et al., 1998). Monocytes that differentiate into macrophages are visible by 24 hours and they continue to be recruited where their numbers peak between 7 and 10 days post-trauma (Schwartz and Yoles, 2006). Schwartz has argued that the inflammatory response should not be abolished but rather controlled and it has been shown that enhancing the T cell response against myelin basic protein improves functional recovery in animals (Hauben et al., 2000; Schwartz, 2003), though this strategy remains controversial (Popovich and Jones, 2003).

The role of microglia has often been amalgamated with that of blood derived macrophages since fully activated microglia are morphologically and immunohistochemically indistinguishable from blood derived macrophages (Matsumoto et al., 2007). Under non-pathologic conditions, resting microglia actively extend and retract their ramified processes presumably to maintain surveillance of the cord parenchyma (Davalos et al., 2005). In addition, microglia provide neurotrophic support to neurons. Microglial activation has been associated with numerous neurodegenerative diseases such as Alzheimer's, Parkinson's, and multiple sclerosis (Block and Hong, 2005) though whether microglia contribute to causing these pathologies remains uncertain (Teismann and Schulz, 2004). Recent studies show microglia are activated by adenosine triphosphate (ATP) that may be released from necrotic cells following trauma (Davalos et al., 2005; Haynes et al., 2006; Xiang et al., 2006). A greater understanding of microglial regulation may assist in attenuating the earliest phases of post-traumatic secondary degeneration.

1.5.1.3 Oxidative Stress

Ischemic and inflammatory process both precipitate the generation of reactive oxygen and nitrogen species which contribute to secondary damage of cellular proteins and lipids (Dugan and Kim-Han, 2006). During hypoxia, mitochondrial respiration is interrupted resulting in an

increased generation of free radicals (Abramov et al., 2007). In addition, intracellular calcium accumulation opens the mitochondrial permeability transition pore (mPTP) that uncouples the electron transport chain, increases mitochondrial swelling and enables the release of pro-apoptotic proteins as well as the free radicals that are normally sequestered within the inner mitochondrial membrane. Upon reperfusion, a more significant increase in reactive oxygen species occurs although the precise localization remains unclear (Abramov et al., 2007). Superoxide dismutase, glutathione, catalase, ascorbic acid, and vitamin E scavenge the reactive oxygen species that normally leak from mitochondria, but these endogenous anti-oxidants are overcome following trauma (Sugawara et al., 2004).

Peroxynitrite (ONOO⁻) is currently thought to be one of the central players in post-traumatic oxidative stress (Deng et al., 2007; Xiong et al., 2007). Nitric oxide synthase generates nitric oxide (NO[•]) which can combine with superoxide (O₂^{-•}) to form peroxynitrite (Dugan and Kim-Han, 2006). Peroxynitrite can further react to form the hydroxyl radical (•OH), nitrogen dioxide (NO₂[•]), and carbonate radical (CO₃^{-•}) which contribute to lipid peroxidation and the reaction with tyrosine residues on proteins to produce nitrotyrosine—a marker of oxidative stress which is used later in this thesis.

The neuroprotective effects of methylprednisolone is believed to stem from its potent anti-oxidant actions in addition to its anti-inflammatory properties (Hsu and Dimitrijevic, 1990; Mu et al., 2000). Therapeutic strategies to counter lipid peroxidation include free radical scavengers such as the 21-aminosteroid U-74006F (Behrmann et al., 1994) and cyclosporin-A (Diaz-Ruiz et al., 1999). Other evidence suggests direct repair of damaged membranes with polyethylene glycol reduces the production of reactive oxygen species (Luo et al., 2002).

1.5.1.4 Calcium & Excitotoxicity

Excessive stimulation of neurons by excitatory neurotransmitters can result in excitotoxic cell death (Choi et al., 1987). Following neurotrauma, lysed cells release neurotransmitters such as glutamate which stimulate N-methyl-D-aspartate (NMDA), α -amino-3-hydroxy-5-methyl-4-isoxazolepropionic acid (AMPA) and kainate receptors on neighbouring neurons and glia. Over-activation of glutamate receptors results in the influx of sodium and calcium ions leading the cellular edema and the initiation of degeneration (Kapoor et al., 2003). In the spinal cord, NMDA

channels appear predominantly localized to neurons while AMPA and kainate channels are predominantly localized to the glia (Mattson, 2003; Park et al., 2004).

The extracellular concentration of calcium ions is on the order of 1mM while the intracellular concentration is on the order of 1 μ m (Young et al., 1982). This steep gradient renders calcium influx a sensitive signalling mechanism. Following SCI, extracellular calcium levels fall precipitously due to the rapid influx of calcium ions into the intracellular space (Young et al., 1982). Excessive calcium influx overloads local calcium buffering mechanisms such as calbindin. The resultant intracellular calcium overload triggers cysteine proteases (calpain) that degrade cytoskeletal proteins such as neurofilaments (Iwasaki et al., 1987; Stys and Jiang, 2002). In addition, calcium triggers mitochondrial oxidative stress that initiates the release of pro-apoptotic factors such as cytochrome *c* and apoptosis inducing factor. Calcium influx following shearing trauma can be attenuated by blocking NMDA channels (LaPlaca and Thibault, 1998)

Due to its deleterious effects in activating proteases, enhancing oxidative stress, and triggering apoptosis, calcium influx was once regarded as possibly the final common pathway to neural degeneration. This paradigm was later revised by the source specificity hypothesis that argued excitotoxicity occurred following influx through specific pathways (e.g. NMDA channels) where intracellular microdomains possessed the correct machinery to execute the degenerative functions (Tymianski et al., 1993; Sattler et al., 1998). More recently, this concept has been further refined as new work indicates differences between subgroups of NMDA channels. Stimulation of NMDA channels with NR2A subunits activates pro-survival signals whereas activation of channels with NR2B subunits generates cell death signals (Deridder et al., 2005; Liu et al., 2007). As the excitotoxic mechanisms continue to be refined, the role of mechanically induced pores in the gray and white matter remains unclear because the proximity of these pores to beneficial or harmful microdomains has not been established. Moreover, although membrane resealing may result in only transient pathways for calcium entry, this may be sufficient to initiate downstream deleterious events (Shi et al., 1989).

1.5.1.5 Apoptosis

Apoptosis is an actively controlled form of cell death characterized by DNA fragmentation, nuclear condensation, cell shrinkage, and gradual degeneration that does not elicit an inflammatory response (Lu et al., 2000). Neuronal apoptosis has been observed to peak at 8 hours following SCI

(Liu et al., 1997). The predominant apoptotic cell population, however, appears to be oligodendrocytes that undergo apoptosis during a second wave of cell death which peaks at 7 to 8 days post-trauma (Liu et al., 1997; Shuman et al., 1997). The protracted time-course of apoptosis may provide a broader time-window for therapeutic interventions.

Apoptosis can be initiated by both an extrinsic and an intrinsic molecular pathway (Harwood et al., 2005). In the extrinsic pathway, a death receptor such as CD95 (also called FAS) on the cell membrane is activated and triggers the formation of activated caspase-3 which in turn activates endonuclease enzymes that fragment DNA. Apoptosis can also be initiated via intrinsic pathways that involve the mitochondria (Wu et al., 2007). Mitochondria under oxidative stress can release cytochrome *c* and apoptotic protease activating factor into the cytoplasm which activates the caspase-3 apoptotic pathway (Springer et al., 1999). Alternatively, in a caspase-independent pathway, mitochondria can release apoptosis inducing factor that translocates to the cell nucleus to activate nucleases (Arundine et al., 2004).

In a model of mild (15g) clip compression SCI, which did not induce cavitation or extensive hemorrhage, ventral motoneurons were found to undergo apoptosis following the release of cytochrome *c* from mitochondria (Sugawara et al., 2002). Caspase-3 mediated apoptosis has been detected following moderate *in vitro* stretch injury but was absent in mild or severe injury (Pike et al., 2000). Mild, sub-lethal *in vitro* stretch injuries that do not activate caspase-3 may still exhibit enhanced sensitivity to secondary excitotoxic injury (Arundine et al., 2004). Hence, at one end of the injury spectrum severe mechanical trauma causes immediate necrosis but there is a broad intermediate range of sub-lethal mechanical injuries whose optimal treatment remains to be fully understood.

1.5.2 Repair & Regeneration

Repair and regeneration of the chronic spinal cord lesion is the most intensely studied field of experimental SCI. In the event of severe primary injury, or failure of neuroprotective efforts, axonal regeneration and repair of dysfunctional fibers may be the only route to functional recovery. The chronic spinal cord lesion is distant in time from the mechanical injury and early neuropathology addressed in this thesis, however, the prevalence of primary axotomy and the rostro-caudal extent of secondary damage analysed in this thesis will strongly influence the feasibility of successful axonal repair and regeneration. A short overview is presented here.

1.5.2.1 The Inhibitory Environment

The inability of neurons in the central nervous system (CNS) to regenerate their transected axons was widely accepted since the time of Cajal's pioneering observations of abortive axonal regeneration over a century ago (Hagg and Oudega, 2006). Axons in the peripheral nervous system, however, were known to regenerate following injury. This dichotomy was resolved in the early 1980's by the demonstration that spinal cord axons could regenerate (~3cm) into peripheral nerve grafts (David and Aguayo, 1981). The seminal result demonstrated the capacity of CNS neurons to regenerate but also showed the environment was a principal cause of failed regeneration.

Since David and Aguayo's report, the CNS environment has been found to contain myelin associated inhibitory proteins (Caroni and Schwab, 1988; Schnell and Schwab, 1990), such as Nogo (Chen et al., 2000; GrandPre et al., 2000; Prinjha et al., 2000), myelin associated glycoprotein (McKerracher et al., 1994; Mukhopadhyay et al., 1994), and oligodendrocyte-myelin glycoprotein (Kottis et al., 2002; Wang et al., 2002). The characteristics of these inhibitory molecules have been widely studied including the identification of their receptor Nogo-66 and co-receptors (p75 neurotrophin receptor, LINGO, TROY/TAJ). Neutralization of these inhibitory proteins has been shown to improve axonal regeneration (Freund et al., 2006).

Instead of neutralizing the inhibitory proteins, the intrinsic growth capacity of the neuron could be augmented to overcome the inhibitory response. In the dorsal root ganglion, which has one axonal process extending into the growth permissive peripheral nervous system and a second branch extending into the inhibitory environment of the CNS, transection of the peripheral branch was shown to amplify the regenerative response into peripheral nerve grafts (Richardson and Issa, 1984). Interestingly, it would not be until 15 years later, using a similar model, that a preconditioning lesion of the peripheral nerve branch would be shown to enhance regeneration of the central branch directly into the non-permissive environment of the CNS (Neumann and Woolf, 1999). An increase in cyclic adenosine monophosphate was found to be an important factor in the neurons ability to overcome environmental inhibition and has since become a focus in regeneration research (Cai et al., 1999; Neumann et al., 2002; Lu et al., 2004; Pearse et al., 2004). The results of regeneration in dorsal root ganglia, however, have been tempered by the relatively poorer regenerative capacity of other key systems such as the corticospinal tract (Ye and Houle, 1997).

An additional environmental barrier to regeneration, particularly in the chronic lesion, is the glial scar. Reactive astrocytes are thought to aid in the containment of the SCI during the acute phase of injury. Indeed, ablation of astrocytes following SCI exacerbates injury suggesting a neuroprotective role for reactive astroglia (Faulkner et al., 2004). However, astrocytes also lay down chondroitin sulphate proteoglycans (CSPGs) that inhibit regenerating neurites. CSPGs constitute a broad family of proteins (e.g. neurocan, versican, NG2, and brevican among others) but they share in common glycosaminoglycan (GAG) chains which are inhibitory. ChondroitinaseABC is an enzyme that digests GAG chains on the CSPGs and appears to promote axonal growth (Bradbury et al., 2002).

1.5.2.2 Growth Factors

Neurons require growth factors to survive and these factors can also be used to enhance their regenerative capacity. Traditionally, neurotrophins were thought to be transported from target innervations, retrogradely to the cell body and hence served as a feedback mechanism to connect neurons to their appropriate targets. Other sources of neurotrophins were discovered such as from afferent inputs and from myelinating glia. Nerve growth factor (NGF) was the original neurotrophin discovered and it binds to the tyrosine kinase receptor TrkA. Other members of the family include brain derived neurotrophic factor (BDNF) that binds to TrkB, neurotrophin-3 (NT-3) that binds to TrkC, as well as NT-4 and NT-5 which also bind to TrkB. The different receptors are expressed in distinct neuronal populations and hence impart specificity in their responses and highlight the heterogeneity of neuronal populations. Following spinal cord injury, axotomy can result in the loss of trophic support which leads to atrophy of the neuronal somata and possibly cell death. Treatment with neurotrophins can revive atrophied neurons (Kwon et al., 2002b) and enhance the regenerative response (Bregman et al., 1997).

1.5.2.3 Axonal Repair

Given the immense challenges that accompany stimulating axonal regeneration, overcoming inhibition in the environment, and guiding axons to their appropriate targets, the repair of spared axonal fibers might be a more feasible therapeutic strategy. Axons that survive the initial primary mechanical trauma and that remain intact following the ensuing secondary degenerative cascade can be dysfunctional. Months following SCI, the myelin sheath of many surviving axons are thinned (dysmyelinated) or completely absent (demyelinated) rendering axonal conduction

dysfunctional (Blight, 1983; Nashmi and Fehlings, 2001). In addition, conduction deficits can also stem from abnormalities in the ionic channels that control the generation of action potentials (Waxman and Wood, 1984; Nashmi et al., 2000).

Potassium channels normally reside in the juxtaparanodal region adjacent to the node of Ranvier where they are covered by myelin (Rasband and Trimmer, 2001). The disruption of the myelin structure exposes potassium channels which is thought to abnormally increase their conductivity and results in conduction deficits that can be ameliorated by pharmacological blockade of these channels by 4-aminopyridine (Shi et al., 1997). Interestingly, 4-aminopyridine appears to be more effective in restoring conduction deficits following stretch injuries compared to compressive injuries (Jensen and Shi, 2003) suggesting an interaction between the biomechanics of trauma and the ensuing pathology. This therapy is currently under clinical investigation (Tator, 2006).

Other repair strategies have included the transplantation of cellular constructs to serve as both a scaffold for regenerating axons and to promote remyelination. Among these are Schwann cells from the peripheral nervous system (Pearse et al., 2004; Oudega and Xu, 2006) and olfactory ensheathing cells (Ruitenbergh et al., 2006; Sasaki et al., 2006). Current repair strategies have an increasing focus on stem cells which have the potential to differentiate into neurons, astrocytes, and oligodendrocytes (McDonald et al., 1999; Liu et al., 2000; Cao et al., 2005; Cirasuolo et al., 2005; Horvath et al., 2006; Eftekharpour et al., 2007). Stem cells preferentially differentiate towards glial cell lines and hence, their effectiveness may be strongly predicated on the survival of neurons from both primary and secondary injuries.

1.5.3 Summary of Neurobiology

Primary mechanical trauma initiates secondary degenerative events that are interrelated and over time appear inseparable. Neuroprotective strategies that limit inflammation and oxidative stress have shown some success in both experimental and clinical studies. Whether the primary injury mechanism alters the characteristics of secondary spinal cord pathology has not been studied. In addition, although robust regeneration has been demonstrated in dorsal root ganglia, the regenerative capacity of supraspinal axons appears more limited and thus, the rostro-caudal length of the SCI lesion and the characteristics of the chronic scar may be critical factors in the success of regenerative therapies.

1.6 Thesis Objectives and Hypotheses

The objective of this thesis was to examine the effect of clinically relevant biomechanical injury mechanisms on the pathology of spinal cord injury (SCI). It was hypothesized that different injury mechanisms would produce different patterns (i.e. spatial distributions) of primary damage within the spinal cord. In addition, since primary injury initiates secondary pathomechanisms, the early neuropathology following different injury mechanisms would also differ.

At the onset of this thesis, distinct injury mechanisms had not been previously compared, and the instrumentation necessary to directly address this clinically relevant question was not in existence. Hence, the specific aims of this thesis were:

1. To develop a new SCI test system capable of modelling different clinically relevant injury mechanisms;
2. To concurrently develop three animal models to enable comparisons between contusion, dislocation, and distraction SCI mechanisms;
3. To characterize the spatial distribution of primary mechanical damage within the spinal cord following contusion, dislocation, and distraction injuries;
4. To broadly characterize the early secondary neuropathology following contusion, dislocation, and distraction injuries.

In the broader perspective, it is hoped that this work might contribute to the development of future clinical treatment paradigms by characterizing the specific structures damaged during primary injury, and highlighting differences in treatment priorities for secondary injury during the early time-window before degeneration converges upon an irreversible destruction of neural tissue.

1.6.1 Scope

This thesis focused on the very early period following traumatic SCI (Figure 1.16) in rat animal models, in order to clearly isolate the effects of the biomechanical injury mechanism from the confounding secondary biochemical effects that will occur during a protracted survival time-course. The spatial distribution of primary mechanical injury within the spinal cord was analysed at 5 minutes post-trauma before any substantial secondary damage could occur. In order to examine any causative relationship between primary and secondary injury, tissue was analysed immunohistochemically at 3 hours post-trauma for a spectrum of the main secondary deleterious phenomena such as oxidative stress and the activation of inflammatory cells. Comparison of

neuroprotective pharmacotherapies, axonal repair and regeneration strategies, and behavioural deficits were outside the scope of this thesis. In this way, this thesis established a framework of the initial conditions of primary mechanical damage and the initiation of secondary degeneration following distinct clinically relevant mechanisms of SCI.

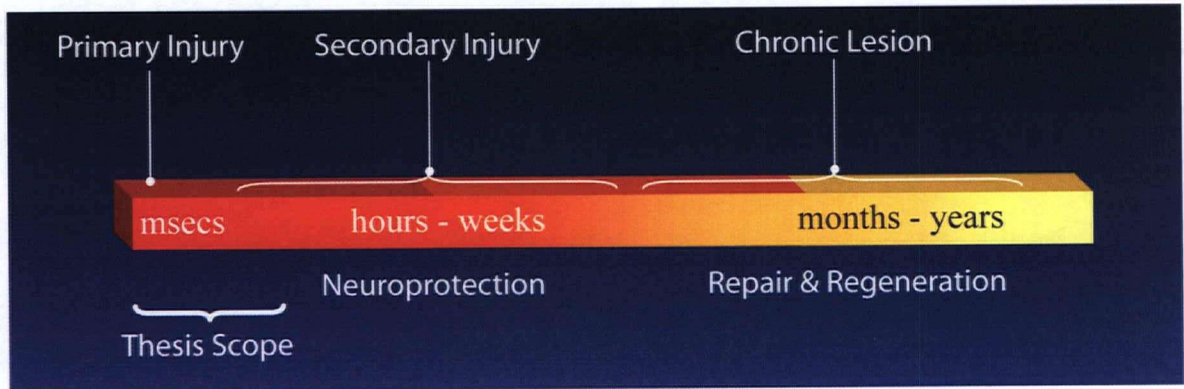


Figure 1.16: Thesis scope

This thesis explicitly varied the biomechanical mechanism of injury in three novel rat animal models of SCI. The thesis examined the characteristics of the initial primary injury and explored how primary injury related to the early cascade of secondary injury. Animal behavioural function, pharmacotherapies for neuroprotection, axonal repair and regeneration were not investigated.

1.7 References

- Abramov AY, Scorziello A, Duchen MR (2007) Three distinct mechanisms generate oxygen free radicals in neurons and contribute to cell death during anoxia and reoxygenation. *J Neurosci* 27:1129-1138.
- Agus H, Kayali C, Arslantas M (2004) Nonoperative treatment of burst-type thoracolumbar vertebra fractures: clinical and radiological results of 29 patients. *Eur Spine J*.
- Allen AR (1911) Surgery of experimental lesion of spinal cord equivalent to crush injury of fracture dislocation of spinal column: A preliminary report. *JAMA* 57:878-880.
- Allen AR (1914) Remarks on the histopathological changes in the spinal cord due to impact. An experimental study. *The Journal of Nervous and Mental Disease* 41:141-147.
- Allen BL, Jr., Ferguson RL, Lehmann TR, O'Brien RP (1982) A mechanistic classification of closed, indirect fractures and dislocations of the lower cervical spine. *Spine* 7:1-27.
- Anderson TE (1982) A controlled pneumatic technique for experimental spinal cord contusion. *J Neurosci Methods* 6:327-333.
- Anderson TE (1985) Spinal cord contusion injury: experimental dissociation of hemorrhagic necrosis and subacute loss of axonal conduction. *J Neurosurg* 62:115-119.
- Arbogast KB, Margulies SS (1998) Material characterization of the brainstem from oscillatory shear tests. *J Biomech* 31:801-807.
- Arbogast KB, Margulies SS (1999) A fiber-reinforced composite model of the viscoelastic behavior of the brainstem in shear. *J Biomech* 32:865-870.
- Arundine M, Aarts M, Lau A, Tymianski M (2004) Vulnerability of central neurons to secondary insults after in vitro mechanical stretch. *J Neurosci* 24:8106-8123.
- Bain AC, Meaney DF (2000) Tissue-level thresholds for axonal damage in an experimental model of central nervous system white matter injury. *J Biomech Eng* 122:615-622.
- Balentine JD (1978) Pathology of experimental spinal cord trauma. I. The necrotic lesion as a function of vascular injury. *Lab Invest* 39:236-253.
- Banks WA, Kastin AJ, Arimura A (1998) Effect of spinal cord injury on the permeability of the blood-brain and blood-spinal cord barriers to the neurotrophin PACAP. *Exp Neurol* 151:116-123.
- Baptiste DC, Fehlings MG (2006) Pharmacological approaches to repair the injured spinal cord. *J Neurotrauma* 23:318-334.
- Basso DM, Beattie MS, Bresnahan JC (1995) A sensitive and reliable locomotor rating scale for open field testing in rats. *J Neurotrauma* 12:1-21.
- Baussart B, Stamegna JC, Polentes J, Tadie M, Gauthier P (2006) A new model of upper cervical spinal contusion inducing a persistent unilateral diaphragmatic deficit in the adult rat. *Neurobiol Dis*.
- Beattie MS, Bresnahan JC, Komon J, Tovar CA, Van Meter M, Anderson DK, Faden AI, Hsu CY, Noble LJ, Salzman S, Young W (1997) Endogenous repair after spinal cord contusion injuries in the rat. *Exp Neurol* 148:453-463.
- Behrmann DL, Bresnahan JC, Beattie MS (1994) Modeling of acute spinal cord injury in the rat: neuroprotection and enhanced recovery with methylprednisolone, U-74006F and YM-14673. *Exp Neurol* 126:61-75.
- Behrmann DL, Bresnahan JC, Beattie MS, Shah BR (1992) Spinal cord injury produced by consistent mechanical displacement of the cord in rats: behavioral and histologic analysis. *J Neurotrauma* 9:197-217.

- Bensch FV, Koivikko MP, Kiuru MJ, Koskinen SK (2006) The incidence and distribution of burst fractures. *Emerg Radiol* 12:124-129.
- Bilston LE, Thibault LE (1996) The mechanical properties of the human cervical spinal cord in vitro. *Ann Biomed Eng* 24:67-74.
- Blight A (1988) Mechanical factors in experimental spinal cord injury. *J Am Paraplegia Soc* 11:26-34.
- Blight AR (1983) Cellular morphology of chronic spinal cord injury in the cat: analysis of myelinated axons by line-sampling. *Neuroscience* 10:521-543.
- Blight AR, Decrescito V (1986) Morphometric analysis of experimental spinal cord injury in the cat: the relation of injury intensity to survival of myelinated axons. *Neuroscience* 19:321-341.
- Block ML, Hong JS (2005) Microglia and inflammation-mediated neurodegeneration: multiple triggers with a common mechanism. *Prog Neurobiol* 76:77-98.
- Boerger TO, Limb D, Dickson RA (2000) Does 'canal clearance' affect neurological outcome after thoracolumbar burst fractures? *J Bone Joint Surg Br* 82:629-635.
- Bohlman HH (1985) Treatment of fractures and dislocations of the thoracic and lumbar spine. *J Bone Joint Surg Am* 67:165-169.
- Bondurant FJ, Cotler HB, Kulkarni MV, McArdle CB, Harris JH, Jr. (1990) Acute spinal cord injury. A study using physical examination and magnetic resonance imaging. *Spine* 15:161-168.
- Borgens RB, Shi R (2000) Immediate recovery from spinal cord injury through molecular repair of nerve membranes with polyethylene glycol. *FASEB J* 14:27-35.
- Bracken MB, Collins WF, Freeman DF, Shepard MJ, Wagner FW, Silten RM, Hellenbrand KG, Ransohoff J, Hunt WE, Perot PL, Jr., et al. (1984) Efficacy of methylprednisolone in acute spinal cord injury. *JAMA* 251:45-52.
- Bracken MB, Shepard MJ, Hellenbrand KG, Collins WF, Leo LS, Freeman DF, Wagner FC, Flamm ES, Eisenberg HM, Goodman JH, et al. (1985) Methylprednisolone and neurological function 1 year after spinal cord injury. Results of the National Acute Spinal Cord Injury Study. *J Neurosurg* 63:704-713.
- Bracken MB, Shepard MJ, Collins WF, Holford TR, Young W, Baskin DS, Eisenberg HM, Flamm E, Leo-Summers L, Maroon J, et al. (1990) A randomized, controlled trial of methylprednisolone or naloxone in the treatment of acute spinal-cord injury. Results of the Second National Acute Spinal Cord Injury Study. *N Engl J Med* 322:1405-1411.
- Bracken MB, Shepard MJ, Collins WF, Jr., Holford TR, Baskin DS, Eisenberg HM, Flamm E, Leo-Summers L, Maroon JC, Marshall LF, et al. (1992) Methylprednisolone or naloxone treatment after acute spinal cord injury: 1-year follow-up data. Results of the second National Acute Spinal Cord Injury Study. *J Neurosurg* 76:23-31.
- Bracken MB, Shepard MJ, Holford TR, Leo-Summers L, Aldrich EF, Fazl M, Fehlings M, Herr DL, Hitchon PW, Marshall LF, Nockels RP, Pascale V, Perot PL, Jr., Piepmeier J, Sonntag VK, Wagner F, Wilberger JE, Winn HR, Young W (1997) Administration of methylprednisolone for 24 or 48 hours or tirilazad mesylate for 48 hours in the treatment of acute spinal cord injury. Results of the Third National Acute Spinal Cord Injury Randomized Controlled Trial. National Acute Spinal Cord Injury Study. *JAMA* 277:1597-1604.
- Bracken MB, Shepard MJ, Holford TR, Leo-Summers L, Aldrich EF, Fazl M, Fehlings MG, Herr DL, Hitchon PW, Marshall LF, Nockels RP, Pascale V, Perot PL, Jr., Piepmeier J, Sonntag

- VK, Wagner F, Wilberger JE, Winn HR, Young W (1998) Methylprednisolone or tirilazad mesylate administration after acute spinal cord injury: 1-year follow up. Results of the third National Acute Spinal Cord Injury randomized controlled trial. *J Neurosurg* 89:699-706.
- Bradbury EJ, Moon LD, Popat RJ, King VR, Bennett GS, Patel PN, Fawcett JW, McMahon SB (2002) Chondroitinase ABC promotes functional recovery after spinal cord injury. *Nature* 416:636-640.
- Braughler JM, Hall ED, Means ED, Waters TR, Anderson DK (1987) Evaluation of an intensive methylprednisolone sodium succinate dosing regimen in experimental spinal cord injury. *J Neurosurg* 67:102-105.
- Bregman BS, McAtee M, Dai HN, Kuhn PL (1997) Neurotrophic factors increase axonal growth after spinal cord injury and transplantation in the adult rat. *Exp Neurol* 148:475-494.
- Breig A (1970) Overstretching of and circumscribed pathological tension in the spinal cord--a basic cause of symptoms in cord disorders. *J Biomech* 3:7-9.
- Bresnahan JC, Beattie MS, Todd FD, 3rd, Noyes DH (1987) A behavioral and anatomical analysis of spinal cord injury produced by a feedback-controlled impaction device. *Exp Neurol* 95:548-570.
- Bresnahan JC, Beattie MS, Stokes BT, Conway KM (1991) Three-dimensional computer-assisted analysis of graded contusion lesions in the spinal cord of the rat. *J Neurotrauma* 8:91-101.
- Brodkey JS, Richards DE, Blasingame JP, Nulsen FE (1972) Reversible spinal cord trauma in cats. Additive effects of direct pressure and ischemia. *J Neurosurg* 37:591-593.
- Bunegin L, Hung TK, Chang GL (1987) Biomechanics of spinal cord injury. *Crit Care Clin* 3:453-470.
- Cai D, Shen Y, De Bellard M, Tang S, Filbin MT (1999) Prior exposure to neurotrophins blocks inhibition of axonal regeneration by MAG and myelin via a cAMP-dependent mechanism. *Neuron* 22:89-101.
- Cao Q, Xu XM, Devries WH, Enzmann GU, Ping P, Tsoulfas P, Wood PM, Bunge MB, Whittemore SR (2005) Functional recovery in traumatic spinal cord injury after transplantation of multilineurotrophin-expressing glial-restricted precursor cells. *J Neurosci* 25:6947-6957.
- Carlson GD, Gorden CD, Oliff HS, Pillai JJ, LaManna JC (2003a) Sustained spinal cord compression: part I: time-dependent effect on long-term pathophysiology. *J Bone Joint Surg Am* 85-A:86-94.
- Carlson GD, Gorden CD, Nakazawa S, Wada E, Smith JS, LaManna JC (2003b) Sustained spinal cord compression: part II: effect of methylprednisolone on regional blood flow and recovery of somatosensory evoked potentials. *J Bone Joint Surg Am* 85-A:95-101.
- Carlson GD, Warden KE, Barbeau JM, Bahniuk E, Kutina-Nelson KL, Biro CL, Bohlman HH, LaManna JC (1997a) Viscoelastic relaxation and regional blood flow response to spinal cord compression and decompression. *Spine* 22:1285-1291.
- Carlson GD, Minato Y, Okada A, Gorden CD, Warden KE, Barbeau JM, Biro CL, Bahniuk E, Bohlman HH, Lamanna JC (1997b) Early time-dependent decompression for spinal cord injury: vascular mechanisms of recovery. *J Neurotrauma* 14:951-962.
- Carlson SL, Parrish ME, Springer JE, Doty K, Dossett L (1998) Acute inflammatory response in spinal cord following impact injury. *Exp Neurol* 151:77-88.
- Caroni P, Schwab ME (1988) Antibody against myelin-associated inhibitor of neurite growth neutralizes nonpermissive substrate properties of CNS white matter. *Neuron* 1:85-96.

- Chang GL, Hung TK, Feng WW (1988) An in-vivo measurement and analysis of viscoelastic properties of the spinal cord of cats. *J Biomech Eng* 110:115-122.
- Chen MS, Huber AB, van der Haar ME, Frank M, Schnell L, Spillmann AA, Christ F, Schwab ME (2000) Nogo-A is a myelin-associated neurite outgrowth inhibitor and an antigen for monoclonal antibody IN-1. *Nature* 403:434-439.
- Cheng S, Bilston LE (2007) Unconfined compression of white matter. *J Biomech* 40:117-124.
- Choi DW, Maulucci-Gedde M, Kriegstein AR (1987) Glutamate neurotoxicity in cortical cell culture. *J Neurosci* 7:357-368.
- Cirasuolo JS, Biernaskie J, Liu J, Choo AM, Mckenzie IA, Miller FD, Tetzlaff W (2005) Skin-Derived Precursors Integrate, Promote Axonal Regeneration, And Produce Myelin After Transplantation Into Rat Spinal Cord Contusion Injuries. In: 35th Annual Meeting of the Society for Neuroscience. Washington, D.C.
- Croul SE, Flanders AE (1997) Neuropathology of human spinal cord injury. *Adv Neurol* 72:317-323.
- Cullen DK, LaPlaca MC (2006) Neuronal response to high rate shear deformation depends on heterogeneity of the local strain field. *J Neurotrauma* 23:1304-1319.
- Cusick JF, Myklebust J, Zyvoloski M, Sances A, Jr., Houterman C, Larson SJ (1982) Effects of vertebral column distraction in the monkey. *J Neurosurg* 57:651-659.
- Dabney KW, Ehrenshteyn M, Agresta CA, Twiss JL, Stern G, Tice L, Salzman SK (2004) A model of experimental spinal cord trauma based on computer-controlled intervertebral distraction: characterization of graded injury. *Spine* 29:2357-2364.
- Darvish KK, Crandall JR (2001) Nonlinear viscoelastic effects in oscillatory shear deformation of brain tissue. *Med Eng Phys* 23:633-645.
- Davalos D, Grutzendler J, Yang G, Kim JV, Zuo Y, Jung S, Littman DR, Dustin ML, Gan WB (2005) ATP mediates rapid microglial response to local brain injury in vivo. *Nat Neurosci* 8:752-758.
- David S, Aguayo AJ (1981) Axonal elongation into peripheral nervous system "bridges" after central nervous system injury in adult rats. *Science* 214:931-933.
- Davis GB, Kohandel M, Sivaloganathan S, Tenti G (2006) The constitutive properties of the brain paraenchyma Part 2. Fractional derivative approach. *Med Eng Phys* 28:455-459.
- Delamarter RB, Sherman J, Carr JB (1995) Pathophysiology of spinal cord injury. Recovery after immediate and delayed decompression. *J Bone Joint Surg Am* 77:1042-1049.
- Demediuk P, Saunders RD, Anderson DK, Means ED, Horrocks LA (1985) Membrane lipid changes in laminectomized and traumatized cat spinal cord. *Proc Natl Acad Sci U S A* 82:7071-7075.
- Deng Y, Thompson BM, Gao X, Hall ED (2007) Temporal relationship of peroxynitrite-induced oxidative damage, calpain-mediated cytoskeletal degradation and neurodegeneration after traumatic brain injury. *Exp Neurol*.
- Denis F (1983) The three column spine and its significance in the classification of acute thoracolumbar spinal injuries. *Spine* 8:817-831.
- Denis F (1984) Spinal instability as defined by the three-column spine concept in acute spinal trauma. *Clin Orthop*:65-76.
- Deridder MN, Simon MJ, Siman R, Auberson YP, Raghupathi R, Meaney DF (2005) Traumatic mechanical injury to the hippocampus in vitro causes regional caspase-3 and calpain activation that is influenced by NMDA receptor subunit composition. *Neurobiol Dis*.

- Diaz-Ruiz A, Rios C, Duarte I, Correa D, Guizar-Sahagun G, Grijalva I, Ibarra A (1999) Cyclosporin-A inhibits lipid peroxidation after spinal cord injury in rats. *Neurosci Lett* 266:61-64.
- Dimar JR, 2nd, Glassman SD, Raque GH, Zhang YP, Shields CB (1999) The influence of spinal canal narrowing and timing of decompression on neurologic recovery after spinal cord contusion in a rat model. *Spine* 24:1623-1633.
- Dohrmann GJ, Panjabi MM, Banks D (1978) Biomechanics of experimental spinal cord trauma. *J Neurosurg* 48:993-1001.
- Dolan EJ, Tator CH, Endrenyi L (1980a) The value of decompression for acute experimental spinal cord compression injury. *J Neurosurg* 53:749-755.
- Dolan EJ, Transfeldt EE, Tator CH, Simmons EH, Hughes KF (1980b) The effect of spinal distraction on regional spinal cord blood flow in cats. *J Neurosurg* 53:756-764.
- Dugan LL, Kim-Han JS (2006) Hypoxic-ischemic brain injury and oxidative stress. In: *Basic Neurochemistry: Molecular, Cellular, and Medical Aspects*, 7th Edition (Siegel GJ, Albers RW, Brady ST, Price DL, eds), pp 559-573. Burlington, MA: Elsevier Academic Press.
- Dumont RJ, Okonkwo DO, Verma S, Hurlbert RJ, Boulos PT, Ellegala DB, Dumont AS (2001) Acute spinal cord injury, part I: pathophysiologic mechanisms. *Clin Neuropharmacol* 24:254-264.
- Eder C, Klee R, Heinemann U (1998) Involvement of stretch-activated Cl⁻ channels in ramification of murine microglia. *J Neurosci* 18:7127-7137.
- Eftekharpour E, Karimi-Abdolrezaee S, Wang J, El Beheiry H, Morshead C, Fehlings MG (2007) Myelination of congenitally dysmyelinated spinal cord axons by adult neural precursor cells results in formation of nodes of Ranvier and improved axonal conduction. *J Neurosci* 27:3416-3428.
- Elder GA, Friedrich VL, Jr., Kang C, Bosco P, Gourov A, Tu PH, Zhang B, Lee VM, Lazzarini RA (1998) Requirement of heavy neurofilament subunit in the development of axons with large calibers. *J Cell Biol* 143:195-205.
- Faden AI, Lemke M, Simon RP, Noble LJ (1988) N-methyl-D-aspartate antagonist MK801 improves outcome following traumatic spinal cord injury in rats: behavioral, anatomic, and neurochemical studies. *J Neurotrauma* 5:33-45.
- Fallenst.Gt, Hulce VD, Melvin JW (1969) Dynamic Mechanical Properties of Human Brain Tissue. *J Biomech* 2:217-&.
- Fallenstein GT, Hulce VD, Melvin JW (1969) Dynamic mechanical properties of human brain tissue. *J Biomech* 2:217-226.
- Faulkner JR, Herrmann JE, Woo MJ, Tansey KE, Doan NB, Sofroniew MV (2004) Reactive astrocytes protect tissue and preserve function after spinal cord injury. *J Neurosci* 24:2143-2155.
- Fehlings MG, Tator CH (1995) The relationships among the severity of spinal cord injury, residual neurological function, axon counts, and counts of retrogradely labeled neurons after experimental spinal cord injury. *Exp Neurol* 132:220-228.
- Fehlings MG, Sekhon LH, Tator C (2001) The role and timing of decompression in acute spinal cord injury: what do we know? What should we do? *Spine* 26:S101-110.
- Ferguson RL, Allen BL, Jr. (1984) A mechanistic classification of thoracolumbar spine fractures. *Clin Orthop Relat Res*:77-88.
- Fiford RJ, Bilston LE, Waite P, Lu J (2004) A vertebral dislocation model of spinal cord injury in rats. *J Neurotrauma* 21:451-458.

- Freund P, Schmidlin E, Wannier T, Bloch J, Mir A, Schwab ME, Rouiller EM (2006) Nogo-A-specific antibody treatment enhances sprouting and functional recovery after cervical lesion in adult primates. *Nat Med* 12:790-792.
- Fung YC (1993) *Biomechanics: mechanical properties of living tissues*. New York: Springer.
- Galbraith JA, Thibault LE, Matteson DR (1993) Mechanical and electrical responses of the squid giant axon to simple elongation. *J Biomech Eng* 115:13-22.
- Galford JE, McElhaney JH (1970) A viscoelastic study of scalp, brain, and dura. *J Biomech* 3:211-221.
- Gallant PE (1992) The direct effects of graded axonal compression on axoplasm and fast axoplasmic transport. *J Neuropathol Exp Neurol* 51:220-230.
- Geddes DM, Cargill RS, 2nd, LaPlaca MC (2003) Mechanical stretch to neurons results in a strain rate and magnitude-dependent increase in plasma membrane permeability. *J Neurotrauma* 20:1039-1049.
- Geisler FH, Dorsey FC, Coleman WP (1991) Recovery of motor function after spinal-cord injury--a randomized, placebo-controlled trial with GM-1 ganglioside. *N Engl J Med* 324:1829-1838.
- Geisler FH, Coleman WP, Grieco G, Poonian D (2001) The Sygen multicenter acute spinal cord injury study. *Spine* 26:S87-98.
- Gensel JC, Tovar CA, Hamers FP, Deibert RJ, Beattie MS, Bresnahan JC (2006) Behavioral and histological characterization of unilateral cervical spinal cord contusion injury in rats. *J Neurotrauma* 23:36-54.
- Ghasemlou N, Kerr BJ, David S (2005) Tissue displacement and impact force are important contributors to outcome after spinal cord contusion injury. *Exp Neurol* 196:9-17.
- GrandPre T, Nakamura F, Vartanian T, Strittmatter SM (2000) Identification of the Nogo inhibitor of axon regeneration as a Reticulon protein. *Nature* 403:439-444.
- Gris D, Marsh DR, Oatway MA, Chen Y, Hamilton EF, Dekaban GA, Weaver LC (2004) Transient blockade of the CD11d/CD18 integrin reduces secondary damage after spinal cord injury, improving sensory, autonomic, and motor function. *J Neurosci* 24:4043-4051.
- Gruner JA (1992) A monitored contusion model of spinal cord injury in the rat. *J Neurotrauma* 9:123-126; discussion 126-128.
- Guha A, Tator CH, Rochon J (1989) Spinal cord blood flow and systemic blood pressure after experimental spinal cord injury in rats. *Stroke* 20:372-377.
- Guha A, Tator CH, Endrenyi L, Piper I (1987) Decompression of the spinal cord improves recovery after acute experimental spinal cord compression injury. *Paraplegia* 25:324-339.
- Hackney DB, Finkelstein SD, Hand CM, Markowitz RS, Black P (1994) Postmortem magnetic resonance imaging of experimental spinal cord injury: magnetic resonance findings versus in vivo functional deficit. *Neurosurgery* 35:1104-1111.
- Hagg T, Oudega M (2006) Degenerative and spontaneous regenerative processes after spinal cord injury. *J Neurotrauma* 23:264-280.
- Hall ED, Braughler JM (1982) Glucocorticoid mechanisms in acute spinal cord injury: a review and therapeutic rationale. *Surg Neurol* 18:320-327.
- Hall ED, Springer JE (2004) Neuroprotection and acute spinal cord injury: a reappraisal. *NeuroRx* 1:80-100.
- Hall ED, Wolf DL, Braughler JM (1984) Effects of a single large dose of methylprednisolone sodium succinate on experimental posttraumatic spinal cord ischemia. Dose-response and time-action analysis. *J Neurosurg* 61:124-130.

- Harrop JS, Sharan AD, Vaccaro AR, Przybylski GJ (2001) The cause of neurologic deterioration after acute cervical spinal cord injury. *Spine* 26:340-346.
- Hart RA (2002) Cervical facet dislocation: when is magnetic resonance imaging indicated? *Spine* 27:116-117.
- Harwood SM, Yaqoob MM, Allen DA (2005) Caspase and calpain function in cell death: bridging the gap between apoptosis and necrosis. *Ann Clin Biochem* 42:415-431.
- Hauben E, Butovsky O, Nevo U, Yoles E, Moalem G, Agranov E, Mor F, Leibowitz-Amit R, Pevsner E, Akselrod S, Neeman M, Cohen IR, Schwartz M (2000) Passive or active immunization with myelin basic protein promotes recovery from spinal cord contusion. *J Neurosci* 20:6421-6430.
- Hayes KC, Kakulas BA (1997) Neuropathology of human spinal cord injury sustained in sports-related activities. *J Neurotrauma* 14:235-248.
- Haynes SE, Hollopeter G, Yang G, Kurpius D, Dailey ME, Gan WB, Julius D (2006) The P2Y₁₂ receptor regulates microglial activation by extracellular nucleotides. *Nat Neurosci* 9:1512-1519.
- Hedel HJ, Curt A (2006) Fighting for Each Segment: Estimating the Clinical Value of Cervical and Thoracic Segments in SCI. *J Neurotrauma* 23:1621-1631.
- Hirokawa N, Glicksman MA, Willard MB (1984) Organization of mammalian neurofilament polypeptides within the neuronal cytoskeleton. *J Cell Biol* 98:1523-1536.
- Horky LL, Galimi F, Gage FH, Horner PJ (2006) Fate of endogenous stem/progenitor cells following spinal cord injury. *J Comp Neurol* 498:525-538.
- Horn EM, Feiz-Erfan I, Lekovic GP, Dickman CA, Sonntag VK, Theodore N (2007) Survivors of occipitotlantal dislocation injuries: imaging and clinical correlates. *J Neurosurg Spine* 6:113-120.
- Hsu CY, Dimitrijevic MR (1990) Methylprednisolone in spinal cord injury: the possible mechanism of action. *J Neurotrauma* 7:115-119.
- Hung TK, Chang GL (1981) Biomechanical and neurological response of the spinal cord of a puppy to uniaxial tension. *J Biomech Eng* 103:43-47.
- Hurlbert RJ (2000) Methylprednisolone for acute spinal cord injury: an inappropriate standard of care. *J Neurosurg* 93:1-7.
- Ichihara K, Taguchi T, Shimada Y, Sakuramoto I, Kawano S, Kawai S (2001) Gray matter of the bovine cervical spinal cord is mechanically more rigid and fragile than the white matter. *J Neurotrauma* 18:361-367.
- Iencean SM (2003) Classification of spinal injuries based on the essential traumatic spinal mechanisms. *Spinal Cord* 41:385-396.
- Iwasaki Y, Yamamoto H, Iizuka H, Yamamoto T, Konno H (1987) Suppression of neurofilament degradation by protease inhibitors in experimental spinal cord injury. *Brain Res* 406:99-104.
- Jacques-Fricke BT, Seow Y, Gottlieb PA, Sachs F, Gomez TM (2006) Ca²⁺ influx through mechanosensitive channels inhibits neurite outgrowth in opposition to other influx pathways and release from intracellular stores. *J Neurosci* 26:5656-5664.
- Jakeman LB, Guan Z, Wei P, Ponnappan R, Dzwonczyk R, Popovich PG, Stokes BT (2000) Traumatic spinal cord injury produced by controlled contusion in mouse. *J Neurotrauma* 17:299-319 ;217(294):299-319.
- Jarzem PF, Kostuik JP, Filiaggi M, Doyle DJ, Ethier R, Tator CH (1991) Spinal cord distraction: an in vitro study of length, tension, and tissue pressure. *J Spinal Disord* 4:177-182.

- Jensen JM, Shi R (2003) Effects of 4-aminopyridine on stretched mammalian spinal cord: the role of potassium channels in axonal conduction. *J Neurophysiol* 90:2334-2340.
- Kapoor R, Davies M, Blaker PA, Hall SM, Smith KJ (2003) Blockers of sodium and calcium entry protect axons from nitric oxide-mediated degeneration. *Ann Neurol* 53:174-180.
- Kearney PA, Ridella SA, Viano DC, Anderson TE (1988) Interaction of contact velocity and cord compression in determining the severity of spinal cord injury. *J Neurotrauma* 5:187-208.
- Khan M, Griebel R, Rozdilsky B, Politis M (1985) Hemorrhagic changes in experimental spinal cord injury models. *Can J Neurol Sci* 12:259-262.
- Kiwerski J (1991) The influence of the mechanism of cervical spine injury on the degree of the spinal cord lesion. *Paraplegia* 29:531-536.
- Kloos AD, Fisher LC, Detloff MR, Hassenzahl DL, Basso DM (2005) Stepwise motor and all-or-none sensory recovery is associated with nonlinear sparing after incremental spinal cord injury in rats. *Exp Neurol* 191:251-265.
- Kobrine AI, Evans DE, Rizzoli H (1978) Correlation of spinal cord blood flow and function in experimental compression. *Surg Neurol* 10:54-59.
- Kohandel M, Sivaloganathan S, Tenti G, Drake JM (2006) The constitutive properties of the brain parenchyma Part 1. Strain energy approach. *Med Eng Phys* 28:449-454.
- Kottis V, Thibault P, Mikol D, Xiao ZC, Zhang R, Dergham P, Braun PE (2002) Oligodendrocyte-myelin glycoprotein (OMgp) is an inhibitor of neurite outgrowth. *J Neurochem* 82:1566-1569.
- Kwon BK, Oxland TR, Tetzlaff W (2002a) Animal models used in spinal cord regeneration research. *Spine* 27:1504-1510.
- Kwon BK, Vaccaro AR, Grauer JN, Fisher CG, Dvorak MF (2006) Subaxial cervical spine trauma. *J Am Acad Orthop Surg* 14:78-89.
- Kwon BK, Liu J, Messerer C, Kobayashi NR, McGraw J, Oschipok L, Tetzlaff W (2002b) Survival and regeneration of rubrospinal neurons 1 year after spinal cord injury. *Proc Natl Acad Sci U S A* 99:3246-3251.
- La Rosa G, Conti A, Cardali S, Cacciola F, Tomasello F (2004) Does early decompression improve neurological outcome of spinal cord injured patients? Appraisal of the literature using a meta-analytical approach. *Spinal Cord* 42:503-512.
- LaMotte C (1980) Early spinal cord trauma assessed by diffuse axonal uptake of HRP. In: *Society for Neuroscience*, p 734.
- LaPlaca MC, Thibault LE (1997) An in vitro traumatic injury model to examine the response of neurons to a hydrodynamically-induced deformation. *Ann Biomed Eng* 25:665-677.
- LaPlaca MC, Thibault LE (1998) Dynamic mechanical deformation of neurons triggers an acute calcium response and cell injury involving the N-methyl-D-aspartate glutamate receptor. *J Neurosci Res* 52:220-229.
- Laplaca MC, Lee VM, Thibault LE (1997) An in vitro model of traumatic neuronal injury: loading rate-dependent changes in acute cytosolic calcium and lactate dehydrogenase release. *J Neurotrauma* 14:355-368.
- LaPlaca MC, Cullen DK, McLoughlin JJ, Cargill RS, 2nd (2005) High rate shear strain of three-dimensional neural cell cultures: a new in vitro traumatic brain injury model. *J Biomech* 38:1093-1105.
- Lippert SA, Rang EM, Grimm MJ (2004) The high frequency properties of brain tissue. *Biorheology* 41:681-691.

- Liu S, Qu Y, Stewart TJ, Howard MJ, Chakraborty S, Holekamp TF, McDonald JW (2000) Embryonic stem cells differentiate into oligodendrocytes and myelinate in culture and after spinal cord transplantation. *Proc Natl Acad Sci U S A* 97:6126-6131.
- Liu XZ, Xu XM, Hu R, Du C, Zhang SX, McDonald JW, Dong HX, Wu YJ, Fan GS, Jacquin MF, Hsu CY, Choi DW (1997) Neuronal and glial apoptosis after traumatic spinal cord injury. *J Neurosci* 17:5395-5406.
- Liu Y, Wong TP, Aarts M, Rooyackers A, Liu L, Lai TW, Wu DC, Lu J, Tymianski M, Craig AM, Wang YT (2007) NMDA receptor subunits have differential roles in mediating excitotoxic neuronal death both in vitro and in vivo. *J Neurosci* 27:2846-2857.
- Lu J, Ashwell KW, Waite P (2000) Advances in secondary spinal cord injury: role of apoptosis. *Spine* 25:1859-1866 ;1825(1814):1859-1866.
- Lu P, Yang H, Jones LL, Filbin MT, Tuszynski MH (2004) Combinatorial therapy with neurotrophins and cAMP promotes axonal regeneration beyond sites of spinal cord injury. *J Neurosci* 24:6402-6409.
- Luo J, Borgens R, Shi R (2002) Polyethylene glycol immediately repairs neuronal membranes and inhibits free radical production after acute spinal cord injury. *J Neurochem* 83:471-480.
- Magerl F, Aebi M, Gertzbein SD, Harms J, Nazarian S (1994) A comprehensive classification of thoracic and lumbar injuries. *Eur Spine J* 3:184-201.
- Maikos JT, Shreiber DI (2007) Immediate damage to the blood-spinal cord barrier due to mechanical trauma. *J Neurotrauma* 24:492-507.
- Maiman DJ, Coats J, Myklebust JB (1989) Cord/spine motion in experimental spinal cord injury. *J Spinal Disord* 2:14-19.
- Matsumoto H, Kumon Y, Watanabe H, Ohnishi T, Shudou M, Ii C, Takahashi H, Imai Y, Tanaka J (2007) Antibodies to CD11b, CD68, and lectin label neutrophils rather than microglia in traumatic and ischemic brain lesions. *J Neurosci Res*.
- Mattson MP (2003) Excitotoxic and excitoprotective mechanisms: abundant targets for the prevention and treatment of neurodegenerative disorders. *Neuromolecular Med* 3:65-94.
- Maxwell WL, Graham DI (1997) Loss of axonal microtubules and neurofilaments after stretch-injury to guinea pig optic nerve fibers. *J Neurotrauma* 14:603-614.
- Maxwell WL, Irvine A, Graham, Adams JH, Gennarelli TA, Tipperman R, Sturatis M (1991) Focal axonal injury: the early axonal response to stretch. *J Neurocytol* 20:157-164.
- McDonald JW, Liu XZ, Qu Y, Liu S, Mickey SK, Turetsky D, Gottlieb DI, Choi DW (1999) Transplanted embryonic stem cells survive, differentiate and promote recovery in injured rat spinal cord. *Nat Med* 5:1410-1412.
- McKerracher L, David S, Jackson DL, Kottis V, Dunn RJ, Braun PE (1994) Identification of myelin-associated glycoprotein as a major myelin-derived inhibitor of neurite growth. *Neuron* 13:805-811.
- Meaney DF (2003) Relationship between structural modeling and hyperelastic material behavior: application to CNS white matter. *Biomech Model Mechanobiol* 1:279-293.
- Means ED, Anderson DK, Waters TR, Kalaf L (1981) Effect of methylprednisolone in compression trauma to the feline spinal cord. *J Neurosurg* 55:200-208.
- Mendis KK, Stalnaker RL, Advani SH (1995a) A constitutive relationship for large deformation finite element modeling of brain tissue. *J Biomech Eng* 117:279-285.
- Mendis KK, Stalnaker RL, Advani SH (1995b) A Constitutive Relationship for Large-Deformation Finite-Element Modeling of Brain-Tissue. *Journal of Biomechanical Engineering-Transactions of the Asme* 117:279-285.

- Mu X, Azbill RD, Springer JE (2000) Riluzole improves measures of oxidative stress following traumatic spinal cord injury. *Brain Res* 870:66-72.
- Mukhopadhyay G, Doherty P, Walsh FS, Crocker PR, Filbin MT (1994) A novel role for myelin-associated glycoprotein as an inhibitor of axonal regeneration. *Neuron* 13:757-767.
- Myklebust JB, Maiman DJ, Cusick JF (1988) Axial tension model of spinal cord injury. *J Am Paraplegia Soc* 11:50-55.
- Nacimientto AC, Bartels M, Loew F (1986) Acute changes in somatosensory evoked potentials following graded experimental spinal cord compression. *Surg Neurol* 25:62-66.
- Naito M, Owen JH, Bridwell KH, Sugioka Y (1992) Effects of distraction on physiologic integrity of the spinal cord, spinal cord blood flow, and clinical status. *Spine* 17:1154-1158.
- Nashmi R, Fehlings MG (2001) Changes in axonal physiology and morphology after chronic compressive injury of the rat thoracic spinal cord. *Neuroscience* 104:235-251;104(231):235-251.
- Nashmi R, Jones OT, Fehlings MG (2000) Abnormal axonal physiology is associated with altered expression and distribution of Kv1.1 and Kv1.2 K⁺ channels after chronic spinal cord injury. *Eur J Neurosci* 12:491-506.
- Neumann S, Woolf CJ (1999) Regeneration of dorsal column fibers into and beyond the lesion site following adult spinal cord injury. *Neuron* 23:83-91.
- Neumann S, Bradke F, Tessier-Lavigne M, Basbaum AI (2002) Regeneration of sensory axons within the injured spinal cord induced by intraganglionic cAMP elevation. *Neuron* 34:885-893.
- Noble LJ, Wrathall JR (1985) Spinal cord contusion in the rat: morphometric analyses of alterations in the spinal cord. *Exp Neurol* 88:135-149.
- Noble LJ, Wrathall JR (1989) Distribution and time course of protein extravasation in the rat spinal cord after contusive injury. *Brain Res* 482:57-66.
- Norenberg MD, Smith J, Marcillo A (2004) The pathology of human spinal cord injury: defining the problems. *J Neurotrauma* 21:429-440.
- Noyes DH (1987a) Electromechanical impactor for producing experimental spinal cord injury in animals. *Med Biol Eng Comput* 25:335-340.
- Noyes DH (1987b) Correlation between parameters of spinal cord impact and resultant injury. *Exp Neurol* 95:535-547.
- Oudega M, Xu XM (2006) Schwann cell transplantation for repair of the adult spinal cord. *J Neurotrauma* 23:453-467.
- Oxland TR (1992) Burst Fractures of the Human Thoracolumbar Spine: A Biomechanical Investigation. In: *Mechanical Engineering*, p 201. New Haven: Yale University.
- Ozawa H, Matsumoto T, Ohashi T, Sato M, Kokubun S (2001) Comparison of spinal cord gray matter and white matter softness: measurement by pipette aspiration method. *J Neurosurg* 95:221-224.
- Panjabi MM, Kifune M, Wen L, Arand M, Oxland TR, Lin RM, Yoon WS, Vasavada A (1995) Dynamic canal encroachment during thoracolumbar burst fractures. *J Spinal Disord* 8:39-48.
- Paoletti P, Ascher P (1994) Mechanosensitivity of NMDA receptors in cultured mouse central neurons. *Neuron* 13:645-655.
- Park E, Velumian AA, Fehlings MG (2004) The role of excitotoxicity in secondary mechanisms of spinal cord injury: a review with an emphasis on the implications for white matter degeneration. *J Neurotrauma* 21:754-774.

- Pearse DD, Pereira FC, Marcillo AE, Bates ML, Berrocal YA, Filbin MT, Bunge MB (2004) cAMP and Schwann cells promote axonal growth and functional recovery after spinal cord injury. *Nat Med* 10:610-616.
- Pearse DD, Lo TP, Jr., Cho KS, Lynch MP, Garg MS, Marcillo AE, Sanchez AR, Cruz Y, Dietrich WD (2005) Histopathological and behavioral characterization of a novel cervical spinal cord displacement contusion injury in the rat. *J Neurotrauma* 22:680-702.
- Petersilge CA, Emery SE (1996) Thoracolumbar burst fracture: evaluating stability. *Semin Ultrasound CT MR* 17:105-113.
- Pettus EH, Christman CW, Giebel ML, Povlishock JT (1994) Traumatically induced altered membrane permeability: its relationship to traumatically induced reactive axonal change. *J Neurotrauma* 11:507-522.
- Pickett GE, Campos-Benitez M, Keller JL, Duggal N (2006) Epidemiology of traumatic spinal cord injury in Canada. *Spine* 31:799-805.
- Pike BR, Zhao X, Newcomb JK, Glenn CC, Anderson DK, Hayes RL (2000) Stretch injury causes calpain and caspase-3 activation and necrotic and apoptotic cell death in septo-hippocampal cell cultures. *J Neurotrauma* 17:283-298.
- Pitzen T, Lane C, Goertzen D, Dvorak M, Fisher C, Barbier D, Steudel WI, Oxland T (2003) Anterior cervical plate fixation: biomechanical effectiveness as a function of posterior element injury. *J Neurosurg* 99:84-90.
- Popovich PG, Jones TB (2003) Manipulating neuroinflammatory reactions in the injured spinal cord: back to basics. *Trends Pharmacol Sci* 24:13-17.
- Popovich PG, Stokes BT, Whitacre CC (1996a) Concept of autoimmunity following spinal cord injury: possible roles for T lymphocytes in the traumatized central nervous system. *J Neurosci Res* 45:349-363.
- Popovich PG, Horner PJ, Mullin BB, Stokes BT (1996b) A quantitative spatial analysis of the blood-spinal cord barrier. I. Permeability changes after experimental spinal contusion injury. *Exp Neurol* 142:258-275.
- Popovich PG, Guan Z, Wei P, Huitinga I, van Rooijen N, Stokes BT (1999) Depletion of hematogenous macrophages promotes partial hindlimb recovery and neuroanatomical repair after experimental spinal cord injury. *Exp Neurol* 158:351-365.
- Prado GR (2004) Neuronal Plasma Membrane Disruption in Traumatic Brain Injury. In: *School of Biomedical Engineering*. Atlanta: Georgia Institute of Technology.
- Prado GR, LaPlaca MC (2004) Neuronal plasma membrane is transiently disrupted by mechanical trauma: an insight into the mechanisms involved. *J Neurotrauma* 21:1331.
- Prado GR, Ross JD, Deweerth SP, Laplaca MC (2005) Mechanical trauma induces immediate changes in neuronal network activity. *J Neural Eng* 2:148-158.
- Prange MT, Margulies SS (2002) Regional, directional, and age-dependent properties of the brain undergoing large deformation. *J Biomech Eng* 124:244-252.
- Prinjha R, Moore SE, Vinson M, Blake S, Morrow R, Christie G, Michalovich D, Simmons DL, Walsh FS (2000) Inhibitor of neurite outgrowth in humans. *Nature* 403:383-384.
- Ramon S, Dominguez R, Ramirez L, Paraira M, Olona M, Castello T, Garcia FL (1997) Clinical and magnetic resonance imaging correlation in acute spinal cord injury. *Spinal Cord* 35:664-673.
- Rasband MN, Trimmer JS (2001) Developmental clustering of ion channels at and near the node of Ranvier. *Dev Biol* 236:5-16.

- Rawe SE, Lee WA, Perot PL, Jr. (1978) The histopathology of experimental spinal cord trauma. The effect of systemic blood pressure. *J Neurosurg* 48:1002-1007.
- Raynor RB, Koplik B (1985) Cervical cord trauma. The relationship between clinical syndromes and force of injury. *Spine* 10:193-197.
- Reindl R, Ouellet J, Harvey EJ, Berry G, Arlet V (2006) Anterior reduction for cervical spine dislocation. *Spine* 31:648-652.
- Richardson PM, Issa VM (1984) Peripheral injury enhances central regeneration of primary sensory neurones. *Nature* 309:791-793.
- Rivlin AS, Tator CH (1978) Effect of duration of acute spinal cord compression in a new acute cord injury model in the rat. *Surg Neurol* 10:38-43.
- Rosenberg LJ, Wrathall JR (2001) Time course studies on the effectiveness of tetrodotoxin in reducing consequences of spinal cord contusion. *J Neurosci Res* 66:191-202.
- Ruitenbergh MJ, Vukovic J, Sarich J, Busfield SJ, Plant GW (2006) Olfactory ensheathing cells: characteristics, genetic engineering, and therapeutic potential. *J Neurotrauma* 23:468-478.
- Sasaki M, Black JA, Lankford KL, Tokuno HA, Waxman SG, Kocsis JD (2006) Molecular reconstruction of nodes of Ranvier after remyelination by transplanted olfactory ensheathing cells in the demyelinated spinal cord. *J Neurosci* 26:1803-1812.
- Sattler R, Charlton MP, Hafner M, Tymianski M (1998) Distinct influx pathways, not calcium load, determine neuronal vulnerability to calcium neurotoxicity. *J Neurochem* 71:2349-2364.
- Sayer FT, Kronvall E, Nilsson OG (2006) Methylprednisolone treatment in acute spinal cord injury: the myth challenged through a structured analysis of published literature. *Spine J* 6:335-343.
- Schaefer DM, Flanders A, Northrup BE, Doan HT, Osterholm JL (1989) Magnetic resonance imaging of acute cervical spine trauma. Correlation with severity of neurologic injury. *Spine* 14:1090-1095.
- Schauer BA, Sokolove PE (2003) Severe cervical spine distraction. *J Emerg Med* 25:445-447.
- Scheff SW, Rabchevsky AG, Fugaccia I, Main JA, Lumpp JE, Jr. (2003) Experimental modeling of spinal cord injury: characterization of a force-defined injury device. *J Neurotrauma* 20:179-193.
- Schnell L, Schwab ME (1990) Axonal regeneration in the rat spinal cord produced by an antibody against myelin-associated neurite growth inhibitors. *Nature* 343:269-272.
- Schnell L, Fearn S, Klassen H, Schwab ME, Perry VH (1999) Acute inflammatory responses to mechanical lesions in the CNS: differences between brain and spinal cord. *Eur J Neurosci* 11:3648-3658.
- Schwartz M (2003) Macrophages and microglia in central nervous system injury: are they helpful or harmful? *J Cereb Blood Flow Metab* 23:385-394.
- Schwartz M, Yoles E (2006) Immune-based therapy for spinal cord repair: autologous macrophages and beyond. *J Neurotrauma* 23:360-370.
- Schweitzer KM, Jr., Vaccaro AR, Lee JY, Grauer JN (2006) Confusion regarding mechanisms of injury in the setting of thoracolumbar spinal trauma: a survey of The Spine Trauma Study Group (STSG). *J Spinal Disord Tech* 19:528-530.
- Sekhon LH, Fehlings MG (2001) Epidemiology, demographics, and pathophysiology of acute spinal cord injury. *Spine* 26:S2-12.
- Shi R, Blight AR (1997) Differential effects of low and high concentrations of 4-aminopyridine on axonal conduction in normal and injured spinal cord. *Neuroscience* 77:553-562.

- Shi R, Borgens RB (1999) Acute repair of crushed guinea pig spinal cord by polyethylene glycol. *J Neurophysiol* 81:2406-2414.
- Shi R, Pryor JD (2000) Temperature dependence of membrane sealing following transection in mammalian spinal cord axons. *Neuroscience* 98:157-166.
- Shi R, Pryor JD (2002) Pathological changes of isolated spinal cord axons in response to mechanical stretch. *Neuroscience* 110:765-777.
- Shi R, Whitebone J (2006) Conduction deficits and membrane disruption of spinal cord axons as a function of magnitude and rate of strain. *J Neurophysiol* 95:3384-3390.
- Shi R, Kelly TM, Blight AR (1997) Conduction block in acute and chronic spinal cord injury: different dose-response characteristics for reversal by 4-aminopyridine. *Exp Neurol* 148:495-501.
- Shi R, Asano T, Vining NC, Blight AR (2000) Control of membrane sealing in injured mammalian spinal cord axons. *J Neurophysiol* 84:1763-1769.
- Shi R, Qiao X, Emerson N, Malcom A (2001) Dimethylsulfoxide enhances CNS neuronal plasma membrane resealing after injury in low temperature or low calcium. *J Neurocytol* 30:829-839.
- Shi RY, Lucas JH, Wolf A, Gross GW (1989) Calcium antagonists fail to protect mammalian spinal neurons after physical injury. *J Neurotrauma* 6:261-276; discussion 277-268.
- Shuck LZ, Advani SH (1972) Rheological Response of Human Brain-Tissue in Shear. *Journal of Basic Engineering* 94:905-911.
- Shuman SL, Bresnahan JC, Beattie MS (1997) Apoptosis of microglia and oligodendrocytes after spinal cord contusion in rats. *J Neurosci Res* 50:798-808.
- Siegel GJ, Albers RW, Brady ST, Price DL (2006) *Basic Neurochemistry: Molecular, Cellular, and Medical Aspects*, 7th Edition. Burlington: Elsevier Academic Press.
- Silberstein M, McLean K (1994) Non-contiguous spinal injury: clinical and imaging features, and postulated mechanism. *Paraplegia* 32:817-823.
- Singleton RH, Povlishock JT (2004) Identification and characterization of heterogeneous neuronal injury and death in regions of diffuse brain injury: evidence for multiple independent injury phenotypes. *J Neurosci* 24:3543-3553.
- Smith DH, Wolf JA, Lusardi TA, Lee VM, Meaney DF (1999) High tolerance and delayed elastic response of cultured axons to dynamic stretch injury. *J Neurosci* 19:4263-4269.
- Somerson SK (1986) Analysis of an electro-mechanical spinal cord injury device. In: *Bio-Medical Engineering*. Columbus: The Ohio State University.
- Somerson SK, Stokes BT (1987) Functional analysis of an electromechanical spinal cord injury device. *Exp Neurol* 96:82-96.
- Sparrey CJ, Choo AM, Liu J, Tetzlaff W, Oxland TR (2004) The effect of impact velocity on spinal cord contusion injuries. *J Neurotrauma* 21:1322.
- Springer JE, Azbill RD, Knapp PE (1999) Activation of the caspase-3 apoptotic cascade in traumatic spinal cord injury. *Nat Med* 5:943-946.
- Squire LR, Bloom FE, McConnell SK, Roberts JL, Spitzer NC, Zigmond MJ (2003) *Fundamental Neuroscience*, 2nd Edition. San Diego: Academic Press.
- Stirling DP, Khodarahmi K, Liu J, McPhail LT, McBride CB, Steeves JD, Ramer MS, Tetzlaff W (2004) Minocycline treatment reduces delayed oligodendrocyte death, attenuates axonal dieback, and improves functional outcome after spinal cord injury. *J Neurosci* 24:2182-2190.

- Stokes BT, Jakeman LB (2002) Experimental modelling of human spinal cord injury: a model that crosses the species barrier and mimics the spectrum of human cytopathology. *Spinal Cord* 40:101-109.
- Stokes BT, Noyes DH, Behrmann DL (1992) An electromechanical spinal injury technique with dynamic sensitivity. *J Neurotrauma* 9:187-195.
- Stone JR, Okonkwo DO, Dialo AO, Rubin DG, Mutlu LK, Povlishock JT, Helm GA (2004) Impaired axonal transport and altered axolemmal permeability occur in distinct populations of damaged axons following traumatic brain injury. *Exp Neurol* 190:59-69.
- Stys PK (1998) Anoxic and ischemic injury of myelinated axons in CNS white matter: from mechanistic concepts to therapeutics. *J Cereb Blood Flow Metab* 18:2-25.
- Stys PK, Jiang Q (2002) Calpain-dependent neurofilament breakdown in anoxic and ischemic rat central axons. *Neurosci Lett* 328:150-154.
- Sugawara T, Lewen A, Gasche Y, Yu F, Chan PH (2002) Overexpression of SOD1 protects vulnerable motor neurons after spinal cord injury by attenuating mitochondrial cytochrome c release. *FASEB J* 16:1997-1999.
- Sugawara T, Fujimura M, Noshita N, Kim GW, Saito A, Hayashi T, Narasimhan P, Maier CM, Chan PH (2004) Neuronal death/survival signaling pathways in cerebral ischemia. *NeuroRx* 1:17-25.
- Tani S, Yamada S, Knighton RS (1987) Extensibility of the lumbar and sacral cord. Pathophysiology of the tethered spinal cord in cats. *J Neurosurg* 66:116-123.
- Tator CH (1983) Spine-spinal cord relationships in spinal cord trauma. *Clin Neurosurg* 30:479-494.
- Tator CH (2006) Review of treatment trials in human spinal cord injury: issues, difficulties, and recommendations. *Neurosurgery* 59:957-982; discussion 982-957.
- Teismann P, Schulz JB (2004) Cellular pathology of Parkinson's disease: astrocytes, microglia and inflammation. *Cell Tissue Res* 318:149-161.
- Teng YD, Choi H, Onario RC, Zhu S, Desilets FC, Lan S, Woodard EJ, Snyder EY, Eichler ME, Friedlander RM (2004) Minocycline inhibits contusion-triggered mitochondrial cytochrome c release and mitigates functional deficits after spinal cord injury. *Proc Natl Acad Sci U S A* 101:3071-3076.
- Tuszynski MH, Gabriel K, Gerhardt K, Szollar S (1999) Human spinal cord retains substantial structural mass in chronic stages after injury. *J Neurotrauma* 16:523-531.
- Tymianski M, Charlton MP, Carlen PL, Tator CH (1993) Source specificity of early calcium neurotoxicity in cultured embryonic spinal neurons. *J Neurosci* 13:2085-2104.
- Velardi F, Fraternali F, Angelillo M (2006) Anisotropic constitutive equations and experimental tensile behavior of brain tissue. *Biomech Model Mechanobiol* 5:53-61.
- Wang KC, Koprivica V, Kim JA, Sivasankaran R, Guo Y, Neve RL, He Z (2002) Oligodendrocyte-myelin glycoprotein is a Nogo receptor ligand that inhibits neurite outgrowth. *Nature* 417:941-944.
- Waxman SG, Wood SL (1984) Impulse conduction in inhomogeneous axons: effects of variation in voltage-sensitive ionic conductances on invasion of demyelinated axon segments and preterminal fibers. *Brain Res* 294:111-122.
- Wrathall JR (1992) Spinal cord injury models. *J Neurotrauma* 9:S129-S134.
- Wrathall JR, Teng YD, Choiniere D (1996) Amelioration of functional deficits from spinal cord trauma with systemically administered NBQX, an antagonist of non-N-methyl-D-aspartate receptors. *Exp Neurol* 137:119-126.

- Wu KL, Hsu C, Chan JY (2007) Impairment of the mitochondrial respiratory enzyme activity triggers sequential activation of apoptosis-inducing factor-dependent and caspase-dependent signaling pathways to induce apoptosis after spinal cord injury. *J Neurochem*.
- Wyndaele M, Wyndaele JJ (2006) Incidence, prevalence and epidemiology of spinal cord injury: what learns a worldwide literature survey? *Spinal Cord* 44:523-529.
- Xiang Z, Chen M, Ping J, Dunn P, Lv J, Jiao B, Burnstock G (2006) Microglial morphology and its transformation after challenge by extracellular ATP in vitro. *J Neurosci Res* 83:91-101.
- Xiong Y, Rabchevsky AG, Hall ED (2007) Role of peroxynitrite in secondary oxidative damage after spinal cord injury. *J Neurochem* 100:639-649.
- Yamada S, Knerium DS, Mandybur GM, Schultz RL, Yamada BS (2004) Pathophysiology of tethered cord syndrome and other complex factors. *Neurol Res* 26:722-726.
- Yamauchi T, Lin Y, Sharp FR, Noble-Haeusslein LJ (2004) Hemin induces heme oxygenase-1 in spinal cord vasculature and attenuates barrier disruption and neutrophil infiltration in the injured murine spinal cord. *J Neurotrauma* 21:1017-1030.
- Ye JH, Houle JD (1997) Treatment of the chronically injured spinal cord with neurotrophic factors can promote axonal regeneration from supraspinal neurons. *Exp Neurol* 143:70-81.
- Young W (1992) Role of calcium in central nervous system injuries. *J Neurotrauma* 9 Suppl 1:S9-25.
- Young W (2002) Spinal cord contusion models. *Prog Brain Res* 137:231-255.
- Young W, Bracken MB (1992) The Second National Acute Spinal Cord Injury Study. *J Neurotrauma* 9 Suppl 1:S397-405.
- Young W, Yen V, Blight A (1982) Extracellular calcium ionic activity in experimental spinal cord contusion. *Brain Res* 253:105-113.
- Zhou C, Khalil TB, King AI (1995) A new model comparing impact responses of the homogeneous and inhomogeneous human brain. In: 39th Stapp Car Crash Conference. San Diego, CA.

Chapter 2

A NOVEL SCI DEVICEⁱ

2.1 Introduction

Transections and contusions of the rodent spinal cord remain the most widely used methods for experimentally modelling spinal cord injury (SCI) (Kwon et al., 2002; Young, 2002). While transection provides an idealized setting for unambiguously examining regeneration across a complete lesion, contusions mimic the more clinically relevant milieu typically characterized by hemorrhagic necrosis, ischemia, and inflammation, evolving into a chronic lesion with central cavitation encapsulated by a glial scar and spared peripheral white matter (Bresnahan et al., 1991). Allen reported the first contusion model nearly a century ago where a mass was dropped from a prescribed height onto the dorsal surface of the canine dura (Allen, 1911, 1914). This weight-drop method, characterized by the product of the mass and drop-height, has since evolved and gained widespread use (Noble and Wrathall, 1985; Gruner, 1992; Young, 2002). Alternate methods have appeared including injuries parameterized by the contusion displacement (Bresnahan et al., 1987; Noyes, 1987b, a; Somerson and Stokes, 1987; Stokes et al., 1992; Jakeman et al., 2000) and the impact force (Scheff et al., 2003). In addition, compression models have also arisen to simulate the persistent spinal canal occlusion that is common in human injuries (Rivlin and Tator, 1978; Joshi and Fehlings, 2002).

When compared to clinically observed injuries, the contusion models are analogous to vertebral burst fractures which account for an estimated 30-48% of human SCI cases (Sekhon and Fehlings, 2001; Pickett et al., 2006). With a combined prevalence of 29-45%, fracture-dislocation and dislocation without fracture are also common SCI mechanisms (Kiwerski, 1991; Sekhon and Fehlings, 2001; Pickett et al., 2006), however, only one other group has modelled this injury (Fiford et al., 2004). Spinal distraction is also believed to cause SCI (Breig, 1970; Silberstein and

ⁱ A version of this chapter has been submitted for publication. Choo AM, Liu J, Liu Z, Dvorak M, Tetzlaff W, Oxland TR. Modelling spinal cord contusion, dislocation, and distraction: Characterization of a novel device and acute injury severities.

McLean, 1994) but again, there are few dynamic experimental models simulating this injury (Myklebust et al., 1988; Maiman et al., 1989a; Maiman et al., 1989b; Dabney et al., 2004) although slow surgical traction has been more frequently investigated (Fried, 1974; Dolan et al., 1980; Salzman et al., 1988; Salzman et al., 1991).

Differences in the biomechanics of trauma could significantly alter the characteristics of neuronal pathology. *In vitro* 3D neuronal cultures subjected to shear deformation exhibit higher cell death compared to planar cultures (Cullen and LaPlaca, 2006). In addition, *in vitro* comparisons between uniaxial and biaxial stretching of neuronal cultures suggest post-traumatic differences in the deleterious entry of calcium ions through N-methyl-D-aspartate channels (Geddes-Klein et al., 2006). While optic nerve and *in vitro* models have been widely used to isolate the role of mechanical tensile and shear strains on axonal (Maxwell et al., 1991; Maxwell and Graham, 1997; Bain et al., 2001; Wolf et al., 2001; Shi and Pryor, 2002; Iwata et al., 2004) as well as neuronal cell body injury (Laplaca et al., 1997; Geddes et al., 2003; Arundine et al., 2004; Lusardi et al., 2004; Cullen and LaPlaca, 2006), *in vivo* models are still essential for replicating the myriad post-traumatic degenerative processes. Hence, although contusion has been shown to be a reliable model—a characteristic paramount to the systematic screening of therapeutic strategies—there is the possibility that treatments optimized in a contusion paradigm may not translate to other injury mechanisms encountered clinically.

This chapter focuses on the methodological aspects of a novel multi-mechanism injury system designed to produce vertebral dislocation, distraction, as well as contusion injuries. There were two components to this investigation. In part 1, we demonstrated the effectiveness of a novel vertebral clamping strategy for holding the cervical spine without slippage or fracture during high-speed injuries. In addition to mechanical strength, the clamp's grasp exhibited a high stiffness indicating injury displacements could be imposed with accuracy. In part 2, we evaluated injury severities based on acute mortality (dislocation, distraction) and intramedullary hemorrhage volumes (dislocation, contusion). Mortality was not observed following contusion while overt hemorrhage was not evident following distraction. In the contusion model, determination of the impactor's initial contact position is a well-known methodological drawback (Scheff et al., 2003) and we analysed its effect on hemorrhage severity.

2.2 Materials and Methods

2.2.1 Multi-Mechanism Injury System

A novel SCI system was developed (Figure 2.1) around an electromagnetic linear actuator (TestBench ELF LM-1, Bose, Eden Prairie, MN). The apparatus had seven degrees of freedom for positioning the actuator and animal at any orientation relative to each other. The actuator was mounted to a rotary axis (ϕ), on a translating radial arm (R, θ), which in turn was mounted to a motorized z-axis (Linear Stage 2DB160UBW-SL, Thomson Industries, Ronkonkoma, NY; Servo Motor, BSM63N-375AA, Baldor, Fort Smith, AR; Controller FlexDriveII, Baldor). The z-axis allowed for continuous and incremental ($50\mu\text{m}$, 0.002in) positioning. A stereotactic frame (Model 900, David Kopf Instruments, Tujunga, CA), mounted to an x-y table (2.54mm , 0.1in lead, pre-loaded antibacklash nut, Thomson), mounted to a turntable (ω), served as the specimen platform. A customized damped-vibration table (78-111-02DR-SPECIAL, TMC, Peabody, MA) acted as the system's base.

The actuator had a nominal stroke of $\pm 6\text{mm}$ with a positional repeatability of $6\mu\text{m}$ root-mean-square compared to an analog dial-gauge ($1\mu\text{m}$ resolution, Kafer, Germany). The actuator was controlled by WinTest software (Bose, Eden Prairie, MN). All injuries were conducted under displacement feedback proportional-integral-derivative control though force feedback was also available. The system was tuned to produce injuries at an intended peak velocity of 100cm/s which is similar in scale to that believed to occur in humans (Panjabi et al., 1995; Nightingale et al., 1996). Transducers were initially sampled at 4kHz and this was increased to 8kHz following software upgrade. Displacement was measured using a linear variable differential transformer (Model MHR250, Schaevitz Sensors, Hampshire, UK) integrated within the actuator chassis. Interchangeable load cells were used to measure forces (reported here in Newtons, where $1\text{N} = 100\text{kdynes}$) in contusion (22N Model 31, Honeywell-Sensotec, Columbus, OH), fracture-dislocation (225N Model 31, Honeywell-Sensotec) and distraction (225N Model 31, Honeywell-Sensotec; 444N Model 208C02 PCB Piezotronics, Depew, NY). Sensor capacities were chosen to accommodate for potentially high inertial forces (i.e. forces required to accelerate the instrumentation's mass irrespective of the forces applied to the specimen) and were calibrated to specific ranges to optimize measurement accuracy. For contusion injuries, the root-mean-square accuracy—a type of average error (Choo and Oxland, 2003)—over a $\pm 15\text{N}$ range was 0.03N with

a maximum error of 0.04N. For dislocation and distraction injuries, the root-mean-square accuracy over a $\pm 100\text{N}$ range was 0.1N with a maximum error of 0.2N. Accelerometers (50G Model 355B03, 500G Model 355B02, PCB Piezotronics) were used for inertial compensation of dynamic force measurements (Stokes et al., 1992). Data were digitally filtered (Lyons, 1997) with a 1kHz zero-phase Butterworth low-pass filter (4kHz data with 4-pole, 8kHz data with 6-pole).

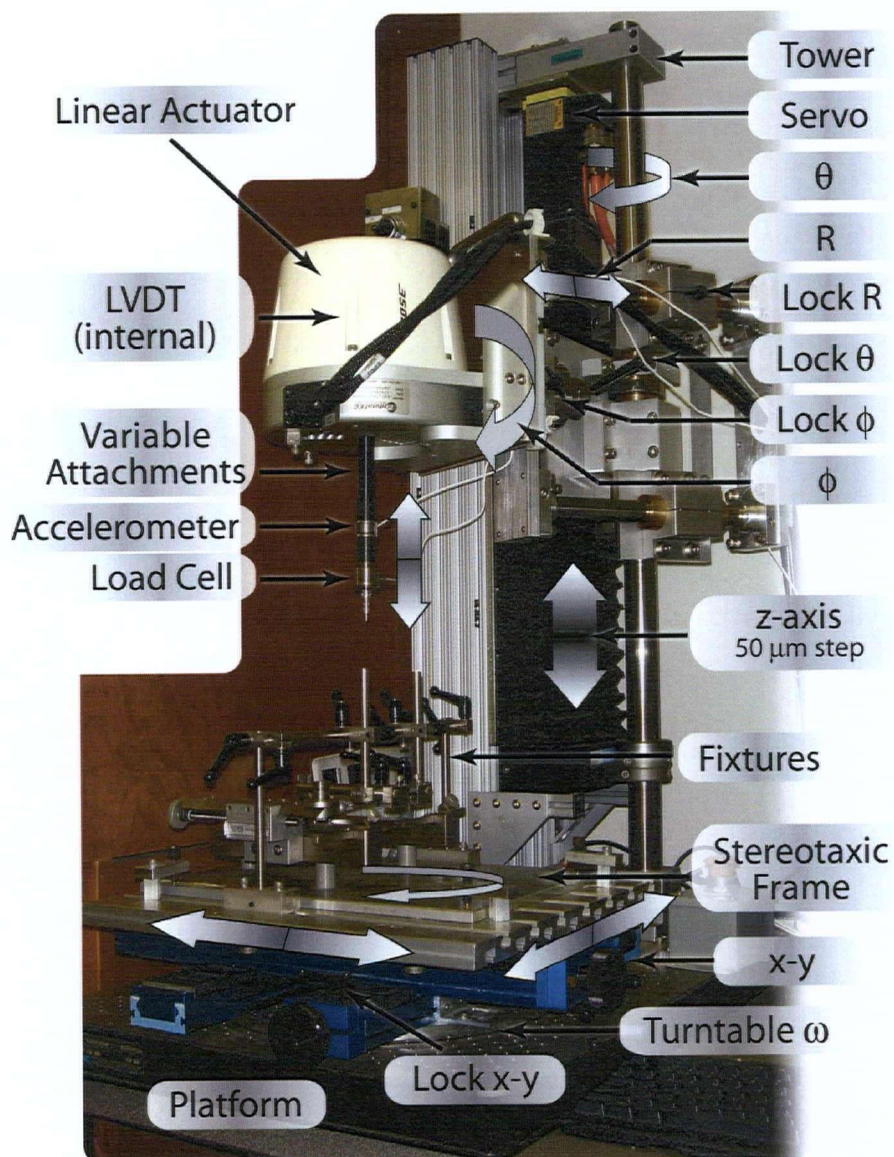


Figure 2.1: Multi-mechanism injury system

Injuries were produced with an electromagnetic linear actuator under displacement feedback control. Seven degrees of freedom enabled positioning of the actuator and animal at any orientation relative each other. Sensors included a linear variable differential transformer (LVDT) to measure displacement, interchangeable load cells (22N, 225N, 444N) and interchangeable accelerometers (50G, 500G).

2.2.2 Part 1: Vertebral Clamps

Mechanical testing was used to evaluate clamping strategies for holding the vertebrae to produce injuries. Clamping stiffness and failure load were used as outcome measures. A high stiffness (i.e. rigid hold of the vertebrae) ensures accuracy in the imposed displacements, while a high failure load ensures the vertebrae do not slip from the clamp's grasp or fracture when injury forces are applied. Spinous process clamps were tested first. Although this method has been successfully applied for contusion (Behrmann et al., 1992), it was unclear whether it would be suitable for the higher forces required to produce dislocation and distraction. Eight fresh-frozen (i.e. without paraformaldehyde fixation) Sprague-Dawley rats (mean \pm S.D. weight = 267 \pm 71g) were used. Allis clamps held the spinous process of T8 and T10. Force was applied dorso-ventrally to the intact lamina of T9 until the spinous processes fractured or slipped from the grasp of the Allis clamps. The maximum force applied prior to vertebral fracture or slippage was defined as the failure load and demarcates the useable limit of the clamping strategy. Forces were applied at a rate of 2.5cm/s using a servohydraulic actuator (Dynamite, Instron Corp., Norwood, MA). The slow rate was a limitation of the actuator. Mechanical tests of biological tissue usually employ cyclic preconditioning or preload to remove measurement artifacts near the beginning of the tests (Fung, 1993), however, neither of these were used because preliminary trials indicated a risk of premature failure.

The results of the Allis clamp tests necessitated the development of stainless-steel vertebral clamps designed to wedge beneath the cervical transverse processes against the lateral masses (Figure 2.2A, B). For dislocation (Figure 2.2C) and distraction (Figure 2.2D), a rostral clamp held C3 and C4 while a caudal clamp held C5 and C6. Extensions in the jaw serrations were incorporated at the C4/5 facet junction in order to eliminate clamp slippage during distraction (Figure 2.2F, G). The contusion clamp (Figure 2.2E) supported C4 and C5 together.

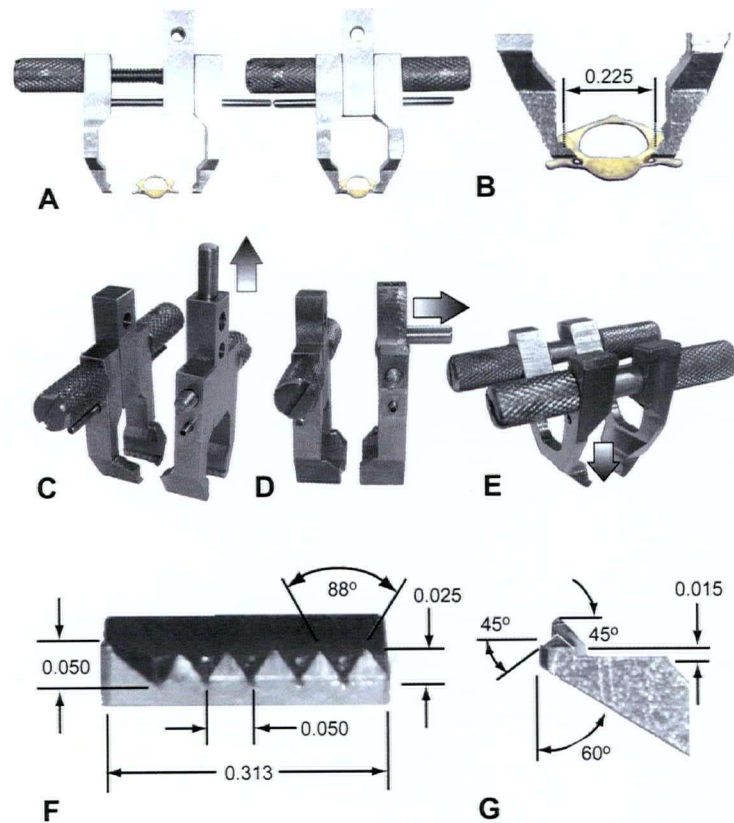


Figure 2.2: Cervical vertebral clamps and dimensions

Clamps closed (A) to support cervical vertebrae beneath the transverse processes (B) for dislocation (C), distraction (D), and contusion (E). Block arrows denote direction of injury vector. Dimensions shown in inches (B, F, G) were suitable for C3 to C6 of 300-350g male Sprague-Dawley rats. Suggested tolerance <0.002 in.

The mechanical characteristics of the novel clamping strategy were evaluated in the (weaker) dorso-ventral direction using the version designed for contusion (Figure 2.2E) with failure loads applied using the new SCI system. Eighteen cadavers of freshly euthanized (without paraformaldehyde fixation) Sprague-Dawley rats (mean \pm S.D. weight = 300 ± 42 g) were used. Specimens were evenly divided into three load-to-failure groups: cervical fast ramp, thoracic fast ramp, and thoracic slow ramp. The prescribed ramp loading rates were 100cm/s (fast) and 3cm/s (slow) applied on the intact laminae of C4 or T10. High rates were used to simulate traumatic injury speeds (Panjabi et al., 1995; Nightingale et al., 1996) while slow rates were used to facilitate comparisons with Allis clamp testing. A preload of 0.1N was used to establish lamina contact. In the cervical tests, the clamp was centered at C4 with support extending to C3 and C5. In the thoracic tests, the clamp was centered at T10 with support extending to T9 and T11. T9 was not selected as the centre because the narrower T8 would not have been supported.

For all mechanical tests, the failure load was manually identified and the stiffness was defined by the steepest regression line fitted to 5 consecutive data points within the initial portion (<1mm) of the force-displacement curve. Ideally, the clamping would be infinitely stiff meaning there would be no loss of injury accuracy due to movement of the vertebrae from the clamp's grasp. The movement of the vertebrae at typical loads for contusion (2N) and dislocation (10N, 20N, 30N) was determined. For the Allis clamps, these deflections were calculated using the slope (deflection = force/stiffness) and hence avoided the displacement artifact in the toe region that resulted from the lack of preconditioning. For the novel clamps, the displacements were taken from the load-displacement curve—including any toe region—and thus the analysis was conservative; biased against the novel design.

2.2.3 Part 2: Injury Models

Immediate injury mortality (dislocation, distraction) and primary hemorrhage volumes (dislocation, contusion) were chosen to characterize acute injury severities. All procedures were approved by our institution's Animal Care Committee in accordance with the guidelines published by the Canadian Council on Animal Care. Forty-three male Sprague-Dawley rats (mean \pm S.D. weight = 311 \pm 26g) were divided into three groups (n = 14 dislocation, n = 21 distraction, n = 8 contusion). Animals were anesthetized with an intraperitoneal injection of ketamine (80mg/kg) and xylazine (10mg/kg) and maintained under deep anesthesia throughout the tests. All animals were secured in a similar manner within a stereotactic frame with the head in flexion to remove cervical lordosis.

To model fracture-dislocation (Figure 2.3A & D), the dorsal ligaments and facets at C4/5 were removed to mimic the type of posterior element fracture and ligament injury commonly seen in a bilateral facet fracture-dislocation. The lamina remained intact at each level. C3 and C4 were clamped together and held stationary while the clamp holding C5 and C6 was coupled to the actuator and dislocated dorsally thus reproducing the displacement pattern seen in human fracture-dislocations. Forces were continuously monitored during coupling between the caudal clamp and the actuator to ensure no cord damage prior to the injury stroke. Dislocations ranging from 2.3mm to 3.7mm were used to investigate severity. Following dislocation, the rostral and caudal vertebral clamps were clamped together to prevent further movement at C4/5.

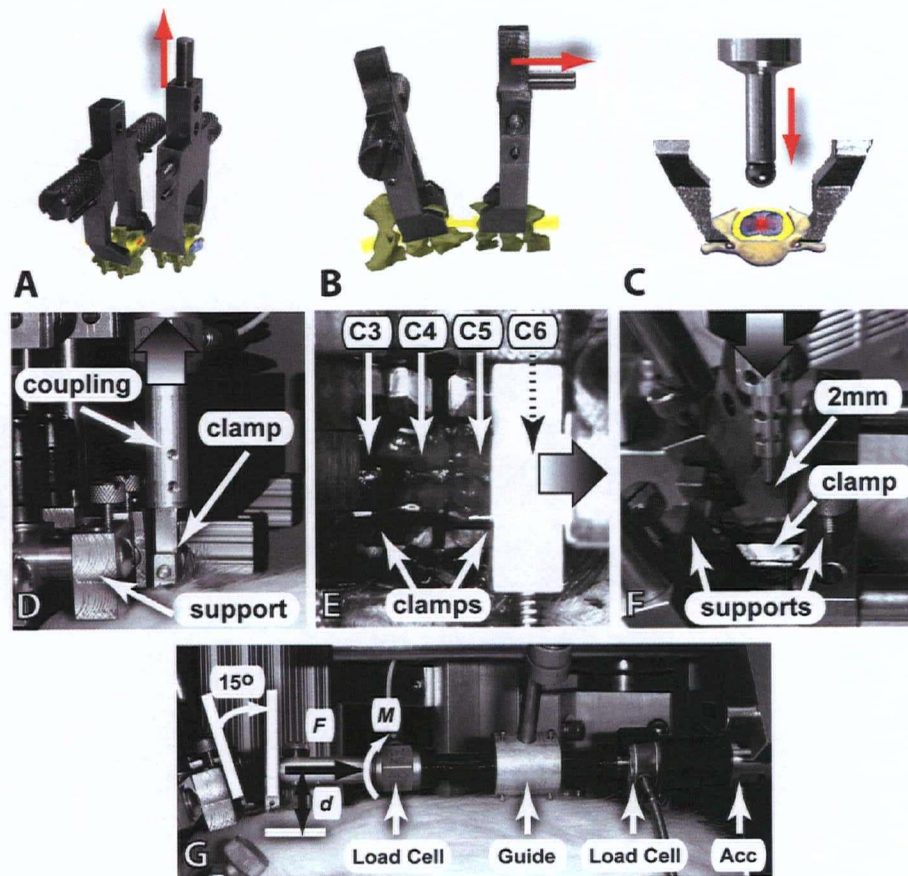


Figure 2.3: Illustrations and photos of experimental injury configurations

To model dislocation (A & D), the rostral (left) vertebral clamp was held stationary while the caudal (right) clamp was coupled to the actuator for dorsal translation. For distraction injuries (B & E), C3 and C4 were held stationary while C5 and C6 were translated caudally. Dorsal view is shown in E. In the contusion model (C & F), the vertebral clamp holding C4 and C5 was supported while the 2mm spherical head impactor injured the cord through a laminectomy. G. Distraction force vector (F) was applied at $d = 25.4\text{mm}$ (1.0 in) from the axis of the clamp. The resultant moment (M) was constrained using a ceramic guide. Continuous monitoring of strain gauge load cell (right) ensured negligible forces were applied during actuator positioning and coupling. Piezoelectric load cell (left) was able to tolerate moment and used to empirically determine dynamic bearing friction. Acc denotes accelerometer. Proportions in A-C are only approximate.

For distraction (Figure 2.3B & E), the facets at C4/5 were removed. Three animals were secured on the stereotactic frame with 0° of flexion at C4/5 measured using a digital inclinometer (0.1° resolution). For the remaining eighteen animals, 15° of flexion (approximate physiological limit) was used to more closely mimic human injuries (Giacobetti et al., 1997). C3 and C4 were clamped and held stationary while the clamp holding C5 and C6 was distracted caudally, held for one second, then returned to its initial position. Displacements ranged from 5.1mm to 6.1mm (without flexion) and 4.1mm to 4.6mm (with flexion). The one second dwell enabled visual confirmation under stereomicroscopy that the clamps did not slip rostro-caudally. For contusion

and dislocation, clamp slippage was not possible without transverse process fracture (Figure 2.2B). The distraction vector was applied at 25.4mm (1.0 in) above the level of the facets (Figure 2.3G). A ceramic guide was used to constrain the resultant moment ($M = F \times d$) and prevent uncontrolled clamp deflection. In separate trials using a piezoelectric load cell (444N Model 208C02, PCB Piezotronics, Depew, NY) capable of tolerating the moment, the bearing friction was found to be $F_{friction} = 0.068 \times F_{max} + 3.554$ and was used to correct the measured peak distraction loads. As in dislocation, forces were monitored during actuator coupling and the vertebral clamps were clamped together post-trauma to prevent additional SCI.

In the contusion experiments (Figure 2.3C & F), the dura was exposed with partial laminectomies on the caudal side of C4 and rostral side of C5. The motorized z-axis was used to lower the actuator chassis in 50 μ m step increments at a rate of approximately two steps per second until an initial touch force of 0.03N was detected, thereby dimpling the dural surface and displacing the cerebrospinal fluid (CSF) beneath (Stokes et al., 1992; Pearse et al., 2005). The actuator's 2mm spherical head impactor, similar in dimension to impactors commonly used (Behrmann et al., 1992; Gruner, 1992; Scheff et al., 2003), was then retracted from the dimpled dura and accelerated downward to produce the contusion. For the first five animals, our 50G accelerometer was saturated during peak deceleration hence the inertial force was determined from air impacts in the absence of any specimen (Somerson, 1986; Somerson and Stokes, 1987). A 500G accelerometer was used for the rest of the study.

Unlike dislocation and distraction, immediate mortality was unlikely even at maximum cord compression (Choo et al., unpublished observations). In addition, moderate-severe cervical contusions at C5 had previously indicated a subacute mortality rate of 12.2% for injuries ranging from 0.95 to 1.1mm over the first several days (Pearse et al., 2005). Hence, we assessed the effect of impactor positioning on hemorrhage severity, which has not been previously addressed.

When the contusion impactor is lowered through the laminectomy, the dura is dimpled as CSF is displaced and the dura contacts the spinal cord. Identification of a 0.03N contact force is difficult because as CSF and fluid components within the dura and spinal cord ebb away from the location of applied pressure, the measured force decays—a process called viscoelastic relaxation that is common in many biological tissues (Fung, 1993). Hence, the contact force is not constant over time thereby introducing variability into the determination of this initial contact position.

Note that the actuator itself delivers a highly repeatable injury displacement (S.D. = 0.02 mm) relative to this initial position. The retraction of the actuator above the touch position prior to the downward impact enabled the detection of dural contact and hence the quantification of the different initial contact positions (i.e. dimpled touch depths). Dura contact was detected as an increase in force before the downward accelerating impactor reached its initial dimpled position.

All animals were transcardially perfused with 250mL phosphate buffered saline followed by 500mL of fresh cold 4% paraformaldehyde at 5 minutes post-trauma in order to analyse primary hemorrhage. Spinal cords were post-fixed overnight in 4% paraformaldehyde and cryoprotected in graded sucrose (12, 18, 24%) before being frozen in isopentane cooled with dry ice. Cords were cryosectioned at 20 μ m parasagittally.

2.2.4 Hemorrhage Analysis

Slides from all animals were stained with hematoxylin and eosine (H&E) for analysis of hemorrhage and general morphology. Sections were imaged (5 \times objective lens) using an AxioPlan2 microscope (Carl Zeiss, Thornwood, NY) equipped with monochrome camera with RGB unit (Retiga-Exi, QImaging, Burnaby, BC) using Northern Eclipse software (Empix Imaging, Mississauga, ON). Images were montaged using a motorized scanning stage (Scan 100 \times 100, Marzhauser, Wetzlar-Steindorf, Germany; MAC5000 controller, Ludl, Hawthorne, NY). Volumes were calculated using Cavalieri's method (Howard and Reed, 1998) with a 50 \times 50 μ m² spacing of point probes on sections (14 to 18 per animal) spaced 160 μ m apart. This probe spacing was found to have an area measurement accuracy of 5.6% (root-mean-square) when compared to manual tracing of 20 sections. Image analysis was performed blinded to the injury mechanism and severity using custom software written in Matlab (The MathWorks, Natick, MA).

For dislocation and distraction, logistic regression was used to determine moderate-severe injury severities that we defined by a 10% mortality rate. This mortality rate is comparable to that previously reported for cervical contusions (Pearse et al., 2005) and may be considered the upper limit for ethical approval of future survival studies. For reference, the 50% lethal threshold is reported as well. For dislocation and contusion, linear regression was used to examine the relationships between displacement, force, and hemorrhage volumes. Significance was set at $p < 0.05$. Data are reported as means \pm standard deviations, or ranges when different severities were investigated.

2.2.5 White Matter Immunohistochemistry

Injury in the white matter was qualitatively assessed by immunostaining simultaneously for large caliber axons (mouse anti-NF200, clone N52, Sigma, Saint Louis, MO) and fine caliber axons (mouse anti- β Tubulin Isotype III, clone SDL3D10, Sigma). Sections were washed 3 \times 5 minutes in 0.01M phosphate buffered saline (PBS). Sections were blocked for 30 minutes in normal donkey serum before being incubated for 3 hours at room temperature in primary antibodies diluted (1:400) in 0.01M PBS with 0.1% Triton X-100. Sections were then washed 3 \times 5 minutes in 0.01M PBS and incubated for 1 hour in Cy3-conjugated donkey anti-mouse (cross adsorbed against rat) secondary antibody (Jackson ImmunoResearch Laboratories, West Grove, PA). Sections were washed 3 \times 5 minutes in 0.01M PBS then mounted with Fluoromount-G (SouthernBiotech, Birmingham, AL).

2.3 Results

2.3.1 Part 1: Vertebral Clamps

Mechanical tests using Allis clamps (Figure 2.4A & B, Table 2.1) to hold T8 and T10 resulted in a mean failure load of the dorsal processes at $7.8 \pm 4.2\text{N}$ with a stiffness of $13.1 \pm 9.2\text{N/mm}$. The low failure load indicated this clamping method could not deliver the higher forces necessary to produce injuries such as fracture-dislocation. In addition, the compliance (i.e. inverse of stiffness, 1mm of vertebral movement or slippage per 13.1N of applied force) of the clamped dorsal processes would compromise the accuracy of the imposed displacements.

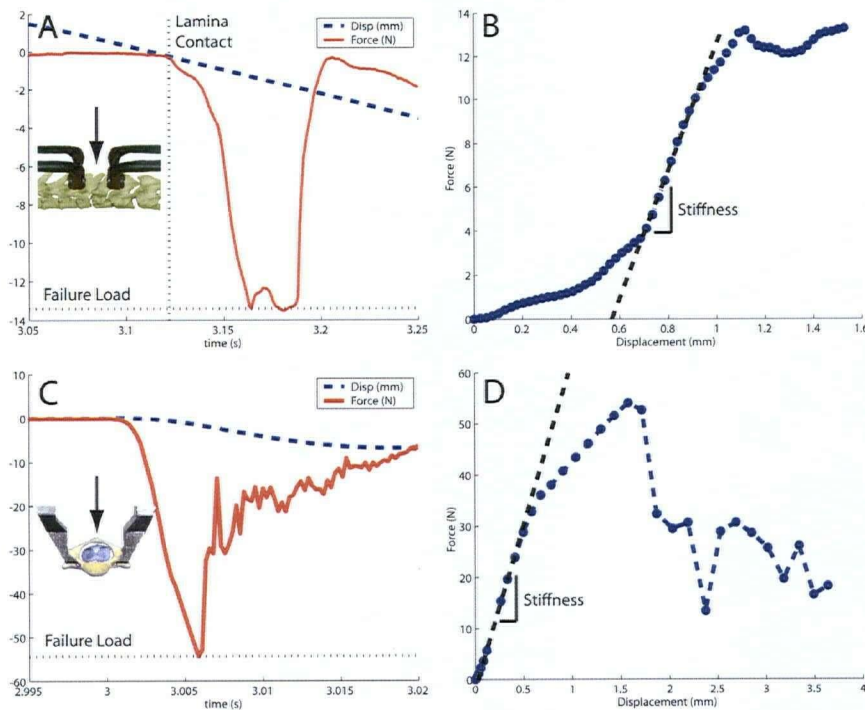


Figure 2.4: Failure and stiffness of Allis clamps and novel vertebral clamps

Representative load-to-failure curves of the mechanical evaluation of the Allis clamps (A & B) and the novel clamps (C & D). Preconditioning was not possible for Allis clamps hence displacement was initiated above the lamina (A). Preload of 0.1N was used to establish contact for testing novel cervical clamps (C). Stiffness was determined from maximum initial slope of force vs. displacement curve (B & D). Insets (A & C) illustrate mechanical testing configuration.

Table 2.1: Vertebral clamping characteristics

	Cervical (fast)	Thoracic (fast)	Thoracic (slow)	Allis (slow)
No. of Animals	6	6	5	8
Loading Rate at Collapse (cm/s)	60.6 (8.3)	72.5 (2.4)	3.0 (0.3)	2.5 (0.2)
Stiffness (N/mm)	83.6 (18.9)	27.4 (2.4)	18.6 (6.3)	13.1 (9.2)
Maximum Load (N)	64.7 (10.2)	38.1 (6.4)	19.9 (7.6)	7.8 (4.2)
Deflections (mm)				
at 2N	0.03 (0.01)	0.12 (0.06)	0.17 (0.12)	0.5 (0.22)
at 10N	0.16 (0.05)	0.56 (0.22)	0.85 (0.32)	-
at 20N	0.32 (0.09)	1.10 (0.34)	1.66 (0.46) ¹	-
at 30N	0.48 (0.11)	1.69 (0.34)	-	-

Clamped vertebrae were loaded to failure with forces (reported in Newtons) applied to the intact lamina of C4 (Cervical), T10 (Thoracic) and T9 (Allis).

Fast and slow refer to loading rates.

Data reported as mean (standard deviation).

Hyphen (-) denotes values not applicable as it exceeds the maximum load

¹ This value was based on $n = 3$ since 2 specimens failed at under 20N.

The optimal vertebral clamping strategy was found to be in the cervical region using the novel clamps (Table 2.1). The cervical spine held with the novel vertebral clamp design (Figure 2.4C & D, Table 2.1) exhibited a stiffness of $83.6 \pm 18.9\text{N/mm}$ and a failure load of $64.7 \pm 10.2\text{N}$ occurred with C4 lamina fracture. The vertebral movement at 2N was found to be $0.03 \pm 0.01\text{mm}$. Larger deflections were found at 10N ($0.16 \pm 0.05\text{mm}$), 20N ($0.3 \pm 0.09\text{mm}$) and 30N ($0.48 \pm 0.11\text{mm}$). When the new clamps were tested in the thoracic spine, the stiffness and failure characteristics were reduced by 40% to 80% (Table 2.1). One specimen in the thoracic slow-ramp group was excluded due to the ambiguity in determining stiffness and failure.

2.3.2 Part 2: Injury Models

The overall maximum loads measured in fracture-dislocation ranged from 13.2N to 30.9N (Table 2.2) and were thus well below the failure loads that characterized the clamp's grasp in the cervical region (64.7N in Table 2.1). Several local peak forces were typically observed, with the initial peak ($19.4 \pm 6.3\text{N}$) at $1.1 \pm 0.5\text{mm}$ likely corresponding to C4 caudal endplate fracture (Figure 2.5A). The loads at maximum displacement ($10.9 \pm 3.5\text{N}$) were less than the maximum forces demonstrating that vertebral column failure had occurred. The peak velocities ranged from 75.3cm/s to 102.6cm/s (mean $95.3 \pm 7.8\text{cm/s}$) with higher velocities achievable for greater injury displacements. Residual dislocation was observed following dislocations greater than 3mm while no measurable residual dislocation was detected at lower severities.

Table 2.2: Mechanical parameters for graded injuries

	Dislocation	Distraction	Contusion
No. of Animals	14	21	8
Displacement (mm)	2.3 – 3.7	4.1 – 6.1	1.1 (0.02)
Force (N)	13.2 – 30.9	24.1 – 43.9	2.1 (0.5)
Velocity (cm/s)	75.3 – 102.6	85.6 – 96.8	97.8 (3.7)
Touch Depth (mm)¹	–	–	0.7 (0.2)
Disp relative to Dura (mm)²	–	–	1.8 (0.2)

For dislocation and distraction, a range of severities are reported. For contusion, means (standard deviations) are reported because a fixed displacement severity was modelled. Hyphen (-) denotes values not applicable.

¹The initial position was inferred from force data (0.03N) and defined as the touch depth. ²Displacement relative to dura was the sum of the actuator displacement and touch depth.

The forces required to axially distract the spinal column (Table 2.2) were higher than for dislocation (Figure 2.5B). The friction correction applied was $6.4 \pm 0.4\text{N}$ in order to account for

the force artifact introduced by the guide bearing. The resulting peak distraction forces ranged from 24.1N to 43.9N (mean 35.6 ± 5.1 N). The peak injury speeds ranged from 85.6cm/s to 96.8cm/s (mean 92.5 ± 2.4 cm/s). Failure of the intervertebral disc at the C4 caudal endplate was consistently observed but was not detectable from the force-time data due to residual support from the surrounding tissue.

A common difficulty of displacement controlled contusion is the need to define the initial position of the impactor and a light contact force of 0.03N is commonly used (Stokes et al., 1992; Pearse et al., 2005) though viscoelastic relaxation of the force introduces variability. As outlined previously in the methods, we lowered the actuator to 0.03N of contact and the resultant touch position was found to be at a 0.7 ± 0.2 mm dimpling of the dura (Figure 2.5C). The actuator was retracted from the dimpled surface and accelerated downward to achieve a high velocity. The mean velocity at dura contact was 109.4 ± 6.4 cm/s and decelerated to 97.8 ± 3.7 cm/s at the initial touch (dimpled) position. The impact depth relative to the initial touch position was 1.1 ± 0.02 mm, however, the impact displacements relative to the dural surface (not dimpled with CSF between the dura and cord) ranged from 1.6mm to 2.2mm with a mean of 1.8 ± 0.2 mm. Since the contusion impacts were directly applied to the spinal cord, the forces (2.1 ± 0.5 N) were lower than in either dislocation or distraction.

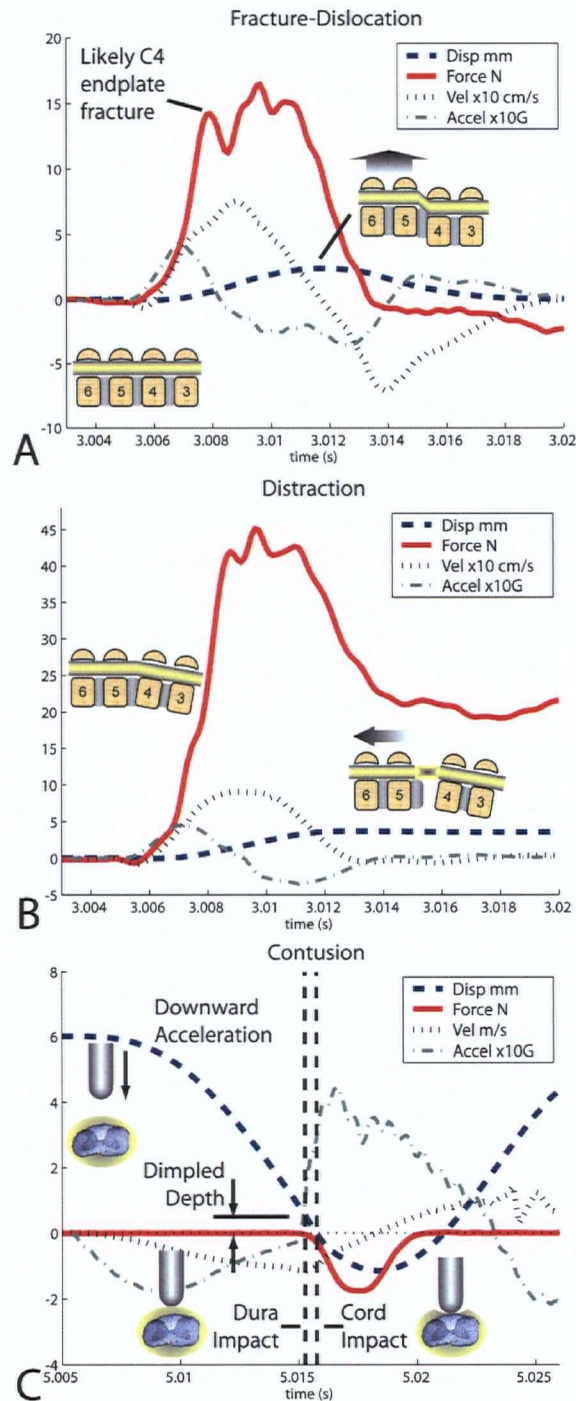


Figure 2.5: Representative curves for graded injuries

Representative curves of mechanical parameters (displacement, force, velocity, acceleration) measured for the three injury models. A. Fracture-dislocation. Inset diagrams show C3 through C6 vertebrae and direction of dislocation. B. Distraction. Inset diagrams show C3 and C4 at 15 degrees of flexion and the distraction vector applied caudally to a clamp holding C5 and C6. C. Contusion. Initial touch position was defined as 0mm and actuator was retracted to +6mm before downward acceleration. Force detected prior to 0mm was indicative of dura contact (i.e. mean 0.7mm dimpled depth).

Logistic regression analysis of fracture-dislocation severity indicated a significant logit fit ($p=0.011$) with estimated mortality rates of 10% at 2.6mm and 50% at 3.1mm of C4/5 dislocation (Figure 2.6A). For vertebral distraction, a significant logistic fit ($p=0.001$) was also found yielding mortality estimates of 10% at 4.1mm and 50% at 4.5mm of distraction between C4 and C5 (Figure 2.6B).

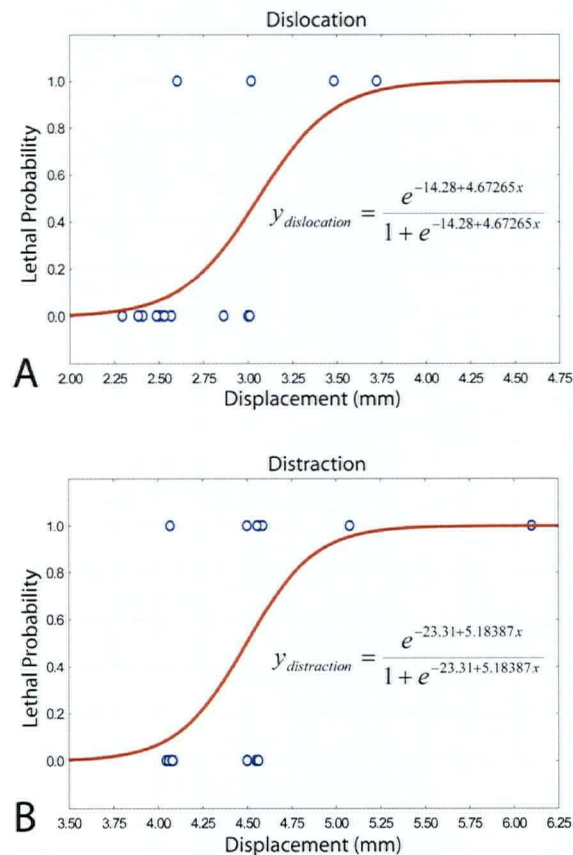


Figure 2.6: Mortality rates for dislocation and distraction injuries

Logistic regression analysis curves for dislocation (A) and distraction (B). Data points at 0 denote non-lethal injuries whereas lethal injuries are plotted at 1.0. Logit fit was significant for both dislocation ($p=0.011$) and distraction ($p=0.001$). The 10% acute mortality rate was found to be 2.6mm of dislocation and 4.1mm of distraction.

Morphology on H&E stained sections showed primary hemorrhage predominantly localized to the gray matter following both contusion (Figure 2.7A) and dislocation (Figure 2.7B). Following dislocation, the hemorrhage volumes ranged from 0.18mm^3 to 2.49mm^3 in the different severities and were observed to extend rostrally from the C4/5 epicentre. In addition, dislocation resulted in shearing of the lateral columns (Figure 2.7C). H&E sections from distraction injuries did not show any obvious hemorrhage (Figure 2.7D).

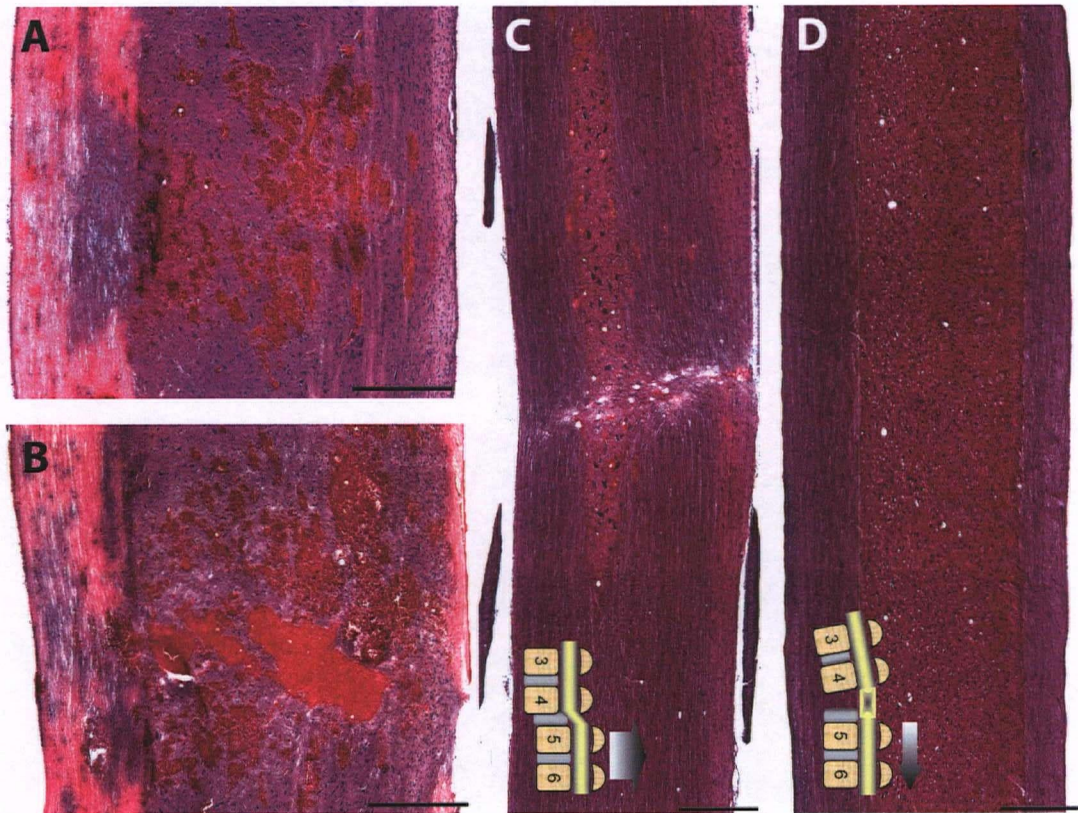


Figure 2.7: Morphology stained with H&E

Central gray matter damage in contusion (A) and fracture-dislocation (B). Lateral column damage was consistently observed following dislocation (C). No obvious pathology following both lethal and non-lethal distraction injuries (D). Scale bars 500 μ m.

Quantitative analysis of hemorrhage following 1.1mm contusion indicated a mean volume of $0.82 \pm 0.52\text{mm}^3$. The variation in the initial touch position ($0.7 \pm 0.2\text{mm}$) used to displace the CSF between the dura and spinal cord did not significantly correlate with differences in the contusion hemorrhage volume ($r^2 = 0.27$, $p = 0.190$; Figure 2.8A). Instead, the contusion force exhibited a significant positive correlation with the hemorrhage volume ($r^2 = 0.51$, $p = 0.048$; Figure 2.8B).

In the dislocation model, no significant correlation was found between the displacement and hemorrhage volume ($r = -0.45$, $r^2 = 0.21$, $p = 0.119$, Figure 2.8C). For dislocations greater than 2.6mm, decreased hemorrhage volumes were observed. There was no correlation between the dislocation force applied to the vertebrae and the hemorrhage volume ($r = 0.26$, $r^2 = 0.07$, $p = 0.391$).

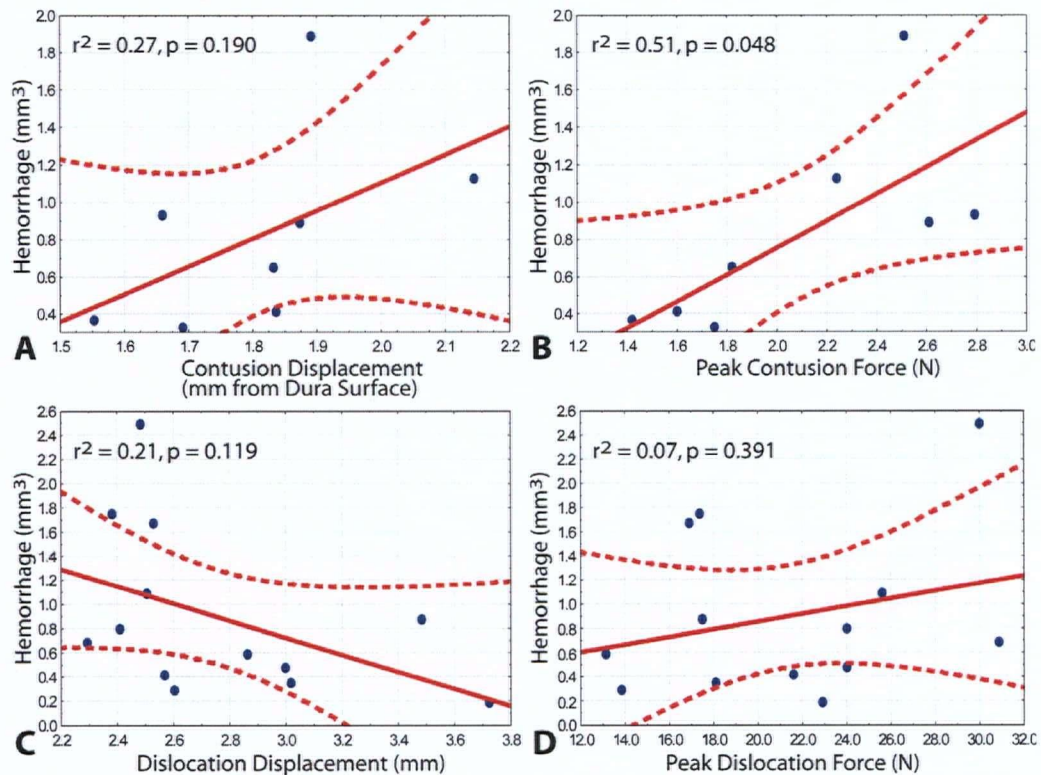


Figure 2.8: Regression curves for hemorrhage versus injury displacement and force

A. Contusion severity was fixed at 1.1mm but variation was caused by viscoelastic relaxation of the spinal cord when determining the initial touch position on dural surface. This variation in touch position did not significantly account for variability in acute hemorrhage volumes. B. Significant correlation was found between hemorrhage volume and peak contusion force. C. As dislocation severity increased beyond 2.5mm, hemorrhage volume decreased. D. The dislocation force applied to the vertebrae was not correlated with the intramedullary hemorrhage severity. Dotted lines mark 95% confidence intervals.

Different patterns of white matter damage were observed on sections immunostained for the neuronal cytoskeleton with neurofilament 200 and β -Tubulin III. At low levels of dislocation (Figure 2.9A), the dorsal and ventral columns were predominantly spared while damage was localized to the gray matter (*asterisk* Figure 2.9A) and the axons bordering this region. At higher magnitudes of dislocation, primary axotomy was observed to extend outward from the gray matter into the dorsal column (Figure 2.9B). Dislocation injury also produced axotomy of fibers in the lateral funiculi (Figure 2.9C & *arrowheads* in D). In contrast, after distraction injuries there were only minor alterations in the neurofilament and β -Tubulin III staining patterns without prominent localized tissue tears or axotomies (Figure 2.9E). In the contusion model, the ventral and dorsal funiculi in most animals were largely spared with damage concentrated centrally (*asterisks* Figure 2.9F). With deeper touch positions, axotomies were also observed in dorsal funiculi following contusion (data not shown).

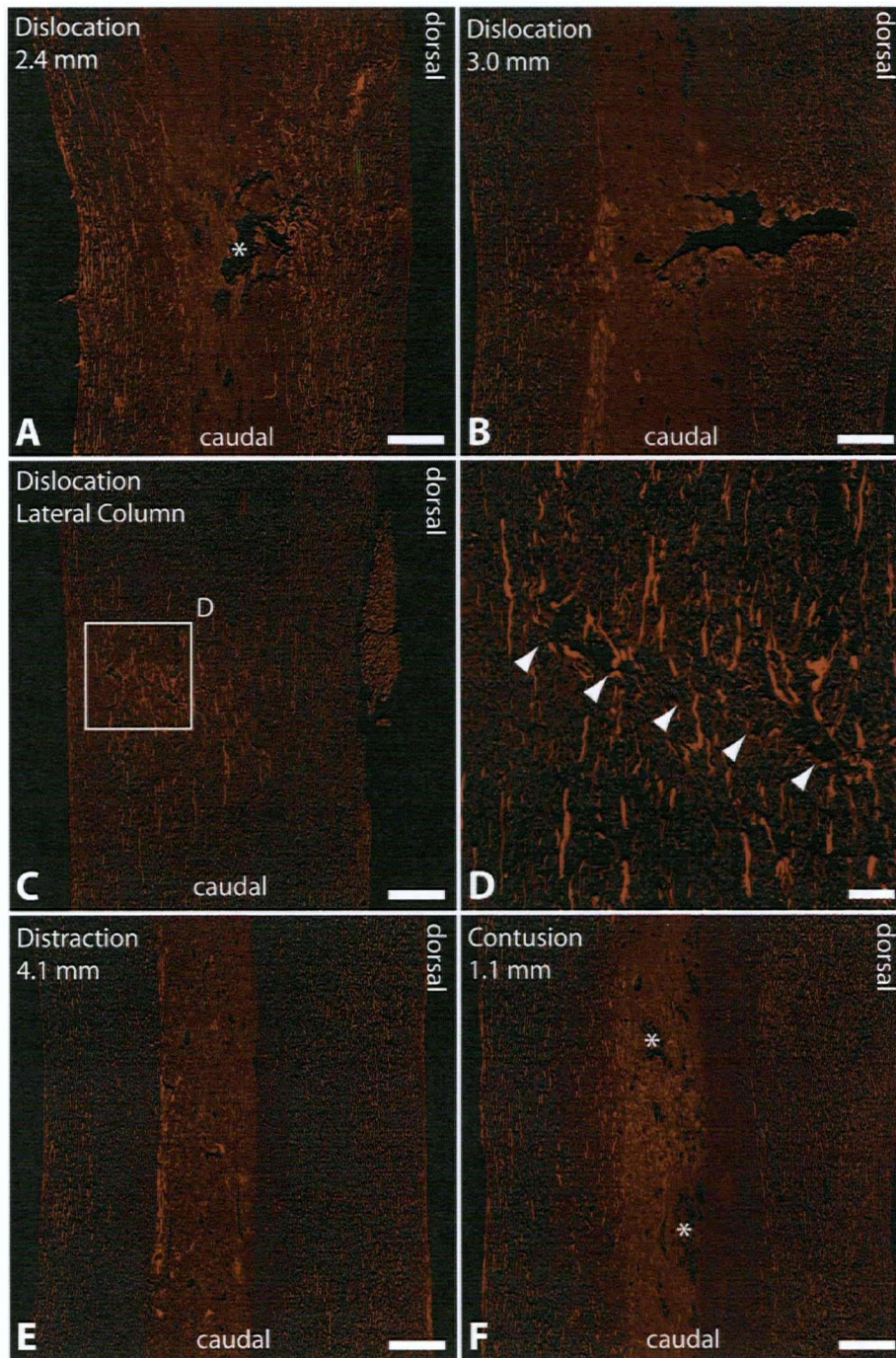


Figure 2.9: White matter damage following three injury mechanisms

Representative parasagittal photomicrographs of white matter immunostained simultaneously for neurofilament 200 (large axons) and β -Tubulin III (fine axons). Near the midsagittal plane, lower magnitudes of dislocation (A) grossly spared the dorsal and ventral white matter with damage originating centrally in the gray matter (*asterisk* in A). At higher magnitudes of dislocation (B), primary damage extended outward into the deep dorsal column. Fracture-dislocation at C4/5 sheared axons in the lateral funiculi (C). *Arrowheads* in D highlight axotomy line. Distraction injuries did not produce gross primary axotomy (E). Peripheral white matter was generally spared following contusion (F) with damage focused in the gray matter (*asterisks* F). Scale bars 250 μ m except in D, 50 μ m.

2.4 Discussion

The objective of this study was to develop a novel device for the experimental modelling of distinct clinically relevant mechanisms of SCI. In part 1, novel vertebral clamps were developed and shown to have a high stiffness (i.e. low vertebral slippage or deflection when force was applied) thereby demonstrating the devices' utility for delivering accurate injury displacements. In addition, the clamping strength (i.e. high failure load) was found to be sufficient to reliably produce high-speed cervical injuries. In part 2, the new devices were used to model contusion, dislocation, and distraction injuries. Injuries were parameterized by controlled displacements rather than forces because in the dislocation and distraction models, forces were applied to the vertebral column rather than to the spinal cord. Moderate-severe injury severities were determined for the dislocation (2.6mm) and distraction (4.1mm) models based on 10% mortality rates that are comparable to rates reported for 0.95-1.1mm cervical contusions (Pearse et al., 2005). In our contusion model, variation in the impactor's contact position on the dura was found to be small (SD = 0.2mm), and did not correlate with intramedullary hemorrhage volumes, suggesting this variation is an acceptable drawback of displacement controlled spinal cord contusion. Primary axotomy in the lateral funiculi was a distinctive feature of dislocation injuries, while contusion and dislocation shared similar patterns of central gray matter damage. Although several reliable injury models are already in widespread use, the methods reported here enable the investigation of distinct biomechanical injuries encountered clinically and hence provide additional pre-clinical paradigms for assessing promising therapies for specific types of injury.

Although the new vertebral clamp design was shown to have optimal mechanical characteristics for producing cervical injuries, we could not draw direct comparisons with Allis clamps. The mechanical testing was performed without the typical contusion model laminectomy. Consequently, the measured failure loads could potentially be higher than with the laminectomized vertebrae. In our hands, Allis clamps tested on intact spinal columns resulted in early failure (<10N) thereby demonstrating the necessity for novel clamps for the dislocation and distraction models. Tests of the new clamp in the cervical spine resulted in fracture of the loaded lamina rather than the pedicle (clamping axis) indicating a conservative estimate of the clamping strength. These failure loads (~65N) were found to be sufficiently high to enable the production of fracture-

dislocation (<31N) and importantly, suggest this clamping method may be adapted as a viable post-traumatic stabilization strategy for longer-term survival studies.

Clinically, intramedullary hemorrhage is a strong predictor of poor neurological outcome (Bondurant et al., 1990; Ramon et al., 1997), though in this study, hemorrhage volumes only correlated with the contusion force. The lack of correlation between contusion displacement and hemorrhage (Figure 2.8A) stems from the relatively narrow variation in the impactor's contact position ($0.7 \pm 0.2\text{mm}$) and thus is a favourable finding in this context – suggesting this undesirable variation has minor effects. In the dislocation model, the injury displacement controls mortality (Figure 2.6A, $p=0.011$) but unexpectedly did not linearly correlate with hemorrhage volumes. *Post hoc* observations indicate, counter-intuitively, that hemorrhage declines at greater severities (Figure 2.8C) but this may reflect hypotension and hypoperfusion caused by the more severe SCIs (Guha and Tator, 1988; Guha et al., 1989). Hence, while hemorrhage is a clinically useful indicator of SCI severity, its utility can potentially be confounded by a reduction in vascular perfusion. The vertebral dislocation force did not correlate with the hemorrhage volume suggesting the model could be improved with additional intramedullary pressure sensors.

The lack of direct visualization of cord-column interaction is a limitation of the closed vertebral column models (i.e. dislocation and distraction). Radiographic studies in the cat suggest a cord-column coupling ratio of approximately 0.5 to 0.8 between the cord and cervical vertebral column (Maiman et al., 1989a) however it is unclear whether this ratio is the same in the rat. The spinal canal diameter and the initial spinal cord tension both likely contribute to variability. In this study, the animal weights varied less than 10% and their position within the stereotactic frame was standardized to minimize these sources of variation. In addition, the surgery time was longer than that typically required for a contusion injury (20-25 minutes vs. 10-15 minutes).

The primary shearing of the lateral columns (Figure 2.7C & 2.9C-D) after fracture-dislocation is distinct from the lateral white matter sparing characteristic of contusion lesions (Blight, 1988; Bresnahan et al., 1991). Both dislocation and contusion severely affect the gray matter of the spinal cord, which will likely lead to the demise of motoneurons and interneurons. Our 5 minute time-window, selected to facilitate comparisons between lethal and non-lethal injuries, was too short to allow for the detection of oxidative stress and apoptotic markers (data not shown) which might be expected to evolve in the dislocation model given the similarity in central

hemorrhage with the contusion model (Hall and Braugher, 1986; Shuman et al., 1997; Springer et al., 1999; Beattie et al., 2002).

The high hemorrhage volume reported in our dislocation injuries differs from the diffuse hemorrhage reported in lateral thoracolumbar dislocation (Fiford et al., 2004). The difference may be attributed to the higher traumatic speed modelled here (95cm/s vs. <15cm/s) as well as the disparity in the vertebral levels (dislocation between two vertebrae [C4 and C5] versus three vertebrae [T12 and T13 and L1]). In addition, although the mechanical tests of the vertebral clamps suggest vertebral compliance of $0.48 \pm 0.11\text{mm}$ at 30N, the loads at maximum displacement were substantially lower ($10.9 \pm 3.5\text{N}$) yielding an estimate of <0.2mm of compliance, reflecting the accuracy of the dislocation magnitude.

Although pure distractive injuries are less common clinically than contusion and dislocation, local tensile forces at the cellular level are widely believed to play an important role in neurotrauma (Breig, 1970; Blight, 1988; Myklebust et al., 1988; Dabney et al., 2004; Henderson et al., 2005). It has often be posited that mechanical failure occurs along principal tensile axes in gray and white matter (Maiman et al., 1989b) producing a central cavitation following contusion (Raynor and Koplik, 1985; Blight, 1988). A distraction model could hypothetically provide a more uniform mechanical loading paradigm for modelling tensile deformation (Myklebust et al., 1988; Dabney et al., 2004; Greaves, 2004) similar to optic nerve stretch methods (Maxwell et al., 1991; Jafari et al., 1998; Bain and Meaney, 2000). However, the distraction modelled here was lethal in the absence of overt mechanical tissue failure and hemorrhage. This appears consistent with reports of cat spinal distraction where it may be interpreted that hemorrhage was rare and cellular injury was not detected until after 24 hours (Myklebust et al., 1988; Maiman et al., 1989b). Although gross disruptions in the cytoskeleton were not detected here, other methods such as electron microscopy might reveal subtler damage (Balentine, 1978; Banik et al., 1982; Maxwell et al., 1991; Anthes et al., 1995; Maxwell and Graham, 1997; Maxwell et al., 1997). Hence, the morbidity reported here is likely a consequence of traumatically induced depolarization of phrenic nuclei spanning C3 through C5 (el-Bohy et al., 1998).

The choice of controlling contusion injuries using force or displacement feedback remains controversial (Scheff et al., 2003; Ghasemlou et al., 2005). Both parameters have correlated with experimental SCI severity (Anderson, 1985; Noyes, 1987a; Behrmann et al., 1992; Scheff et al.,

2003; Ghasemlou et al., 2005). In a behavioural analysis of displacement controlled contusions, a force window of ± 1.3 standard deviations was necessary to isolate distinct biomechanical groups resulting in an exclusion rate of approximately 30% (Kloos et al., 2005). An analogous displacement window has also been advocated for force controlled injuries (Ghasemlou et al., 2005). In the contusions reported here, a new method of vertebral clamping eliminated the vertebral slippage (Stokes et al., 1992; Stokes and Jakeman, 2002) that reduces impact accuracy (Gruner, 1992), and enabled us to isolate the variability of the impactor's initial contact position which we found to be minor. Instead, the relation between force and displacement is likely dominated by variation in the dura, cerebrospinal fluid, spinal cord, vascular anatomy, and perfusion pressure. Given this biological variation, numerous trials over wider severity ranges (i.e. greater than the 0.2mm variation in contact position) are required to clearly see the relation between force and displacement (Scheff et al., 2003; Ghasemlou et al., 2005). Our contusion force, however, significantly correlated with hemorrhage (Figure 2.8B), thereby lending support for the force controlled injury paradigm and its ability to accommodate for potential differences in perfusion pressure, vascular anatomy, and if it occurs, vertebral slippage from the clamps.

In summary, we have developed a novel SCI device and demonstrated the utility of an innovative vertebral clamping method for the production of three biomechanically distinct cervical SCI models. Although cervical models are functionally more severe (Schrimsher and Reier, 1993; el-Bohy et al., 1998), regaining hand function has been identified as by far the highest priority of tetraplegic individuals (Anderson, 2004) and cervical contusions have only recently been addressed (Pearse et al., 2005; Baussart et al., 2006; Gensel et al., 2006). The functional significance of neurons in the cervical enlargement allows for the assessment of both gray and white matter protective strategies utilizing forelimb tests which may have a higher sensitivity than hindlimb locomotor scoring (Onifer et al., 2005). The multi-mechanism system and methods are adaptable for modelling a broad spectrum of clinically relevant injuries in the cervical (Choo et al., 2004), thoracic (Sjovold et al., 2005), and thoraco-lumbar (Clarke et al., 2006) spines. Hence, although well characterized thoracic contusions with their lower morbidity are the most efficient models for exploring novel therapies, other models, such as the set detailed here, may play a valuable role as intermediaries for verifying the robustness of treatments prior to human testing.

2.5 References

- Allen AR (1911) Surgery of experimental lesion of spinal cord equivalent to crush injury of fracture dislocation of spinal column: A preliminary report. *JAMA* 57:878-880.
- Allen AR (1914) Remarks on the histopathological changes in the spinal cord due to impact. An experimental study. *The Journal of Nervous and Mental Disease* 41:141-147.
- Anderson KD (2004) Targeting recovery: priorities of the spinal cord-injured population. *J Neurotrauma* 21:1371-1383.
- Anderson TE (1985) Spinal cord contusion injury: experimental dissociation of hemorrhagic necrosis and subacute loss of axonal conduction. *J Neurosurg* 62:115-119.
- Anthes DL, Theriault E, Tator CH (1995) Characterization of axonal ultrastructural pathology following experimental spinal cord compression injury. *Brain Res* 702:1-16.
- Arundine M, Aarts M, Lau A, Tymianski M (2004) Vulnerability of central neurons to secondary insults after in vitro mechanical stretch. *J Neurosci* 24:8106-8123.
- Bain AC, Meaney DF (2000) Tissue-level thresholds for axonal damage in an experimental model of central nervous system white matter injury. *J Biomech Eng* 122:615-622.
- Bain AC, Raghupathi R, Meaney DF (2001) Dynamic stretch correlates to both morphological abnormalities and electrophysiological impairment in a model of traumatic axonal injury. *J Neurotrauma* 18:499-511.
- Balentine JD (1978) Pathology of experimental spinal cord trauma. II. Ultrastructure of axons and myelin. *Lab Invest* 39:254-266.
- Banik NL, Hogan EL, Powers JM, Whetstone LJ (1982) Degradation of cytoskeletal proteins in experimental spinal cord injury. *Neurochem Res* 7:1465-1475.
- Baussart B, Stamegna JC, Polentes J, Tadie M, Gauthier P (2006) A new model of upper cervical spinal contusion inducing a persistent unilateral diaphragmatic deficit in the adult rat. *Neurobiol Dis.*
- Beattie MS, Hermann GE, Rogers RC, Bresnahan JC (2002) Cell death in models of spinal cord injury. *Prog Brain Res* 137:37-47.
- Behrmann DL, Bresnahan JC, Beattie MS, Shah BR (1992) Spinal cord injury produced by consistent mechanical displacement of the cord in rats: behavioral and histologic analysis. *J Neurotrauma* 9:197-217.
- Blight A (1988) Mechanical factors in experimental spinal cord injury. *J Am Paraplegia Soc* 11:26-34.
- Bondurant FJ, Cotler HB, Kulkarni MV, McArdle CB, Harris JH, Jr. (1990) Acute spinal cord injury. A study using physical examination and magnetic resonance imaging. *Spine* 15:161-168.
- Breig A (1970) Overstretching of and circumscribed pathological tension in the spinal cord--a basic cause of symptoms in cord disorders. *J Biomech* 3:7-9.
- Bresnahan JC, Beattie MS, Todd FD, 3rd, Noyes DH (1987) A behavioral and anatomical analysis of spinal cord injury produced by a feedback-controlled impaction device. *Exp Neurol* 95:548-570.
- Bresnahan JC, Beattie MS, Stokes BT, Conway KM (1991) Three-dimensional computer-assisted analysis of graded contusion lesions in the spinal cord of the rat. *J Neurotrauma* 8:91-101.
- Choo AM, Oxland TR (2003) Improved RSA accuracy with DLT and balanced calibration marker distributions with an assessment of initial-calibration. *J Biomech* 36:259-264.

- Choo AM, Liu J, Lam CK, Dvorak M, Tetzlaff W, Oxland TR (2004) Contrasting Mechanisms of Spinal Cord Injury - Contusion, Dislocation, and Distraction. *J Neurotrauma* 21:1273.
- Clarke EC, Choo AM, Liu J, Lam CK, Bilston LE, Tetzlaff W, Oxland TR (2006) Early Spinal Cord Injury Pathology Development Following Experimental Fracture Dislocation. *J Neurotrauma* 23:770.
- Cullen DK, LaPlaca MC (2006) Neuronal response to high rate shear deformation depends on heterogeneity of the local strain field. *J Neurotrauma* 23:1304-1319.
- Dabney KW, Ehrenshteyn M, Agresta CA, Twiss JL, Stern G, Tice L, Salzman SK (2004) A model of experimental spinal cord trauma based on computer-controlled intervertebral distraction: characterization of graded injury. *Spine* 29:2357-2364.
- Dolan EJ, Transfeldt EE, Tator CH, Simmons EH, Hughes KF (1980) The effect of spinal distraction on regional spinal cord blood flow in cats. *J Neurosurg* 53:756-764.
- el-Bohy AA, Schrimsher GW, Reier PJ, Goshgarian HG (1998) Quantitative assessment of respiratory function following contusion injury of the cervical spinal cord. *Exp Neurol* 150:143-152.
- Fiford RJ, Bilston LE, Waite P, Lu J (2004) A vertebral dislocation model of spinal cord injury in rats. *J Neurotrauma* 21:451-458.
- Fried LC (1974) Cervical spinal cord injury during skeletal traction. *JAMA* 229:181-183.
- Fung YC (1993) *Biomechanics: mechanical properties of living tissues*. New York: Springer.
- Geddes-Klein DM, Schiffman KB, Meaney DF (2006) Mechanisms and consequences of neuronal stretch injury in vitro differ with the model of trauma. *J Neurotrauma* 23:193-204.
- Geddes DM, Cargill RS, 2nd, LaPlaca MC (2003) Mechanical stretch to neurons results in a strain rate and magnitude-dependent increase in plasma membrane permeability. *J Neurotrauma* 20:1039-1049.
- Gensel JC, Tovar CA, Hamers FP, Deibert RJ, Beattie MS, Bresnahan JC (2006) Behavioral and histological characterization of unilateral cervical spinal cord contusion injury in rats. *J Neurotrauma* 23:36-54.
- Ghasemlou N, Kerr BJ, David S (2005) Tissue displacement and impact force are important contributors to outcome after spinal cord contusion injury. *Exp Neurol* 196:9-17.
- Giacobetti FB, Vaccaro AR, Bos-Giacobetti MA, Deeley DM, Albert TJ, Farmer JC, Cotler JM (1997) Vertebral artery occlusion associated with cervical spine trauma. A prospective analysis. *Spine* 22:188-192.
- Greaves CY (2004) *Spinal Cord Injury Mechanisms: A Finite Element Study*. In: *Mechanical Engineering*. Vancouver: University of British Columbia.
- Gruner JA (1992) A monitored contusion model of spinal cord injury in the rat. *J Neurotrauma* 9:123-126; discussion 126-128.
- Guha A, Tator CH (1988) Acute cardiovascular effects of experimental spinal cord injury. *J Trauma* 28:481-490.
- Guha A, Tator CH, Rochon J (1989) Spinal cord blood flow and systemic blood pressure after experimental spinal cord injury in rats. *Stroke* 20:372-377.
- Hall ED, Braughler JM (1986) Role of lipid peroxidation in post-traumatic spinal cord degeneration: a review. *Cent Nerv Syst Trauma* 3:281-294.
- Henderson FC, Geddes JF, Vaccaro AR, Woodard E, Berry KJ, Benzel EC (2005) Stretch-associated injury in cervical spondylotic myelopathy: new concept and review. *Neurosurgery* 56:1101-1113; discussion 1101-1113.

- Howard CV, Reed MG (1998) *Unbiased Stereology - Three Dimensional Measurement in Microscopy*. New York: Springer-Verlag.
- Iwata A, Stys PK, Wolf JA, Chen XH, Taylor AG, Meaney DF, Smith DH (2004) Traumatic axonal injury induces proteolytic cleavage of the voltage-gated sodium channels modulated by tetrodotoxin and protease inhibitors. *J Neurosci* 24:4605-4613.
- Jafari SS, Nielson M, Graham DI, Maxwell WL (1998) Axonal cytoskeletal changes after nondisruptive axonal injury. II. Intermediate sized axons. *J Neurotrauma* 15:955-966.
- Jakeman LB, Guan Z, Wei P, Ponnappan R, Dzwonczyk R, Popovich PG, Stokes BT (2000) Traumatic spinal cord injury produced by controlled contusion in mouse. *J Neurotrauma* 17:299-319 ;217(294):299-319.
- Joshi M, Fehlings MG (2002) Development and characterization of a novel, graded model of clip compressive spinal cord injury in the mouse: Part 1. Clip design, behavioral outcomes, and histopathology. *J Neurotrauma* 19:175-190.
- Kiwerski J (1991) The influence of the mechanism of cervical spine injury on the degree of the spinal cord lesion. *Paraplegia* 29:531-536.
- Kloos AD, Fisher LC, Detloff MR, Hassenzuhl DL, Basso DM (2005) Stepwise motor and all-or-none sensory recovery is associated with nonlinear sparing after incremental spinal cord injury in rats. *Exp Neurol* 191:251-265.
- Kwon BK, Oxland TR, Tetzlaff W (2002) Animal models used in spinal cord regeneration research. *Spine* 27:1504-1510.
- Laplaca MC, Lee VM, Thibault LE (1997) An in vitro model of traumatic neuronal injury: loading rate-dependent changes in acute cytosolic calcium and lactate dehydrogenase release. *J Neurotrauma* 14:355-368.
- Lusardi TA, Wolf JA, Putt ME, Smith DH, Meaney DF (2004) Effect of acute calcium influx after mechanical stretch injury in vitro on the viability of hippocampal neurons. *J Neurotrauma* 21:61-72.
- Lyons RG (1997) *Understanding Digital Signal Processing*.
- Maiman DJ, Coats J, Myklebust JB (1989a) Cord/spine motion in experimental spinal cord injury. *J Spinal Disord* 2:14-19.
- Maiman DJ, Myklebust JB, Ho KC, Coats J (1989b) Experimental spinal cord injury produced by axial tension. *J Spinal Disord* 2:6-13.
- Maxwell WL, Graham DI (1997) Loss of axonal microtubules and neurofilaments after stretch-injury to guinea pig optic nerve fibers. *J Neurotrauma* 14:603-614.
- Maxwell WL, Povlishock JT, Graham DL (1997) A mechanistic analysis of nondisruptive axonal injury: a review. *J Neurotrauma* 14:419-440.
- Maxwell WL, Irvine A, Graham, Adams JH, Gennarelli TA, Tipperman R, Sturatis M (1991) Focal axonal injury: the early axonal response to stretch. *J Neurocytol* 20:157-164.
- Myklebust JB, Maiman DJ, Cusick JF (1988) Axial tension model of spinal cord injury. *J Am Paraplegia Soc* 11:50-55.
- Nightingale RW, McElhaney JH, Richardson WJ, Best TM, Myers BS (1996) Experimental impact injury to the cervical spine: relating motion of the head and the mechanism of injury. *J Bone Joint Surg Am* 78:412-421.
- Noble LJ, Wrathall JR (1985) Spinal cord contusion in the rat: morphometric analyses of alterations in the spinal cord. *Exp Neurol* 88:135-149.
- Noyes DH (1987a) Correlation between parameters of spinal cord impact and resultant injury. *Exp Neurol* 95:535-547.

- Noyes DH (1987b) Electromechanical impactor for producing experimental spinal cord injury in animals. *Med Biol Eng Comput* 25:335-340.
- Onifer SM, Zhang YP, Burke DA, Brooks DL, Decker JA, McClure NJ, Floyd AR, Hall J, Proffitt BL, Shields CB, Magnuson DS (2005) Adult rat forelimb dysfunction after dorsal cervical spinal cord injury. *Exp Neurol* 192:25-38.
- Panjabi MM, Kifune M, Wen L, Arand M, Oxland TR, Lin RM, Yoon WS, Vasavada A (1995) Dynamic canal encroachment during thoracolumbar burst fractures. *J Spinal Disord* 8:39-48.
- Pearse DD, Lo TP, Jr., Cho KS, Lynch MP, Garg MS, Marcillo AE, Sanchez AR, Cruz Y, Dietrich WD (2005) Histopathological and behavioral characterization of a novel cervical spinal cord displacement contusion injury in the rat. *J Neurotrauma* 22:680-702.
- Pickett GE, Campos-Benitez M, Keller JL, Duggal N (2006) Epidemiology of traumatic spinal cord injury in Canada. *Spine* 31:799-805.
- Ramon S, Dominguez R, Ramirez L, Paraira M, Olona M, Castello T, Garcia FL (1997) Clinical and magnetic resonance imaging correlation in acute spinal cord injury. *Spinal Cord* 35:664-673.
- Raynor RB, Koplik B (1985) Cervical cord trauma. The relationship between clinical syndromes and force of injury. *Spine* 10:193-197.
- Rivlin AS, Tator CH (1978) Effect of duration of acute spinal cord compression in a new acute cord injury model in the rat. *Surg Neurol* 10:38-43.
- Salzman SK, Mendez AA, Dabney KW, Daley JC, Freeman GM, el-Tantawi S, Beckman AL, Bunnell WP (1991) Serotonergic response to spinal distraction trauma in experimental scoliosis. *J Neurotrauma* 8:45-54.
- Salzman SK, Dabney KW, Mendez AA, Beauchamp JT, Daley JC, Freeman GM, Fonseca A, Ingersoll EB, Beckman AL, Bunnell WP (1988) The somatosensory evoked potential predicts neurologic deficits and serotonergic pathochemistry after spinal distraction injury in experimental scoliosis. *J Neurotrauma* 5:173-186.
- Scheff SW, Rabchevsky AG, Fugaccia I, Main JA, Lumpp JE, Jr. (2003) Experimental modeling of spinal cord injury: characterization of a force-defined injury device. *J Neurotrauma* 20:179-193.
- Schrimsher GW, Reier PJ (1993) Forelimb motor performance following dorsal column, dorsolateral funiculi, or ventrolateral funiculi lesions of the cervical spinal cord in the rat. *Exp Neurol* 120:264-276.
- Sekhon LH, Fehlings MG (2001) Epidemiology, demographics, and pathophysiology of acute spinal cord injury. *Spine* 26:S2-12.
- Shi R, Pryor JD (2002) Pathological changes of isolated spinal cord axons in response to mechanical stretch. *Neuroscience* 110:765-777.
- Shuman SL, Bresnahan JC, Beattie MS (1997) Apoptosis of microglia and oligodendrocytes after spinal cord contusion in rats. *J Neurosci Res* 50:798-808.
- Silberstein M, McLean K (1994) Non-contiguous spinal injury: clinical and imaging features, and postulated mechanism. *Paraplegia* 32:817-823.
- Sjovold SG, Choo AM, Liu J, Lam CK, Tetzlaff W, Oxland TR (2005) A Controlled Model of Residual Compression Subsequent to a Contusion Injury. *J Neurotrauma* 22:1219.
- Somerson SK (1986) Analysis of an electro-mechanical spinal cord injury device. In: *Bio-Medical Engineering*. Columbus: The Ohio State University.

- Somerson SK, Stokes BT (1987) Functional analysis of an electromechanical spinal cord injury device. *Exp Neurol* 96:82-96.
- Springer JE, Azbill RD, Knapp PE (1999) Activation of the caspase-3 apoptotic cascade in traumatic spinal cord injury. *Nat Med* 5:943-946.
- Stokes BT, Jakeman LB (2002) Experimental modelling of human spinal cord injury: a model that crosses the species barrier and mimics the spectrum of human cytopathology. *Spinal Cord* 40:101-109.
- Stokes BT, Noyes DH, Behrmann DL (1992) An electromechanical spinal injury technique with dynamic sensitivity. *J Neurotrauma* 9:187-195.
- Wolf JA, Stys PK, Lusardi T, Meaney D, Smith DH (2001) Traumatic axonal injury induces calcium influx modulated by tetrodotoxin-sensitive sodium channels. *J Neurosci* 21:1923-1930.
- Young W (2002) Spinal cord contusion models. *Prog Brain Res* 137:231-255.

Chapter 3

DISTRIBUTION OF PRIMARY INJURYⁱⁱ

3.1 Introduction

The tissue damage in spinal cord injury (SCI) is typically described as a central cavitating lesion surrounded by a peripheral rim of spared white matter (Bresnahan et al., 1991). Although transection models are highly prevalent, particularly in regeneration research where spared fibers can introduce ambiguity, contusions are felt to be biomechanically similar to vertebral burst fractures and thus provide the most realistic experimental setting in which to test potential neuroprotective and regenerative strategies (Kwon et al., 2002; Rabchevsky et al., 2002; Pearse et al., 2004; Teng et al., 2004). The pattern of central damage has been consistently reported in numerous experimental animal models that injure the spinal cord by contusion and compression injury mechanisms (Noyes, 1987a; Anderson and Stokes, 1992; Gruner, 1992; Jakeman et al., 2000; Young, 2002; Scheff et al., 2003).

Alternative models to contusion have lagged in development due in part to the current understanding that the secondary biochemical cascade overwhelmingly dominates the neuropathology of SCI. However, the pattern of primary mechanical injury to the spinal cord has rarely been examined in other clinical injury mechanisms such as vertebral fracture-dislocation and distraction. Spinal distraction has been studied by some (Dolan et al., 1980; Myklebust et al., 1988; Maiman et al., 1989a; Maiman et al., 1989b; Dabney et al., 2004) as well as slow distraction for scoliosis correction (Salzman et al., 1988; Sarwark et al., 1988; Salzman et al., 1991), but only one study has modelled dynamic vertebral dislocation (Fiford et al., 2004). Fracture-dislocation shears the spinal cord between adjacent vertebral levels whereas distraction injuries hypothetically stretch the cord axially. These traumatic loading conditions are mechanically distinct from the

ⁱⁱ A version of this chapter has been published. Choo AM, Liu J, Lam CK, Dvorak M, Tetzlaff W, Oxland TR (2007) Contusion, dislocation, and distraction: Primary hemorrhage and membrane permeability in distinct mechanisms of spinal cord injury. *J Neurosurg Spine* 6(3): 255-266.

transient transverse compression of a contusion injury. The spinal cord is comprised of heterogeneous cellular populations that are organized into a tissue structure that is mechanically anisotropic (Arbogast and Margulies, 1998). Biomechanically, one would expect the characteristics of the tissue damage to depend on the direction of trauma.

It has previously not been possible to experimentally compare clinical injury mechanisms in order to identify any mechanism-specific characteristics which may be exploited to enhance treatment strategies. The multi-mechanism devices and animal models profiled in chapter 2 of this thesis enabled the comparison of primary mechanical injuries that are addressed in the current chapter.

The objective of this study was to compare the primary damage in three distinct models of cervical SCI – contusion, fracture-dislocation and flexion-distraction. We focused on vascular damage and compromised membrane integrity as injuries to these structures are key primary events in the neuropathology of SCI. Hemorrhage has been widely correlated in the clinical literature with poor functional outcomes (Bondurant et al., 1990; Flanders et al., 1990; Flanders et al., 1996; Ramon et al., 1997). Meanwhile, traumatically induced increases in membrane permeability and the subsequent loss of ionic homeostasis results in a range of pathologic sequelae including signal conduction failure (Galbraith et al., 1993; Shi and Blight, 1996) and the influx of calcium ions which has been linked to myriad degenerative processes (Young, 1992; Stys, 2004; Sullivan et al., 2005).

3.2 Materials and Methods

All procedures were approved by our institution's Animal Care Committee in accordance with the guidelines published by the Canadian Council on Animal Care. Thirty-six male Sprague-Dawley rats (mean \pm SD weight = 319 \pm 26g) were divided into three injury groups ($n = 9$ contusion, $n = 10$ dislocation, $n = 9$ distraction) and three sham surgical control groups ($n = 2$ contusion, $n = 3$ dislocation, $n = 3$ distraction). Animals were anesthetized with an intraperitoneal injection of ketamine (80mg/kg) and xylazine (10mg/kg) and maintained under deep anesthesia throughout the tests. Fluorescein-dextran with a molecular weight of 10kDa (0.375mg diluted in 15 μ L dH₂O, Molecular Probes, Eugene, OR) was infused into the cisterna magna 1.5 hours prior to injury in order to detect increases in membrane permeability (Pettus et al., 1994; Singleton and

Povlishock, 2004; Stone et al., 2004). Custom designed stereotactic clamps were used to rigidly hold the cervical vertebrae between C3 and C6 laterally beneath the transverse processes.

All injuries were produced under displacement feedback control using the SCI multi-mechanism system described in chapter 2 of this thesis (Figure 2.1). The surgical procedures are described in chapter 2 and summarized briefly here. For contusion, C4 to C5 were held as a single continuously supported unit while partial laminectomies on the caudal side of C4 and rostral side of C5 allowed a 2mm spherical head indenter to strike the cord to a depth of $1.1 \pm 0.06\text{mm}$ (SD) to produce a moderate-severe injury (Behrmann et al., 1992; Kloos et al., 2005; Pearse et al., 2005). A touch force of 0.03N on the dural surface was used to establish the initial position (Stokes et al., 1992; Pearse et al., 2005).

For fracture-dislocation, the dorsal ligaments and facets at C4/5 were removed to reduce the possibility of residual dislocation following injury. C3 and C4 were clamped together and held stationary while the vertebral clamp holding C5 and C6 was coupled to the actuator, dislocated dorsally $2.5 \pm 0.16\text{mm}$ (SD), and then returned to its initial position. Trials over a range of displacements indicated 2.5mm was severe, but not lethal (Figure 2.6A), and the likelihood of residual dislocation was negligible.

For flexion-distraction, the facets at C4/5 were removed. The animals were secured on the stereotactic frame with 15° of flexion at C4/5 measured using a digital inclinometer (0.1° resolution). C3 and C4 were clamped and held stationary while the clamp holding C5 and C6 was distracted caudally to a displacement of $4.1 \pm 0.01\text{mm}$ (SD) and held for one second before being returned to its initial position. Preliminary trials indicated the chosen severity was severe but not lethal (Figure 2.6B). The one second dwell was introduced into the protocol to allow visual confirmation under stereomicroscopy that the vertebral clamps did not slip. In contusion and dislocation, dorso-ventral clamp slippage was not possible without fracture of the transverse processes.

Immediately following dislocation and distraction, the vertebral clamps were themselves clamped together to prevent further injury at the now unstable C4/5 joint. Sham injured controls underwent identical surgical procedures and were secured within the stereotactic frame. For contusion, the same touch load was applied then removed. For dislocation and distraction the caudal vertebral clamp was coupled to the actuator without the injury stroke being applied.

Animals were transcardially perfused with 250mL phosphate buffered saline followed by 500mL of freshly hydrolyzed cold 4% paraformaldehyde at 5 minutes post-trauma in order to analyse the primary injury. Spinal cords were post-fixed overnight in 4% paraformaldehyde and cryoprotected in graded sucrose (12, 18, 24% in phosphate buffer) before being frozen in isopentane cooled with dry ice. Cords were cryosectioned at 20 μ m parasagittally.

One set of slides from all animals was stained with hematoxylin and eosin (H&E) for hemorrhage analysis. Fluorescein-dextran was immediately visualizable under epifluorescent microscopy and slides from all animals were also immunostained with mouse anti-NeuN (Serotec, Raleigh, NC) to colocalize dextran-positive neuronal somata. A subset of slides was immunostained with rabbit anti-Kv1.2 (Alomone Labs, Jerusalem, Israel) to detect potassium channels at the nodes of Ranvier. For immunohistochemistry, sections were washed 3 \times 5 minutes in 0.01M phosphate buffered saline (PBS). Sections were blocked for 30 minutes in normal donkey serum before being incubated for 3 hours at room temperature in the primary antibody diluted (1:100 mouse anti-NeuN; 1:500 rabbit anti-Kv1.2) in 0.01M PBS with 0.1% Triton X-100). Sections were then washed 3 \times 5 minutes in 0.01M PBS and incubated in Cy3-conjugated donkey anti-mouse (Jackson ImmunoResearch Laboratories, West Grove, PA). Sections were washed 3 \times 5 minutes in 0.01M PBS then mounted in ProLong anti-fade (Molecular Probes) and sealed with nail polish.

For hemorrhage analysis, sections were imaged using a 5 \times objective on an AxioPlan2 microscope (Carl Zeiss, Thornwood, NY) equipped with monochrome camera with RGB unit (Retiga Exi, QImaging, Burnaby, BC) using Northern Eclipse acquisition software (Empix Imaging, Mississauga, ON). Volumes were calculated using Cavalieri's method (Howard and Reed, 1998) with a 50 \times 50 μ m² spacing of point probes on sections (14 to 18 per animal) spaced 160 μ m apart. The area root-mean-square measurement accuracy of this probe spacing was found to be 5.6% compared to manual tracing of 20 sections.

Fluorescein-dextran and NeuN were imaged with a 20 \times objective. The ventral gray matter and four white matter columns (dorsal, lateral, ventro-lateral, ventro-medial) were imaged at 1mm intervals from (-) 5mm caudal to (+) 5mm rostral to the apparent lesion epicentre using a motorized scanning stage (Scan 100 \times 100, Marzhauser, Wetzlar-Steindorf, Germany; MAC5000 controller, Ludl, Hawthorne, NY). For each specimen, 13 series (3 \times ventral gray, 2 \times dorsal,

2×lateral, 3×ventro-lateral, 3×ventro-medial) of 11 rostro-caudal images (-5mm ... +5mm) were captured.

Dextran penetration into neuronal somata was quantified using $100\times 100\mu\text{m}^2$ unbiased sampling frames (Howard and Reed, 1998). Four frames were randomly placed on each image entirely within the gray matter. To classify neurons, NeuN outlines were superimposed on fluorescein-dextran images (Figure 3.1). The intensity within the outline was compared to the intensity in the background region defined as a perimeter 10 pixels deep. Neurons were classified as positive, negative or neutral (where the mean intensity was within one standard deviation of the background). In addition, dextran-positive cells with neuronal morphology but completely negative for NeuN were classified as a separate group. Counts were normalized to percent cells counted per specimen at the specified rostro-caudal position.

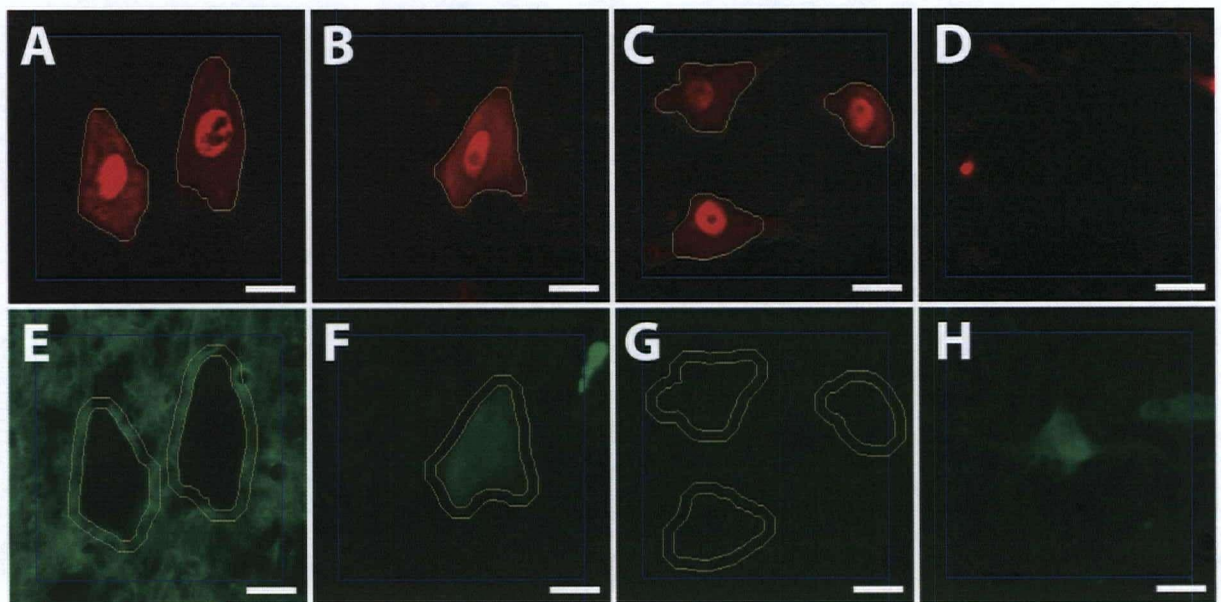


Figure 3.1: Classification of membrane permeability into neuronal somata

Perimeters of NeuN-positive cells (A-C) were overlaid on fluorescein-dextran images and background perimeters were defined (E-G). Cells were counted as negative (E), positive (F), or neutral (G, intensity within one standard deviation of the background) if they fell within randomly placed $100\times 100\mu\text{m}^2$ counting frames. Dextran-positive cells morphologically appearing to be neurons (H) but completely negative for NeuN (D) were classified separately. Scale bar $20\mu\text{m}$. © Journal of Neurosurgery, 2007, by permission.

Dextran entry into axons was quantified using $100\mu\text{m}$ line probes (3 per image) randomly placed within $250\mu\text{m}$ of the superficial tissue boundary. Dextran diffusion into the white matter was found to be inconsistent below this depth. In addition, the boundary constraint improved homogeneity of axon calibers since counts were normalized to axons per millimeter. Profiles

intersecting the line probe were counted as positive if the intensity was above a background threshold and the axon followed a discernable course of $75\mu\text{m}$ (half the distance to next probe) without evidence of dextran excluded and accumulating at nodes of Ranvier (Figure 3.2).

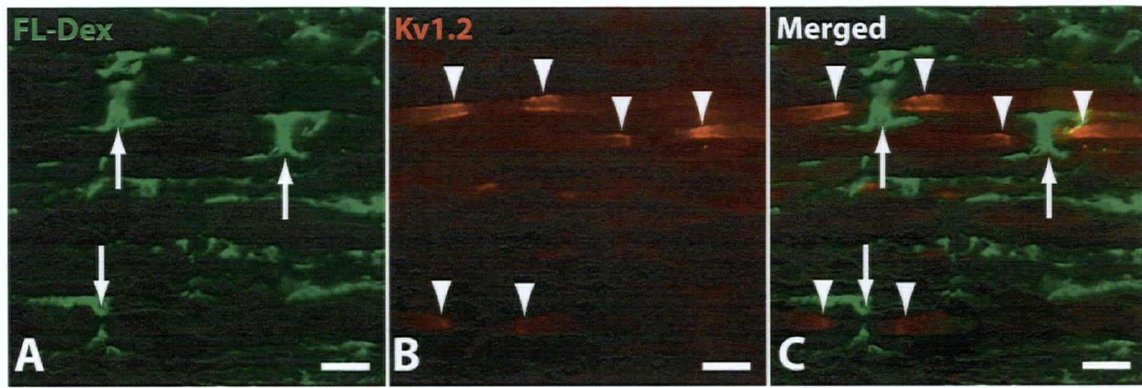


Figure 3.2: Dextran accumulation at nodes of Ranvier

Fluoresceine-dextran (FL-Dex) with a molecular weight of 10kDa is excluded from the intracellular space and accumulates at nodes of Ranvier (*arrows A & C*) that are identified with immunostaining for Kv1.2 potassium channels in the juxtapanodal region (*arrowheads B & C*). Scale bars $10\mu\text{m}$.

All image analysis was performed blinded to the injury mechanism using custom software written in Matlab (The MathWorks, Natick, MA). Quantification was accelerated using routine image analysis tools (Nikolaidis and Pitas, 2001) to semi-automate segmentation, detection, classification and counting. All counts were subjected to human verification and correction for cases where the general algorithms failed.

As count data exhibits a Poisson distribution, where the variance is proportional to the mean, square root transformations were used to ensure homoscedasticity prior to statistical testing (Zar, 1999). Two-way repeated-measures analysis of variance was used to compare the effects of mechanism and rostro-caudal position on membrane permeability in each gray and white matter column. In the two ventral white matter columns, the -5mm position was removed from the ANOVA as there was no variance on which to perform the analysis. Planned comparisons were used to compare the three mechanisms at the lesion (0mm) and rostro-caudal extremes ($\pm 5\text{mm}$, -4mm substituted where necessary). Student-Newman-Keuls post-hoc tests were used to explore the rostro-caudal extent of membrane compromise within in each mechanism. Significance was set at $p < 0.05$.

3.3 Results

One dislocation specimen was excluded due to fracture of the transverse process during the injury. The intervertebral disc at C4/5 consistently failed at the vertebral endplate in all dislocation and distraction injuries. No measurable residual dislocation was detected.

The mechanical data for each injury mechanism differed due to the unique characteristics of each model (Figure 3.3 and Table 3.1). The mean peak injury force for contusion was found to be $2.0 \pm 0.5\text{N}$ (SD). The forces were higher to produce fracture-dislocation ($20.7 \pm 6.5\text{N}$ (SD) and flexion-distraction ($38.6 \pm 3.0\text{N}$ [SD]) as these loads were applied to the spinal column rather than onto the exposed dura/cord. Although the actuator's control system was tuned to deliver the injuries at 100cm/s , some variation was observed with the measured speeds ranging from $91.9 \pm 2.9\text{cm/s}$ (SD) in distraction to $96.7 \pm 4.8\text{cm/s}$ (SD) in contusion.

Table 3.1: Injury parameters for primary injury study

Mechanism	<i>n</i>	Displacement (mm)	Force (N)	Velocity (cm/s)
Contusion	9	1.1 (0.06)	2.0 (0.5)	96.7 (4.8)
Dislocation	9	2.5 (0.16)	20.7 (6.5)	95.1 (9.5)
Distraction	9	4.1 (0.01)	38.6 (3.0)	91.9 (2.9)
Shams	8	—	—	—

Mean and standard deviation of injuries produced under displacement feedback control.

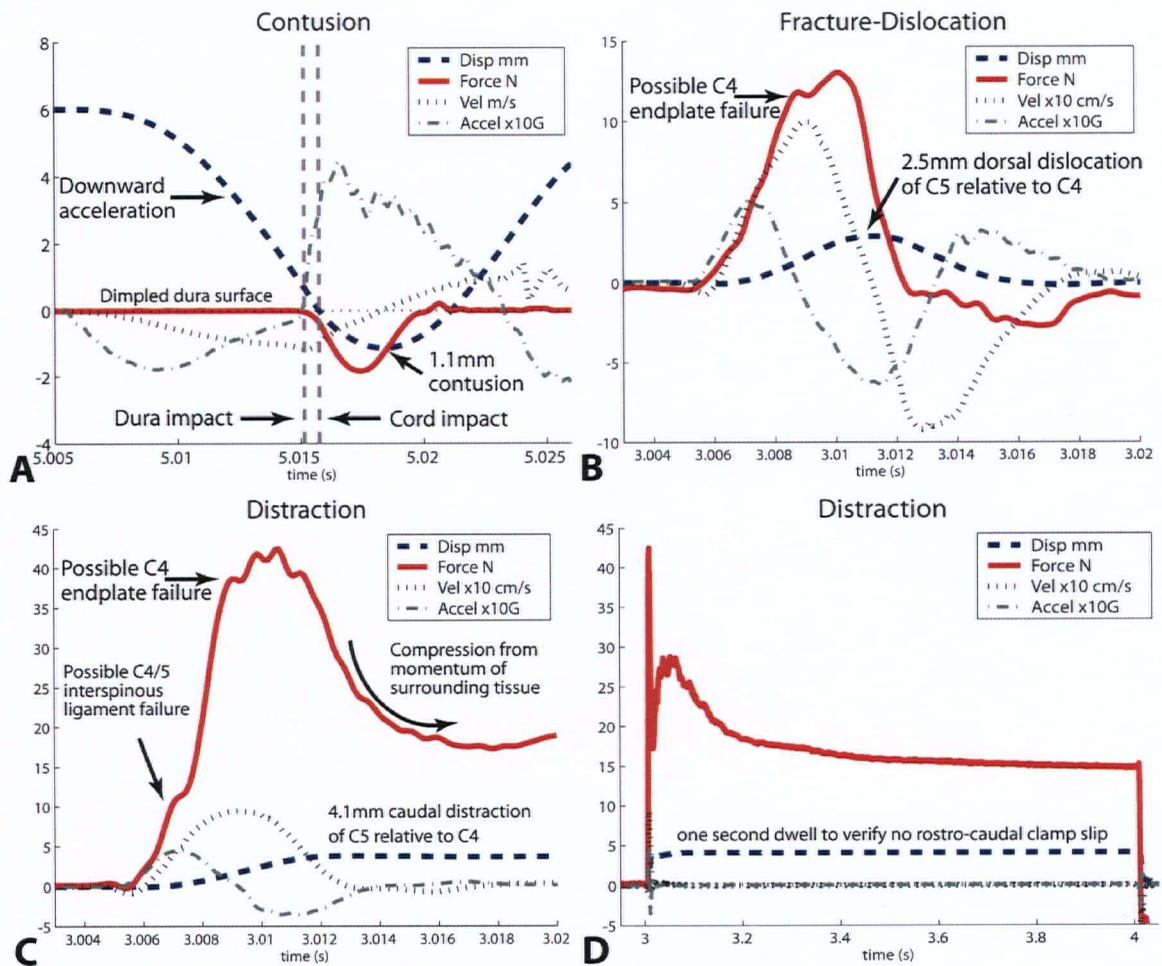


Figure 3.3: Representative mechanical injury curves

A) Dashed line at 0 shows initial touch (0.03N) position which dimpled the cord. The actuator was retracted from the dimpled position and began its downward acceleration from 6mm above the cord. The compressive load prior to 0mm shows impact with dura. B) Fluctuations in force curve during dislocation reflected the failure of different soft-tissues and structures such as the C4 endplate. C) Highest forces were observed in distraction. The initial decline in force at peak displacement was due to the continuing caudal motion of tissue producing compression after the actuator had stopped. Increasing the timescale (D) shows the load increased again before exhibiting viscoelastic decay. Note, y-axis units are listed beside labels. © Journal of Neurosurgery, 2007, by permission.

Contusion and dislocation injuries produced similar patterns of hemorrhage concentrated in the gray matter while no appreciable hemorrhage was observed following distraction (Figure 3.4). Contusion resulted in a mean hemorrhage volume of $1.03 \pm 0.3\text{mm}^3$ (SEM) while a similar volume was found for dislocation ($1.08 \pm 0.2\text{mm}^3$ [SEM]).

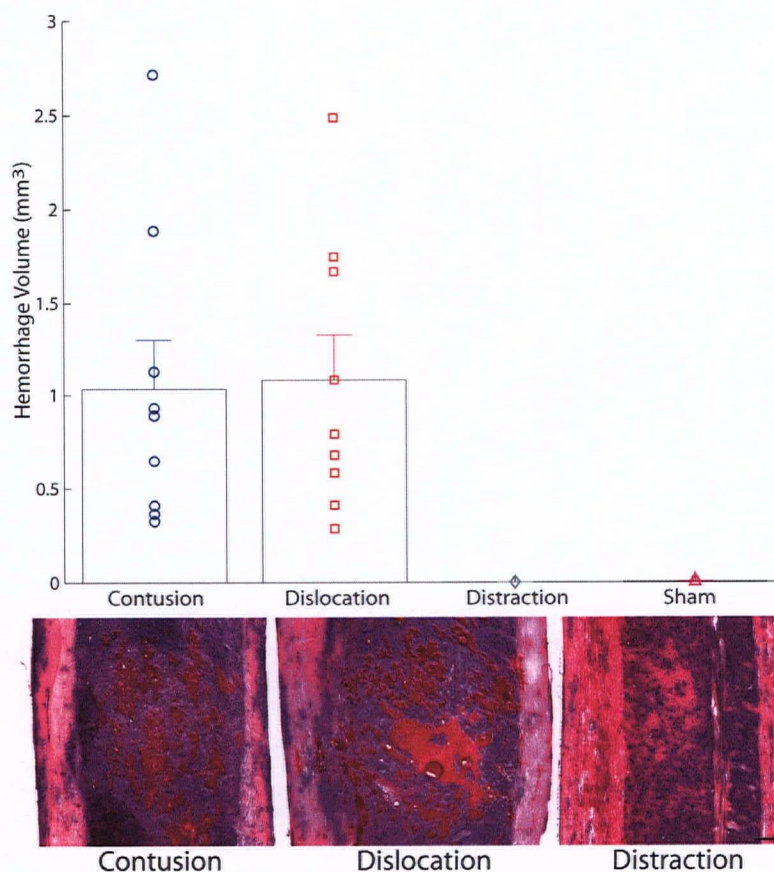


Figure 3.4: Primary hemorrhage volumes following three injury mechanisms

Bar graph and H&E photomicrographs showing that hemorrhage was concentrated in the gray matter following contusion and dislocation but not distraction. Mean hemorrhage volumes and SEMs (nine animals per injury group; eight combined surgical shams) were calculated using point probes and Cavalieri's method. Scale bar 250 μ m. © Journal of Neurosurgery, 2007, by permission.

Qualitatively, different patterns of membrane compromise were observed between the three mechanisms. Following contusion (Figure 3.5, *top panel*), the extent of increased membrane permeability to fluorescein-dextran was generally localized to the lesion epicentre in the gray matter (Figure 3.5E *arrowhead*) and white matter (Figure 3.5B, H *arrowheads*). Distal to the contusion lesion, dextran was observed to be excluded from neuronal somata (Figure 3.5D, F *arrows*) and axons (Figure 3.5A, C, G, I). In this region, dextran accumulated at the nodes of Ranvier (Figure 3.5, *top panel*, *vertical arrows*) and in the vascular endothelium (Figure 3.5, *top panel*, "v") similar to uninjured tissue (data not shown). A transition zone between 1mm and 2mm distal to the lesion was observed where neither dextran-positive axons, nor dextran accumulations at the nodes of Ranvier, were clearly visible suggesting that the myelin sheath had been compromised without axonal damage (Anthes et al., 1995).

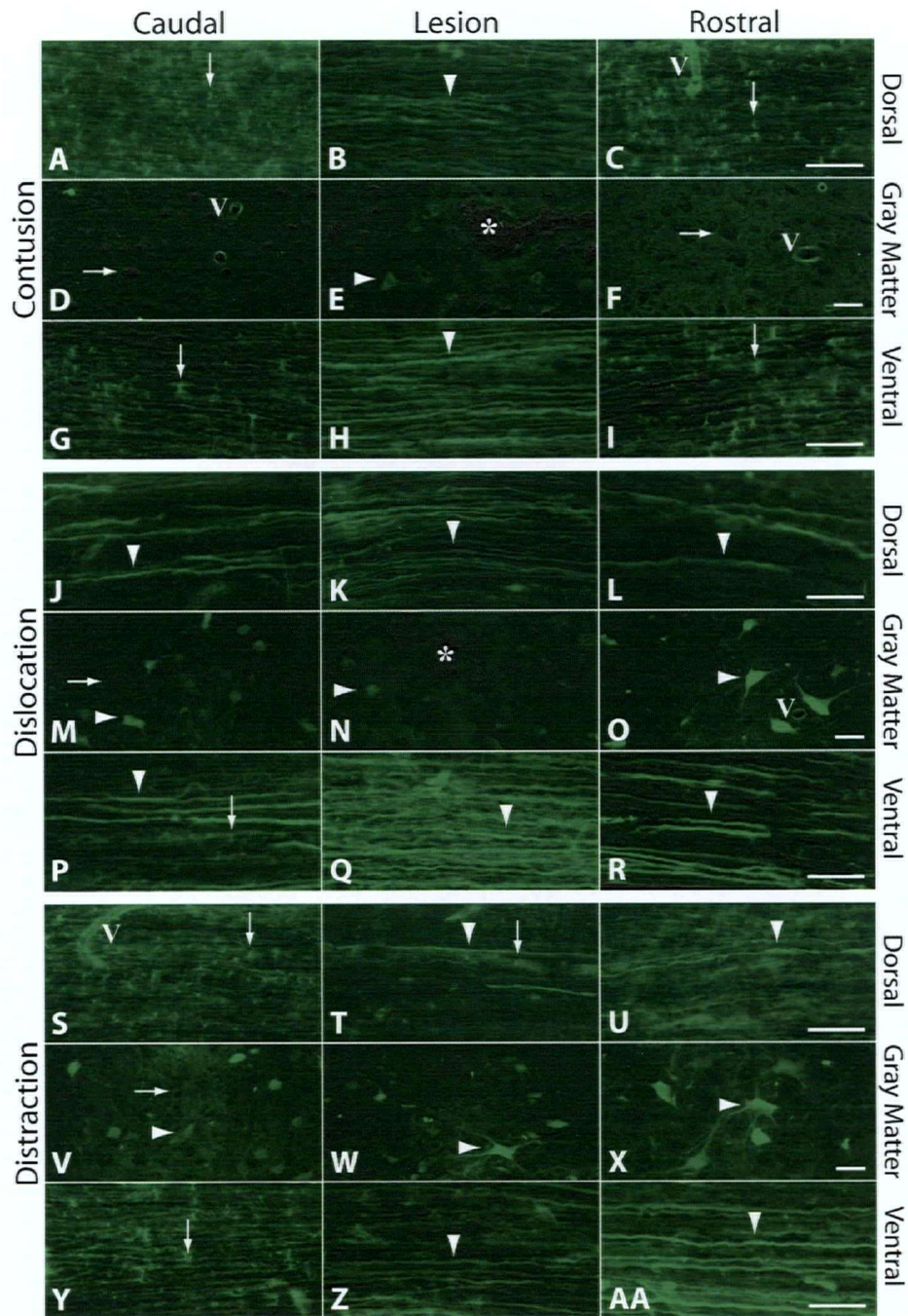


Figure 3.5: Axonal membrane compromise detected with fluorescein-dextran

Photomicrographs demonstrating that membrane compromise evidenced by permeability to fluorescein-dextran was limited to the lesion segment following contusion and extended rostro-caudally following dislocation and distraction. Representative parasagittal images taken from 3mm caudal, the lesion epicentre, and 3mm rostral in the dorsal column, ventral gray matter, and ventro-medial column. Arrows and arrow heads mark one example per image tile. Dextran was observed to accumulate at the nodes of Ranvier of axons with intact membrane integrity (*vertical arrows*). Neuronal somata excluding dextran appeared dark relative to the background (*horizontal arrows*). Dextran-filled axons (*vertical arrow heads*) and neuronal cell bodies (*horizontal arrow heads*) indicated membrane compromise. Immediate necrosis (*) was observed at the lesion following contusion and dislocation. Dextran also enveloped the vascular endothelium highlighting blood vessels (v). Scale bars 50 μ m. © Journal of Neurosurgery, 2007, by permission.

The dislocation lesion epicentre appeared similar to that of contusion with areas of necrosis in the gray matter (Figure 3.5N *asterisk*) and some dextran-positive neuronal somata (Figure 3.5N *arrowhead*) as well as many dextran-positive axons in the white matter (Figure 3.5K, Q *arrowheads*). In contrast to contusion, membrane compromise after dislocation was qualitatively observed to extend several vertebral levels rostrally (Figure 3.5L, O, R *arrowheads*) and caudally (Figure 3.5J, M, P *arrowheads*) to the apparent epicentre. In addition, consistent primary axonal damage was observed in the lateral columns.

Membrane compromise following distraction appeared more diffuse than in either of the other two mechanisms. Necrosis was not observed at the lesion epicentre (Figure 3.5W) in contrast to the other two models (Figure 3.5E, N). Some neuronal somata at the epicentre were dextran-positive (Figure 3.5W, *arrowhead*) and similar to dislocation, elevated membrane compromise was encountered to extend rostro-caudally in the gray matter (Figure 3.5X, V, *arrowheads*). We noticed fewer dextran-positive axons, in the dorsal and ventral white matter at the distraction centre (Figure 3.5T *arrow*) in contrast to contusion and dislocation (Figure 3.5B and K). Similar to dislocation, axonal membrane compromise in the ventral and ventro-lateral columns was observed to extend further rostrally (Figure 3.5U, AA *arrowheads*), however, not caudally (Figure 3.5S, Y *arrows*). Interestingly, in the distraction model we found regions without dextran-positive axons yet lacking the typical dextran accumulations at the nodes of Ranvier reminiscent of the transition zone flanking the contusion lesion.

Quantitative analysis detected statistically significant interactions between the three mechanisms of injury and the rostro-caudal profile of membrane compromise in all gray and white matter columns ($p < 0.001$ for interaction in all ANOVAs). Comparisons in the two ventral columns (Figure 3.6C, D) indicated contusion and dislocation exhibited significantly more axolemma compromise than distraction at the lesion epicentre ($p < 0.015$). However, the pattern was different at 5mm rostral where more dextran-positive axons were detected following dislocation and distraction than resulting from contusion ($p < 0.026$). In the dorsal column (Figure 3.6A), more dextran-filled axons were counted at the contusion and dislocation epicentres than in distraction ($p < 0.001$). Distraction resulted in a greater loss of membrane integrity at 5mm rostral in the lateral column (Figure 3.6B) relative to the other two mechanisms ($p < 0.001$).

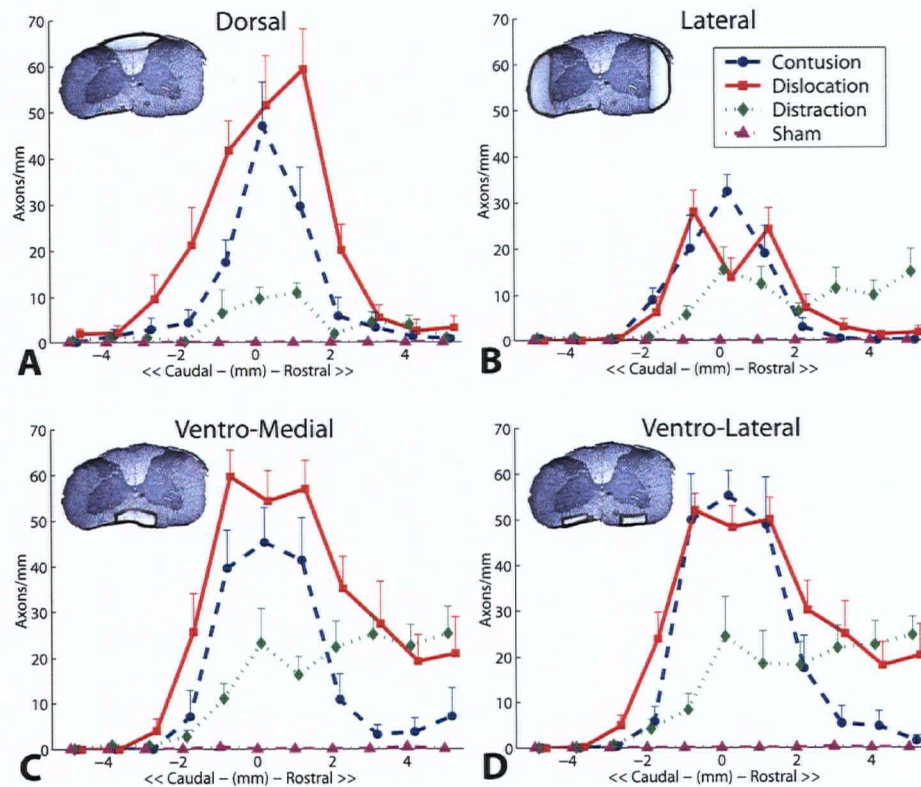


Figure 3.6: Quantitative measurements of dextran-positive axons

Line graphs showing the asymmetric rostro-caudal counts of dextran-positive axons. Zero denotes lesion epicentre. Systematic random sampling was used to quantify axons within $250\mu\text{m}$ of the superficial tissue border. Fluorescein-dextran diffusion past this boundary was inconsistent. Insets highlight sampled regions. Whiskers denote SEM. © Journal of Neurosurgery, 2007, by permission.

Post-hoc analysis revealed distinct rostro-caudal boundaries of axolemma compromise in the ventral white matter (Figure 3.6C-D). In contusion, a significant increase in dextran-positive axons was detected spanning -1mm to $+1\text{mm}$ when compared to boundaries at $\pm 2\text{mm}$ ($p < 0.001$). In dislocation, the degree of axolemma compromise increased between -3mm and -2mm ($p = 0.001$) and remained significantly elevated, although declining, towards 5mm rostral of the lesion ($p < 0.008$ for all comparisons relative to -3mm). Following distraction, significant membrane permeability was seen between -1mm and the lesion epicentre ($p = 0.028$) and maintained a similar level out to 5mm rostral. In the dorsal column (Figure 3.6A), axonal damage after distraction appeared to have a bimodal profile with peaks at $+1\text{mm}$ (11 ± 2 axons/mm [SEM]) and $+3\text{mm}$ (5 ± 2 axons/mm [SEM]). However, *post hoc* analysis of the depression at $+2\text{mm}$ (2 ± 1 axons/mm [SEM]) was not detected as significantly lower than at $+1\text{mm}$ ($p = 0.061$). Sham animals exhibited no membrane compromise in the white matter (Figure 3.6).

In the gray matter, contusion and dislocation resulted in greater plasma membrane compromise than distraction at the lesion epicentre ($p < 0.036$, Figure 3.7A). Dextran-positive neuronal somata were detected rostrally following dislocation and distraction but the counts were not statistically greater than those in contusion ($p > 0.139$). Some increased membrane permeability was found in the gray matter extending from 3mm caudal to 1mm rostral of the sham lesion at C4/5 (Figure 3.7A). Cell bodies morphologically appearing like neurons or larger astrocytes filled with dextran but immunostaining negative for NeuN (Figure 3.2D & H) generally constituted less than 5% of total counts (Figure 3.7B). Peaks of $10.2 \pm 3.5\%$ (SEM) and $5.6 \pm 2.9\%$ (SEM) were found at 2mm rostral to the dislocation and contusion lesion respectively. Contusion and dislocation exhibited peaks at ± 2 mm while the peak in distraction was observed at the lesion epicentre. Neurons that were not distinguishable from the background (Figure 3.2C & G) and hence classified as neutral accounted for $42.1 \pm 7.3\%$ (SEM) to $55.8 \pm 9.1\%$ (SEM) of the counts in sham control animals. This ambiguous population was considered a result of random sectioning of background tissue above and below neuronal somata and hence was not analysed further.

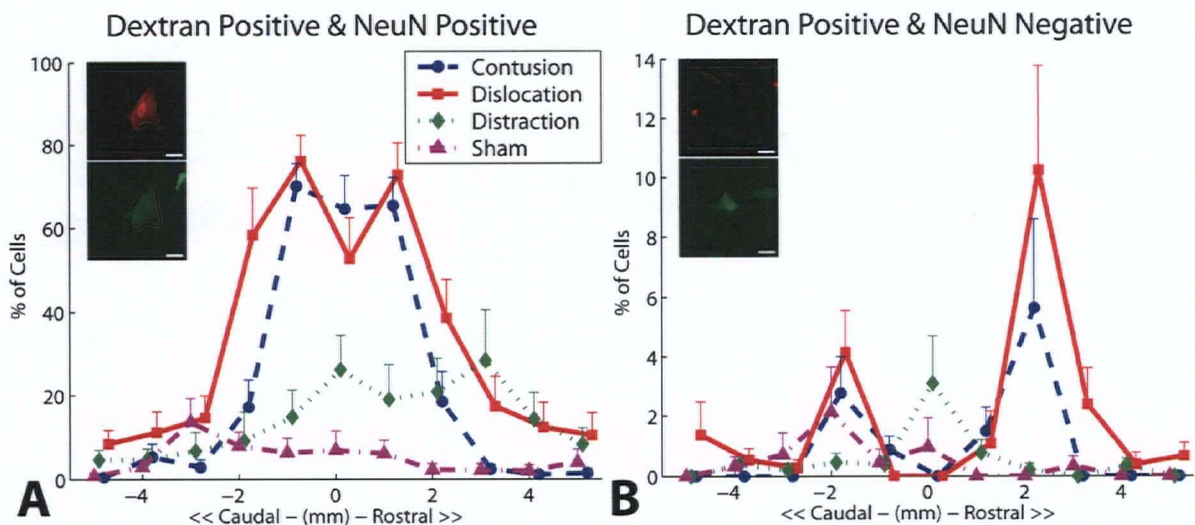


Figure 3.7: Quantitative measurements dextran-positive cell bodies

Line graphs showing the distinct rostro-caudal patterns of dextran-positive neuronal somata. Zero denotes apparent lesion epicentre at C4/5. Counts were normalized to total number of cells counted (NeuN positive + cells with neuronal/large astroglial morphology negative for NeuN) per animal per rostro-caudal location. A) colocalization of dextran-positive cells and NeuN immunostaining. B) dextran-positive cells with neuronal morphology but negative for NeuN. Whiskers denote SEM. Insets show example classifications. © Journal of Neurosurgery, 2007, by permission.

3.4 Discussion

The objective of this study was to experimentally compare three clinically relevant mechanisms of primary spinal cord injury at 5 minutes post-trauma in order to identify differences which may potentially be exploited to guide future clinical paradigms. Hemorrhage and cellular membrane compromise were used as indicators of primary damage since their central role in the initiation of subsequent neuropathology has been well established. The results showed each injury mechanism produced distinct rostro-caudal distributions of primary membrane compromise in both the gray and white matter. Contusion caused localized increases in membrane permeability while fracture-dislocation and flexion-distraction resulted in asymmetric membrane compromise with increased rostral damage. Hemorrhage was similar between contusion and dislocation although not evident following distraction.

There were several limitations to this study. First, given the short survival time, we were not yet able to assess the evolution of the ensuing secondary degeneration nor to determine convergence or divergence of the injury patterns observed. Since the variable under control was the biomechanical injury paradigm, early sacrifice was necessary to enable us to map the initial spatial distribution of mechanically induced damage while limiting confounding secondary events. In addition, without long-term survival data, it remains unclear whether identical injury severities were produced in the three models. Ideally, behavioural measures showing similar functional deficits would be the most clinically relevant demonstration of comparable severities. However, as dislocation and distraction in the rat cervical spine were novel models, a survival study at this stage was considered premature without first establishing that meaningful differences existed to ethically warrant longer survival times. Instead, the lethal thresholds for dislocation and distraction were used as surrogate measures of function and the injury magnitudes in this study were reduced to a level estimated as moderate-severe. Although hemorrhage was not observed following distraction, lethal injuries in graded severity studies also did not exhibit obvious hemorrhage. The use of techniques such as the detection of molecular tracer extravasation across the compromised blood-brain-barrier could have increased the sensitivity of detecting vascular injury following distraction (Noble and Maxwell, 1983; Noble and Wrathall, 1988; Popovich et al., 1996). Recognizing these limitations of a short survival, the study design and analysis focused on generating a detailed rostro-caudal profile in several regions to detect consistent patterns rather than focusing on the

absolute count magnitudes. Alterations in severity would change the individual number of dextran-positive neurons or axons, but the rostro-caudal distributions and differences between tracts would likely remain similar.

Second, the diffusion depth of the 10kDa fluorescein-dextran used in this study prevented analysis of deeper axonal populations. A smaller molecular-weight dextran may have increased the penetration depth, however, *in vitro* data in the literature had indicated the ability of 10kDa to discriminate moderate-severe stretch levels whereas smaller dextrans were able to penetrate uninjured control cells (Geddes et al., 2003).

Third, the counts of dextran-positive neuronal somata and axons have a limited resolution. Extracellular tissue above and below axons and cell bodies appears to obscure the fluorescent dextran signal. This phenomenon likely introduced some bias by reducing the count sensitivity of small neurons, fine axons, and cells with “milder” dextran penetration. In preliminary analysis, dextran penetration or uptake into the fine processes of astrocytes and microglia were found to be difficult to reliably distinguish from background levels while dextran-positive oligodendrocytes were usually detected only at the lesion epicentre in all models (A.M. Choo et al. unpublished observations). Consequently, glial membrane compromise was not quantified. The use of cryosections thinner than the 20 μ m used here could potentially improve the sensitivity of dextran measurement.

The injuries in the three mechanisms reported here showed similarities as well as differences compared to those in the literature. The pattern of central damage in contusion was similar to that reported by many groups (Bresnahan et al., 1991; Gruner et al., 1996; Scheff et al., 2003). The 2.5mm dislocation examined in this study produced more severe hemorrhage than the 3.2mm to 7.5mm injuries modelled in lateral thoraco-lumbar dislocation (Fiford et al., 2004). The differences may be attributed to the slower speed used in that study (5.7-12.7cm/s) as well as the lateral dislocation being distributed across three vertebral segments in contrast to the adjacent vertebrae (C4/5) dislocated here. The distraction magnitude of 4.1mm used in this study was lower than the moderate (5mm) to severe (7mm) injuries reported in a rat thoracic distraction model utilizing Harrington rods (Dabney et al., 2004). Pilot trials at 5mm indicated this to be a lethal severity in the cervical spine. In addition, the injury velocity used in the current study (91.9 ± 2.9 cm/s [SD]) was aimed to model traumatic injury as opposed to surgical distraction (0.9cm/s).

The pivotal nature of hemorrhage and increased membrane permeability has been well described in the literature. Hemorrhage and hemorrhagic necrosis have been shown to increase with injury severity and are predictive of functional outcomes experimentally and clinically (Anderson, 1985; Noyes, 1987b; Bondurant et al., 1990; Flanders et al., 1990; Boldin et al., 2006). In addition, the associated ischemia and infiltration of inflammatory cells both precipitate free radical generation causing oxidation of lipid membranes, proteins and DNA thereby exacerbating damage (Young, 1987, 1992; Popovich, 2000; Bao et al., 2004; Park et al., 2004). Concurrently, the release of glutamate from depolarized or necrotic cells initiates the influx of calcium ions through NMDA and AMPA glutamate receptor channels resulting in excitotoxicity (Choi et al., 1987). Although antagonists to these channels have been explored to halt calcium influx (Shi et al., 1989; LaPlaca and Thibault, 1998; Li and Tator, 1999; Lipton, 2006), alternate routes through larger membrane pores permeable to macromolecules have also been detected with *in vitro* biaxial neuronal stretch models (Geddes et al., 2003; Geddes-Klein et al., 2006), *ex vivo* white matter preparations (Shi and Borgens, 2000; Luo et al., 2002; Shi and Pryor, 2002), *in vivo* spinal cord compression injuries (Shi, 2004), and *in vivo* traumatic brain injury (Pettus et al., 1994; Singleton and Povlishock, 2004; Stone et al., 2004).

Evidence in the literature suggests changing the characteristics of the primary mechanical trauma alters the fate of the injured neurons. *In vitro* cell stretching has been shown to result in both calpain and caspase-3 mediated necrotic and apoptotic cell death (Pike et al., 2000). However, at sub-lethal stretch levels, DNA fragmentation and apoptosis has been found to result from mitochondrial dysfunction leading to excessive reactive oxygen species rather than from caspase-3 mediated pathways (Arundine et al., 2004). In a recent *in vitro* study, biaxial stretching of neurons caused significantly greater increases in acute intracellular calcium compared to uniaxial stretching. However, by twenty-four hours post-trauma, the uniaxially stretched population exhibited heightened calcium influx through NMDA channels (Geddes-Klein et al., 2006). In addition, our unexpected observation of membrane compromise in the gray matter (Figure 3.7A) of sham controls in contrast to the sham white matter (Figure 3.6) also reinforces the mechanical and biological anisotropy of these two tissue components. The increased susceptibility of gray matter to damage, particularly hemorrhagic necrosis, has commonly been attributed to its increased capillary network (Tator and Koyanagi, 1997). The observations here suggest that in addition to the vascular differences, the susceptibility to membrane compromise between cell

bodies and myelinated axons may also be a distinguishing factor in their susceptibility to injury. The subtler relations between the injury biomechanics and the neuronal response remain unclear, but together, these observations suggest a more sophisticated role for primary injury than simply initiating an independent secondary cascade.

The patterns of primary injury found at 5 minutes provide some insight into the injury biomechanics of the three models. The strain-field in contusion has been previously modelled with gel demonstrating maximal axial displacement occurring in the central region of the cord (Blight, 1988). At the speed and impact depth used in this study, this field appears to be contained within two to four millimeters ($\pm 1\text{mm}$ to $\pm 2\text{mm}$ rostro-caudal to lesion) corresponding to one to two impactor diameters (2mm). In fracture-dislocation, a consideration of the direction of vertebral motion (C4 translating ventrally relative to C5) indicates the rostral injury field in the ventral tracts stems from the transduction of traumatic loads, perhaps tensile in nature, from the lesion epicentre rather than due to rostral vertebral contact. In flexion-distraction, the biomechanics of load transfer between the column and the cord remains unclear. Qualitatively, the depression in dextran-positive dorsal axons at -2, 2, and 5mm may imply the coupling takes place via the nerve roots which are roughly spaced at this interval. In the ventral tracts, it may be more likely that injury occurred due to contact with translating vertebrae as opposed to any sort of axial tensile coupling. The slight increasing slope in rostral membrane compromise could be related to a narrowing of the cord cross-section resulting in an increase in stress (force/unit area), however, horizontal sections along the longitudinal axis would have been better suited to detect this.

Hence, the distinct biomechanics of each model produced mechanism-specific injury regions with potential therapeutic implications. Our finding after dislocation showed a similar zone of hemorrhagic necrosis at the lesion epicentre as previously described after contusion (Anderson, 1985). This similar primary damage likely triggers analogous pathomechanisms including ischemia, excitotoxicity, and inflammation giving rise to secondary damage (Tator and Koyanagi, 1997; Popovich, 2000; Dumont et al., 2001; Park et al., 2004; Starkov et al., 2004). However, the primary shearing of lateral axonal tracts by fracture-dislocation reduces the available rim of spared white matter (Blight, 1983b; Blight and Decrescito, 1986; Bresnahan et al., 1991) normally targeted for neuroprotection, thereby potentially reducing clinical treatment efficacy in some of these injuries. In addition, dislocation and distraction appeared to establish a distinct

rostral region of gray and white matter damage which at this early acute stage appears to be spared of major vascular compromise but exhibited extensive membrane compromise. The optimal treatment for this sub-population remains to be determined and appears complex. If the permeability changes in neuronal somata are transient and sublethal, the neurons may exhibit heightened susceptibility to delayed excitotoxicity (Arundine et al., 2004) originating from the growing lesion. On the other hand, calcium activation of calpain appears to be a necessary component of endogenous membrane repair (Shi et al., 2000; Prado and LaPlaca, 2004).

The widespread membrane compromise in white matter tracts following dislocation or distraction may ultimately result in a wider gap for repair and regeneration. The membrane resealing rate of *in vitro* white matter strips appears to be slower when subjected to forceps compression relative to a discrete transection (Shi et al., 2000; Shi and Pryor, 2000; Luo et al., 2002) and therefore axolemma recovery could be further delayed by an extended rostro-caudal injury. Abnormal axonal permeability to horseradish peroxidase has been reported to persist for up to 7 days following an *in vivo* compression injury (Shi, 2004). In optic nerve stretch models, ultrastructural evidence suggests axonal damage initiates at the nodes of Ranvier (Maxwell et al., 1991) with the subsequent loss of nodal microtubules detected within minutes of injury (Maxwell and Graham, 1997). Similarly, in traumatic brain and spinal cord injury, the loss of axolemma integrity has been associated with extensive cytoskeletal degradation (Banik et al., 1982; Pettus et al., 1994). This deterioration may be ameliorated by therapies aimed at limiting ionic dysregulation (Rosenberg et al., 1999; Rosenberg and Wrathall, 2001; Schwartz and Fehlings, 2001; Hains et al., 2004) and calcium mediated protease activation (Springer et al., 1997; Schumacher et al., 2000). Even for the surviving axons, however, secondary alterations to ion channels in the nodal region (Maxwell et al., 1999; Nashmi et al., 2000) combined with damage of myelin lamellae (Balentine, 1978; Bresnahan, 1978; Banik et al., 1982; Blight and Decrescito, 1986; Anthes et al., 1995) may still result in residual conduction deficits (Blight, 1983a; Blight and Someya, 1985; Waxman et al., 1991; Nashmi and Fehlings, 2001). Thus, the pattern of dextran entry may indicate that the biomechanics of dislocation and distraction could heighten the rostro-caudal field of degeneration and chronic dysfunction relative to that previously observed in contusion models.

In summary, this study profiled differences in the primary damage created by three clinically relevant mechanisms of spinal cord injury. Different distributions of acute hemorrhage and membrane compromise were detected reflecting distinctions between the injury biomechanics of these mechanisms. The injury patterns may have implications in the targeting of distinct injury populations and hence be useful for guiding future experimental and clinical treatment strategies.

3.5 References

- Anderson TE (1985) Spinal cord contusion injury: experimental dissociation of hemorrhagic necrosis and subacute loss of axonal conduction. *J Neurosurg* 62:115-119.
- Anderson TE, Stokes BT (1992) Experimental models for spinal cord injury research: physical and physiological considerations. *J Neurotrauma* 9:S135-S142.
- Anthes DL, Theriault E, Tator CH (1995) Characterization of axonal ultrastructural pathology following experimental spinal cord compression injury. *Brain Res* 702:1-16.
- Arbogast KB, Margulies SS (1998) Material characterization of the brainstem from oscillatory shear tests. *J Biomech* 31:801-807.
- Arundine M, Aarts M, Lau A, Tymianski M (2004) Vulnerability of central neurons to secondary insults after in vitro mechanical stretch. *J Neurosci* 24:8106-8123.
- Balentine JD (1978) Pathology of experimental spinal cord trauma. II. Ultrastructure of axons and myelin. *Lab Invest* 39:254-266.
- Banik NL, Hogan EL, Powers JM, Whetstone LJ (1982) Degradation of cytoskeletal proteins in experimental spinal cord injury. *Neurochem Res* 7:1465-1475.
- Bao F, Chen Y, Dekaban GA, Weaver LC (2004) Early anti-inflammatory treatment reduces lipid peroxidation and protein nitration after spinal cord injury in rats. *J Neurochem* 88:1335-1344.
- Behrmann DL, Bresnahan JC, Beattie MS, Shah BR (1992) Spinal cord injury produced by consistent mechanical displacement of the cord in rats: behavioral and histologic analysis. *J Neurotrauma* 9:197-217.
- Blight A (1988) Mechanical factors in experimental spinal cord injury. *J Am Paraplegia Soc* 11:26-34.
- Blight AR (1983a) Axonal physiology of chronic spinal cord injury in the cat: intracellular recording in vitro. *Neuroscience* 10:1471-1486.
- Blight AR (1983b) Cellular morphology of chronic spinal cord injury in the cat: analysis of myelinated axons by line-sampling. *Neuroscience* 10:521-543.
- Blight AR, Someya S (1985) Depolarizing afterpotentials in myelinated axons of mammalian spinal cord. *Neuroscience* 15:1-12.
- Blight AR, Decrescito V (1986) Morphometric analysis of experimental spinal cord injury in the cat: the relation of injury intensity to survival of myelinated axons. *Neuroscience* 19:321-341.
- Boldin C, Raith J, Fankhauser F, Haunschmid C, Schwantzer G, Schweighofer F (2006) Predicting neurologic recovery in cervical spinal cord injury with postoperative MR imaging. *Spine* 31:554-559.
- Bondurant FJ, Cotler HB, Kulkarni MV, McArdle CB, Harris JH, Jr. (1990) Acute spinal cord injury. A study using physical examination and magnetic resonance imaging. *Spine* 15:161-168.
- Bresnahan JC (1978) An electron-microscopic analysis of axonal alterations following blunt contusion of the spinal cord of the rhesus monkey (*Macaca mulatta*). *J Neurol Sci* 37:59-82.
- Bresnahan JC, Beattie MS, Stokes BT, Conway KM (1991) Three-dimensional computer-assisted analysis of graded contusion lesions in the spinal cord of the rat. *J Neurotrauma* 8:91-101.
- Choi DW, Maulucci-Gedde M, Kriegstein AR (1987) Glutamate neurotoxicity in cortical cell culture. *J Neurosci* 7:357-368.

- Dabney KW, Ehrenshteyn M, Agresta CA, Twiss JL, Stern G, Tice L, Salzman SK (2004) A model of experimental spinal cord trauma based on computer-controlled intervertebral distraction: characterization of graded injury. *Spine* 29:2357-2364.
- Dolan EJ, Transfeldt EE, Tator CH, Simmons EH, Hughes KF (1980) The effect of spinal distraction on regional spinal cord blood flow in cats. *J Neurosurg* 53:756-764.
- Dumont RJ, Okonkwo DO, Verma S, Hurlbert RJ, Boulos PT, Ellegala DB, Dumont AS (2001) Acute spinal cord injury, part I: pathophysiologic mechanisms. *Clin Neuropharmacol* 24:254-264.
- Fiford RJ, Bilston LE, Waite P, Lu J (2004) A vertebral dislocation model of spinal cord injury in rats. *J Neurotrauma* 21:451-458.
- Flanders AE, Spettell CM, Tartaglino LM, Friedman DP, Herbison GJ (1996) Forecasting motor recovery after cervical spinal cord injury: value of MR imaging. *Radiology* 201:649-655.
- Flanders AE, Schaefer DM, Doan HT, Mishkin MM, Gonzalez CF, Northrup BE (1990) Acute cervical spine trauma: correlation of MR imaging findings with degree of neurologic deficit. *Radiology* 177:25-33.
- Galbraith JA, Thibault LE, Matteson DR (1993) Mechanical and electrical responses of the squid giant axon to simple elongation. *J Biomech Eng* 115:13-22.
- Geddes-Klein DM, Schiffman KB, Meaney DF (2006) Mechanisms and consequences of neuronal stretch injury in vitro differ with the model of trauma. *J Neurotrauma* 23:193-204.
- Geddes DM, Cargill RS, 2nd, LaPlaca MC (2003) Mechanical stretch to neurons results in a strain rate and magnitude-dependent increase in plasma membrane permeability. *J Neurotrauma* 20:1039-1049.
- Gruner JA (1992) A monitored contusion model of spinal cord injury in the rat. *J Neurotrauma* 9:123-126; discussion 126-128.
- Gruner JA, Yee AK, Blight AR (1996) Histological and functional evaluation of experimental spinal cord injury: evidence of a stepwise response to graded compression. *Brain Res* 729:90-101.
- Hains BC, Saab CY, Lo AC, Waxman SG (2004) Sodium channel blockade with phenytoin protects spinal cord axons, enhances axonal conduction, and improves functional motor recovery after contusion SCI. *Exp Neurol* 188:365-377.
- Howard CV, Reed MG (1998) *Unbiased Stereology - Three Dimensional Measurement in Microscopy*. New York: Springer-Verlag.
- Jakeman LB, Guan Z, Wei P, Ponnappan R, Dzwonczyk R, Popovich PG, Stokes BT (2000) Traumatic spinal cord injury produced by controlled contusion in mouse. *J Neurotrauma* 17:299-319 ;217(294):299-319.
- Kloos AD, Fisher LC, Detloff MR, Hassenzahl DL, Basso DM (2005) Stepwise motor and all-or-none sensory recovery is associated with nonlinear sparing after incremental spinal cord injury in rats. *Exp Neurol* 191:251-265.
- Kwon BK, Oxland TR, Tetzlaff W (2002) Animal models used in spinal cord regeneration research. *Spine* 27:1504-1510.
- LaPlaca MC, Thibault LE (1998) Dynamic mechanical deformation of neurons triggers an acute calcium response and cell injury involving the N-methyl-D-aspartate glutamate receptor. *J Neurosci Res* 52:220-229.
- Li S, Tator CH (1999) Effects of MK801 on evoked potentials, spinal cord blood flow and cord edema in acute spinal cord injury in rats. *Spinal Cord* 37:820-832.

- Lipton SA (2006) Paradigm shift in neuroprotection by NMDA receptor blockade: memantine and beyond. *Nat Rev Drug Discov* 5:160-170.
- Luo J, Borgens R, Shi R (2002) Polyethylene glycol immediately repairs neuronal membranes and inhibits free radical production after acute spinal cord injury. *J Neurochem* 83:471-480.
- Maiman DJ, Coats J, Myklebust JB (1989a) Cord/spine motion in experimental spinal cord injury. *J Spinal Disord* 2:14-19.
- Maiman DJ, Myklebust JB, Ho KC, Coats J (1989b) Experimental spinal cord injury produced by axial tension. *J Spinal Disord* 2:6-13.
- Maxwell WL, Graham DI (1997) Loss of axonal microtubules and neurofilaments after stretch-injury to guinea pig optic nerve fibers. *J Neurotrauma* 14:603-614.
- Maxwell WL, Kosanlavit R, McCreath BJ, Reid O, Graham DI (1999) Freeze-fracture and cytochemical evidence for structural and functional alteration in the axolemma and myelin sheath of adult guinea pig optic nerve fibers after stretch injury. *J Neurotrauma* 16:273-284.
- Maxwell WL, Irvine A, Graham, Adams JH, Gennarelli TA, Tipperman R, Sturatis M (1991) Focal axonal injury: the early axonal response to stretch. *J Neurocytol* 20:157-164.
- Myklebust JB, Maiman DJ, Cusick JF (1988) Axial tension model of spinal cord injury. *J Am Paraplegia Soc* 11:50-55.
- Nashmi R, Fehlings MG (2001) Mechanisms of axonal dysfunction after spinal cord injury: with an emphasis on the role of voltage-gated potassium channels. *Brain Res Brain Res Rev* 38:165-191.
- Nashmi R, Jones OT, Fehlings MG (2000) Abnormal axonal physiology is associated with altered expression and distribution of Kv1.1 and Kv1.2 K⁺ channels after chronic spinal cord injury. *Eur J Neurosci* 12:491-506.
- Nikolaidis N, Pitas I (2001) *3-D Image Processing Algorithms*. New York: John Wiley & Sons.
- Noble LJ, Maxwell DS (1983) Blood-spinal cord barrier response to transection. *Exp Neurol* 79:188-199.
- Noble LJ, Wrathall JR (1988) Blood-spinal cord barrier disruption proximal to a spinal cord transection in the rat: time course and pathways associated with protein leakage. *Exp Neurol* 99:567-578.
- Noyes DH (1987a) Electromechanical impactor for producing experimental spinal cord injury in animals. *Med Biol Eng Comput* 25:335-340.
- Noyes DH (1987b) Correlation between parameters of spinal cord impact and resultant injury. *Exp Neurol* 95:535-547.
- Park E, Velumian AA, Fehlings MG (2004) The role of excitotoxicity in secondary mechanisms of spinal cord injury: a review with an emphasis on the implications for white matter degeneration. *J Neurotrauma* 21:754-774.
- Pearse DD, Pereira FC, Marcillo AE, Bates ML, Berrocal YA, Filbin MT, Bunge MB (2004) cAMP and Schwann cells promote axonal growth and functional recovery after spinal cord injury. *Nat Med* 10:610-616.
- Pearse DD, Lo TP, Jr., Cho KS, Lynch MP, Garg MS, Marcillo AE, Sanchez AR, Cruz Y, Dietrich WD (2005) Histopathological and behavioral characterization of a novel cervical spinal cord displacement contusion injury in the rat. *J Neurotrauma* 22:680-702.
- Pettus EH, Christman CW, Giebel ML, Povlishock JT (1994) Traumatically induced altered membrane permeability: its relationship to traumatically induced reactive axonal change. *J Neurotrauma* 11:507-522.

- Pike BR, Zhao X, Newcomb JK, Glenn CC, Anderson DK, Hayes RL (2000) Stretch injury causes calpain and caspase-3 activation and necrotic and apoptotic cell death in septo-hippocampal cell cultures. *J Neurotrauma* 17:283-298.
- Popovich PG (2000) Immunological regulation of neuronal degeneration and regeneration in the injured spinal cord. *Prog Brain Res* 128:43-58.
- Popovich PG, Horner PJ, Mullin BB, Stokes BT (1996) A quantitative spatial analysis of the blood-spinal cord barrier. I. Permeability changes after experimental spinal contusion injury. *Exp Neurol* 142:258-275.
- Prado GR, LaPlaca MC (2004) Neuronal plasma membrane is transiently disrupted by mechanical trauma: an insight into the mechanisms involved. *J Neurotrauma* 21:1331.
- Rabchevsky AG, Fugaccia I, Sullivan PG, Blades DA, Scheff SW (2002) Efficacy of methylprednisolone therapy for the injured rat spinal cord. *J Neurosci Res* 68:7-18.
- Ramon S, Dominguez R, Ramirez L, Paraira M, Olona M, Castello T, Garcia FL (1997) Clinical and magnetic resonance imaging correlation in acute spinal cord injury. *Spinal Cord* 35:664-673.
- Rosenberg LJ, Wrathall JR (2001) Time course studies on the effectiveness of tetrodotoxin in reducing consequences of spinal cord contusion. *J Neurosci Res* 66:191-202.
- Rosenberg LJ, Teng YD, Wrathall JR (1999) Effects of the sodium channel blocker tetrodotoxin on acute white matter pathology after experimental contusive spinal cord injury. *J Neurosci* 19:6122-6133.
- Salzman SK, Mendez AA, Dabney KW, Daley JC, Freeman GM, el-Tantawi S, Beckman AL, Bunnell WP (1991) Serotonergic response to spinal distraction trauma in experimental scoliosis. *J Neurotrauma* 8:45-54.
- Salzman SK, Dabney KW, Mendez AA, Beauchamp JT, Daley JC, Freeman GM, Fonseca A, Ingersoll EB, Beckman AL, Bunnell WP (1988) The somatosensory evoked potential predicts neurologic deficits and serotonergic pathochemistry after spinal distraction injury in experimental scoliosis. *J Neurotrauma* 5:173-186.
- Sarwark JF, Dabney KW, Salzman SK, Wakabayashi T, Kitadai HK, Beauchamp JT, Beckman AL, Bunnell WP (1988) Experimental scoliosis in the rat. I. Methodology, anatomic features and neurologic characterization. *Spine* 13:466-471.
- Scheff SW, Rabchevsky AG, Fugaccia I, Main JA, Lumpp JE, Jr. (2003) Experimental modeling of spinal cord injury: characterization of a force-defined injury device. *J Neurotrauma* 20:179-193.
- Schumacher PA, Siman RG, Fehlings MG (2000) Pretreatment with calpain inhibitor CEP-4143 inhibits calpain I activation and cytoskeletal degradation, improves neurological function, and enhances axonal survival after traumatic spinal cord injury. *J Neurochem* 74:1646-1655.
- Schwartz G, Fehlings MG (2001) Evaluation of the neuroprotective effects of sodium channel blockers after spinal cord injury: improved behavioral and neuroanatomical recovery with riluzole. *J Neurosurg* 94:245-256.
- Shi R (2004) The dynamics of axolemmal disruption in guinea pig spinal cord following compression. *J Neurocytol* 33:203-211.
- Shi R, Blight AR (1996) Compression injury of mammalian spinal cord in vitro and the dynamics of action potential conduction failure. *J Neurophysiol* 76:1572-1580.
- Shi R, Pryor JD (2000) Temperature dependence of membrane sealing following transection in mammalian spinal cord axons. *Neuroscience* 98:157-166.

- Shi R, Borgens RB (2000) Anatomical repair of nerve membranes in crushed mammalian spinal cord with polyethylene glycol. *J Neurocytol* 29:633-643.
- Shi R, Pryor JD (2002) Pathological changes of isolated spinal cord axons in response to mechanical stretch. *Neuroscience* 110:765-777.
- Shi R, Asano T, Vining NC, Blight AR (2000) Control of membrane sealing in injured mammalian spinal cord axons. *J Neurophysiol* 84:1763-1769.
- Shi RY, Lucas JH, Wolf A, Gross GW (1989) Calcium antagonists fail to protect mammalian spinal neurons after physical injury. *J Neurotrauma* 6:261-276; discussion 277-268.
- Singleton RH, Povlishock JT (2004) Identification and characterization of heterogeneous neuronal injury and death in regions of diffuse brain injury: evidence for multiple independent injury phenotypes. *J Neurosci* 24:3543-3553.
- Springer JE, Azbill RD, Kennedy SE, George J, Geddes JW (1997) Rapid calpain I activation and cytoskeletal protein degradation following traumatic spinal cord injury: attenuation with riluzole pretreatment. *J Neurochem* 69:1592-1600.
- Starkov AA, Chinopoulos C, Fiskum G (2004) Mitochondrial calcium and oxidative stress as mediators of ischemic brain injury. *Cell Calcium* 36:257-264.
- Stokes BT, Noyes DH, Behrmann DL (1992) An electromechanical spinal injury technique with dynamic sensitivity. *J Neurotrauma* 9:187-195.
- Stone JR, Okonkwo DO, Dialo AO, Rubin DG, Mutlu LK, Povlishock JT, Helm GA (2004) Impaired axonal transport and altered axolemmal permeability occur in distinct populations of damaged axons following traumatic brain injury. *Exp Neurol* 190:59-69.
- Stys PK (2004) White matter injury mechanisms. *Curr Mol Med* 4:113-130.
- Sullivan PG, Rabchevsky AG, Waldmeier PC, Springer JE (2005) Mitochondrial permeability transition in CNS trauma: cause or effect of neuronal cell death? *J Neurosci Res* 79:231-239.
- Tator CH, Koyanagi I (1997) Vascular mechanisms in the pathophysiology of human spinal cord injury. *J Neurosurg* 86:483-492.
- Teng YD, Choi H, Onario RC, Zhu S, Desilets FC, Lan S, Woodard EJ, Snyder EY, Eichler ME, Friedlander RM (2004) Minocycline inhibits contusion-triggered mitochondrial cytochrome c release and mitigates functional deficits after spinal cord injury. *Proc Natl Acad Sci U S A* 101:3071-3076.
- Waxman SG, Ransom BR, Stys PK (1991) Non-synaptic mechanisms of Ca(2+)-mediated injury in CNS white matter. *Trends Neurosci* 14:461-468.
- Young W (1987) The post-injury responses in trauma and ischemia: secondary injury or protective mechanisms? *Cent Nerv Syst Trauma* 4:27-51.
- Young W (1992) Role of calcium in central nervous system injuries. *J Neurotrauma* 9 Suppl 1:S9-25.
- Young W (2002) Spinal cord contusion models. *Prog Brain Res* 137:231-255.
- Zar JH (1999) *Biostatistical Analysis*, 4 Edition. New Jersey: Prentice Hall.

Chapter 4

INITIATION OF SECONDARY INJURYⁱⁱⁱ

4.1 Introduction

Spinal cord injury (SCI) occurs when distinct types of vertebral column failure injure the cord by different primary injury mechanisms. For example, vertebral burst fracture, which has a prevalence of 30-48% (Sekhon and Fehlings, 2001; Pickett et al., 2006), results in contusion and ongoing compression of the cord from retropulsed bone fragments. In contrast, vertebral dislocation—occurring in 29-45% of human cases (Sekhon and Fehlings, 2001; Pickett et al., 2006)—shears the cord between adjacent segments. Hyper-flexion of the vertebrae can cause SCI by tensile stretching (Breig, 1970; Silberstein and McLean, 1994) and this mode of trauma is widely studied *in vitro* (Shi and Pryor, 2002; Geddes et al., 2003; Lusardi et al., 2004). Neuroprotective strategies designed to mitigate the biochemical cascade that exacerbates the lesion (Tator and Fehlings, 1999), have been extensively tested in pre-clinical models of spinal cord contusion (Gruner, 1992; Stokes et al., 1992; Scheff et al., 2003) and compression (Rivlin and Tator, 1978). Clinical translation of these strategies has been modest, and suggests that current animal models may not reflect the spectrum of human SCI (Tator, 2006).

Since the spinal cord is rarely transected (Norenberg et al., 2004), neuroprotective sparing of tissue from secondary degeneration holds the promise of enabling functional recovery. Myriad strategies have been explored including: the management of blood flow to minimize ischemia (Guha et al., 1989; Tator, 1992), the attenuation of inflammation to limit bystander damage (Xu et al., 1998; Gris et al., 2004; Stirling et al., 2004), the inhibition of free radicals to reduce oxidative stress (Diaz-Ruiz et al., 1999), and the blockade of glutamate receptors to prevent excitotoxicity (Faden et al., 1988; Wrathall et al., 1996; Gaviria et al., 2000b). Although methylprednisolone

ⁱⁱⁱ A version of this chapter has been submitted for publication. Choo AM, Liu J, Dvorak M, Tetzlaff W, Oxland TR. Contusion, dislocation, and distraction: Evolution of membrane permeability and early secondary pathology of neuronal somata, axons, astrocytes, and microglial in clinically relevant mechanisms of spinal cord injury.

(Bracken et al., 1990; Bracken et al., 1997) initially gained widespread clinical application, its efficacy remains intensely controversial (Hurlbert, 2000; Hall and Springer, 2004). The interaction between neurodegenerative processes confounds the identification of treatment priorities. Some pre-clinical investigations have favoured early intervention within a few hours of injury (Wrathall et al., 1997; Diaz-Ruiz et al., 1999; Gaviria et al., 2000a; Rosenberg and Wrathall, 2001; Gris et al., 2004). Given that pre-clinical therapies have had limited success against the broader spectrum of clinical injuries, it seems imperative to understand if the early secondary cascades are modified by different injury mechanisms.

Although mechanical trauma triggers secondary pathomechanisms, few have addressed the influence of different primary injury mechanisms on secondary pathophysiology. In neuronal cultures, biaxial stretching initiates greater calcium influx than uniaxial stretching, however counter-intuitively, delayed excitotoxicity is heightened in the uniaxial injury model (Geddes-Klein et al., 2006). Biomechanically, compression, tension, and shear produce different deformations (Fung, 1993). Neural tissue is mechanically anisotropic (Arbogast and Margulies, 1998); meaning it is not homogeneous and its susceptibility to traumatic deformation depends on the direction of force application. In chapter 3 it was found that contusion, dislocation, and distraction established distinctive patterns of primary damage when analysed immediately after injury. Here, the early secondary pathology that evolves from these three clinically relevant SCI mechanisms was compared.

4.2 Materials and Methods

4.2.1 Animal Models

All procedures were approved by our institution's Animal Care Committee in accordance with the guidelines published by the Canadian Council on Animal Care. Thirty-nine male Sprague-Dawley rats (weight 347 ± 28 g [SD]) were divided into three injury groups ($n = 10$ contusion, $n = 10$ dislocation, $n = 10$ distraction), three sham surgical control groups ($n = 2$ contusion, $n = 2$ dislocation, $n = 3$ distraction) and one group of controls for dextran incubation ($n = 2$, described below). Animals were anesthetized with an intramuscular injection of ketamine (80mg/kg) and xylazine (10mg/kg) and maintained under deep anesthesia throughout the tests. Fluorescein-dextran with a molecular weight of 10kDa (0.375mg diluted in 15 μ L dH₂O, Molecular Probes, Eugene, OR) was infused into the cisterna magna 1.5 hours prior to injury in order to

detect increases in membrane permeability (Pettus et al., 1994; Singleton and Povlishock, 2004; Stone et al., 2004). Custom designed stereotactic clamps were used to hold the cervical vertebrae between C3 and C6 laterally beneath the transverse processes as described in chapter 2.

Moderate-severe contusion, fracture-dislocation and flexion-distraction injuries were produced as previously described using an SCI multi-mechanism system equipped with an electromagnetic linear actuator and sensors to measure force, displacement, and acceleration (refer to chapter 2). Briefly, for contusion, a circular laminectomy window was produced between C4 and C5. A 2-mm spherical head impactor (Figure 4.1A) was lowered in 50 μ m step-increments on to the dural surface until a touch force of 0.03N was detected (Stokes et al., 1992). The actuator was retracted and the touch force was re-verified. The actuator was then retracted to 6mm above the dural before being accelerated downward to strike the cord to an injury depth of 1.1 ± 0.02 mm (SD). To model vertebral fracture-dislocation, the dorsal ligaments and facets between C4 and C5 were removed. The C3 and C4 vertebrae were held stationary, while a vertebral clamp holding C5 and C6 together was coupled to the actuator and translated dorsally to produce a transient 2.5 ± 0.12 mm (SD) C4/5 dislocation (Figure 4.1B). For flexion-distraction, the facets between C4 and C5 were removed and the animals were secured within a stereotactic frame with 15° of flexion at C4/5. With the C3 and C4 vertebrae held stationary, C5 and C6 were held with a vertebral clamp and were distracted caudally 4.1 ± 0.03 mm (SD), held for one second, then returned to their initial position (Figure 4.1C). For sham contusions, the animals were secured within the stereotactic frame and underwent identical procedures, however, only the touch force was applied. For sham dislocations and distractions, the procedure was halted after the vertebral clamp holding C5 and C6 was coupled to the actuator.

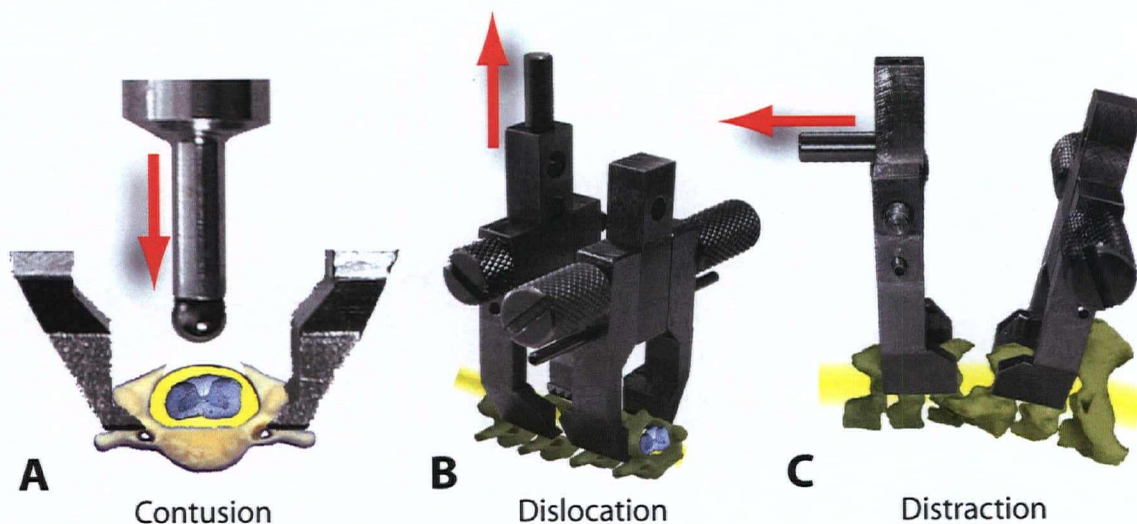


Figure 4.1: Illustration of three injury mechanisms

A: Contusion injury was produced with a 2mm diameter impactor that struck the cord through a laminectomy between C4 and C5. B: Dislocation was modelled by holding C3 and C4 stationary while C5 and C6 were displaced together dorsally. C: Distraction injuries were generated by translating C5 and C6 caudally. Proportions and perspectives in illustrations are approximations. Instrumentation used to constrain stationary vertebral clamps is not shown.

Following dislocation and distraction injuries, the rostral and caudal vertebral clamps were clamped together to prevent further movement at the now unstable C4/5 joint. Animals were removed from the stereotactic frame and the vertebral clamps were carefully removed under stereomicroscopy. For animals in the dislocation and distraction groups, 0.8mm stainless steel rods were bonded (Vetbond, 3M, St Paul, MN) to the C4 and C5 laminae to prevent additional movement. The wound was covered with saline-soaked gauze and closed. Animals were carefully maintained under anesthesia in a warmed chamber with temperature monitored via rectal probe (RET-2, Kopf Instruments, Tujunga, CA) and heart rate and blood oxygenation were monitored using a pulse-oximeter (8600V, Nonin, Plymouth, MN).

At two hours post-trauma, 10kDa cascade blue-dextran (0.75mg diluted in 20 μ L dH₂O) was infused into the cerebrospinal fluid to detect secondary changes in membrane permeability. A higher concentration of cascade blue-dextran was used compared to fluorescein-dextran in order to accommodate for its weaker photostability. For three animals (one per injury mechanism), the order of dextran infusion was reversed (i.e. cascade blue-dextran used 1.5 hours prior to trauma and fluorescein-dextran used 2 hours post-trauma) in order to confirm the observations were independent of the sequence of dextran infusion. At three hours post-trauma, all animals were transcardially perfused with 250mL phosphate buffered saline followed by 500mL of freshly

hydrolyzed cold 4% paraformaldehyde. Spinal cords were post-fixed overnight in 4% paraformaldehyde and cryoprotected in graded sucrose (12, 18, 24% in phosphate buffer) before being frozen in isopentane cooled with dry ice and stored at -80°C . Thirty-four spinal cords were cryosectioned at $20\mu\text{m}$ parasagittally while three cords (one per injury mechanism) were sectioned in the horizontal plane from dorsal to ventral. Sections from each spinal cord were systematically distributed over eight slides (16 to 18 sections per slide) yielding eight replicates for each cord.

The remaining two animals served as controls for dextran incubation in the absence of vertebral column exposure. These animals were anesthetized and infused with 10kDa dextran conjugated to fluorescein or cascade blue (Molecular Probes). Animals were maintained under deep anesthesia and perfused at four hours after infusion. Tissue processing was identical to the injury and sham surgical control groups.

4.2.2 Immunohistochemistry

Fluorescein-dextran and cascade blue-dextran were immediately visible under epifluorescent microscopy, however, to improve photostability, slides from all animals were also immunostained with goat anti-fluorescein and rabbit anti-cascade blue (Table 4.1). Oxidative stress in neuronal somata was analysed by immunostaining ($n = 37$) for 3-nitrotyrosine (3NT), which is generated by the reactive oxygen species peroxynitrite (Deng et al., 2007; Xiong et al., 2007), and early indications of apoptosis were investigated by immunostaining ($n = 22$) for cytochrome *c* (Springer et al., 1999; Vanderluit et al., 2003). Immunohistochemistry for non-phosphorylated ($n = 37$) and phosphorylated ($n = 12$) neurofilament epitopes was used to detect axonal degeneration. In addition, accumulation of β -Amyloid Precursor Protein (βAPP , $n = 37$) demonstrated axonal transport dysfunction (Li et al., 1995; Cornish et al., 2000; Stone et al., 2004). Anti-Iba1 (Imai et al., 1996; Ito et al., 1998) revealed activated microglial morphology ($n = 37$) while the extent of reactive astrocytes was assessed by staining for glial fibrillary acidic protein (GFAP, $n = 21$).

Table 4.1: Immunohistochemical markers for secondary injury

Analysis	Antibody	Type	Target	Vendor	Dilution	Animals Sampled ¹			
						CT	DL	DT	SH
Membrane Permeability	A-11095	goat polyclonal	fluorescein-dextran	Molecular Probes	1:200	10	10	10	7
	A-5760	rabbit polyclonal	cascade blue-dextran	Molecular Probes	1:200	10	10	10	7
Cell Bodies in Gray Matter ²	1A6	mouse monoclonal	nitrotyrosine	Upstate	1:100	10	10	10	7
	6H2.B4	mouse monoclonal	cytochrome c	Pharmingen	1:500	5	5	5	7
Axons in White Matter ²	SMI 32	mouse monoclonal	non-phosphorylated neurofilament	Sternberger Monoclonals	1:1000	10	10	10	7
	SMI 31	mouse monoclonal	phosphorylated neurofilament	Sternberger Monoclonals	1:1000	3	3	3	3
	CT695 ³	rabbit polyclonal	β -Amyloid Precursor Protein	Invitrogen	1:500	10	10	10	7
Microglial Activation	01-1974	rabbit polyclonal	Iba1	Wako	1:1000	10	10	10	7
Reactive Astrocytes ²	G-A-5	mouse monoclonal	Glial Fibrillary Acidic Protein	Sigma	1:400	6	6	6	3

¹ Cryosections from each spinal cord were systematically distributed over eight slides to produce eight replicates of the cord from each animal (16 to 18 sections per slide). CT = Contusion, DL = Dislocation, DT = Distraction, SH = Sham.

² Where there was no conflict in the primary antibodies, sections were also multilabelled with anti-fluorescein and anti-cascade blue.

³ β -Amyloid Precursor Protein that was visualized in brightfield whereas immunofluorescence was used for all other analyses (refer to methods).

For immunofluorescence, sections were washed 3×5 minutes in 0.01M phosphate buffered saline (PBS). Sections were blocked for 30 minutes in normal donkey serum before being incubated for 3 hours at room temperature in primary antibodies (Table 4.1) diluted in 0.01M PBS with 0.1% Triton X-100. Sections were then washed 3×5 minutes in 0.01M PBS and incubated for 1 hour in the appropriate donkey secondary antibody. Alexa488 donkey anti-goat (Molecular Probes) was used as the secondary antibody for anti-fluorescein while AMCA donkey anti-rabbit (Jackson ImmunoResearch Laboratories, West Grove, PA) was used to visualize anti-cascade blue. Cy3-conjugated donkey secondary antibodies (Jackson ImmunoResearch; cross adsorbed against rat in the case of anti-mouse primaries) were used to detect all other primary antibodies. Sections were washed 3×5 minutes in 0.01M PBS then mounted with Fluoromount-G (SouthernBiotech, Birmingham, AL).

For brightfield immunohistochemistry (i.e. β APP), sections were washed 3 \times 5 minutes in PBS then incubated under agitation for 30 minutes in 0.3% hydrogen peroxide in 100% methanol to quench endogenous peroxidase activity. Sections were washed 3 \times 5 minutes in PBS then blocked for 30 minutes in normal donkey serum before being incubated for 3 hours at room temperature in rabbit anti- β APP (Table 4.1) diluted in 0.01M PBS with 0.1% Triton X-100. Sections were then washed 3 \times 5 minutes in 0.01M PBS and incubated for 30 minutes in avidin-biotin complex (ABC Standard Elite, Vector Laboratories, Burlingame, CA). Sections were washed, incubated for 1 hour in biotinylated donkey anti-rabbit (Jackson ImmunoResearch) and then washed again. Sections were visualized using 3,3'-diaminobenzidine (DAB) substrate with nickel (Vector Laboratories), then washed in distilled water, dehydrated in graded ethanol (50, 70, 90, 95, 100%), cleared in isopropanol, followed by toluene, then mounted with Entellan (EM Science, Gibbstown, NJ).

4.2.3 General Image Acquisition & Analysis

All images were acquired using a Zeiss AxioPlan2 (Carl Zeiss, Thornwood, NY) equipped with a motorized scanning stage (Scan 100 \times 100, Marzhauser, Wetzlar-Steindorf, Germany; MAC5000 controller, Ludl, Hawthorne, NY) for systematic random sampling of tissue at either 1mm rostro-caudal intervals or image montaging of contiguous segments as specified below. Sampling at 1mm intervals spanned from 4mm caudal to 4mm rostral to the apparent lesion epicentre (i.e. 9 images, -4mm ... +4mm) with three series captured (i.e. 3 \times 9 images) per region of interest (e.g. ventral gray matter) in each animal. For montaged images, the rostro-caudal length differed between injury markers, however, for all analyses, three montages were captured per tract per animal. Image analysis was conducted with the investigator blind to the mechanism of injury using customized software (Appendix B) written in Matlab (The MathWorks, Natick, MA) to semiautomate thresholding and counting with basic analysis tools (Nikolaidis and Pitas, 2001). All image analysis was subjected to manual verification and correction for cases where the general algorithms failed. Random placement of quantitative probes such as counting frames was achieved using a random vector of length 0 to 50 μ m. As detailed below, one-way, two-way and three-way Analysis of Variance (ANOVA) were carried out with Student-Newman-Keuls *post hoc* tests using an alpha level of 0.05.

4.2.4 Changes in Membrane Permeability

Intracellular penetration of fluorescein-dextran and cascade blue-dextran was analysed to assess changes in membrane permeability over the post-traumatic period. Nine specimens were excluded from quantitative analysis due to poor visibility of either dextran tracer (2 contusion, 2 dislocation, 3 distraction, 2 sham controls). Systematic random sampling (-4mm ... +4mm) was used to image the ventral gray matter (20× objective lens) and ventro-medial white matter (40× objective lens) as these regions were previously representative of the primary membrane compromise in these three injury models (refer to chapter 3 Figures 4.6 & 4.7). Cell bodies were selected using 100×100µm² unbiased sampling frames (Howard and Reed, 1998). Four frames were randomly placed entirely within the gray matter in each image and cells were manually counted if the intensity of either dextran was three times greater than the background. Dextran penetration into axons was quantified using 100µm line probes (three per image) randomly placed within 250µm of the ventral tissue border (as in chapter 3). Similar to the gray matter, axons crossing the line probe were manually selected if they exhibited dextran fluorescence above a consistent background threshold. The intensities of fluorescein-dextran (I_{FL}) and cascade blue-dextran (I_{CB}) within the cell body or axon was defined by averaging 3×3 image pixels around the selection point within the cytoplasm of the cell bodies or at the intersection between the axon and the line probe. In order to accommodate for variations in the background level of dextran, the intensity of the dextran within cell bodies and axons was normalized to the background level within the same image: $\hat{I}_{FL} = \frac{I_{FL}}{I_{FL_Background}}$ and $\hat{I}_{CB} = \frac{I_{CB}}{I_{CB_Background}}$. Changes in membrane permeability were analysed using three-way repeated-measures ANOVA to compare the effects of injury mechanism, dextran infusion time (pre-injury vs. post-injury with \hat{I}_{FL} and \hat{I}_{CB} as appropriate for the sequence used), and rostral-caudal position.

4.2.5 Cell Bodies in the Gray Matter

To compare patterns of oxidative stress between injury models, sections stained for 3NT were systematically imaged (-4mm ... +4mm) using a 20× objective lens. Cells exhibiting neuronal morphology and positive for 3NT above a fixed background threshold were counted if they fell within four randomly placed 100×100µm² unbiased sampling frames. Two-way repeated-measures ANOVA compared the effects of injury mechanism and rostral-caudal position on the

number of 3NT-positive cells per square millimeter. Since count data exhibits a Poisson distribution, where the standard deviation is proportional to the mean, square-root transformations were used to ensure equal variances prior to statistical testing (Zar, 1999). Potentially apoptotic neurons are identifiable by the release of cytochrome *c* from mitochondria into the cytoplasm (Springer et al., 1999; Sugawara et al., 2002; Vanderluit et al., 2003), however, classification appeared unreliable in our sections. Hence, cytochrome *c* immunostaining was analysed qualitatively only.

4.2.6 Axons in the White Matter

The ventro-medial white matter tract on slides stained for non-phosphorylated neurofilament were systematically imaged with a 40× objective from 4mm caudal to 4mm rostral to the lesion epicentre thereby paralleling the analysis of axonal membrane compromise, which is thought to initiate the collapse of neurofilament sidearms (Pettus et al., 1994; Jafari et al., 1998; Okonkwo et al., 1998). A 200µm wide sampling frame, occupying the entire rostro-caudal length of the image, was randomly placed within 250µm of the superficial tissue border. A fixed threshold segmented individually identified axonal profiles for area measurements. Two-way repeated-measures ANOVA compared the effects of mechanism and rostro-caudal position on changes in the percent area of non-phosphorylated neurofilaments. To confirm the apparent loss of neurofilaments, a subset of adjacent sections was also analysed for phosphorylated neurofilament epitopes. Phosphorylated neurofilaments were not quantified because the staining pattern was not amenable to segmentation of individual axons.

Accumulation of βAPP was imaged using a 20× objective lens to capture the dorsal ascending columns, dorsal corticospinal tract, lateral white matter and ventro-medial column. Since βAPP generally exhibits isolated regions of punctate staining, contiguous rostro-caudal montages centered at the lesion epicentre were acquired. For the corticospinal tract 4.5mm image montages were used whereas 3.5mm montages were used for the remaining tracts. βAPP staining outside these regions was negligible. To quantify βAPP accumulation, a sampling frame (200µm×4.5mm [corticospinal tract] or 200µm×3.5mm [dorsal, lateral, and ventral tracts]) was randomly overlaid on each montaged image and a fixed threshold was used to determine the total area of βAPP immunostaining. For each animal, three montages from each tract were quantified except for the lateral column where two montages were used. In addition, the rostro-caudal profile

of β APP accumulation was analysed by projecting the 200 μ m width onto the rostro-caudal axis. Nine specimens (2 contusion, 2 dislocation, 2 distraction, 3 shams) were excluded from quantitative analysis because the level of endogenous peroxidase quenching was not comparable to the level in the remaining slides. For each tract, one-way ANOVA compared β APP accumulation between injury mechanisms. Square-root transformations were used to ensure homoscedasticity prior to statistical testing.

4.2.7 Reactive Astrocytes

Sections stained for GFAP were montaged with a 10 \times objective from -4.5mm to +4.5mm rostro-caudal to the lesion epicentre. Area sampling frames, 500 μ m \times 9mm, were randomly placed entirely within the central region of the gray matter and a threshold was applied to determine the percent area of GFAP immunostaining. Arcsine transformations were applied to ensure equal variances of percent data (Zar, 1999) followed by one-way ANOVA to compare the area of reactive astrocytes between injury mechanisms. The rostro-caudal profile of GFAP was analysed by projecting the 500 μ m sampling frame onto the rostro-caudal axis. White matter astrocytes were not quantified because an immunoreactive gradient was observed between the white/gray matter boundary and the glia limitans thus confounding the placement of a random sampling frame.

4.2.8 Microglial Activation

A new method was developed and validated to quantify microglial activation. Ramified microglia exhibit thin, highly branched processes which thicken and retract during activation (Glenn et al., 1992; Stence et al., 2001). This activation is often characterized qualitatively or by using semi-quantitative methods to grade microglia as resting, activated, or phagocytic. However, the consistency of subjective classification was deemed untenable for the large current dataset (37 animals \times 9 rostro-caudal positions \times 4 regions \times 3 samples). Quantitative methods such as fractal analysis have shown promise though some disparity remains compared to manual classification (Soltys et al., 2001). To validate our method, a set of 154 cropped images of microglia, visualized with anti-Iba1, were manually classified into fully ramified (Figure 4.2A, from sham surgical controls), initial activation indicated by increased immunoreactivity (Figure 4.2B), low activation indicated by thickened processes (Figure 4.2C), medium activation indicated by retracted processes (Figure 4.2D), high activation indicated by few processes (Figure 4.2E), and full activation indicated by a spherical amoeboid morphology (Figure 4.2F). A threshold was used to segment

microglial areas (outlined in red Figure 4.2A to 4.2F). As activation progresses, immunoreactive area initially increases, but this increase is eventually offset by the retraction of processes, thereby rendering area an ambiguous measure of the activation state (Figure 4.2G).

In the novel method, each microglia's "skeleton"—a common quantity in computational image analysis (Nikolaidis and Pitas, 2001)—was determined by thinning the area profiles (*bwmorph(Image, 'thin', inf)* Matlab command) until only a one-pixel thick skeleton representation of each microglia remained (blue pixels in Figure 4.2A to 4.2F). A ramification index was defined as the ratio of skeleton pixels to area pixels ($R = \text{Skeleton}/\text{Area}$). For a highly ramified microglia with thin processes, the majority of area pixels will also be skeleton pixels (Figure 4.2A and 4.2B) resulting in a greater index (Figure 4.2H A-B on x-axis). As microglial processes thicken, the area pixels will increase, while process retraction will reduce the number of skeleton pixels, resulting in a progressive decline in the ramification index (Figure 4.2H C-F on x-axis). Hence, once initially activated, microglia exhibit a monotonic decrease in the ramification index (Figure 4.2H B-F on x-axis) making the index a useful metric for quantitative comparisons.

Slides stained for Iba1 were imaged (20× objective) at 1mm intervals from 4mm caudal to 4mm rostral of the lesion in the ventral gray matter, ventro-medial funiculus, lateral funiculus, and dorsal ascending column. A threshold was applied and the ramification index was calculated within a randomly placed sampling frame ($250 \times 325 \mu\text{m}^2$). Two-way repeated-measures ANOVA compared the effects of injury mechanism and rostro-caudal position in each gray and white matter region analysed.

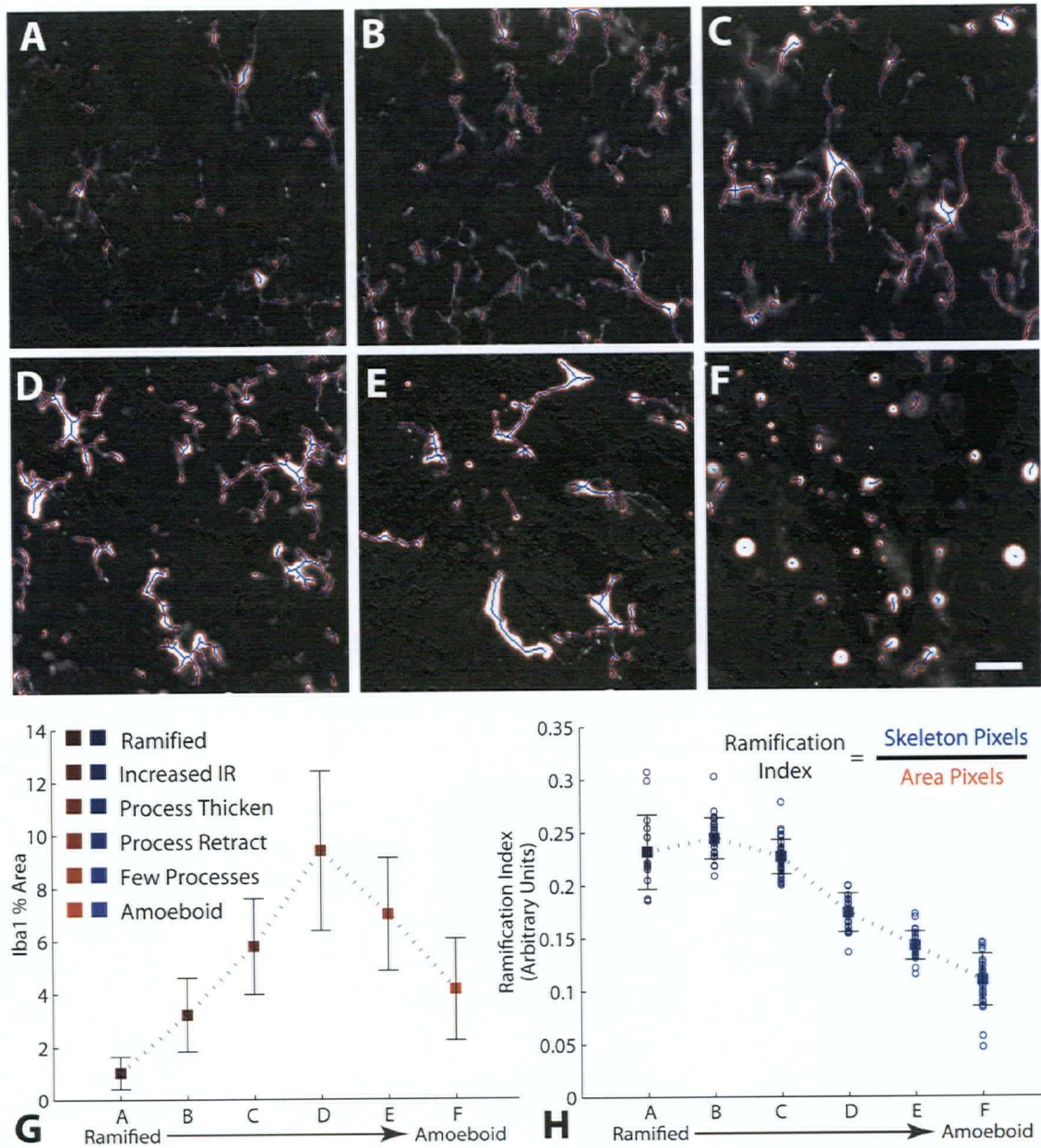


Figure 4.2: Novel microglial ramification index

Iba1 immunohistochemistry demonstrating progressive microglial activation and validation curves for novel ramification index used to quantify morphology. Ramified microglia (A) exhibit low Iba1 immunoreactivity (IR) and fine highly branched (ramified) processes. On initial microglial activation, Iba1-IR increases (B), followed by a thickening of processes (C). As activation evolves, processes retract (D) until microglia exhibit few processes (E). Fully activated microglia (F) exhibit a spherical, amoeboid morphology similar to phagocytic macrophages. In A-F, red pixels outline areas above the background threshold, while blue pixels mark the skeleton of the areas above threshold (refer to methods). G: Percent Iba1-IR area of 154 images manually classified from ramified (A) to amoeboid (F) demonstrates ambiguity of area measurements in delineating the state of microglial activation. H: Ramification index of same images in G shows a progressive decline in the ramification index as microglia evolve from initial activation (B) to amoeboid (F) thereby validating the utility of the (continuous) index for quantitative analysis in place of (discrete) manual classification. Scale bar 20 μ m applies to A-F. Scatter of individual data points are shown in H. Whiskers denote SD.

4.3 Results

The multi-mechanism injury system produced contusion, dislocation, and distraction injuries with a high repeatability (<5% SD) in the controlled displacements and velocities (Table 4.2). The mean resultant contusion force was 1.5 ± 0.4 N (SD). In the dislocation model, the peak force was 24.7 ± 5.7 N (SD) while the peak distraction force was 37.9 ± 5.4 N (SD). Following dislocation and distraction, repositioning of slight misalignment between C4 and C5 was achieved with gentle axial tension on the vertebrae prior to stabilization with stainless steel rods. The integrity of the stabilization was confirmed during tissue harvest.

Table 4.2: Mechanical injury parameters in secondary injury study

Mechanism	<i>n</i>	Displacement (mm)	Force (N)	Velocity (cm/s)
Contusion [†]	10	1.1 ± 0.02	1.5 ± 0.4	99.8 ± 3.7
Dislocation [†]	10	2.5 ± 0.12	24.7 ± 5.7	95.6 ± 3.2
Distraction	10	4.1 ± 0.03	37.9 ± 5.4	111.2 ± 3.5
Surgery Controls	7	–	–	–
Dextran Controls	2	–	–	–

Values represent the means \pm standard deviations for injuries produced under displacement feedback control. Values not applicable are denoted by a hyphen (–).

[†]Mechanical parameters for this group are based on 9 of 10 animals due to software write-error for one animal.

4.3.1 Changes in Membrane Permeability

In order to detect changes in membrane permeability, two different dextran-conjugated fluorophores were infused, 1.5 hours before and 2 hours after injury, and analysed by histology at 3 hours. Compromise of membrane integrity due to primary or secondary injury is reflected by characteristic changes in dextran penetration into axons and cell bodies previously shown to be predominantly neurons (i.e. NeuN-positive refer to chapter 3 Figure 3.7). In the gray matter of surgical controls, dextran incubation controls, and uninjured regions distal to the contusion epicentre, the pre-injury and post-injury dextran molecules were excluded from some neurons (*arrows* Figure 4.3A-C). In these controls, many somata, however, exhibited trace intracellular dextran fluorescence that was similar to background levels (*arrows* Figure 4.3D-F) suggesting a “mild” level of dextran penetration or uptake in the absence of trauma. In uninjured white matter, both dextran tracers accumulated at the nodes of Ranvier (*arrows* Figure 4.3G-I, chapter 3 Figure 3.2) and remained outside the intracellular compartment. In contrast to the gray matter, uninjured white matter rarely exhibited a “mild” level of dextran penetration.

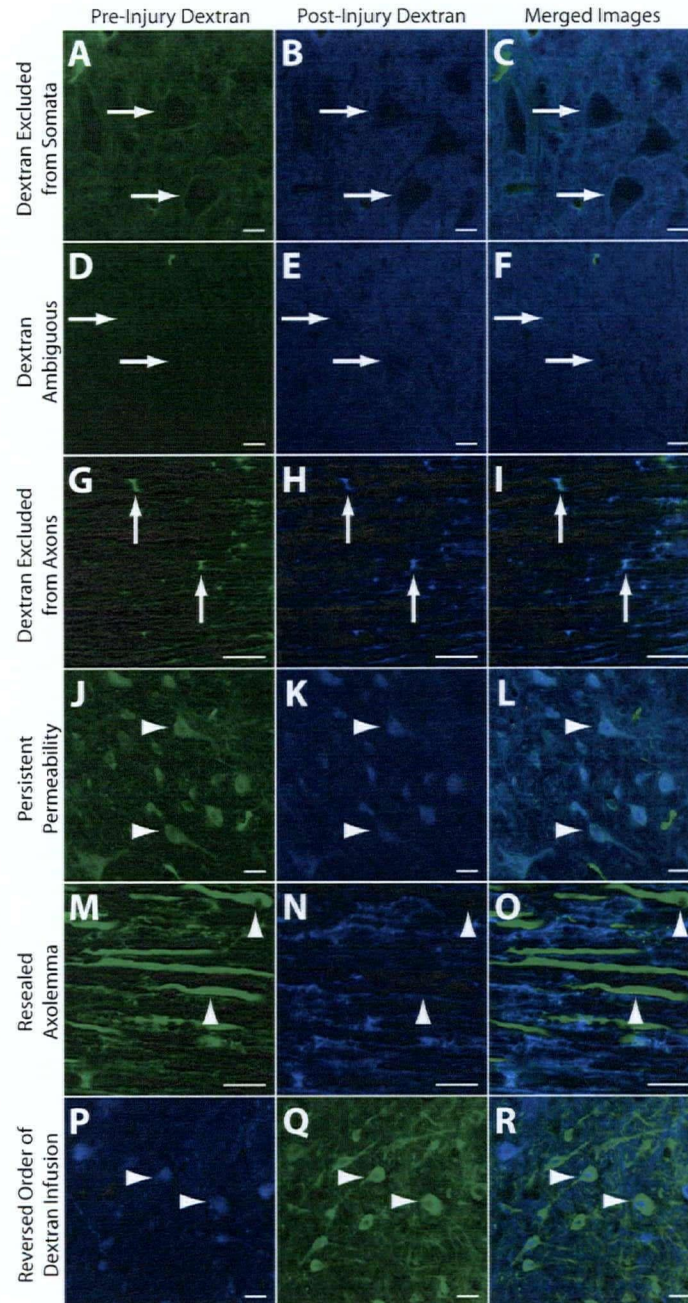


Figure 4.3: Representative micrographs showing evolution of membrane permeability

Photomicrographs contrast the evolution of membrane permeability in neuronal somata and axons. The intracellular penetration of 10kDa dextran-conjugated fluorophores (fluorescein and cascade blue) infused 1.5 hours before injury and 2 hours after injury revealed the time-course of membrane compromise. Uninjured cell bodies excluded both dextran species (*arrows A-C*). Fluorescence from overlaying tissue and mild dextran penetration could obscure neuronal somata (*arrows D-F*). Dextran accumulated at the nodes of Ranvier of axons with an intact axolemma (*arrows G-H*). Injured neuronal somata were usually positive for both the dextran infused before injury (*arrowheads J & L*) and the dextran infused after injury (*arrowheads K & L*) indicating persistent membrane compromise. In contrast, axons flooded with the dextran infused before injury (*arrowheads M & O*) were typically negative for the dextran infused at 2 hours post-trauma (*arrowheads N & O*) indicating membrane resealing. Observations were similar when the order of dextran infusion was reversed (*arrowheads P-R*). Scale bars 25 μ m.

In the SCI region (contrasts between mechanisms is given below), neurons were flooded with the dextran that had been infused before injury (*arrowheads* Figure 4.3J & L), as well as the dextran infused after injury (*arrowheads* Figure 4.3K & L) indicating a persistence in membrane compromise from the time of injury to at least 2 hours post-trauma. In the ventro-medial white matter, axons filled with the pre-injury dextran (*arrowheads* Figure 4.3M & O) were generally negative for the post-injury dextran (*arrowheads* Figure 4.3N & O) signifying that the axolemma had resealed before the second dextran infusion. Dextran infused at 2 hours post-injury was rarely observed to accumulate at “resealed” nodes of Ranvier suggesting damaged nodal structures following primary membrane compromise. Spinal cords in which the order of dextran incubation was reversed showed similar results (Figure 4.3P-R) demonstrating the observations were independent of the dextran species.

Mechanism-specific patterns of primary membrane compromise were still detectable, particularly in the white matter, with the first dextran; however, the second dextran infusion revealed the evolution of membrane permeability was dominated by differences in resealing between neuronal somata and axons. Within neuronal cell bodies, ANOVA revealed a significant difference between the normalized intensity of the pre-injury dextran (1.69) and the post-injury dextran (1.55); an 8% reduction suggesting a gradual resealing of the membranes ($p=0.021$, Figure 4.4A & B). No significant interaction was found between the dextran infusion time and the injury mechanism ($p=0.092$) indicating all mechanisms exhibited parallel resealing patterns. A significant interaction between injury mechanism and rostro-caudal position was detected ($p=0.002$) with dislocation injuries producing the greatest increase in both dextran intensities at the lesion epicentre compared to sham controls ($p=0.030$ pre-injury dextran, $p=0.002$ post-injury dextran).

Axons individually identified to be positive for either or both dextrans exhibited a significantly higher intensity of the pre-injury dextran ($p<0.001$) when analysed over all injury mechanisms and all rostro-caudal positions (Figure 4.4C versus D). Overall, the normalized intensity of the dextran infused after injury was 40% lower than the dextran infused before injury (2.50 vs. 1.47), demonstrating a more pronounced recovery of membrane integrity in axons relative to cell bodies. A significant interaction between rostro-caudal position and injury mechanism ($p=0.004$) was detected indicating the intensity of dextran penetration varied along the length of

the spinal cord. For example, in the dislocation and distraction models, the dextran infused before injury exhibited intensities, approximately 3 times the background level of fluorescence, and this elevated intensity of intra-axonal dextran extended rostrally (at 4mm rostral: $p=0.040$ contusion vs. dislocation, $p=0.048$ contusion vs. distraction). These rostro-caudal differences between injury mechanisms were no longer visible in the analysis of the dextran infused at 2 hours post-injury which may be attributed to the apparent resealing of injured axons. The variability in the sham group at -4mm caudal appeared to be related to excessive manipulation of the vertebral clamp and underscores the sensitivity of the dextran for detecting membrane compromise.

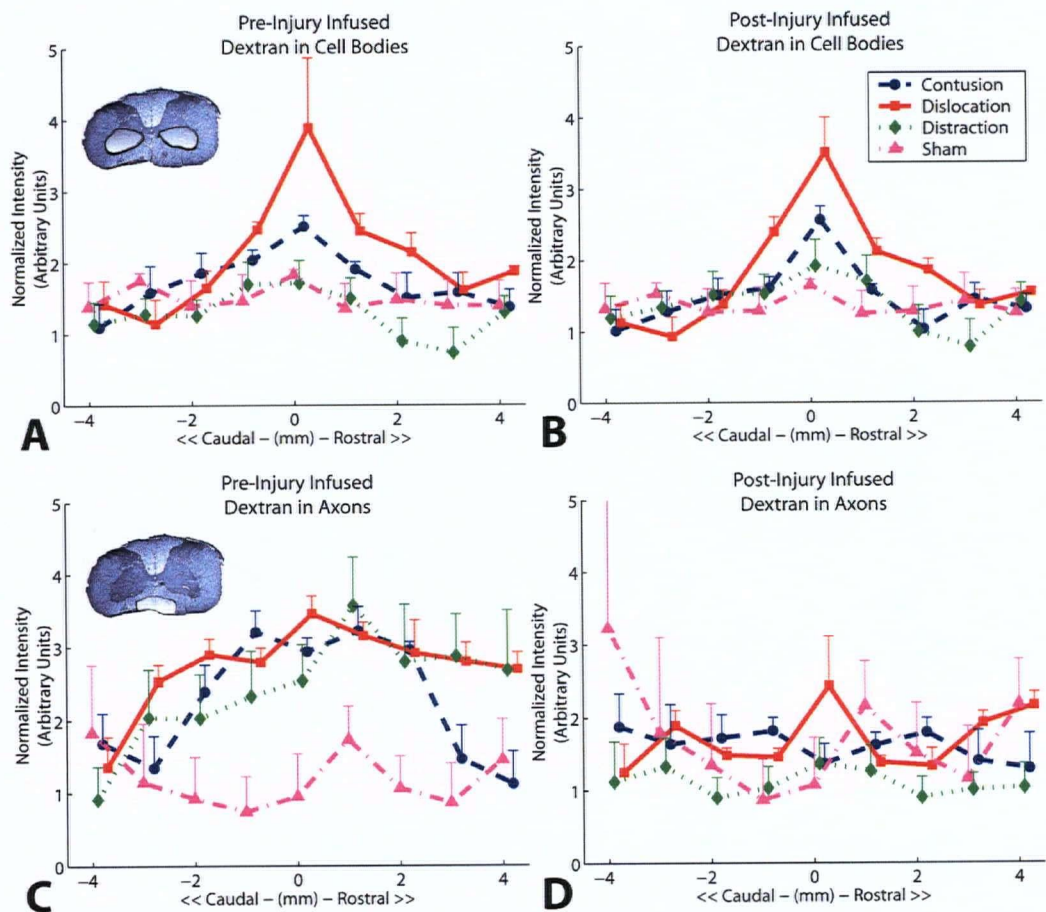


Figure 4.4: Quantitative analysis of dextran penetration into somata and axons

Line graphs comparing the intracellular dextran fluorescence (normalized to the background) in individually identified neuronal cell bodies and axons. In the ventral gray matter (highlighted in A inset), the intensity was similar between the dextran infused before injury (A) and the dextran infused 2 hours after injury (B) suggesting a persistence in membrane permeability. In the ventro-medial white matter (highlighted in C inset), the intensity of dextran infused before injury (C) was greater than that infused after injury (D) indicating membrane resealing. Whiskers denote SEM.

4.3.2 Cell Bodies in the Gray Matter

Sham controls exhibited little immunostaining for the oxidative stress marker 3NT (Figure 4.5A) whereas extensive staining throughout the neurophil near the lesion epicentre was observed in spinal cords injured by contusion (Figure 4.5B) and dislocation (Figure 4.5C). At the distraction epicentre, 3NT staining appeared localized to sparse hemorrhagic areas (Figure 4.5D). The fluorescent intensity of 3NT-positive cells was generally near background levels (*arrowheads* Figure 4.5B-D).

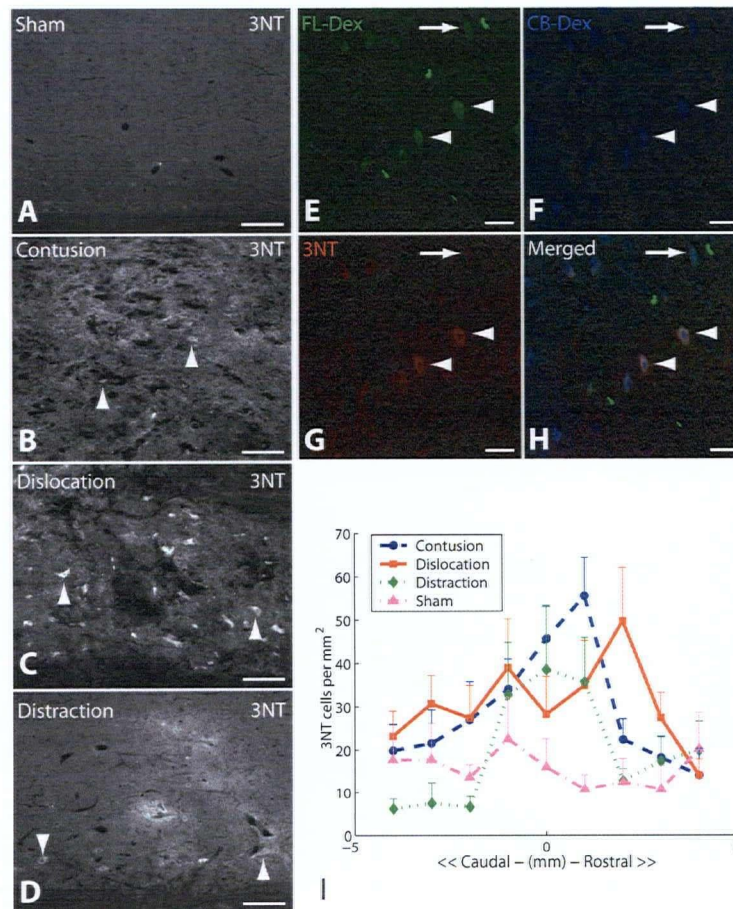


Figure 4.5: Photomicrographs and quantitative counts of 3-NT immunostaining

Representative photomicrographs of immunohistochemistry for the oxidative stress marker 3-nitrotyrosine (3NT) and line graphs showing quantitative distribution of 3NT-positive cells. Spinal cords from sham animals exhibited little 3NT immunostaining (A). Similar patterns of 3NT staining were observed in the gray matter of spinal cords injured by contusion (B) and dislocation (C). Less 3NT immunostaining was detected following distraction injury (D). Near the lesion epicentre, cell bodies permeable to dextran infused before (*arrowheads* E) and after injury (*arrowheads* F) were often positive for 3NT (*arrowheads* G & H). Other dextran-positive cells (*arrow* E & F), however, were negative for 3NT (*arrow* G & H) indicating only a weak association between membrane compromise and oxidative stress at this time-point. A significant interaction ($p=0.023$) between the injury mechanism and rostro-caudal distribution of 3NT-positive cells (I) was found with peak counts in the dislocation model biased rostrally. Scale bars 150 μ m (A-D) and 50 μ m (E-H). *Whiskers* denote SEM.

Near the lesion, neurons positive for 3NT (*arrowheads* Figure 4.5G & H) often exhibited persistent membrane permeability to dextran (*arrowheads* Figure 4.5E & F), however, dextran-positive neurons were also observed to be negative, or only weakly positive, for 3NT (*arrow* Figure 4.5E-H). The overall number of 3NT-positive cells was similar between injury groups ($p=0.072$) though a significant interaction ($p=0.007$, Figure 4.5I) was detected between the injury mechanism and the rostro-caudal distribution of cells. SNK *post hoc* analysis showed a rostral bias in the number of 3NT-positive cells with more 3NT-positive cells detected at 2mm rostral to the dislocation lesion compared to similar regions in the contusion ($p=0.053$) and distraction ($p=0.012$) injuries.

There were subtle differences in the pattern of cytochrome *c* immunostaining between injury groups. Cytochrome *c* is normally localized within mitochondria (Gulyas et al., 2006) and its release into the cytosol is an early marker of apoptosis as demonstrated by immunohistochemistry (Springer et al., 1999; Sugawara et al., 2002; Vanderluit et al., 2003) and western blot (Springer et al., 1999; Teng et al., 2004). In uninjured animals, the mitochondria within the cytoplasm of neuronal somata exhibited a high intensity of cytochrome *c* immunofluorescence (*arrows* Figure 4.6A) against a backdrop of scattered cytochrome *c*-positive mitochondria in the neurophil (Figure 4.6A). A small population in the lateral penumbra of the contusion lesion exhibited a profound loss of cytochrome *c* immunostaining (*arrowheads* Figure 4.6B) indicative of complete cytochrome *c* release from mitochondria. Attenuation of cytochrome *c* in neuronal cell bodies was also found in the rostral and caudal penumbra of the dislocation epicentre (*arrowhead* Figure 4.6C). Distraction injury produced cytochrome *c* immunostaining patterns similar to that observed in spinal cords from sham surgical controls (*arrows* Figure 4.6D). Cells displaying a loss of cytochrome *c* were consistently positive for both dextran tracers (*arrowheads* Figure 4.6E-H), although dextran-positive neuronal somata were also observed to maintain cytochrome *c* immunoreactivity (*arrow* Figure 4.6I-L), suggesting persistent membrane compromise was a necessary, but not sufficient condition to abolish cytochrome *c* immunostaining. This subpopulation with attenuated immunostaining for cytochrome *c* was consistently observed following contusion and dislocation, however, the sparseness of these cells, and their narrow localization within the penumbrae of the lesion epicentres, precluded systematic random sampling. Hence, quantitative analysis was not conducted.

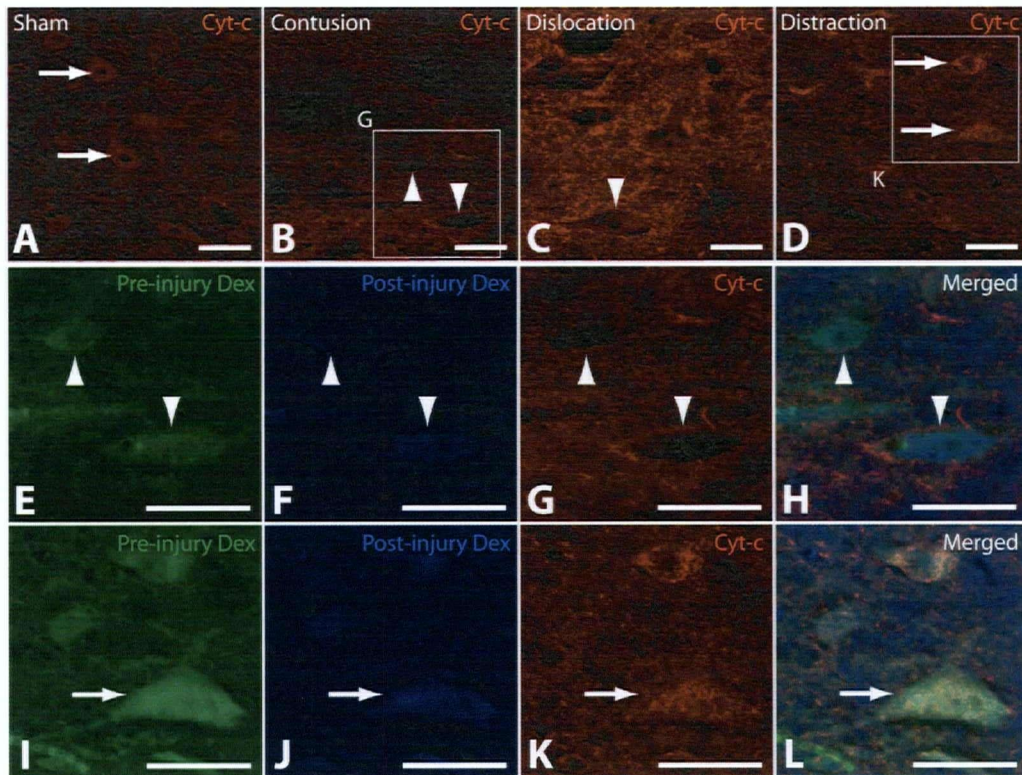


Figure 4.6: Cytochrome *c* immunostaining

Photomicrographs showing cytochrome *c* immunohistochemistry and its association with membrane compromise near the lesion epicentre. Spinal cords from sham surgical controls exhibited granular cytochrome *c* immunostaining localized to the neuronal cytoplasm (arrows A) with less intense granular staining of mitochondria in the surrounding tissue. In the lateral penumbra of the contusion epicentre, a reduction in cytochrome *c* was observed in neurons (arrowheads B) and the surrounding hemorrhagic tissue. In the rostro-caudal penumbrae of the dislocation lesion, a loss of cytochrome *c* immunoreactivity was observed in a small population of cells (arrowhead C) while an increase in immunostaining was observed in surrounding non-hemorrhagic tissue. Cytochrome *c* immunostaining following distraction injury was similar to that observed in sham animals (arrows D). Cytochrome *c*-negative neurons in the contusion and dislocation lesion penumbra were consistently positive for dextran (arrowheads E-H), though many dextran-positive neurons were also cytochrome *c*-positive (arrow I-L). Scale bars 50 μ m.

4.3.3 Axons in the White Matter

The compaction of neurofilaments is characteristic of early axonal damage following axolemmal compromise (Pettus et al., 1994) and likely results from the dephosphorylation and collapse of sidearms (Maxwell et al., 1997; Okonkwo et al., 1998). This dephosphorylation exposes the neurofilament core to earlier proteolytic degradation than its phosphorylated counterparts (Pant, 1988; Schumacher et al., 1999). SMI32 binds to non-phosphorylated neurofilament (npNF) epitopes in heavy and medium neurofilaments (Sternberger and Sternberger, 1983) revealing thick axons such as those in the ventral white matter (Figure 4.7A), whereas SMI31 detects phosphorylated epitopes (pNF, Figure 4.7B). At the contusion epicentre, non-phosphorylated neurofilament immunostaining declined (Figure 4.7C) while phosphorylated

neurofilaments were still readily detectable on the adjacent section (Figure 4.7D). In contrast, the dislocation injury mechanism produced an extensive loss of immunostaining for both non-phosphorylated (Figure 4.7E) and phosphorylated (Figure 4.7F) epitopes signifying irreversible white matter damage. Ventral axons at the distraction epicentre appeared predominantly intact and stained robustly for both neurofilament epitopes (Figure 4.7G & H).

The differences in immunoreactive areas between contusion and dislocation were more apparent at the high magnification (40× objective) used for quantification. At the contusion epicentre, ventral peripheral axons appeared predominantly intact (*arrows* Figure 4.7I). In contrast, at the dislocation epicentre, axonal fragmentation of ventral axons was frequently observed (*arrowheads* Figure 4.7J) and subpial areas of complete axonal loss were also evident (*asterisk* Figure 4.7J). Quantitative analysis (Figure 4.7K) showed a significant effect of mechanism ($p=0.024$), rostro-caudal position ($p<0.001$) and interaction of these two parameters ($p<0.001$). At the lesion epicentre, dislocation injuries resulted in a greater loss of non-phosphorylated neurofilament area compared to both contusion ($p=0.004$) and distraction ($p<0.001$). The area of non-phosphorylated neurofilaments at the contusion site was not significantly less than the area at the sham lesion ($p=0.167$) and reflects that many axons at the contusion epicentre were still detectable above the background threshold, while areas of axonal loss were partially offset by axonal swelling. The elevation in the mean area of non-phosphorylated neurofilaments following distraction (*green profile* Figure 4.7K), though not significant ($p>0.127$) compared to sham controls, may be indicative of subtle neurofilament dephosphorylation.

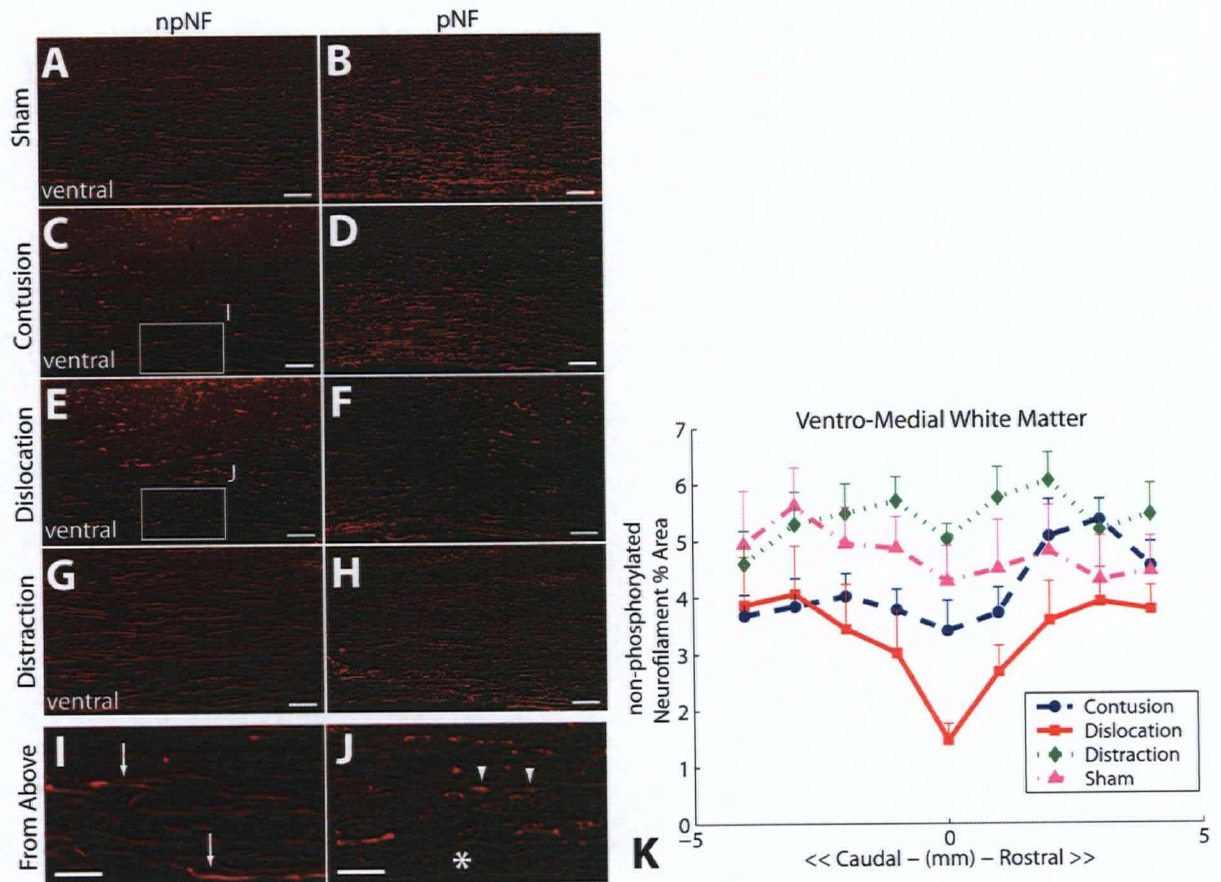


Figure 4.7: Neurofilament degradation in the ventro-medial white matter

Representative photomicrographs and quantitative line graphs show the dislocation injury mechanism accelerates the degeneration of neurofilaments in the ventro-medial white matter. Robust non-phosphorylated (npNF) and phosphorylated (pNF) neurofilament immunostaining was observed in spinal cords from sham surgical controls (A & B). A reduction in immunostaining for non-phosphorylated neurofilaments was observed at the contusion epicentre (C) though staining for phosphorylated neurofilament epitopes revealed many axons were still intact (D). Extensive loss of ventro-medial neurofilaments – both non-phosphorylated (E) and phosphorylated (F) – was observed in the dislocation model. The majority of ventral axons appeared intact in the distraction injury model (G & H). High magnification images at the lesion epicentres reveal peripheral ventral axons were generally spared following contusion (arrows I). In contrast, dislocation injury resulted in more axonal fragmentation (arrowheads J) and regions completely devoid of peripheral axons (asterisk J). Quantitative measurements of the percent area of non-phosphorylated neurofilament immunoreactivity showed the greatest loss in neurofilaments at the dislocation epicentre ($p < 0.004$ vs. contusion and distraction). A reduction in non-phosphorylated neurofilament area was detected at the contusion epicentre though most axons exhibited immunoreactivity above the background threshold at high magnification. Scale bars 100 μ m (A-H) and 50 μ m (I & J). Whiskers denote SEM.

We next assessed the accumulation of β APP which is indicative of disrupted fast axonal transport and reveals white matter injury following neurotrauma in humans (Cornish et al., 2000; Smith et al., 2003) and animals (Li et al., 1995; Gomes-Leal et al., 2005). In the lateral white matter, following contusion (Figure 4.8A & D) and distraction injuries (Figure 4.8C & F), diffuse punctate staining of β APP was observed. In contrast, dislocation produced widespread staining of

β APP accumulation in ascending and descending fibers of the lateral funiculi (Figure 4.8B & E) near primary axotomies from the direct shearing between C4 and C5 vertebrae (*arrowheads* Figure 4.8B). Quantitatively in the distraction model, the diffuse level of β APP accumulation in all white matter tracts rendered these areas negligible relative to the more extensive accumulations observed following contusion and dislocation injuries (Figure 4.8G & H, $p < 0.001$ for all comparisons relative to distraction). In contrast to the diffuse staining observed in distraction, contusion and dislocation injury mechanisms produced similar levels of β APP accumulation in the dorsal column ($p = 0.647$), dorsal corticospinal tract ($p = 0.145$), and ventro-medial column ($p = 0.206$). However, as observed qualitatively, dislocation injuries resulted in quantitatively much greater β APP immunostaining in the lateral column than either contusion ($p = 0.001$) or distraction ($p < 0.001$) injuries. Although β APP accumulation levels were often similar between the contusion and dislocation groups – indicating a comparable number of axons injured – the rostro-caudal position of the β APP accumulation front in the corticospinal tract was shifted rostrally following dislocation indicating a more extensive damage of this tract by a dislocation injury mechanism (Figure 4.8I).

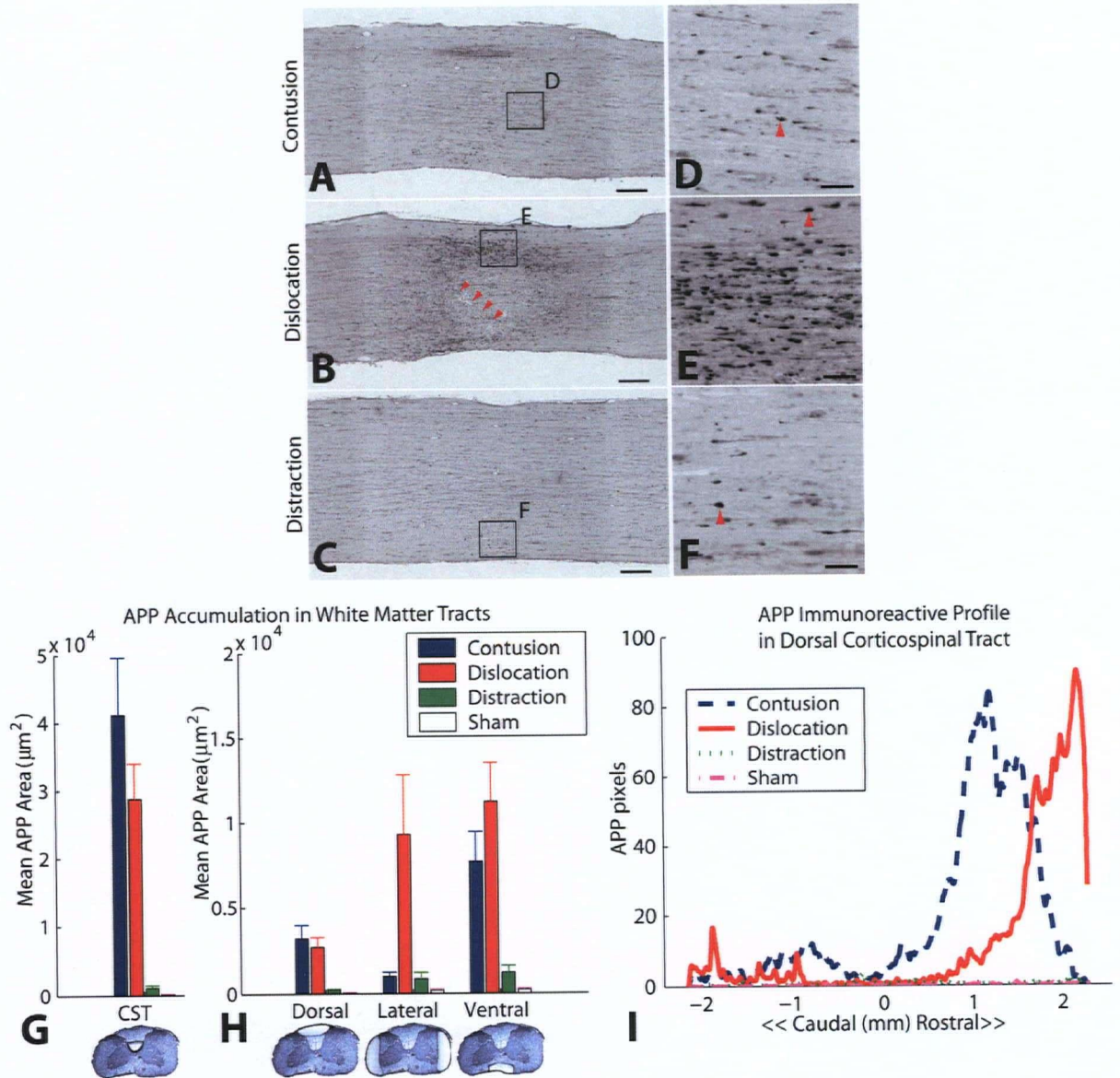


Figure 4.8: β APP accumulation in white matter

Representative photomicrographs, bar graphs and rostro-caudal profile of β APP immunostaining. In the lateral funiculi of spinal cords injured by contusion (A & D), dislocation (B & E) and distraction (C & F), β APP accumulation was most extensive following dislocation injury. Characteristic axotomy from the dislocation mechanism's shear forces was evident in the lateral column (*arrowheads* B). Quantitative analysis of β APP accumulation in the dorsal corticospinal tract (G), dorsal column, lateral column, and ventral column (H) showed relatively diffuse injury following distraction. In the white matter, contusion and dislocation injuries produced similar areas of β APP immunostaining except in the lateral column where dislocation resulted in significantly greater β APP accumulation ($p=0.001$). A rostral bias in the boundary of descending β APP accumulation was observed in spinal cords injured by dislocation (I). The profile in I was averaged over all animals analysed excluding 9 slides due to differences in the background level of endogenous peroxidase quenching (refer to methods). Scale bars 250 μ m (A-C) and 50 μ m (D-F). *Whiskers* denote SEM.

4.3.4 *Reactive Astrocytes*

Both contusion and dislocation injury mechanisms resulted in extensive astrogliosis near the boundary of the lesion epicentre. GFAP immunostaining in spinal cords from sham surgical controls revealed well defined astrocytes that exhibited dim immunofluorescence (Figure 4.9A). The intensity of GFAP immunoreactivity was increased near the spinal cord lesion following contusion (Figure 4.9B & E), dislocation (Figure 4.9C & G) and distraction (Figure 4.9D) injuries. In the contusion injury model, astrogliosis appeared predominantly contained within 2mm of the lesion epicentre (compare Figure 4.9E versus 4.9F). In contrast, following dislocation, astrogliosis was evident near the lesion boundary (Figure 4.9G) but also in regions at 3 to 4mm distal to the epicentre (Figure 4.9H). In spite of this qualitative observation, quantitative analysis of GFAP immunoreactive areas showed no significant difference in percent GFAP area between contusion and dislocation (Figure 4.9I, $p=0.992$). An analysis of the rostro-caudal distribution of GFAP (Figure 4.9J) suggests the average density of GFAP after dislocation and contusion was indeed similar, though it was more confined to the lesion following contusion, and extended more rostrally following dislocation.

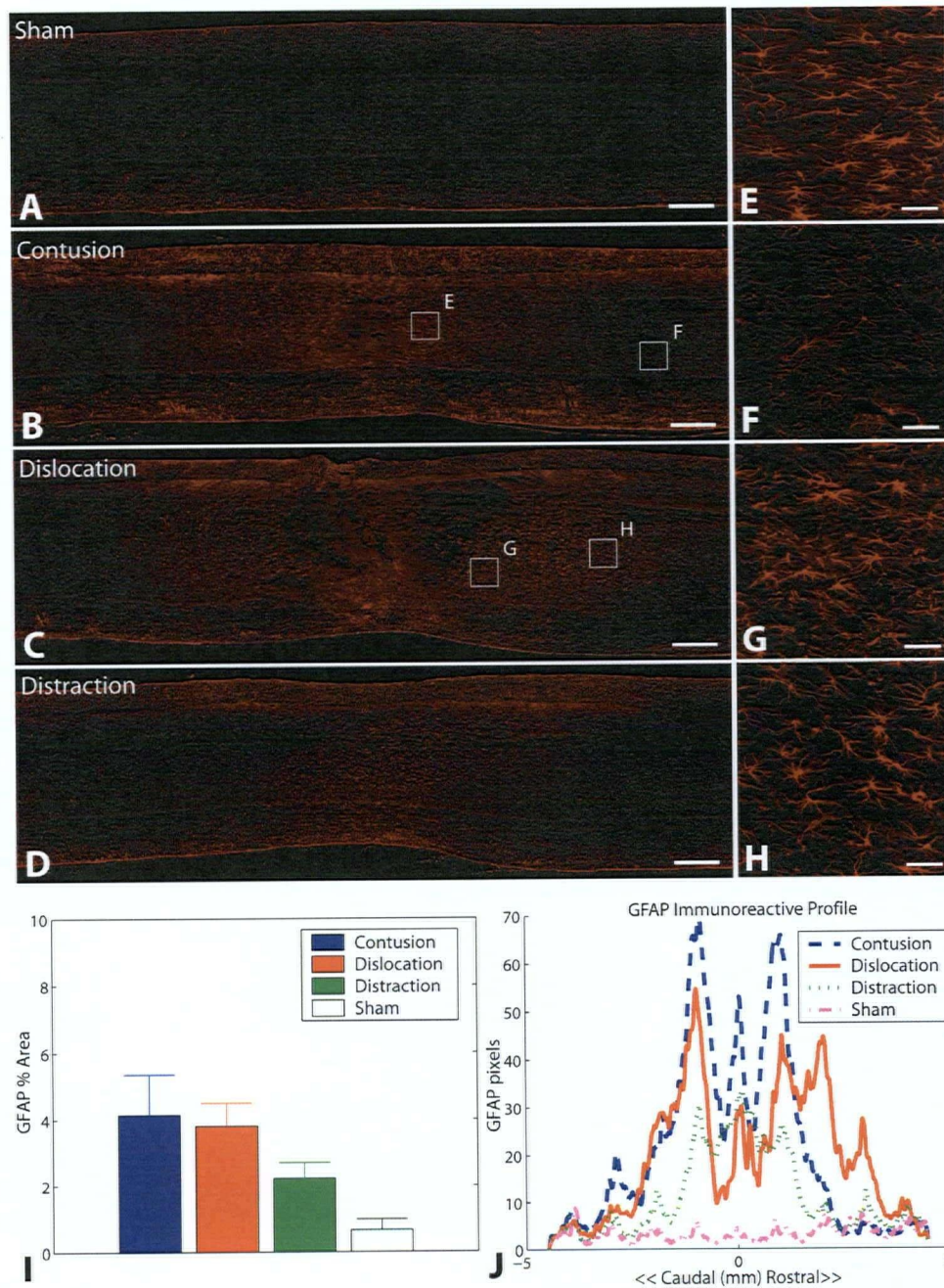


Figure 4.9: Distribution of reactive astrocytes

Low and high magnification photomicrographs, quantitative bar graphs and rostro-caudal profile of GFAP immunostaining. Spinal cords from sham surgical controls exhibited low levels of GFAP (A) while an increase in reactive astrocytes was observed following contusion (B), dislocation (C), and distraction (D) spinal cord injuries. The increase in astrogliosis was localized to the lesion epicentre following contusion (E vs. F) while following dislocation, reactive astrocytes were observed both near the lesion epicentre and rostrally (G vs. H). Quantitative analysis in the gray matter showed no significant differences in immunoreactive areas between the injury mechanisms (I), however, the rostro-caudal profile of immunostaining suggests a broader distribution of reactive astrocytes following dislocation injury (J). Percent areas in I were based on $500\mu\text{m} \times 9\text{mm}$ sampling frames. Identical exposure and background thresholds were used for all images. These levels were selected to prevent saturation of the exposure and threshold areas in images from injured animals resulting in very low GFAP levels in sham surgical controls (A and I). Scale bars $500\mu\text{m}$ (A-D) and $50\mu\text{m}$ (E-H). Whiskers denote SEM.

4.3.5 Microglial Activation

Microglial activation is another hallmark of central nervous system trauma and is characterized by a morphological transition from a resting ramified to an activated amoeboid shape (Figure 4.2 and methods section). Each injury mechanism resulted in distinct rostro-caudal patterns of microglial activation. Microglia in sham surgical control animals exhibited fine highly ramified processes characteristic of resting microglia although some evidence of low activation was observed at the sham lesion presumably due to surgical manipulation of the vertebral column (Figure 4.10A). Microglia at the contusion (Figure 4.10B) and dislocation (Figure 4.10C) gray matter epicentres were predominantly amoeboid in morphology indicative of full activation. In contrast, following distraction injury, few microglia were fully activated except those found near regions exhibiting tissue necrosis (Figure 4.10D). At 4mm rostral to the lesion, microglia in sham (Figure 4.10E), contusion (Figure 4.10F) and distraction (Figure 4.10H) groups exhibited morphologies indicative of resting microglia or microglia in a low activation state. In contrast, highly activated microglia with few processes were still observed at 4mm rostral to the dislocation epicentre (Figure 4.10G). Quantitatively, in the gray matter, contusion and dislocation resulted in similar levels of microglial activation at the lesion epicentre ($p = 0.210$) which were significantly greater than those detected at the distraction lesion ($p < 0.001$, Figure 10I 0mm). Microglial activation in the dislocation model remained elevated along the length of the spinal cord from -4mm caudal ($p = 0.017$ compared to sham controls) to +4mm rostral ($p = 0.003$ compared to sham controls) of the lesion epicentre. Microglia in animals injured by vertebral distraction tended to have a greater ramification index compared to shams at 2mm ($p < 0.001$), 3mm ($p < 0.004$), and 4mm ($p = 0.052$); indicative of the increased immunoreactivity of microglia in the earliest phase of activation (Figure 4.10I, cross-reference with Figure 4.2B & 2H).

Within the white matter, microglial activation patterns in animals injured by dislocation differed between tracts. Following dislocation, microglial activation was greater rostrally in the lateral (Figure 4.10J) and dorsal (Figure 4.10K) columns but symmetric about the lesion epicentre in the ventro-medial tract (Figure 4.10L). In contrast, contusion injuries produced symmetric patterns of microglial activation with the highest activation in the dorsal (Figure 4.10K) and ventral columns (Figure 4.10L). In the distraction model, the microglia in the white matter were quantitatively similar to those in sham surgical control specimens.

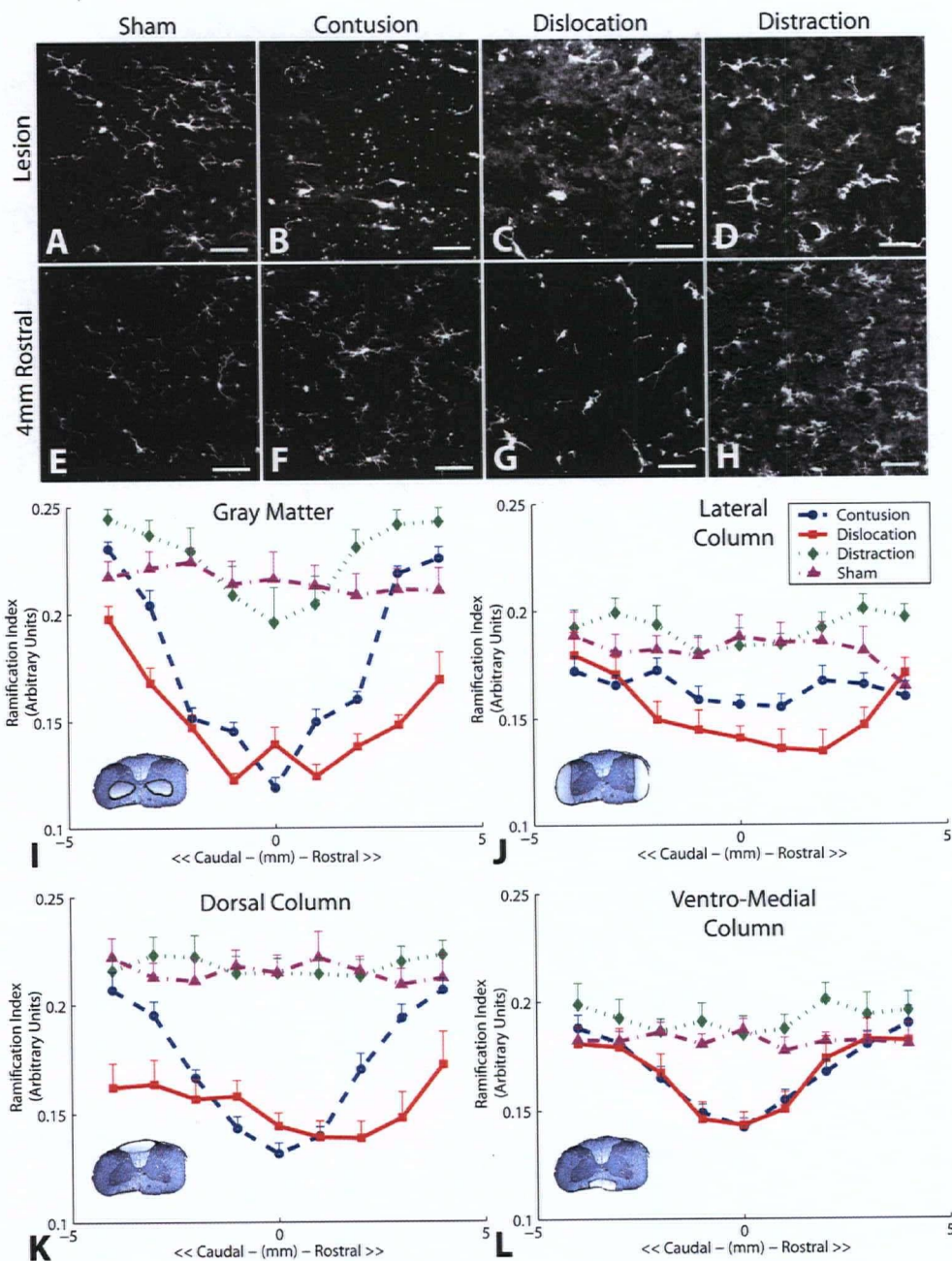


Figure 4.10: Microglial activation

Representative photomicrographs of Iba1 immunostaining and morphometry of microglia in the gray and white matter show asymmetry of microglial activation following dislocation injury. Microglia in sham surgical controls were highly ramified and exhibited low levels of Iba1 immunostaining at the lesion and rostrally (A & E). Microglia at the contusion epicentre were amoeboid (B) while rostrally, only low levels of activation were detected (F). Microglia were highly activated at both the dislocation epicentre (C) and rostrally (G). At the distraction epicentre, microglia exhibited process thickening characteristic of low levels of activation (D) while rostrally, most microglia exhibited increased Iba1 immunoreactivity but remained highly ramified (H). Analysis of the ramification index (Figure 2) in the gray matter (I) showed greater rostral-caudal microglial activation following dislocation injury. Microglial morphology in the lateral (J), dorsal (K), and ventral (L) funiculi showed a dorsal to ventral asymmetry in activation following dislocation injury. Scale bars 50 μ m (A-H). *Insets* I-L highlight region quantified. *Whiskers* denote SEM.

4.4 Discussion

This study compared the initiation of secondary pathology following distinct clinically relevant mechanisms of SCI. An early post-traumatic time-point was examined because it is within this acute phase that neuroprotective strategies have demonstrated promising efficacy, and thus it is here, where an understanding of residual secondary effects from differences in primary damage (chapter 3) might eventually improve future clinical treatment paradigms. Relative to spinal cord contusion, the dislocation injury accelerated neurofilament degeneration, produced a wider axonal regeneration gap, and extended the rostro-caudal zone of microglial and astrocyte activation. In contrast, although distraction injury has been previously shown to produce widespread primary cellular membrane compromise (chapter 3), in this study, modest secondary pathology was detected that might be attributable to the combination of membrane resealing and this model's modest primary hemorrhage that is central to the initiation of degeneration (Balentine, 1978; Guha and Tator, 1988).

A study limitation was that the short survival period prevented the analysis of post-traumatic behaviour. The profound functional deficits from cervical injuries (Pearse et al., 2005; Gensel et al., 2006) ethically necessitate the demonstration of meaningful differences between these injury mechanisms before proceeding with a survival study. The degeneration in the lateral funiculi following dislocation injury could precipitate deficits in digit dexterity due to damage of the rubrospinal tracts (Schrimsher and Reier, 1993) or hindlimb impairments due to loss of ventro-lateral reticulospinal fibers (Loy et al., 2002; Schucht et al., 2002). Clinically, spinal shock confounds the reliability of functional scores taken at the time of hospital admission (Tator, 2006), while later, initial differences may be masked by irreversible degeneration of the spinal cord. Hence, the focus was on contrasting the early secondary cascade that precedes the period of reliable functional assessments.

In the present study dextran tracers were used but this technique has some limitations in detecting membrane compromise. Fluorescence from extracellular dextran blurs the intracellular signal and reduces the reliability of detecting dextran within fine structures (chapter 3). A wider range of graded dextran penetration was observed at three hours post-trauma compared to a primary injury time-point (chapter 3) and is likely due to a combination of protracted endogenous uptake mechanisms (Vercelli et al., 2000) and membranes exhibiting variable stages of progressive

degeneration or recovery. Approximately 40% of cells have been observed to reseal to Texas Red-conjugated dextran by 2 hours following diffuse traumatic brain injury (Farkas et al., 2006). In the current study, the limited resealing detected in the gray matter reflects the greater severity of the injuries produced. The limited resealing observed in the gray matter is unlikely to be an artifact of retrograde transport of the second dextran tracer back to the cell body because there was little penetration of the second dextran into axons and the duration of incubation of the second dextran species was only 1 hour prior to euthanasia. Differences between the studies due to the dextran species utilized (Nance and Burns, 1990) are unlikely since the results were consistent with preliminary trials employing tetramethylrhodamine-dextran (Choo et al., 2005) and confirmed by reversing the order of dextran infusion. In addition, the use of two dextran-conjugated fluorophores limited our ability to use multiple labels for detecting pathologies such as oligodendroglial apoptosis; though the literature indicates this population is more readily detectable at one week after the period analysed here (Shuman et al., 1997).

In the three injury models, dextran penetration across compromised cell membranes previously demarcated distinct primary injury fields but these boundaries have been obscured by the evolution in membrane permeability. Contusion was previously shown to damage cell membranes in a symmetric pattern at the lesion epicentre while the injury fields following dislocation and distraction were asymmetric – extending rostrally (chapter 3). These primary differences were less evident following the secondary evolution of membrane integrity (Figure 4.4B & D). The pre-injury dextran in the white matter, however, still reflected the primary injury asymmetry (Figure 4.4C) suggesting membrane resealing retains the dextran that entered during mechanical injury (Figure 4.4A). Although transient, the loss of membrane integrity is associated with delayed cell death (Geddes et al., 2003; Geddes-Klein et al., 2006) and axonal degradation (Banik et al., 1982; Pettus et al., 1994; Jafari et al., 1998), while membrane repair strategies have shown therapeutic benefits (Borgens and Shi, 2000; Serbest et al., 2006).

The rostro-caudal patterns of secondary neuropathology appeared related to the characteristics of primary injury. In the dislocation model, the distribution of activated microglia, and to a lesser extent reactive astrocytes, parallels the extended rostral primary membrane injury previously observed in chapter 3 for this model. This rostral bias in glial activation may suggest mechanically induced membrane compromise allows the release of adenosine triphosphate

(Ahmed et al., 2000) into the extracellular space which in turn activates glia via purinergic receptors (Rathbone et al., 1999; Inoue, 2002; Davalos et al., 2005). Microglial activation also exhibited a dorsal to ventral asymmetry. This phenomena may highlight the susceptibility to injury of dorsal funiculi that has also been reported in contusion models (Bresnahan et al., 1991). Moreover, signs of primary damage in the lateral funiculi following dislocation injury (chapter 3) were evident in the rapid accumulation of β APP at this lateral epicentre. Parallels between primary and early secondary damage following distraction injury were difficult to draw. This seems consistent with the delayed time-course of neuropathology reported in other animal models of distraction (Myklebust et al., 1988; Maiman et al., 1989; Dabney et al., 2004), as well as *in vitro* models that have demonstrated the robustness of neurons to stretch injury (Smith et al., 1999; Lusardi et al., 2004; Chung et al., 2005) and their vulnerability to delayed apoptosis (Pike et al., 2000; Arundine et al., 2004).

In the current study, although similar primary injury severities were modelled, distinct secondary axonal injury populations were identifiable. Neurofilament degradation and β APP accumulation are well characterized hallmarks of axonal pathology (Banik et al., 1982; Iizuka et al., 1987; Li et al., 1995). The loss of axolemmal integrity is thought to precipitate the collapse of neurofilament sidearms (Jafari et al., 1998), possibly by proteolytic cleavage (Pettus et al., 1994) or dephosphorylation (Okonkwo et al., 1998), rendering these cytoskeletal proteins more susceptible to calpain degradation than their phosphorylated counterparts (Pant, 1988; Schumacher et al., 1999). Non-phosphorylated neurofilaments were not lost following distraction injury; an observation similar to diffuse axonal injury models where an increase in neurofilament dephosphorylation has been reported (Chen et al., 1999; Saatman et al., 2003). In contrast, both contusion and dislocation injuries resulted in reduced immunostaining for non-phosphorylated neurofilament, with degeneration in the dislocation model extending to the phosphorylated epitopes that degrade slower (Pant, 1988). Thus, treatments such as calpain inhibition (Banik et al., 1998; Schumacher et al., 2000), may have a broader time-window in contusion and distraction injuries.

In the gray matter, contusion and dislocation injury mechanisms shared similarities as well as differences that could indicate which processes initiate degeneration regionally. The oxidative stress marker 3NT has been shown in both traumatic brain and spinal cord injuries to increase by

one hour post-trauma (Deng et al., 2007; Xiong et al., 2007). Overall, the similar counts of 3NT-positive cells following contusion and dislocation suggest an equal priority for anti-oxidant or anti-lipid peroxidation strategies in these two mechanisms with a lower priority for this degenerative pathway in distraction injuries. However, the broader microglial activation in the gray matter of spinal cords injured by dislocation suggests this glial response may lead the degeneration in the rostral and caudal fields (Inoue, 2002; Schwartz, 2003; Block and Hong, 2005; Bye et al., 2006) with other pathologies trailing soon after. In addition, the release of cytochrome *c* from mitochondria has been established to precede caspase-3 mediated apoptosis (Springer et al., 1999). The few cytochrome *c*-negative neurons observed in the lateral and rostro-caudal penumbrae of the contusion and dislocation lesions respectively may presage the leading edge of apoptosis that could be amendable to targeted pharmacotherapies (Teng et al., 2004).

This study contributes some perspective on the clinical translation of the myriad therapies directed at mitigating secondary damage. Clinically, vertebral fracture-dislocation have been associated with more severe functional deficits (Marar, 1974; Tator, 1983). The contusion and dislocation injury severities used in this study were previously shown to produce nearly identical levels of intramedullary hemorrhage as well as comparable levels of membrane compromise at the lesion epicentre (chapter 3). The accelerated axonal degeneration and widespread resident inflammatory response of microglia suggest a narrower neuroprotective time-window following dislocation injuries, and may partially explain the limited efficacy of therapies tested in the heterogeneous human population (Pointillart et al., 2000; Geisler et al., 2001; Tadie et al., 2003). Moreover, the rostral asymmetry in the dislocation model may explain the increased clinical severity of fracture-dislocations since the loss of each cervical level is highly detrimental to neurological function (Hedel and Curt, 2006). In a clinical series of 186 cervical SCI's (Harrop et al., 2001), ascension of the lesion was observed in 12 (6%) patients, of which 9 appeared to have suffered a vertebral dislocation injury with concomitant flexion-distraction reported in 6 patients.

This study also suggests that repair and regenerative strategies, specifically targeted to contusion injuries, may have limited efficacy when applied to other injuries. Although in this study astrogliosis was far from complete, our early observations might suggest that dislocation generates a wider astrocytic barrier to regeneration. In the dorsal corticospinal tract, the rostral shift in the β APP accumulation front following dislocation delineates a longer regeneration

distance. When combined with the extensive damage detected in the lateral funiculi, the differences in white matter deterioration suggest repair strategies may favour contusion and distraction injuries, whereas for dislocations, substantial axonal regeneration, however elusive, may be required for improving function.

4.5 References

- Ahmed SM, Rzigalinski BA, Willoughby KA, Sitterding HA, Ellis EF (2000) Stretch-induced injury alters mitochondrial membrane potential and cellular ATP in cultured astrocytes and neurons. *J Neurochem* 74:1951-1960.
- Arbogast KB, Margulies SS (1998) Material characterization of the brainstem from oscillatory shear tests. *J Biomech* 31:801-807.
- Arundine M, Aarts M, Lau A, Tymianski M (2004) Vulnerability of central neurons to secondary insults after in vitro mechanical stretch. *J Neurosci* 24:8106-8123.
- Balentine JD (1978) Pathology of experimental spinal cord trauma. I. The necrotic lesion as a function of vascular injury. *Lab Invest* 39:236-253.
- Banik NL, Hogan EL, Powers JM, Whetstone LJ (1982) Degradation of cytoskeletal proteins in experimental spinal cord injury. *Neurochem Res* 7:1465-1475.
- Banik NL, Shields DC, Ray S, Davis B, Matzelle D, Wilford G, Hogan EL (1998) Role of calpain in spinal cord injury: effects of calpain and free radical inhibitors. *Ann N Y Acad Sci* 844:131-137.
- Block ML, Hong JS (2005) Microglia and inflammation-mediated neurodegeneration: multiple triggers with a common mechanism. *Prog Neurobiol* 76:77-98.
- Borgens RB, Shi R (2000) Immediate recovery from spinal cord injury through molecular repair of nerve membranes with polyethylene glycol. *FASEB J* 14:27-35.
- Bracken MB, Shepard MJ, Collins WF, Holford TR, Young W, Baskin DS, Eisenberg HM, Flamm E, Leo-Summers L, Maroon J, et al. (1990) A randomized, controlled trial of methylprednisolone or naloxone in the treatment of acute spinal-cord injury. Results of the Second National Acute Spinal Cord Injury Study. *N Engl J Med* 322:1405-1411.
- Bracken MB, Shepard MJ, Holford TR, Leo-Summers L, Aldrich EF, Fazl M, Fehlings M, Herr DL, Hitchon PW, Marshall LF, Nockels RP, Pascale V, Perot PL, Jr., Piepmeier J, Sonntag VK, Wagner F, Wilberger JE, Winn HR, Young W (1997) Administration of methylprednisolone for 24 or 48 hours or tirilazad mesylate for 48 hours in the treatment of acute spinal cord injury. Results of the Third National Acute Spinal Cord Injury Randomized Controlled Trial. National Acute Spinal Cord Injury Study. *JAMA* 277:1597-1604.
- Breig A (1970) Overstretching of and circumscribed pathological tension in the spinal cord--a basic cause of symptoms in cord disorders. *J Biomech* 3:7-9.
- Bresnahan JC, Beattie MS, Stokes BT, Conway KM (1991) Three-dimensional computer-assisted analysis of graded contusion lesions in the spinal cord of the rat. *J Neurotrauma* 8:91-101.
- Bye N, Habgood MD, Callaway JK, Malakooti N, Potter A, Kossmann T, Morganti-Kossmann MC (2006) Transient neuroprotection by minocycline following traumatic brain injury is associated with attenuated microglial activation but no changes in cell apoptosis or neutrophil infiltration. *Exp Neurol*.
- Chen XH, Meaney DF, Xu BN, Nonaka M, McIntosh TK, Wolf JA, Saatman KE, Smith DH (1999) Evolution of neurofilament subtype accumulation in axons following diffuse brain injury in the pig. *J Neuropathol Exp Neurol* 58:588-596.
- Choo AM, Liu J, Lam CK, Dvorak M, Tetzlaff W, Oxland TR (2005) Primary and Secondary Damage in Three Mechanisms of Spinal Cord Injury - Contusion, Dislocation & Distraction. *J Neurotrauma* 22:1241.

- Chung RS, Staal JA, McCormack GH, Dickson TC, Cozens MA, Chuckowree JA, Quilty MC, Vickers JC (2005) Mild axonal stretch injury in vitro induces a progressive series of neurofilament alterations ultimately leading to delayed axotomy. *J Neurotrauma* 22:1081-1091.
- Cornish R, Blumbergs PC, Manavis J, Scott G, Jones NR, Reilly PL (2000) Topography and severity of axonal injury in human spinal cord trauma using amyloid precursor protein as a marker of axonal injury. *Spine* 25:1227-1233.
- Dabney KW, Ehrenshteyn M, Agresta CA, Twiss JL, Stern G, Tice L, Salzman SK (2004) A model of experimental spinal cord trauma based on computer-controlled intervertebral distraction: characterization of graded injury. *Spine* 29:2357-2364.
- Davalos D, Grutzendler J, Yang G, Kim JV, Zuo Y, Jung S, Littman DR, Dustin ML, Gan WB (2005) ATP mediates rapid microglial response to local brain injury in vivo. *Nat Neurosci* 8:752-758.
- Deng Y, Thompson BM, Gao X, Hall ED (2007) Temporal relationship of peroxynitrite-induced oxidative damage, calpain-mediated cytoskeletal degradation and neurodegeneration after traumatic brain injury. *Exp Neurol*.
- Diaz-Ruiz A, Rios C, Duarte I, Correa D, Guizar-Sahagun G, Grijalva I, Ibarra A (1999) Cyclosporin-A inhibits lipid peroxidation after spinal cord injury in rats. *Neurosci Lett* 266:61-64.
- Faden AI, Lemke M, Simon RP, Noble LJ (1988) N-methyl-D-aspartate antagonist MK801 improves outcome following traumatic spinal cord injury in rats: behavioral, anatomic, and neurochemical studies. *J Neurotrauma* 5:33-45.
- Farkas O, Lifshitz J, Povlishock JT (2006) Mechanoporation induced by diffuse traumatic brain injury: an irreversible or reversible response to injury? *J Neurosci* 26:3130-3140.
- Fung YC (1993) *Biomechanics: mechanical properties of living tissues*. New York: Springer.
- Gaviria M, Privat A, d'Arbigny P, Kamenka JM, Haton H, Ohanna F (2000a) Neuroprotective effects of gacyclidine after experimental photochemical spinal cord lesion in adult rats: dose-window and time-window effects. *J Neurotrauma* 17:19-30.
- Gaviria M, Privat A, d'Arbigny P, Kamenka J, Haton H, Ohanna F (2000b) Neuroprotective effects of a novel NMDA antagonist, Gacyclidine, after experimental contusive spinal cord injury in adult rats. *Brain Res* 874:200-209.
- Geddes-Klein DM, Schiffman KB, Meaney DF (2006) Mechanisms and consequences of neuronal stretch injury in vitro differ with the model of trauma. *J Neurotrauma* 23:193-204.
- Geddes DM, Cargill RS, 2nd, LaPlaca MC (2003) Mechanical stretch to neurons results in a strain rate and magnitude-dependent increase in plasma membrane permeability. *J Neurotrauma* 20:1039-1049.
- Geisler FH, Coleman WP, Grieco G, Poonian D (2001) The Sygen multicenter acute spinal cord injury study. *Spine* 26:S87-98.
- Gensel JC, Tovar CA, Hamers FP, Deibert RJ, Beattie MS, Bresnahan JC (2006) Behavioral and histological characterization of unilateral cervical spinal cord contusion injury in rats. *J Neurotrauma* 23:36-54.
- Glenn JA, Ward SA, Stone CR, Booth PL, Thomas WE (1992) Characterisation of ramified microglial cells: detailed morphology, morphological plasticity and proliferative capability. *J Anat* 180 (Pt 1):109-118.

- Gomes-Leal W, Corkill DJ, Picanco-Diniz CW (2005) Systematic analysis of axonal damage and inflammatory response in different white matter tracts of acutely injured rat spinal cord. *Brain Res* 1066:57-70.
- Gris D, Marsh DR, Oatway MA, Chen Y, Hamilton EF, Dekaban GA, Weaver LC (2004) Transient blockade of the CD11d/CD18 integrin reduces secondary damage after spinal cord injury, improving sensory, autonomic, and motor function. *J Neurosci* 24:4043-4051.
- Gruner JA (1992) A monitored contusion model of spinal cord injury in the rat. *J Neurotrauma* 9:123-126; discussion 126-128.
- Guha A, Tator CH (1988) Acute cardiovascular effects of experimental spinal cord injury. *J Trauma* 28:481-490.
- Guha A, Tator CH, Rochon J (1989) Spinal cord blood flow and systemic blood pressure after experimental spinal cord injury in rats. *Stroke* 20:372-377.
- Gulyas AI, Buzsaki G, Freund TF, Hirase H (2006) Populations of hippocampal inhibitory neurons express different levels of cytochrome c. *Eur J Neurosci* 23:2581-2594.
- Hall ED, Springer JE (2004) Neuroprotection and acute spinal cord injury: a reappraisal. *NeuroRx* 1:80-100.
- Harrop JS, Sharan AD, Vaccaro AR, Przybylski GJ (2001) The cause of neurologic deterioration after acute cervical spinal cord injury. *Spine* 26:340-346.
- Hedel HJ, Curt A (2006) Fighting for Each Segment: Estimating the Clinical Value of Cervical and Thoracic Segments in SCI. *J Neurotrauma* 23:1621-1631.
- Howard CV, Reed MG (1998) *Unbiased Stereology - Three Dimensional Measurement in Microscopy*. New York: Springer-Verlag.
- Hurlbert RJ (2000) Methylprednisolone for acute spinal cord injury: an inappropriate standard of care. *J Neurosurg* 93:1-7.
- Iizuka H, Yamamoto H, Iwasaki Y, Yamamoto T, Konno H (1987) Evolution of tissue damage in compressive spinal cord injury in rats. *J Neurosurg* 66:595-603.
- Imai Y, Ibata I, Ito D, Ohsawa K, Kohsaka S (1996) A novel gene *iba1* in the major histocompatibility complex class III region encoding an EF hand protein expressed in a monocytic lineage. *Biochem Biophys Res Commun* 224:855-862.
- Inoue K (2002) Microglial activation by purines and pyrimidines. *Glia* 40:156-163.
- Ito D, Imai Y, Ohsawa K, Nakajima K, Fukuuchi Y, Kohsaka S (1998) Microglia-specific localisation of a novel calcium binding protein, *Iba1*. *Brain Res Mol Brain Res* 57:1-9.
- Jafari SS, Nielson M, Graham DI, Maxwell WL (1998) Axonal cytoskeletal changes after nondisruptive axonal injury. II. Intermediate sized axons. *J Neurotrauma* 15:955-966.
- Li GL, Farooque M, Holtz A, Olsson Y (1995) Changes of beta-amyloid precursor protein after compression trauma to the spinal cord: an experimental study in the rat using immunohistochemistry. *J Neurotrauma* 12:269-277.
- Loy DN, Magnuson DS, Zhang YP, Onifer SM, Mills MD, Cao QL, Darnall JB, Fajardo LC, Burke DA, Whitemore SR (2002) Functional redundancy of ventral spinal locomotor pathways. *J Neurosci* 22:315-323.
- Lusardi TA, Wolf JA, Putt ME, Smith DH, Meaney DF (2004) Effect of acute calcium influx after mechanical stretch injury in vitro on the viability of hippocampal neurons. *J Neurotrauma* 21:61-72.
- Maiman DJ, Myklebust JB, Ho KC, Coats J (1989) Experimental spinal cord injury produced by axial tension. *J Spinal Disord* 2:6-13.

- Marar BC (1974) The pattern of neurological damage as an aid to the diagnosis of the mechanism in cervical-spine injuries. *J Bone Joint Surg Am* 56:1648-1654.
- Maxwell WL, Povlishock JT, Graham DL (1997) A mechanistic analysis of nondisruptive axonal injury: a review. *J Neurotrauma* 14:419-440.
- Myklebust JB, Maiman DJ, Cusick JF (1988) Axial tension model of spinal cord injury. *J Am Paraplegia Soc* 11:50-55.
- Nance DM, Burns J (1990) Fluorescent dextrans as sensitive anterograde neuroanatomical tracers: applications and pitfalls. *Brain Res Bull* 25:139-145.
- Nikolaidis N, Pitas I (2001) *3-D Image Processing Algorithms*. New York: John Wiley & Sons.
- Norenberg MD, Smith J, Marcillo A (2004) The pathology of human spinal cord injury: defining the problems. *J Neurotrauma* 21:429-440.
- Okonkwo DO, Pettus EH, Moroi J, Povlishock JT (1998) Alteration of the neurofilament sidearm and its relation to neurofilament compaction occurring with traumatic axonal injury. *Brain Res* 784:1-6.
- Pant HC (1988) Dephosphorylation of neurofilament proteins enhances their susceptibility to degradation by calpain. *Biochem J* 256:665-668.
- Pearse DD, Lo TP, Jr., Cho KS, Lynch MP, Garg MS, Marcillo AE, Sanchez AR, Cruz Y, Dietrich WD (2005) Histopathological and behavioral characterization of a novel cervical spinal cord displacement contusion injury in the rat. *J Neurotrauma* 22:680-702.
- Pettus EH, Christman CW, Giebel ML, Povlishock JT (1994) Traumatically induced altered membrane permeability: its relationship to traumatically induced reactive axonal change. *J Neurotrauma* 11:507-522.
- Pickett GE, Campos-Benitez M, Keller JL, Duggal N (2006) Epidemiology of traumatic spinal cord injury in Canada. *Spine* 31:799-805.
- Pike BR, Zhao X, Newcomb JK, Glenn CC, Anderson DK, Hayes RL (2000) Stretch injury causes calpain and caspase-3 activation and necrotic and apoptotic cell death in septo-hippocampal cell cultures. *J Neurotrauma* 17:283-298.
- Pointillart V, Petitjean ME, Wiart L, Vital JM, Lassie P, Thicoipe M, Dabadie P (2000) Pharmacological therapy of spinal cord injury during the acute phase. *Spinal Cord* 38:71-76.
- Rathbone MP, Middlemiss PJ, Gysbers JW, Andrew C, Herman MA, Reed JK, Ciccarelli R, Di Iorio P, Caciagli F (1999) Trophic effects of purines in neurons and glial cells. *Prog Neurobiol* 59:663-690.
- Rivlin AS, Tator CH (1978) Effect of duration of acute spinal cord compression in a new acute cord injury model in the rat. *Surg Neurol* 10:38-43.
- Rosenberg LJ, Wrathall JR (2001) Time course studies on the effectiveness of tetrodotoxin in reducing consequences of spinal cord contusion. *J Neurosci Res* 66:191-202.
- Saatman KE, Abai B, Grosvenor A, Vorwerk CK, Smith DH, Meaney DF (2003) Traumatic axonal injury results in biphasic calpain activation and retrograde transport impairment in mice. *J Cereb Blood Flow Metab* 23:34-42.
- Scheff SW, Rabchevsky AG, Fugaccia I, Main JA, Lumpkin JE, Jr. (2003) Experimental modeling of spinal cord injury: characterization of a force-defined injury device. *J Neurotrauma* 20:179-193.
- Schrimsher GW, Reier PJ (1993) Forelimb motor performance following dorsal column, dorsolateral funiculi, or ventrolateral funiculi lesions of the cervical spinal cord in the rat. *Exp Neurol* 120:264-276.

- Schucht P, Raineteau O, Schwab ME, Fouad K (2002) Anatomical correlates of locomotor recovery following dorsal and ventral lesions of the rat spinal cord. *Exp Neurol* 176:143-153.
- Schumacher PA, Eubanks JH, Fehlings MG (1999) Increased calpain I-mediated proteolysis, and preferential loss of dephosphorylated NF200, following traumatic spinal cord injury. *Neuroscience* 91:733-744.
- Schumacher PA, Siman RG, Fehlings MG (2000) Pretreatment with calpain inhibitor CEP-4143 inhibits calpain I activation and cytoskeletal degradation, improves neurological function, and enhances axonal survival after traumatic spinal cord injury. *J Neurochem* 74:1646-1655.
- Schwartz M (2003) Macrophages and microglia in central nervous system injury: are they helpful or harmful? *J Cereb Blood Flow Metab* 23:385-394.
- Sekhon LH, Fehlings MG (2001) Epidemiology, demographics, and pathophysiology of acute spinal cord injury. *Spine* 26:S2-12.
- Serbest G, Horwitz J, Jost M, Barbee K (2006) Mechanisms of cell death and neuroprotection by poloxamer 188 after mechanical trauma. *FASEB J* 20:308-310.
- Shi R, Pryor JD (2002) Pathological changes of isolated spinal cord axons in response to mechanical stretch. *Neuroscience* 110:765-777.
- Shuman SL, Bresnahan JC, Beattie MS (1997) Apoptosis of microglia and oligodendrocytes after spinal cord contusion in rats. *J Neurosci Res* 50:798-808.
- Silberstein M, McLean K (1994) Non-contiguous spinal injury: clinical and imaging features, and postulated mechanism. *Paraplegia* 32:817-823.
- Singleton RH, Povlishock JT (2004) Identification and characterization of heterogeneous neuronal injury and death in regions of diffuse brain injury: evidence for multiple independent injury phenotypes. *J Neurosci* 24:3543-3553.
- Smith DH, Chen XH, Iwata A, Graham DI (2003) Amyloid beta accumulation in axons after traumatic brain injury in humans. *J Neurosurg* 98:1072-1077.
- Smith DH, Wolf JA, Lusardi TA, Lee VM, Meaney DF (1999) High tolerance and delayed elastic response of cultured axons to dynamic stretch injury. *J Neurosci* 19:4263-4269.
- Soltys Z, Ziaja M, Pawlinski R, Setkowicz Z, Janeczko K (2001) Morphology of reactive microglia in the injured cerebral cortex. Fractal analysis and complementary quantitative methods. *J Neurosci Res* 63:90-97.
- Springer JE, Azbill RD, Knapp PE (1999) Activation of the caspase-3 apoptotic cascade in traumatic spinal cord injury. *Nat Med* 5:943-946.
- Stence N, Waite M, Dailey ME (2001) Dynamics of microglial activation: a confocal time-lapse analysis in hippocampal slices. *Glia* 33:256-266.
- Sternberger LA, Sternberger NH (1983) Monoclonal antibodies distinguish phosphorylated and nonphosphorylated forms of neurofilaments in situ. *Proc Natl Acad Sci U S A* 80:6126-6130.
- Stirling DP, Khodarahmi K, Liu J, McPhail LT, McBride CB, Steeves JD, Ramer MS, Tetzlaff W (2004) Minocycline treatment reduces delayed oligodendrocyte death, attenuates axonal dieback, and improves functional outcome after spinal cord injury. *J Neurosci* 24:2182-2190.
- Stokes BT, Noyes DH, Behrmann DL (1992) An electromechanical spinal injury technique with dynamic sensitivity. *J Neurotrauma* 9:187-195.

- Stone JR, Okonkwo DO, Dialo AO, Rubin DG, Mutlu LK, Povlishock JT, Helm GA (2004) Impaired axonal transport and altered axolemmal permeability occur in distinct populations of damaged axons following traumatic brain injury. *Exp Neurol* 190:59-69.
- Sugawara T, Lewen A, Gasche Y, Yu F; Chan PH (2002) Overexpression of SOD1 protects vulnerable motor neurons after spinal cord injury by attenuating mitochondrial cytochrome c release. *FASEB J* 16:1997-1999.
- Tadie M, Gaviria M, Mathe J-F, Menthonnex P, Loubert G, Lagarrigue J, Saint-Marc C, Argenson C, Kempf C, D'Arbigny P, Kamenka JM, Privat A, Carli P (2003) Early care and treatment with a neuroprotective drug, Gacyclidine, in patients with acute spinal cord injury. *Rachis* 15:363-376.
- Tator CH (1983) Spine-spinal cord relationships in spinal cord trauma. *Clin Neurosurg* 30:479-494.
- Tator CH (1992) Hemodynamic issues and vascular factors in acute experimental spinal cord injury. *J Neurotrauma* 9:139-140; discussion 141.
- Tator CH (2006) Review of treatment trials in human spinal cord injury: issues, difficulties, and recommendations. *Neurosurgery* 59:957-982; discussion 982-957.
- Tator CH, Fehlings MG (1999) Review of clinical trials of neuroprotection in acute spinal cord injury. *Neurosurg Focus* 6:e8.
- Teng YD, Choi H, Onario RC, Zhu S, Desilets FC, Lan S, Woodard EJ, Snyder EY, Eichler ME, Friedlander RM (2004) Minocycline inhibits contusion-triggered mitochondrial cytochrome c release and mitigates functional deficits after spinal cord injury. *Proc Natl Acad Sci U S A* 101:3071-3076.
- Vanderluit JL, McPhail LT, Fernandes KJ, Kobayashi NR, Tetzlaff W (2003) In vivo application of mitochondrial pore inhibitors blocks the induction of apoptosis in axotomized neonatal facial motoneurons. *Cell Death Differ* 10:969-976.
- Vercelli A, Repici M, Garbossa D, Grimaldi A (2000) Recent techniques for tracing pathways in the central nervous system of developing and adult mammals. *Brain Res Bull* 51:11-28.
- Wrathall JR, Teng YD, Choiniere D (1996) Amelioration of functional deficits from spinal cord trauma with systemically administered NBQX, an antagonist of non-N-methyl-D-aspartate receptors. *Exp Neurol* 137:119-126.
- Wrathall JR, Teng YD, Marriott R (1997) Delayed antagonism of AMPA/kainate receptors reduces long-term functional deficits resulting from spinal cord trauma. *Exp Neurol* 145:565-573.
- Xiong Y, Rabchevsky AG, Hall ED (2007) Role of peroxynitrite in secondary oxidative damage after spinal cord injury. *J Neurochem* 100:639-649.
- Xu J, Fan G, Chen S, Wu Y, Xu XM, Hsu CY (1998) Methylprednisolone inhibition of TNF-alpha expression and NF-kB activation after spinal cord injury in rats. *Brain Res Mol Brain Res* 59:135-142.
- Zar JH (1999) *Biostatistical Analysis*, 4 Edition. New Jersey: Prentice Hall.

Chapter 5

DISCUSSION & CONCLUSION

5.1 Overview

A novel multi-mechanism device was developed that enabled the first direct comparison of clinically relevant mechanisms of SCI. In these new animal models, the biomechanical injury mechanism dictated the pattern of primary damage within the spinal cord which in turn influenced the initial characteristics of secondary pathology. Contusion injuries were highly focused at the lesion epicentre whereas primary damage following dislocation and distraction injuries was distributed over several vertebral levels. Secondary degeneration following dislocation was particularly rapid perhaps indicating a narrower therapeutic time-window for this injury mechanism. In contrast, the extent of secondary pathology following distraction injuries was less pronounced than in either spinal cord contusion or dislocation. These mechanism-specific patterns of injury emphasize that novel therapies should be tested in a broader range of clinically relevant injury mechanisms prior to human trials. The work presented in this thesis demonstrates how an understanding of the biomechanical injury mechanism may contribute to the development of future clinical treatment paradigms.

5.2 Modelling Considerations

The three SCI models developed in this thesis are unique from the animal models already in widespread use. Cervical dislocation and distraction in the rat spine are entirely new experimental paradigms while cervical contusion models have only been developed recently (Pearse et al., 2005; Baussart et al., 2006; Gensel et al., 2006). The SCI animal models that are widely used control variables such as the injury force or injury displacement while maintaining a transverse contusion or compression mechanism of injury. In this thesis, the biomechanical mechanism of injury was explicitly varied in order to characterize its effect on primary damage and the subsequent initiation of secondary neuropathology in the spinal cord.

The injuries in all three novel models were delivered at speeds of approximately 100cm/s. This high speed is on the order of that believed to occur in human SCI (Panjabi et al., 1995; Nightingale et al., 1996; Wilcox et al., 2002). In spinal cord contusion injuries, the impact velocity has been previously shown to control the extent of blood-spinal cord barrier disruption (Maikos and Shreiber, 2007), intramedullary hemorrhage (Anderson, 1985), and electrophysiological function (Kearney et al., 1988). Several *in vitro* and *ex vivo* studies have also emphasized the need to model trauma at high rates (Cargill and Thibault, 1996; Geddes et al., 2003; LaPlaca et al., 2005; Shi and Whitebone, 2006). Pneumatic devices can produce contusion injuries at impact speeds of several meters per second (Anderson, 1982; Kearney et al., 1988) though these devices are not widely used today. In the most common contusion models, impact speeds can range from 13cm/s (Scheff et al., 2003) to approximately 100cm/s (Maikos and Shreiber, 2007), while other injury models such as the aneurysm clip compression (Rivlin and Tator, 1978) and forceps compression (Gruner et al., 1996) do not control the injury speed.

Thoracolumbar dislocation has been modelled at injury velocities between 5cm/s and 15cm/s (Fiford et al., 2004) while the first computer-controlled distraction model utilized Harrington rods and laminar hooks to displace vertebrae at speeds of 0.5cm/s to 1cm/s (Dabney et al., 2004). In the cervical spine, I observed the lamina to fracture when applied displacements exceeded speeds of a few centimeters per second (A.M. Choo et al., unpublished observations). In this thesis, injuries at 100cm/s were achievable due to the novel vertebral clamping strategy developed which held the vertebrae laterally beneath the transverse processes. In addition to the reduced vascular damage (Anderson, 1985; Maikos and Shreiber, 2007) discussed above, slower impact speeds appear to produce less primary axotomy thereby enhancing the relative significance of demyelination in this type of lesion (W. Tetzlaff, personal communication). Some injuries in humans likely occur at lower velocities and hence, it is important that injury devices are capable of modelling both high and low speed trauma.

Cervical contusion models have been recently reported that use the weight-drop to produce unilateral (off-centre) contusions (Gensel et al., 2006) and controlled displacements to produce contusions centred at C5 (Pearse et al., 2005). The contusions reported in this thesis utilized novel vertebral clamping devices that were developed to continuously support the vertebrae beneath the transverse processes. This new design eliminates the vertebral slippage that is a well known

criteria for excluding animals from an experiment following contusion injuries (Stokes et al., 1992; Jakeman et al., 2000; Scheff et al., 2003). These cervical vertebral clamps have also been utilized with other injury devices such as the Ohio State University impactor where cervical hemi-contusion injuries with impact forces of $1.6 \pm 0.2\text{N}$ (SD) have been found to produce highly repeatable behavioural deficits (Plunet et al., unpublished observations). In addition, this new clamping strategy has also been successfully adapted to the thoracic spine (Sjovold et al., 2005).

In this thesis, the variability of the contusion forces was on the order of 25% which is somewhat higher than the 5-20% reported by others who have modelled thoracic contusion injuries (Bresnahan et al., 1987; Somerson and Stokes, 1987; Bresnahan et al., 1991; Behrmann et al., 1992). This increase in variability may stem from the infusion of dextran tracers into the cerebrospinal fluid (CSF). In thoracic spinal cord contusions, sectioning of the dura in order to release CSF prior to impact results in a ~50% reduction in the impact force ($n = 1$, A.M. Choo et al., unpublished observations). Hence, the infusion of dextran into the CSF may introduce some variability into the pressure within the subarachnoid space. In the cervical contusion injuries modelled, the 0.3N contact force used to define the initial position of the impactor was observed to be immediately fully reversible thereby suggesting dextran infusion did not disrupt CSF dynamics. Given that the focus of the study was to compare differences between injury mechanisms, an increase in the within-group variability was deemed an acceptable compromise in order to gain insight into the distribution of primary membrane compromise which was afforded by the infusion of dextran-conjugated fluorophores.

All animal models, including the novel set developed in this thesis, possess strengths that are ideally suited for distinct objectives. Although, spinal cord transections are believed to be rare (Norenberg et al., 2004), these models are important for the clear demonstration of axonal regeneration (Kwon et al., 2002). Similarly, slow contusion or compression injuries might produce a more focal lesion that involves less variability in cellular damage and thus could enhance the detection of therapeutic benefits. The novel models developed in this thesis are surgically more invasive than thoracic contusion injury paradigms and require more extensive post-traumatic care because the lesions are in the cervical region. Consequently, these new models may be inefficient for screening of pharmacotherapies. However, the models add a new dimension—the biomechanical injury mechanism—to the range of injury paradigms available for research.

Typically, animal models are designed to possess mild, moderate, and severe injury grades (Rivlin and Tator, 1978; Behrmann et al., 1992; Jakeman et al., 2000; Scheff et al., 2003). Therapeutic strategies are often honed at moderate injury severities because in mild injuries, control animals recover as well as treated animals whereas in severe injuries, neither treated nor control animals recover. Additional injury mechanisms may provide the flexibility to produce different damage patterns while maintaining an overall level of moderate functional deficits thereby augmenting the repertoire of models for assessing the robustness of novel therapies prior to clinical trials.

5.3 Biomechanics of Primary Injury Patterns

Primary mechanical injury is generally deemed to be irreversible and hence studies have typically focused on mitigating secondary pathomechanisms as well as enhancing repair and regeneration strategies. Primary injury in spinal cord contusions are characterized by central hemorrhagic necrosis (Balentine, 1978a; Rawe et al., 1978) to the highly vascularized gray matter with prominent sparing of the surrounding white matter tracts (Blight, 1983; Bresnahan et al., 1991). The primary injury pattern in other clinically relevant injuries had not been addressed to determine the role of the biomechanical injury mechanism in the pathophysiology of SCI.

In traumatic SCI, the primary mechanical injury occurs on the order of milliseconds thereby making it difficult to capture the dynamic strain distribution within the spinal cord. Mechanical trauma has been shown to induce breaches in the cellular plasma membrane which can be detected by the intracellular penetration of macro molecules (Pettus et al., 1994; Shi and Pryor, 2002). *In vitro* neuronal stretch models demonstrated that 10kDa dextrans were able to differentiate moderate injury severities (Geddes et al., 2003). Hence, it was hypothesized that the spatial distribution of primary injury could be captured by analyzing the patterns of intracellular dextran penetration immediately after trauma before secondary degenerative events had progressed.

5.3.1 Contusion

Following contusion, the distribution of primary damage was similar to that widely reported in thoracic contusion models with primary hemorrhage focused in the central gray matter (Balentine, 1978a; Rawe et al., 1978). Membrane compromise in both the gray and white matter was localized within 1 to 2mm from the lesion epicentre (Figures 3.6 and 3.7). The biomechanical basis for this pattern has been discussed by Blight and Decrescito (Blight and Decrescito, 1986;

Blight, 1988) who used a gel filled cylinder with ink tracks to show that the maximum rostro-caudal displacement of tissue occurred centrally (Figure 5.1A).

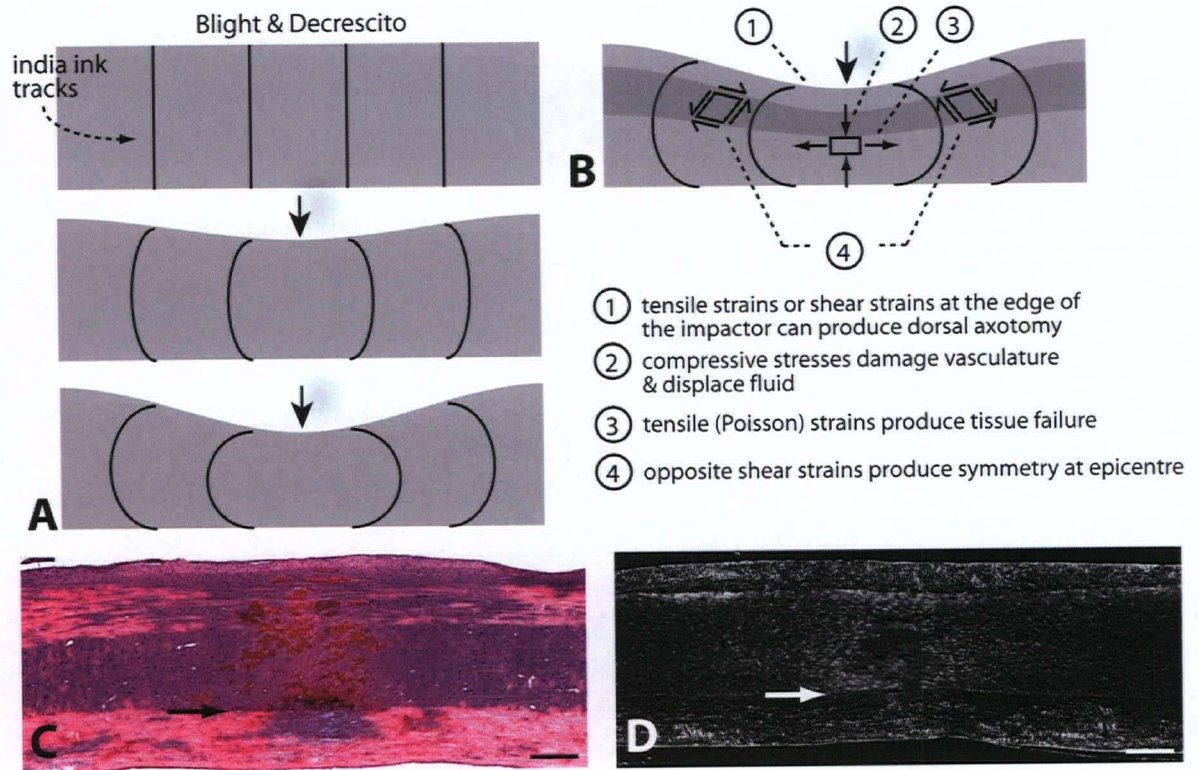


Figure 5.1: Central damage pattern in contusion injuries

A. Deformation pattern of a gelatin model of the spinal cord under compression, adapted from Blight and Decrescito, *Neuroscience* 19(1) 1986, who used india ink tracks to show that gel displacement during compression was greatest at the centre of the gelatin filled tube. B. Analysis of the deformation pattern shows distinct biomechanical strain regions. Axons on the surface (*zone 1*) experience tensile strains, though shear strains may also be present at the contact point between the impactor's edge and the spinal cord. The injury is symmetric about the line of impact with compressive stresses (*zone 2*) resulting in substantial rostro-caudal and lateral tensile strains (*zone 3*) since neural tissue is often considered incompressible. Away from the lesion epicentre, shear strains dominate (*zone 4*). C. Photomicrograph of parasagittal section stained with H&E from an animal perfused immediately following contusion injury shows the pattern of primary hemorrhage. D. Photomicrograph of parasagittal section stained with anti-GFAP to reveal reactive astrocytes at 3 hours following contusion injury shows central pattern of primary damage and surrounding reactive astrocytes. Arrows in C and D highlight discontinuity in damage between gray and white matter. Scale bars 500 μ m in C and D. (Illustration in A © IBRO, 1986, adapted by permission)

Blight and Decrescito proposed that this central tissue displacement accounted for the sparing of subpial axons and the progressive loss of central white matter axons which is observed in the chronic SCI lesion (Blight and Decrescito, 1986; Blight, 1988). In another study, compression of isolated white matter strips resulted in greater membrane compromise at the centre of the white matter strips compared to the superficial fibres (Shi and Pryor, 2002). More recently, finite element analysis of the mechanics of contusion has indicated a similar pattern of von Mises

strains (average of three-dimensional strains) focused centrally within the spinal cord (Greaves et al., 2004). The finite element analysis also showed stress concentrations at the superficial surface of the spinal cord at the point of contact with a cylindrical impactor (Greaves et al., 2004). Somewhat counterintuitively, the superficial axons at the site of contact with the impactor are usually spared except in cases of deeper impact displacement into the spinal cord (Blight, 1988). Impactors with a beveled edge are often used to reduce shear stress concentrations at the contact point between the edge of the impactor and the spinal cord (Stokes et al., 1992). In this thesis, a spherical head impactor was selected to further minimize these edge effects.

Further analysis of the displacement pattern of the gel filled tube shows there are distinct biomechanical injury zones during contusion (Figure 5.1B). Subpial axons in the dorsal column are subjected to tensile strains, though the local strain distribution at the point of contact will depend on the geometry of the impactor (zone 1 in Figure 5.1B). Neural tissue is generally considered to be incompressible (King et al., 1995) and hence, dorso-ventral compressive stresses (zone 2 in Figure 5.1B) will result in substantial tensile Poisson strains (zone 3 in Figure 5.1B) that stretch tissue rostro-caudally and laterally. There is some symmetry along the line of impact though the true strain field in the transverse plane will be complicated by geometric factors such as the shape of the dorsal and ventral gray horns. The tensile strains (zone 3 in Figure 5.1B) along the line of impact have lead some to the hypothesize that white matter is predominantly injured in tension (Fiford et al., 2004; Henderson et al., 2005). Although tension certainly produces axonal injury (Smith et al., 1999; Wolf et al., 2001), shear strains (zone 4 in Figure 5.1B) along the axis of axons are likely also important in white matter injury. Away from the centre of impact, shear strains may be responsible for damage to myelin laminae which have been reported to exhibit early ultrastructural disruption, sometimes in the presence of an intact axolemma (Balentine, 1978b; Anthes et al., 1995). In this thesis, dextran-conjugated fluorophores often accumulated at nodes of Ranvier thereby highlighting them. As reported in chapter 3, however, the zones flanking the contusion epicentre (e.g. zone 4 in Figure 5.1B) were often devoid of dextran positive axons as well as visible nodes of Ranvier. This observation may suggest that in the penumbra of the contusion lesion epicentre, longitudinal shear strains disrupt the organization of myelin at the nodes of Ranvier without causing the axolemma compromise that leads to intracellular dextran penetration.

This analysis of the central displacement pattern during contusion can also apply to the gray matter. Primary hemorrhage was localized to the compressive region (Figure 5.1C) while secondary astrocyte activation extended into the lesion penumbra (Figure 5.1D). Interestingly, a discontinuity in tissue damage was often encountered at the gray and white matter tissue boundary (*arrows* Figure 5.1C & D) in contrast to the continuous pattern of gel deformation discussed above (Figure 5.1A). This phenomenon may reflect the greater susceptibility of gray matter to mechanical damage compared to white matter.

Several lines of evidence predict injury during contusion will initiate in the central gray matter due to its inherent susceptibility to primary damage. *In vitro* evidence suggests gray matter fails at lower tensile stress levels than white matter (Ichihara et al., 2001), though the relative strength of these two tissue components remains uncertain (Ozawa et al., 2001). The gray matter is more highly vascularized than the white matter rendering it more susceptible to hemorrhagic necrosis when the impact speed is high enough (Anderson, 1985). In addition, the blood-spinal cord barrier exhibits a lower mechanical injury threshold in the gray matter compared to the white matter (Maikos and Shreiber, 2007). In this thesis, neuronal somata in the vicinity of the surgical exposure of sham control animals exhibited some susceptibility to primary membrane compromise (Figure 3.7A) in contrast to white matter axons (Figure 3.6). In addition, the extent of plasma membrane resealing appears to be slower in neuronal cell bodies than axons (Figure 4.4).

In summary, contusion impacts produce a central zone of compressive strains and tensile Poisson strains encapsulated by a region of shear strains. These strains produce hemorrhagic necrosis at the contusion epicentre which is flanked by sublethal zones of neurons and axons that exhibited primary membrane compromise. Shear strains in the lesion penumbra may be responsible for primary disruption of myelin structure at the nodes of Ranvier as well as activation of secondary effects such as reactive astrocytes. In addition to the pattern of biomechanical strains, the primary injury is also influenced by the apparent susceptibility of gray matter to injury. The net result is a focal region consisting of both necrotic and salvagable populations of neurons, axons, and glia.

5.3.2 Dislocation

The dislocation injury resulted in primary hemorrhagic necrosis within the gray matter similar to that observed in contusion, but spinal cords injured by a dislocation mechanism also

exhibited primary injury patterns that were unique from the central cavitation of the contusion model.

Primary axotomy in the lateral funiculi was a distinctive feature of the dislocation model that was not observed in either of the other two injury mechanisms. During dislocation, the lateral white matter column is sheared between the vertebral margins of C4 and C5 (Figure 5.2A). Given the high prevalence of dislocation injuries in the human population, this feature of the dislocation injury mechanism may suggest some axotomy occurs during clinical fracture-dislocations which is not evident with post-traumatic imaging.

Damage to the lateral aspect of the spinal cord has also been reported in a model of thoracolumbar dislocation where the vertebrae are dislocated laterally (Fiford et al., 2004). However, the biomechanics of this thoracolumbar model differs from the cervical fracture-dislocation developed in this thesis. In the thoracolumbar model, the lateral dislocation was distributed over T12, T13, and L1. Further analysis of this model has shown this distributed dislocation results in two injury epicentres at the junction of T12-T13 and T13-L1 (Clarke et al., 2006). The region between T12 and L1 appear to be under tensile strain that produces diffuse hemorrhage in the lateral gray matter (Fiford et al., 2004) in contrast to the lateral white matter axotomy observed following the C4/5 dislocation injuries modelled in this thesis. In addition, dislocation between T12 and L1 produced tissue failure in the T13 region (Clarke et al., 2006) along an axis that indicates tissue rupture occurs in tension (*arrows* Figure 5.2B).

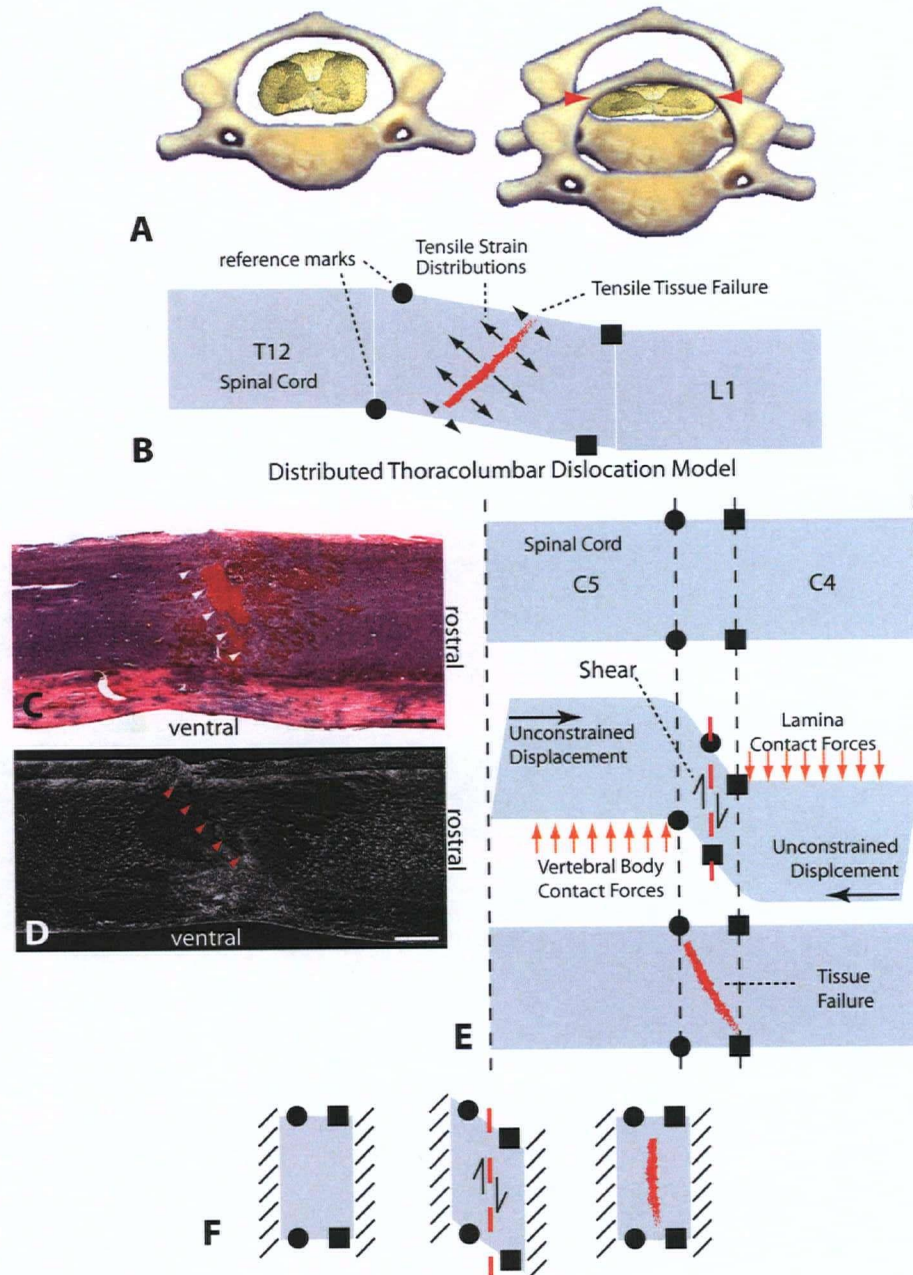


Figure 5.2: Injury patterns following fracture-dislocation

A. Illustration of C4/5 vertebral dislocation that results in shearing of the lateral white matter funiculi (*arrows*). B. Illustration of distributed thoracolumbar dislocation (T12-T13-L1) where tissue fails in tension (*arrows*) producing an oblique pattern of tissue rupture. C. Photomicrograph of parasagittal section stained with H&E from an animal perfused immediately following C4/5 dislocation injury shows central hemorrhage with some evidence of primary tissue failure in an oblique plane opposite to that expected of tensile failure (*arrowheads*). D. Photomicrograph of parasagittal section stained with anti-GFAP to reveal reactive astrocytes at 3 hours following dislocation injury shows oblique pattern of tissue failure that is also opposite to the hypothetical principal tensile plane (*arrowheads*). E. The strain distribution within the spinal cord is complex, but the pattern of injury may be explained by the unconstrained movement of the free surfaces and shear failure between the narrow margins of C4 and C5. F. Hypothetical tissue failure pattern if the spinal cord is fully constrained (i.e. via greater cranial flexion that increases spinal cord axial tension). Illustration in B is adapted from data in Clarke et al. *J Neurotrauma* 23, 2006. *Circles* and *squares* are reference marks for tracking deformation. Scale bars 500 μ m in C and D.

In the C4/5 dislocation modelled in this thesis, the gray matter usually—though not always—failed along an oblique plane that might suggest a shear mode of tissue failure rather than a tensile mode (*arrowheads* Figure 5.2C & D). The internal strains within the spinal cord are complex and vary rostro-caudally as well as laterally. The cervical spinal cord (~2×3mm) is not fully constrained within the vertebral canal (~3×4.5mm) and this may allow unconstrained displacement of the free surfaces (i.e. surfaces without vertebral contact) during dislocation that results in the oblique failure pattern often observed (Figure 5.2E). In this thesis, the angle of the rat's cranium within the stereotaxic frame was standardized such that the dorsal surface of the skull was vertical, thereby placing the head in flexion and removing cervical lordosis. An increase in flexion angle should increase the axial tension in the spinal cord (Breig, 1970) which may constrain the spinal cord and alter the angle of tissue failure (Figure 5.2F).

These differences in failure patterns demonstrate the need to understand contrasting injury patterns even within seemingly similar injury mechanisms. In this thesis, the intracellular penetration of dextran-conjugated fluorophores was used to map the distribution of primary mechanical damage within the spinal cord. This technique gave an indication of the traumatic strain distributions, but the technique does not yield information regarding the local strain components (i.e. local tension, compression, and shear) relative to the orientation of the cells and their processes. The local strain field sensed by individual neurons was recently analysed *in vitro* (Cullen and LaPlaca, 2006). Neurons cultured in a three-dimensional matrix exhibited greater cell death following shear strain trauma compared to neurons cultured in a planar configuration. An analysis of the orientation of the neurite processes extending from the neuronal cell body showed that the neurites of neurons cultured in three-dimensions sampled a broader range of shear, tensile, and compressive strains. Consequently, neurons cultured in three-dimensions were more likely to experience a broader range of traumatic strains thereby increasing the likelihood of neuronal injury.

The cervical dislocation modelled in this thesis also produced a distinctive rostral bias in the membrane compromise particularly in the ventral white matter (Figure 5.3A). This pattern of membrane compromise suggests a region of tensile strain rostral to the C4/5 epicentre (*label 2* Figure 5.3B). A complementary caudal bias was not detected in the dorsal white matter. This is likely due to the reduced sensitivity of detecting fine caliber dextran-positive axons. As discussed

in chapter 3, dextran fluorescence above and below fine processes and smaller cell bodies reduces the sensitivity of discriminating the intracellular level of dextran penetration relative to the background.

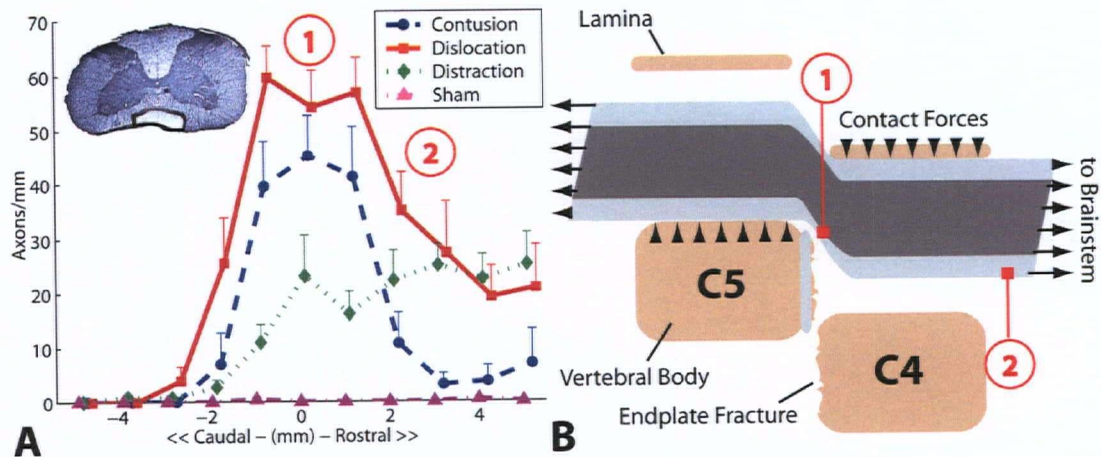


Figure 5.3: Ventro-medial axolemma compromise following dislocation injury

A. Rostro-caudal pattern of primary axolemma compromise evidenced by the intracellular penetration of 10kDa fluorescein-dextran in ventro-medial axons from animals euthanized immediately following dislocation injury (repeated from chapter 3). B. Expected distribution of contact loads (*arrowheads*) delivered to the spinal cord during fracture-dislocation. Maximum number of dextran-positive axons are located near the lesion epicentre (1). Tensile forces within the ventral aspect of the spinal cord result in membrane compromise rostral to the lesion epicentre (2). Inset in A highlights region of tissue sampled. Illustration in B is not to scale and does not include the dura and cerebrospinal fluid. (Graphics in A from: Choo AM, et al. 2007. Contusion, dislocation, and distraction: primary hemorrhage and membrane permeability in distinct mechanisms of spinal cord injury. *J Neurosurg Spine* 6:261. © Journal of Neurosurgery, 2007, adapted by permission.)

Hence, fracture-dislocation produces a distinct primary injury pattern compared to the focal central damage typically reported in contusion models. The dislocation lesion epicentre shares similarities with both contusion and partial transection models. The rostral membrane compromise, however, is a unique feature of this injury model and demonstrates this injury mechanism produces a broader population of injured cells within the spinal cord.

5.3.3 Distraction

In contrast to the contusion and dislocation injury models, distraction injury did not exhibit a focal hemorrhagic lesion epicentre and the extent of membrane compromise was similar at C4/5 and the rostral spinal cord suggesting a more diffuse and uniform injury pattern. The coupling between the vertebral column and the spinal cord remains unresolved. Others have suggested that distractive forces are transmitted to the spinal cord through the denticulate ligaments (Tani et al., 1987). In the dorsal column, membrane compromise was detected in axons between 2mm caudal

and 2mm rostral to the lesion epicentre (label 1 Figure 5.4A). Some axolemma compromise was also detected between 2 and 4mm rostral to the lesion. This periodic pattern of primary dextran penetration into dorsal axons might suggest that the translating vertebrae apply traction forces through the nerve roots (label 1 & 2 Figure 5.4B). The greater membrane compromise in the ventral column suggests traction forces are mainly transferred from the flexed vertebrae and the ventral aspect of the spinal cord (*arrowheads* Figure 5.4B).

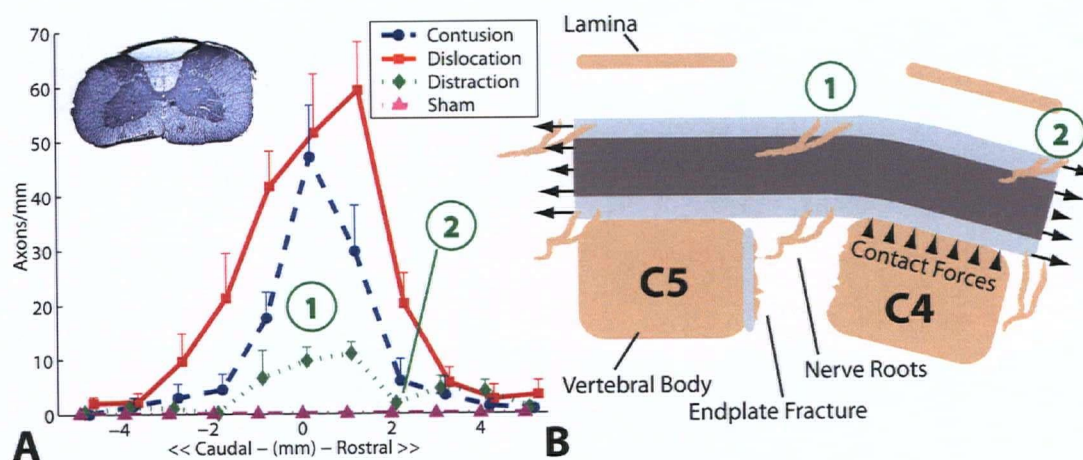


Figure 5.4: Dorsal axolemma compromise following distraction injury

A. Rostro-caudal pattern of primary axolemma compromise evidenced by the intracellular penetration of 10kDa fluorescein-dextran in dorsal axons from animals euthanized immediately following distraction injury (repeated from chapter 3). B. Expected distribution of contact loads (*arrowheads*) delivered to the spinal cord during flexion-distraction. Maximum number of dextran-positive axons are located near the lesion epicentre (1). The mechanism of coupling between the spinal cord and vertebral column remains uncertain. Tensile forces (*arrows* show hypothetical distribution) may be transferred to the dorsal column via the nerve roots (2) that are spaced at approximately 2mm intervals. Inset in A highlights tissue region sampled. Illustration in B is not to scale and does not include the dura and cerebrospinal fluid. (Graphics in A from: Choo AM, et al. 2007. Contusion, dislocation, and distraction: primary hemorrhage and membrane permeability in distinct mechanisms of spinal cord injury. *J Neurosurg Spine* 6:261. © Journal of Neurosurgery, 2007, adapted by permission.)

Maiman et al. used radio-opaque markers to estimate the extent of vertebral column and spinal cord coupling during distraction of cat spines (Maiman et al., 1989a). When the spinal column was placed under 147N (15kg) of distraction, the coupling ratio between the column and cord ranged from 0.38 at C2/3 to 0.62 at C6/7. The difference in coupling ratios may suggest the presence of distributed coupling mechanisms such as spinal nerve roots but could also stem from differences in the cross-sectional area of the spinal cord. The study was not able to isolate the source of vertebral column-spinal cord force transfer. The coupling between the spinal cord and vertebral column might be estimated by tracking the deformation of superficial vasculature within the spinal cord which is visible through the translucent dura. Glare from changes in reflected

lighting as the cord deforms, camera vibration, and slow camera acquisition speeds are some challenges that need to be overcome in order to realize this method (A.M. Choo et al., unpublished observations). Distraction is a frequently observed component of spinal injuries such as flexion-distraction and extension-distraction, and hence, a great deal remains to be learned about the characteristics of this important component of SCI. In the absence of overt hemorrhage, it is possible that spinal cords injured by a distractive injury mechanism may undergo a protracted time-course of pathology that results in delayed pathologic features (Maiman et al., 1989b; Dabney et al., 2004).

5.4 Association of Primary and Secondary Injury

The injury mechanisms modelled produced different patterns of primary damage, but also altered the characteristics of early secondary pathology. This relationship between primary and secondary injury suggests that a consideration of the injury mechanism may aid in the targeting of post-traumatic neuroprotective as well as repair and regeneration strategies. The interaction between primary and secondary damage mechanisms have been advocated before (Blight, 1988; LaPlaca and Thibault, 1997) and evidence continues to accumulate which shows how mechanical injury alters the course of secondary molecular events (Deridder et al., 2005; Geddes-Klein et al., 2006).

5.4.1 Contusion

The secondary pathologies observed following contusion were localized to the vicinity of the lesion epicentre where primary damage was focused. The inflammatory response of activated microglia was localized to ± 2 mm (*blue circles* Figure 5.5B) which corresponds to the central primary hemorrhagic necrosis and distribution of primary membrane compromise of neuronal somata (*blue circles* Figure 5.5A). Likewise, the rostro-caudal distribution of reactive astrocytes was also predominantly restricted to this ± 2 mm injury field. The presence of cytochrome *c* negative neurons in the lateral penumbra of the lesion, but not in the rostro-caudal penumbra, might stem from a greater primary strain field in the lateral zone because it is rigidly confined by the boundaries of the spinal canal compared to the unconfined gray matter displacement rostro-caudally along the axis of the spinal cord.

In the white matter, axonal degeneration was most prominent near the boundary of hemorrhagic gray matter while subpial axonal fibers that exhibited extensive primary membrane

compromise were still largely intact at the 3 hour time-point analysed. This observation suggests that primary hemorrhagic necrosis accelerates degeneration of axonal fibers adjacent to the gray matter while subpial fibers are able to repair breaches in the axolemma. The most prominent accumulation of β AAPP was found in the dorsal and ventral funiculi (Figure 4.8G & H) along the direct line of the contusion impact and further demonstrates the role of the primary injury in dictating the pattern of secondary pathology.

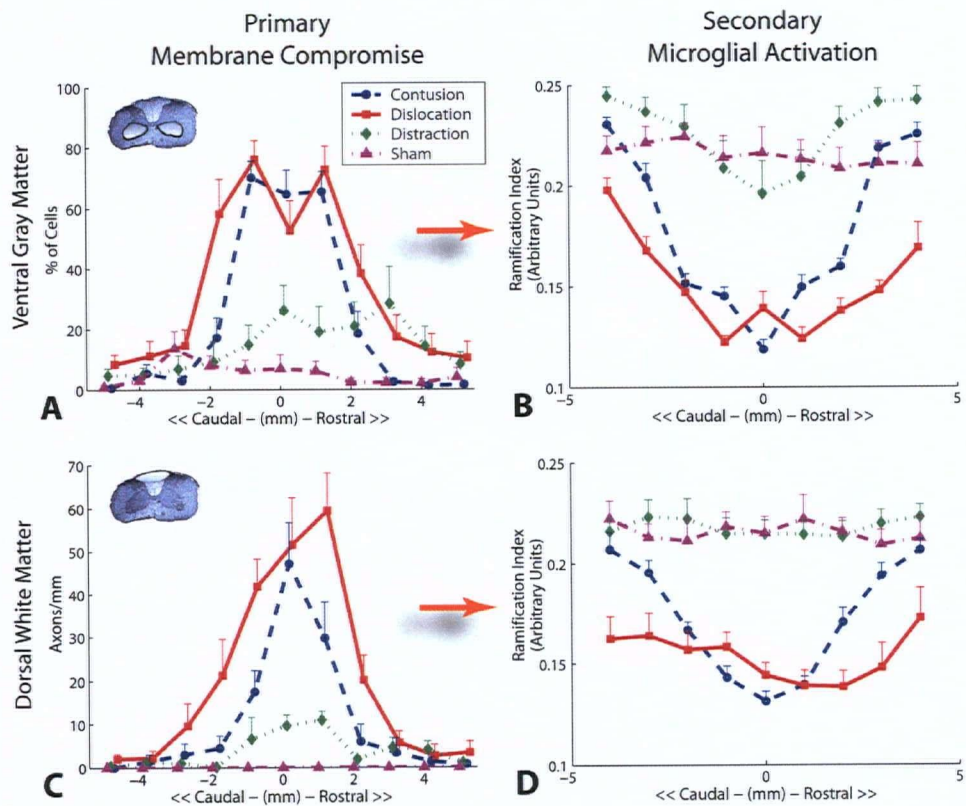


Figure 5.5: Parallel patterns of primary and secondary injury

Distribution of primary mechanical injury was detected by the intracellular penetration of fluorescein-dextran (A & C, repeated from chapter 3) in animals euthanized immediately following injury. Indicators of secondary pathology, such as microglial activation (B & C, repeated from chapter 4), appear to parallel primary injury thereby demonstrating that secondary injury was not yet an independent cascade at 3 hours following SCI. Measurement of primary and secondary injury markers demonstrated mechanism-specific patterns that may aid in the targeting of therapeutic strategies. A. Percent of dextran-positive neuronal somata immediately following injury. B. Ramification index of microglial morphology in the gray matter at 3 hours post-trauma. A lower index represents increased microglial activation. C. Number of dextran-positive axons in the dorsal column immediately following injury. D. Ramification index of microglial morphology in the dorsal column at 3 hours post-trauma. (Graphics in A & C from: Choo AM, et al. 2007. Contusion, dislocation, and distraction: primary hemorrhage and membrane permeability in distinct mechanisms of spinal cord injury. *J Neurosurg Spine* 6:261. © Journal of Neurosurgery, 2007, adapted by permission.)

5.4.2 Dislocation

The secondary degeneration in the dislocation model also closely paralleled the primary mechanical damage observed in this injury mechanism. In the gray matter, the rostro-caudal extent of microglial activation (*red squares* Figure 5.5B) strongly coincided with the central hemorrhage and rostro-caudal distribution of primary membrane compromise in the gray matter (*red squares* Figure 5.5A). A distinct rostral bias was observed in the activation of microglia in the dorsal column (*red squares* Figure 5.5D). This feature may be related to the slight rostral bias in membrane compromise in dorsal axons (*red squares* Figure 5.5C) but could also stem from hemorrhagic necrosis in the dorsal gray horns that are likely subjected to a contusive impact with the C4 lamina. As with the microglia, reactive astrocytes also extended rostrally thereby paralleling the asymmetric distribution of primary injury in the dislocation injury mechanism. In contrast to contusion, cytochrome *c* negative neurons were not located in the lateral penumbra of the lesion but instead were localized to the rostral and caudal boundaries of the lesion epicentre. In the lateral penumbra of the lesion, cytochrome *c*-negative neurons were not observed due to the extensive necrosis in this region.

The pattern of secondary white matter damage following dislocation further reduced the population of available axons that might be salvaged with neuroprotection. In the lateral funiculi, primary axotomy lead to β APP accumulation in transected axons, but the surrounding spared white matter also exhibited extensive axonal transport dysfunction resulting from the high shear strains in this “lateral epicentre” following vertebral fracture-dislocation. All white matter tracts exhibited extensive β APP accumulation following dislocation though it is not clear why less β APP accumulation was detected in the dorsal ascending columns (Figure 4.8H). Although the boundary conditions likely differ between the dorsal and ventral columns, a similar disparity in β APP accumulation was observed in the contusion model and suggests this may be a physiological difference between these axonal populations. In the ventro-medial white matter, axonal degeneration was observed to extend outward from the hemorrhagic gray matter, as well as inward from the subpial rim. This suggests that in the dislocation injury mechanism, primary gray matter hemorrhage and shear strains of ventral axons may combine to narrow the therapeutic time-window available for this population. This may emphasize that urgent treatment priority should be given to axonal cytoskeletal protective strategies such as calpain inhibition (Stys and Jiang, 2002; Zhang et al., 2003; Thompson et al., 2006).

5.4.3 *Distraction*

Although distraction injury exhibited extensive rostro-caudal membrane compromise in both the gray and white matter, the overall extent of secondary pathology was much less than that observed in both the contusion and dislocation injury models. The patterns of secondary degeneration following contusion and dislocation emphasized that vascular damage exacerbates processes such as microglial activation and axonal degeneration. Little overt mechanical damage to vascular structures was detected in the distraction model and this appears to be an important factor in the early progression of secondary damage. Vascular damage was widely studied in the past (Balentine, 1978a; Rawe et al., 1978; Anderson, 1985; Khan et al., 1985; Fehlings et al., 1989; Guha et al., 1989; Noble and Wrathall, 1989) but has received less attention recently as the field has gravitated towards the precision afforded by molecular approaches. It has been suggested that it would be beneficial to further investigate the role of hemorrhagic factors in SCI research (Norenberg et al., 2004).

Following distraction, some evidence of increased neurofilament dephosphorylation was detected though complete cytoskeletal degeneration was not observed suggesting a high tolerance of axons to mechanical injury when hemorrhagic factors are absent. This tolerance to trauma could be a consequence of both axolemma resealing (Figure 4.4D) and the lack of overt primary intramedullary hemorrhage (Figure 3.4). Recovery of axons to stretch injuries has been widely observed in both *ex vivo* (Shi et al., 2000; Shi and Pryor, 2000, 2002) and *in vitro* (Galbraith et al., 1993; Smith et al., 1999) injury preparations where hemorrhage is absent. Indeed, axons of cultured dorsal root ganglion can be elongated up to 8mm/day without any obvious pathology (Pfister et al., 2004). Neuronal somata also exhibit membrane resealing characteristics (Prado and LaPlaca, 2004) though at sub-lethal levels, they may be more vulnerable to delayed secondary insults (Arundine et al., 2004; Geddes-Klein et al., 2006).

5.4.4 *Summary of Primary and Secondary Injury*

By analysing an early post-traumatic time-point, it was possible to identify early secondary injury features that relate to the mechanism of SCI. The patterns of primary mechanical tissue damage immediately restrict the effectiveness of neuroprotective strategies. From a secondary injury perspective, the primary mechanism of injury alters the rostro-caudal distribution of salvageable populations. Following contusion, it is thought that secondary factors spread outward

to destroy otherwise healthy tissue. In dislocation and distraction, however, the sublethal injury in the rostral and caudal zones may already prime these cells for delayed apoptosis (Arundine et al., 2004) or heighten their sensitivity to secondary insults (Geddes et al., 2003). Thus, the cells in these sublethal zones are distinct from necrotic populations as well as naïve uninjured populations. The balance between different cellular populations could, hypothetically, be crucial in the calculation to determine which treatment combination will preserve the maximum number of neurons, axons, and glia.

As the lesion grows over time, it may be increasingly difficult to detect functional differences between injury mechanisms. Degeneration of the lateral column following contusion would likely result in similar deficits as primary axotomy following fracture-dislocation. Indeed, the pattern of membrane recovery in the white matter at 3 hours already masks the primary injury distribution. However, these effects should not diminish the significance of the injury mechanism. For example, though the lateral columns may eventually deteriorate in both the contusion and dislocation injury mechanisms, the rostro-caudal extent of the injury is still critical. Greater rostro-caudal injury following dislocation may translate to greater axonal die-back requiring a longer distance for axonal regeneration. Alternatively, sublethal biomechanical injuries in the rostro-caudal zone may increase the extent of oligodendroglial apoptosis and the resultant dysmyelination or demyelination of spared fibers. In addition, in the cervical spine, a rostral degeneration of gray matter has profound implications for the neurons in this region which control forelimb and respiratory function.

An SCI treatment needs to save a diverse population of motoneurons, sensory neurons, interneurons, large axons, small axons, myelinated axons, unmyelinated axons, and supporting glia, amidst a cascade of interrelated and sometimes competing events. Calcium entry precipitates secondary degeneration (Young, 1992), yet, calcium entry is also needed for membrane resealing (Shi et al., 2000; Prado and LaPlaca, 2004). Oxygen is essential to maintain respiration, yet reoxygenation produces more free radicals (Stys, 2004). Inflammation risks bystander damage, but debris clearance is an essential phase of repair. The mechanism of injury alters the initial distribution of these populations and so may serve as a rationale for identifying treatment strategies.

5.5 Clinical Relevance

It is understood and accepted that experimental animal models can only reflect an idealized typical human SCI (Tator, 2006). Human clinical trials are therefore necessary in order to prove the efficacy of novel therapies. In recent years, the rodent-to-human paradigm for testing pharmacotherapies has increased in prevalence compared to the traditional progression of testing therapies in higher mammals (Tator, 2006). The work presented in this thesis demonstrates that it is technically feasible to examine other types of clinically relevant injury mechanisms, and more importantly, that these injury mechanisms alter the characteristics of the SCI lesion. Hence, pre-clinical therapies designed in a contusion or compression injury paradigm, may not directly apply to the broader range of injury mechanisms encountered clinically. Pre-clinical therapies have had limited success in clinical trials and thus it is imperative that any novel strategy prove its robustness in alternate clinically relevant injury paradigms before making the leap from rodents, to higher mammals, to humans.

The results in this thesis further highlight the importance of the early post-traumatic period as a critical time-window for intervention. The results showed that vertebral fracture-dislocation consistently produced primary axotomy in the lateral funiculi and white matter pathology that was further exacerbated by rapid axonal cytoskeletal degeneration at the shear epicentre. This pattern of white matter damage may explain the greater deficits often associated with vertebral dislocations (Kiwerski, 1991) while the rostro-caudal injury distribution may hypothetically contribute to some instances of ascension of the SCI lesion (Harrop et al., 2001).

The mechanism of SCI may be inferred from the type of vertebral column injury that is visible on radiographs and magnetic resonance images. From the primary and secondary injury patterns found in this thesis, the injury mechanism may give clinicians an indication of the distribution of neuropathology within the cord and eventually aid in the development of therapies targeted to salvage these cellular populations that are established in a mechanism-specific manner.

5.6 Limitations

This thesis focused on the primary mechanical injury and the secondary events that were initiated soon after trauma. As time elapses after injury, secondary events contribute to the characteristics of the lesion thereby confounding the ability to specifically attribute differences to either the initial mechanical insult or secondary factors. It is important to distinguish between these two components as some characteristics of the primary insult, such as direct axotomy, immediately constrain the amount of tissue that can be spared by therapeutic intervention. Hence, it was reasoned that primary mechanical injury should first be characterized and then its relation to early secondary injury could be delineated at later time-points. The feasible time-window to exploit differences between injury mechanisms could be determined by systematically lengthening the survival time. This rationale was supported by both experimental (Rosenberg and Wrathall, 2001; Gris et al., 2004) and clinical (Bracken et al., 1990; Bracken et al., 1997) observations that earlier treatment was often more effective at preserving post-traumatic function.

The short survival time analyzed in this thesis introduced several limitations. Post-traumatic behavioural function was not assessed. Cervical SCI are more severe than thoracic injuries and thus ethically necessitated that relevant differences be first established at short survival times. Cervical SCI models have some advantage over thoracic models. Approximately 55% of SCIs occur in the cervical region in humans (Sekhon and Fehlings, 2001). In addition, among quadriplegics, restoration of upper limb function—rather than walking—has been identified as the most important treatment priority (Anderson, 2004). Cervical injury paradigms are more sensitive for testing both gray and white matter neuroprotective strategies than thoracic lesions which are largely insensitive to gray matter sparing (Onifer et al., 2005). Also, the mobility of the cervical region facilitated modelling SCIs at clinically relevant injury velocities and this was an important consideration given the clinical rationale behind comparing contusion, dislocation, and distraction injury mechanisms. Modelling injuries such as vertebral dislocation in the thoracic region are not without some drawbacks. A deeper surgical exposure is necessary in order to hold the vertebral body in this region since the transverse processes may not have sufficient strength to support a high-speed fracture-dislocation (~38N chapter 2 table 1). Given this invasiveness, longer-term survival in thoracic dislocation injuries has also been difficult to achieve (Clarke et al., 2006).

This thesis aimed to compare clinically relevant SCI mechanisms using a rat model, though there are clearly differences between rats and humans. In the rat, the dorsal corticospinal tract located in the deep dorsal column was found to be extensively injured in both the contusion and dislocation models. In humans, however, the main corticospinal tract is located in the dorso-lateral funiculus—a region which was pooled with the lateral column in this thesis. There are also some differences in the cellular response between rats and humans. In rats, the infiltration of neutrophils during the early inflammatory response peaks at 1 day whereas in humans, the number of neutrophils peaks between 1 and 3 days post-trauma (Fleming et al., 2006). In addition, humans exhibit less demyelination than has been observed in rat models (Norenberg et al., 2004). In spite of these differences, rats, along with mice, are widely used as they are currently the most practical *in vivo* models of experimentally modelling SCI.

This thesis did not assess pre-clinical therapies. The greater rostro-caudal microglial response observed in the dislocation model could suggest a greater therapeutic benefit from anti-inflammatory treatment such as minocycline (Stirling et al., 2004; Teng et al., 2004) which is currently under clinical investigation (Baptiste and Fehlings, 2006). In addition, calpain inhibitors have previously been shown to spare white matter and improve behavioural function following contusion (Schumacher et al., 2000) and this treatment strategy may have a greater efficacy in a dislocation injury paradigm. The investigation of pre-clinical interventions must be deferred until long-term survival has been established.

The three injury mechanisms analysed—contusion, dislocation, and distraction—are themselves still only representative of a portion of SCI mechanisms encountered in humans. Human SCI occur in different combinations such as flexion-distraction with facet dislocation or extension-distraction. In addition, torsion also occurs in human SCI resulting in unilateral facet dislocation (Magerl et al., 1994). Hence, the mechanisms modelled here were chosen as stereotypical vertebral fracture patterns that cover a range of clinically relevant injuries to the spinal cord though there are many other injury mechanisms that merit investigation.

5.7 Recommendations

The injury models should be further developed in order to examine additional biomechanical aspects. In the contusion model, the correlation between the impact force and the hemorrhage volume over a relatively narrow range of displacements might suggest vascular

perfusion pressure, which is not typically regulated in experimental models, might contribute to the undesirable variability observed in contusion models (Scheff et al., 2003; Ghasemlou et al., 2005; Kloos et al., 2005). In addition, both the dislocation and distraction models could benefit from additional pressure sensors (Chavko et al., 2007) to provide force feedback from within the spinal canal. In the distraction model, the coupling between the vertebral column and spinal cord remains an important quantity that should be determined in order to better understand the mechanics of distractive force transfer to the cord.

In addition, this thesis did not vary the extent of axial tension on the spinal cord prior to injury. Traction on the spinal cord has been shown in a small series of animals to increase the cord's susceptibility to compression injury (Fujita and Yamamoto, 1989). Hence, the extent of cranial flexion, or extension, may change the pattern of spinal cord damage as hypothesized in the discussion on failure patterns following fracture-dislocation (Figure 5.2).

Although the recommended approach for the near future would be to further develop the existing models, the multi-mechanism injury system was designed to be a flexible device that can be adapted to model injury mechanisms beyond contusion, dislocation, and distraction. The devices developed have already been adapted to produce oblique hemi-contusions (Choo and Tetzlaff, unpublished observations), cervical hemi-contusions (Plunet, Liu, and Tetzlaff, unpublished observations), thoracic contusions with residual compression (Sjovold et al., 2005), as well as thoracolumbar fracture-dislocation (Clarke et al., 2006). Hyper-extension is also a common injury mechanism associated with falls (Pickett et al., 2006) that was not addressed in this thesis that should likely be investigated.

From a neurobiology perspective, a survival model, particularly for fracture-dislocation would be an important next step given the high prevalence of this injury mechanism in humans. Some important questions would be to determine if the rostro-caudal increase in primary membrane compromise eventually translates to greater oligodendroglial apoptosis, axonal die-back, demyelination, and a broader chronic glial scar. Also important might be to determine if the axonal cytoskeletal degradation near the lesion epicentre might be amendable to treatment by early calpain inhibition (Banik et al., 1998; Schumacher et al., 2000).

Clinically, a retrospective review of patients stratified by injury mechanism might be used to compare the pattern of functional deficits with the distribution of primary and secondary damage

observed in this thesis. A reanalysis of the results of the National Acute Spinal Cord Injury Studies might yield interesting results regarding the efficacy of methylprednisolone in mechanism-specific patient populations.

5.8 Contributions

In the broader scope, this thesis attempts to bridge the relation between the biomechanics of injury and the neurobiology of SCI through animal models that bear closer resemblance to the injuries encountered clinically in humans. The significance of the work can only be assessed as the knowledge matures over time. It is hoped that this work contributes some small perspective on the broad range of SCI in humans and stimulates thoughts about alternative approaches to solving this devastating injury. Some specific contributions include:

1. The development of a novel multi-mechanism injury system. The device can be used to model a broad range of injuries in addition to those analysed in this thesis.
2. The development of three clinically relevant cervical SCI models. This is the first development of vertebral clamps for delivering distinct high-speed injuries to the rat vertebral column. This is the first development of dislocation and distraction injuries in the rat cervical spine.
3. The characterization of primary injury fields in contusion, dislocation, and distraction injuries. This established a comparative reference map of how traumatic injury is distributed in these injury mechanisms.
4. The characterization of similarities and differences in early secondary injury resulting from differences in the mechanism of spinal cord injury.
5. The development of a novel method to quantitatively analyse the morphology of microglia during activation. Although the method is a minor aspect of this thesis, it may be of general interest in other areas of neuroinflammation.

5.9 Conclusion

In humans, spinal cord injury can occur by a range of injury mechanisms that have not been previously compared experimentally. Three new animal models were concurrently developed in this thesis to compare three clinically relevant injury mechanisms—contusion, dislocation, and distraction. The results showed that the mechanism of injury dictates the pattern of primary mechanical damage within the spinal cord which in turn alters the initial characteristics of secondary neuropathology. The primary and secondary neuropathology in human SCI is more diverse than the central cavitating lesion produced by the commonly used contusion and compression injury paradigms and hence pre-clinical therapies should be tested in a range of injury mechanisms before human trials. This interaction between the biomechanical mechanism of injury and the neuropathology of SCI suggests future clinical treatment paradigms may be guided in a mechanism-specific manner.

5.10 References

- Anderson KD (2004) Targeting recovery: priorities of the spinal cord-injured population. *J Neurotrauma* 21:1371-1383.
- Anderson TE (1982) A controlled pneumatic technique for experimental spinal cord contusion. *J Neurosci Methods* 6:327-333.
- Anderson TE (1985) Spinal cord contusion injury: experimental dissociation of hemorrhagic necrosis and subacute loss of axonal conduction. *J Neurosurg* 62:115-119.
- Anthes DL, Theriault E, Tator CH (1995) Characterization of axonal ultrastructural pathology following experimental spinal cord compression injury. *Brain Res* 702:1-16.
- Arundine M, Aarts M, Lau A, Tymianski M (2004) Vulnerability of central neurons to secondary insults after in vitro mechanical stretch. *J Neurosci* 24:8106-8123.
- Balentine JD (1978a) Pathology of experimental spinal cord trauma. I. The necrotic lesion as a function of vascular injury. *Lab Invest* 39:236-253.
- Balentine JD (1978b) Pathology of experimental spinal cord trauma. II. Ultrastructure of axons and myelin. *Lab Invest* 39:254-266.
- Banik NL, Shields DC, Ray S, Davis B, Matzelle D, Wilford G, Hogan EL (1998) Role of calpain in spinal cord injury: effects of calpain and free radical inhibitors. *Ann N Y Acad Sci* 844:131-137.
- Baptiste DC, Fehlings MG (2006) Pharmacological approaches to repair the injured spinal cord. *J Neurotrauma* 23:318-334.
- Baussart B, Stamegna JC, Polentes J, Tadie M, Gauthier P (2006) A new model of upper cervical spinal contusion inducing a persistent unilateral diaphragmatic deficit in the adult rat. *Neurobiol Dis*.
- Behrmann DL, Bresnahan JC, Beattie MS, Shah BR (1992) Spinal cord injury produced by consistent mechanical displacement of the cord in rats: behavioral and histologic analysis. *J Neurotrauma* 9:197-217.
- Blight A (1988) Mechanical factors in experimental spinal cord injury. *J Am Paraplegia Soc* 11:26-34.
- Blight AR (1983) Cellular morphology of chronic spinal cord injury in the cat: analysis of myelinated axons by line-sampling. *Neuroscience* 10:521-543.
- Blight AR, Decrescito V (1986) Morphometric analysis of experimental spinal cord injury in the cat: the relation of injury intensity to survival of myelinated axons. *Neuroscience* 19:321-341.
- Bracken MB, Shepard MJ, Collins WF, Holford TR, Young W, Baskin DS, Eisenberg HM, Flamm E, Leo-Summers L, Maroon J, et al. (1990) A randomized, controlled trial of methylprednisolone or naloxone in the treatment of acute spinal-cord injury. Results of the Second National Acute Spinal Cord Injury Study. *N Engl J Med* 322:1405-1411.
- Bracken MB, Shepard MJ, Holford TR, Leo-Summers L, Aldrich EF, Fazl M, Fehlings M, Herr DL, Hitchon PW, Marshall LF, Nockels RP, Pascale V, Perot PL, Jr., Piepmeier J, Sonntag VK, Wagner F, Wilberger JE, Winn HR, Young W (1997) Administration of methylprednisolone for 24 or 48 hours or tirilazad mesylate for 48 hours in the treatment of acute spinal cord injury. Results of the Third National Acute Spinal Cord Injury Randomized Controlled Trial. National Acute Spinal Cord Injury Study. *JAMA* 277:1597-1604.

- Breig A (1970) Overstretching of and circumscribed pathological tension in the spinal cord--a basic cause of symptoms in cord disorders. *J Biomech* 3:7-9.
- Bresnahan JC, Beattie MS, Todd FD, 3rd, Noyes DH (1987) A behavioral and anatomical analysis of spinal cord injury produced by a feedback-controlled impaction device. *Exp Neurol* 95:548-570.
- Bresnahan JC, Beattie MS, Stokes BT, Conway KM (1991) Three-dimensional computer-assisted analysis of graded contusion lesions in the spinal cord of the rat. *J Neurotrauma* 8:91-101.
- Cargill RS, 2nd, Thibault LE (1996) Acute alterations in $[Ca^{2+}]_i$ in NG108-15 cells subjected to high strain rate deformation and chemical hypoxia: an in vitro model for neural trauma. *J Neurotrauma* 13:395-407.
- Chavko M, Koller WA, Prusaczyk WK, McCarron RM (2007) Measurement of blast wave by a miniature fiber optic pressure transducer in the rat brain. *J Neurosci Methods* 159:277-281.
- Clarke EC, Choo AM, Liu J, Lam CK, Bilston LE, Tetzlaff W, Oxland TR (2006) Early Spinal Cord Injury Pathology Development Following Experimental Fracture Dislocation. *J Neurotrauma* 23:770.
- Cullen DK, LaPlaca MC (2006) Neuronal response to high rate shear deformation depends on heterogeneity of the local strain field. *J Neurotrauma* 23:1304-1319.
- Dabney KW, Ehrenshteyn M, Agresta CA, Twiss JL, Stern G, Tice L, Salzman SK (2004) A model of experimental spinal cord trauma based on computer-controlled intervertebral distraction: characterization of graded injury. *Spine* 29:2357-2364.
- Deridder MN, Simon MJ, Siman R, Auberson YP, Raghupathi R, Meaney DF (2005) Traumatic mechanical injury to the hippocampus in vitro causes regional caspase-3 and calpain activation that is influenced by NMDA receptor subunit composition. *Neurobiol Dis.*
- Fehlings MG, Tator CH, Linden RD (1989) The effect of nimodipine and dextran on axonal function and blood flow following experimental spinal cord injury. *J Neurosurg* 71:403-416.
- Fiford RJ, Bilston LE, Waite P, Lu J (2004) A vertebral dislocation model of spinal cord injury in rats. *J Neurotrauma* 21:451-458.
- Fleming JC, Norenberg MD, Ramsay DA, Dekaban GA, Marcillo AE, Saenz AD, Pasquale-Styles M, Dietrich WD, Weaver LC (2006) The cellular inflammatory response in human spinal cords after injury. *Brain* 129:3249-3269.
- Fujita Y, Yamamoto H (1989) An experimental study on spinal cord traction effect. *Spine* 14:698-705.
- Galbraith JA, Thibault LE, Matteson DR (1993) Mechanical and electrical responses of the squid giant axon to simple elongation. *J Biomech Eng* 115:13-22.
- Geddes-Klein DM, Schiffman KB, Meaney DF (2006) Mechanisms and consequences of neuronal stretch injury in vitro differ with the model of trauma. *J Neurotrauma* 23:193-204.
- Geddes DM, Cargill RS, 2nd, LaPlaca MC (2003) Mechanical stretch to neurons results in a strain rate and magnitude-dependent increase in plasma membrane permeability. *J Neurotrauma* 20:1039-1049.
- Gensel JC, Tovar CA, Hamers FP, Deibert RJ, Beattie MS, Bresnahan JC (2006) Behavioral and histological characterization of unilateral cervical spinal cord contusion injury in rats. *J Neurotrauma* 23:36-54.
- Ghasemlou N, Kerr BJ, David S (2005) Tissue displacement and impact force are important contributors to outcome after spinal cord contusion injury. *Exp Neurol* 196:9-17.

- Greaves CY, Gadala MS, Oxland TR (2004) Spinal cord injury mechanisms: A finite element study. *J Neurotrauma* 21:1307.
- Gris D, Marsh DR, Oatway MA, Chen Y, Hamilton EF, Dekaban GA, Weaver LC (2004) Transient blockade of the CD11d/CD18 integrin reduces secondary damage after spinal cord injury, improving sensory, autonomic, and motor function. *J Neurosci* 24:4043-4051.
- Gruner JA, Yee AK, Blight AR (1996) Histological and functional evaluation of experimental spinal cord injury: evidence of a stepwise response to graded compression. *Brain Res* 729:90-101.
- Guha A, Tator CH, Rochon J (1989) Spinal cord blood flow and systemic blood pressure after experimental spinal cord injury in rats. *Stroke* 20:372-377.
- Harrop JS, Sharan AD, Vaccaro AR, Przybylski GJ (2001) The cause of neurologic deterioration after acute cervical spinal cord injury. *Spine* 26:340-346.
- Henderson FC, Geddes JF, Vaccaro AR, Woodard E, Berry KJ, Benzel EC (2005) Stretch-associated injury in cervical spondylotic myelopathy: new concept and review. *Neurosurgery* 56:1101-1113; discussion 1101-1113.
- Ichihara K, Taguchi T, Shimada Y, Sakuramoto I, Kawano S, Kawai S (2001) Gray matter of the bovine cervical spinal cord is mechanically more rigid and fragile than the white matter. *J Neurotrauma* 18:361-367.
- Jakeman LB, Guan Z, Wei P, Ponnappan R, Dzwonczyk R, Popovich PG, Stokes BT (2000) Traumatic spinal cord injury produced by controlled contusion in mouse. *J Neurotrauma* 17:299-319 ;217(294):299-319.
- Kearney PA, Ridella SA, Viano DC, Anderson TE (1988) Interaction of contact velocity and cord compression in determining the severity of spinal cord injury. *J Neurotrauma* 5:187-208.
- Khan M, Griebel R, Rozdilsky B, Politis M (1985) Hemorrhagic changes in experimental spinal cord injury models. *Can J Neurol Sci* 12:259-262.
- King AI, Ruan JS, Zhou C, Hardy WN, Khalil TB (1995) Recent advances in biomechanics of brain injury research: a review. *J Neurotrauma* 12:651-658.
- Kiwerski J (1991) The influence of the mechanism of cervical spine injury on the degree of the spinal cord lesion. *Paraplegia* 29:531-536.
- Kloos AD, Fisher LC, Detloff MR, Hassenzahl DL, Basso DM (2005) Stepwise motor and all-or-none sensory recovery is associated with nonlinear sparing after incremental spinal cord injury in rats. *Exp Neurol* 191:251-265.
- Kwon BK, Oxland TR, Tetzlaff W (2002) Animal models used in spinal cord regeneration research. *Spine* 27:1504-1510.
- LaPlaca MC, Thibault LE (1997) An in vitro traumatic injury model to examine the response of neurons to a hydrodynamically-induced deformation. *Ann Biomed Eng* 25:665-677.
- LaPlaca MC, Cullen DK, McLoughlin JJ, Cargill RS, 2nd (2005) High rate shear strain of three-dimensional neural cell cultures: a new in vitro traumatic brain injury model. *J Biomech* 38:1093-1105.
- Magerl F, Aebi M, Gertzbein SD, Harms J, Nazarian S (1994) A comprehensive classification of thoracic and lumbar injuries. *Eur Spine J* 3:184-201.
- Maikos JT, Shreiber DI (2007) Immediate damage to the blood-spinal cord barrier due to mechanical trauma. *J Neurotrauma* 24:492-507.
- Maiman DJ, Coats J, Myklebust JB (1989a) Cord/spine motion in experimental spinal cord injury. *J Spinal Disord* 2:14-19.

- Maiman DJ, Myklebust JB, Ho KC, Coats J (1989b) Experimental spinal cord injury produced by axial tension. *J Spinal Disord* 2:6-13.
- Nightingale RW, McElhaney JH, Richardson WJ, Best TM, Myers BS (1996) Experimental impact injury to the cervical spine: relating motion of the head and the mechanism of injury. *J Bone Joint Surg Am* 78:412-421.
- Noble LJ, Wrathall JR (1989) Distribution and time course of protein extravasation in the rat spinal cord after contusive injury. *Brain Res* 482:57-66.
- Norenberg MD, Smith J, Marcillo A (2004) The pathology of human spinal cord injury: defining the problems. *J Neurotrauma* 21:429-440.
- Onifer SM, Zhang YP, Burke DA, Brooks DL, Decker JA, McClure NJ, Floyd AR, Hall J, Proffitt BL, Shields CB, Magnuson DS (2005) Adult rat forelimb dysfunction after dorsal cervical spinal cord injury. *Exp Neurol* 192:25-38.
- Ozawa H, Matsumoto T, Ohashi T, Sato M, Kokubun S (2001) Comparison of spinal cord gray matter and white matter softness: measurement by pipette aspiration method. *J Neurosurg* 95:221-224.
- Panjabi MM, Kifune M, Wen L, Arand M, Oxland TR, Lin RM, Yoon WS, Vasavada A (1995) Dynamic canal encroachment during thoracolumbar burst fractures. *J Spinal Disord* 8:39-48.
- Pearse DD, Lo TP, Jr., Cho KS, Lynch MP, Garg MS, Marcillo AE, Sanchez AR, Cruz Y, Dietrich WD (2005) Histopathological and behavioral characterization of a novel cervical spinal cord displacement contusion injury in the rat. *J Neurotrauma* 22:680-702.
- Pettus EH, Christman CW, Giebel ML, Povlishock JT (1994) Traumatically induced altered membrane permeability: its relationship to traumatically induced reactive axonal change. *J Neurotrauma* 11:507-522.
- Pfister BJ, Iwata A, Meaney DF, Smith DH (2004) Extreme stretch growth of integrated axons. *J Neurosci* 24:7978-7983.
- Pickett GE, Campos-Benitez M, Keller JL, Duggal N (2006) Epidemiology of traumatic spinal cord injury in Canada. *Spine* 31:799-805.
- Prado GR, LaPlaca MC (2004) Neuronal plasma membrane is transiently disrupted by mechanical trauma: an insight into the mechanisms involved. *J Neurotrauma* 21:1331.
- Rawe SE, Lee WA, Perot PL, Jr. (1978) The histopathology of experimental spinal cord trauma. The effect of systemic blood pressure. *J Neurosurg* 48:1002-1007.
- Rivlin AS, Tator CH (1978) Effect of duration of acute spinal cord compression in a new acute cord injury model in the rat. *Surg Neurol* 10:38-43.
- Rosenberg LJ, Wrathall JR (2001) Time course studies on the effectiveness of tetrodotoxin in reducing consequences of spinal cord contusion. *J Neurosci Res* 66:191-202.
- Scheff SW, Rabchevsky AG, Fugaccia I, Main JA, Lumpp JE, Jr. (2003) Experimental modeling of spinal cord injury: characterization of a force-defined injury device. *J Neurotrauma* 20:179-193.
- Schumacher PA, Siman RG, Fehlings MG (2000) Pretreatment with calpain inhibitor CEP-4143 inhibits calpain I activation and cytoskeletal degradation, improves neurological function, and enhances axonal survival after traumatic spinal cord injury. *J Neurochem* 74:1646-1655.
- Sekhon LH, Fehlings MG (2001) Epidemiology, demographics, and pathophysiology of acute spinal cord injury. *Spine* 26:S2-12.

- Shi R, Pryor JD (2000) Temperature dependence of membrane sealing following transection in mammalian spinal cord axons. *Neuroscience* 98:157-166.
- Shi R, Pryor JD (2002) Pathological changes of isolated spinal cord axons in response to mechanical stretch. *Neuroscience* 110:765-777.
- Shi R, Whitebone J (2006) Conduction deficits and membrane disruption of spinal cord axons as a function of magnitude and rate of strain. *J Neurophysiol* 95:3384-3390.
- Shi R, Asano T, Vining NC, Blight AR (2000) Control of membrane sealing in injured mammalian spinal cord axons. *J Neurophysiol* 84:1763-1769.
- Sjovold SG, Choo AM, Liu J, Lam CK, Tetzlaff W, Oxland TR (2005) A Controlled Model of Residual Compression Subsequent to a Contusion Injury. *J Neurotrauma* 22:1219.
- Smith DH, Wolf JA, Lusardi TA, Lee VM, Meaney DF (1999) High tolerance and delayed elastic response of cultured axons to dynamic stretch injury. *J Neurosci* 19:4263-4269.
- Somerson SK, Stokes BT (1987) Functional analysis of an electromechanical spinal cord injury device. *Exp Neurol* 96:82-96.
- Stirling DP, Khodarahmi K, Liu J, McPhail LT, McBride CB, Steeves JD, Ramer MS, Tetzlaff W (2004) Minocycline treatment reduces delayed oligodendrocyte death, attenuates axonal dieback, and improves functional outcome after spinal cord injury. *J Neurosci* 24:2182-2190.
- Stokes BT, Noyes DH, Behrmann DL (1992) An electromechanical spinal injury technique with dynamic sensitivity. *J Neurotrauma* 9:187-195.
- Stys PK (2004) White matter injury mechanisms. *Curr Mol Med* 4:113-130.
- Stys PK, Jiang Q (2002) Calpain-dependent neurofilament breakdown in anoxic and ischemic rat central axons. *Neurosci Lett* 328:150-154.
- Tani S, Yamada S, Knighton RS (1987) Extensibility of the lumbar and sacral cord. Pathophysiology of the tethered spinal cord in cats. *J Neurosurg* 66:116-123.
- Tator CH (2006) Review of treatment trials in human spinal cord injury: issues, difficulties, and recommendations. *Neurosurgery* 59:957-982; discussion 982-957.
- Teng YD, Choi H, Onario RC, Zhu S, Desilets FC, Lan S, Woodard EJ, Snyder EY, Eichler ME, Friedlander RM (2004) Minocycline inhibits contusion-triggered mitochondrial cytochrome c release and mitigates functional deficits after spinal cord injury. *Proc Natl Acad Sci U S A* 101:3071-3076.
- Thompson SN, Gibson TR, Thompson BM, Deng Y, Hall ED (2006) Relationship of calpain-mediated proteolysis to the expression of axonal and synaptic plasticity markers following traumatic brain injury in mice. *Exp Neurol* 201:253-265.
- Wilcox RK, Boerger TO, Hall RM, Barton DC, Limb D, Dickson RA (2002) Measurement of canal occlusion during the thoracolumbar burst fracture process. *J Biomech* 35:381-384.
- Wolf JA, Stys PK, Lusardi T, Meaney D, Smith DH (2001) Traumatic axonal injury induces calcium influx modulated by tetrodotoxin-sensitive sodium channels. *J Neurosci* 21:1923-1930.
- Young W (1992) Role of calcium in central nervous system injuries. *J Neurotrauma* 9 Suppl 1:S9-25.
- Zhang SX, Bondada V, Geddes JW (2003) Evaluation of conditions for calpain inhibition in the rat spinal cord: effective postinjury inhibition with intraspinal MDL28170 microinjection. *J Neurotrauma* 20:59-67.

Appendix A

SCI TEST SYSTEM

5.11 Test System Assembly

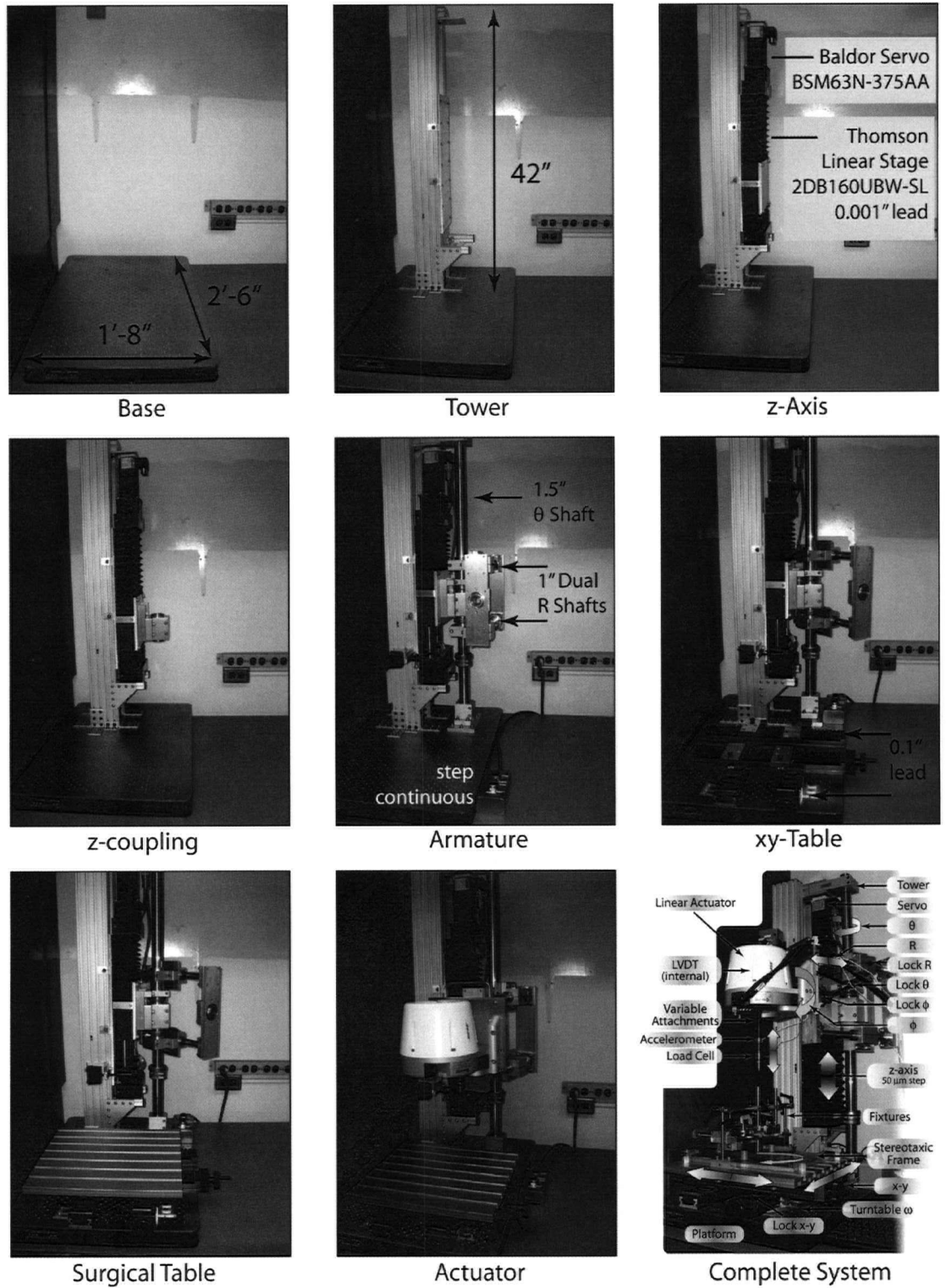
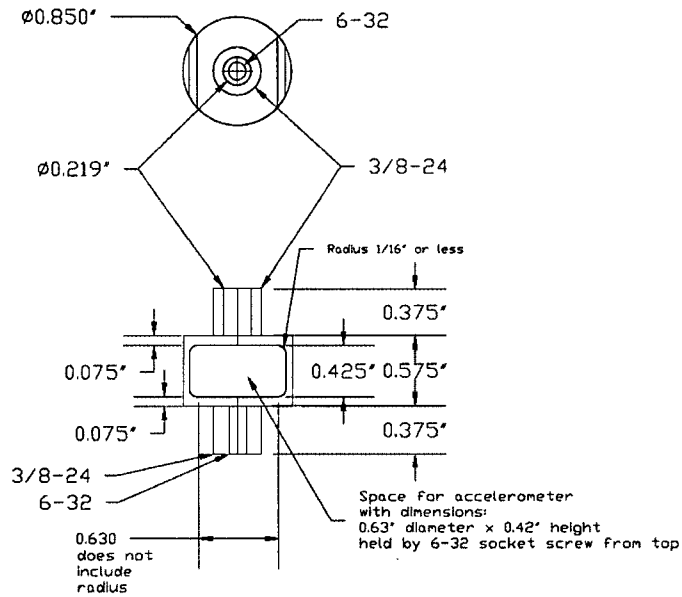


Figure A.1: Test system assembly sequence

5.12 Test System Drawings

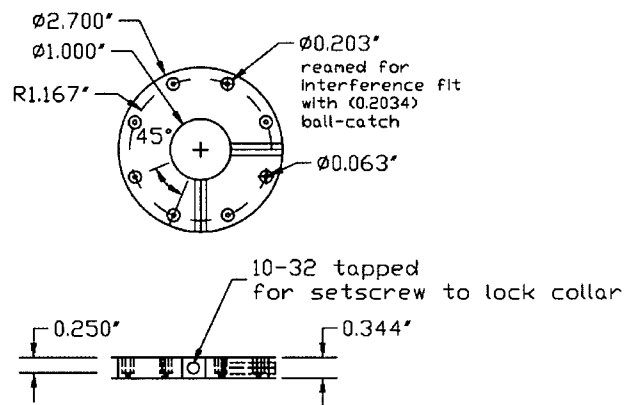
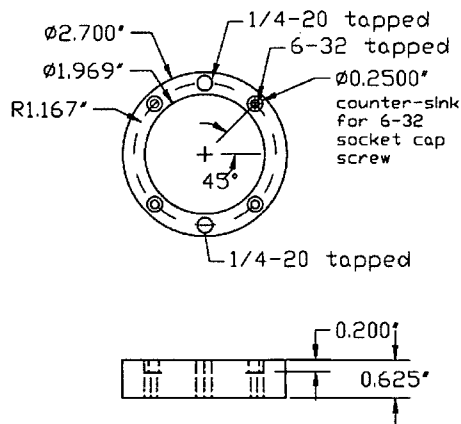


Material: Aluminum
Tolerance: $\pm 0.001''$

Figure A.2: Accelerometer housing

Flange for ball-nose spring plunger

Flange for ball-catches



Material: 304 or 316 Stainless Steel
Tolerances: nominal $\pm 0.005''$ non-critical dims

Figure A.3: Rotary detent

5.13 Sensors

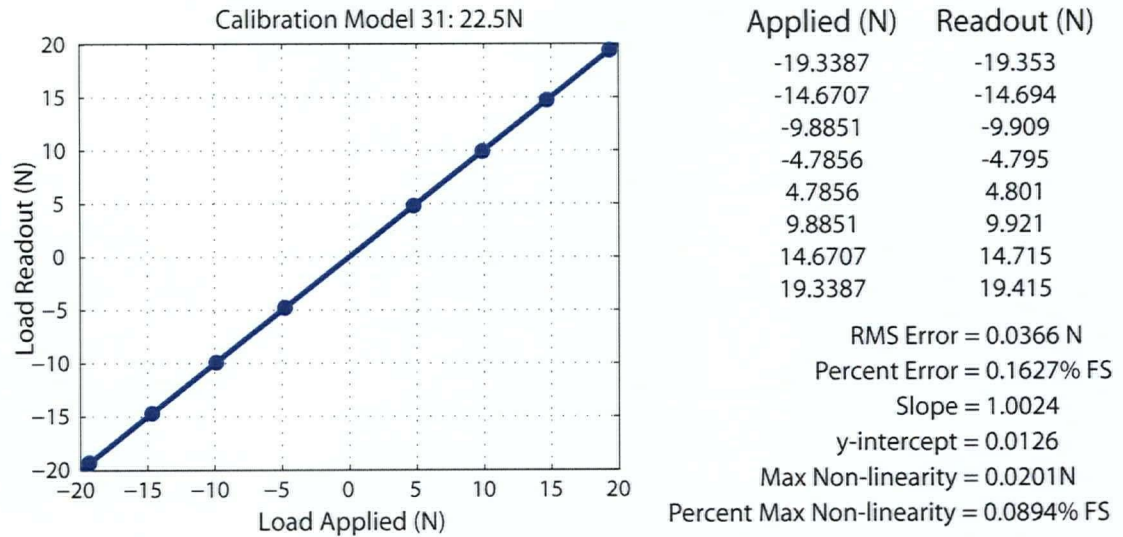


Figure A.4: Load cell calibration model 31: 22.5N

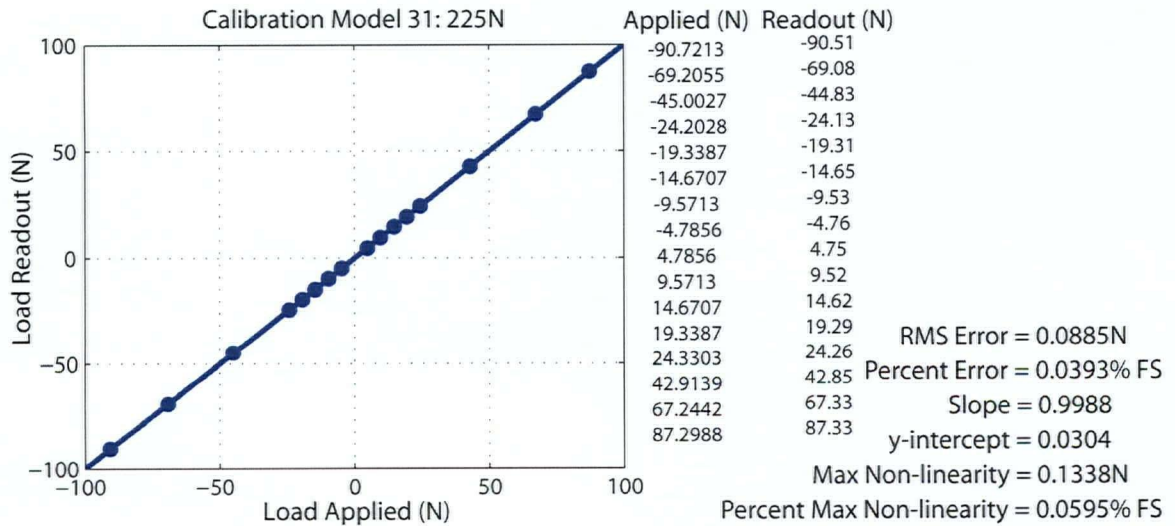


Figure A.5: Load cell calibration model 31: 225N

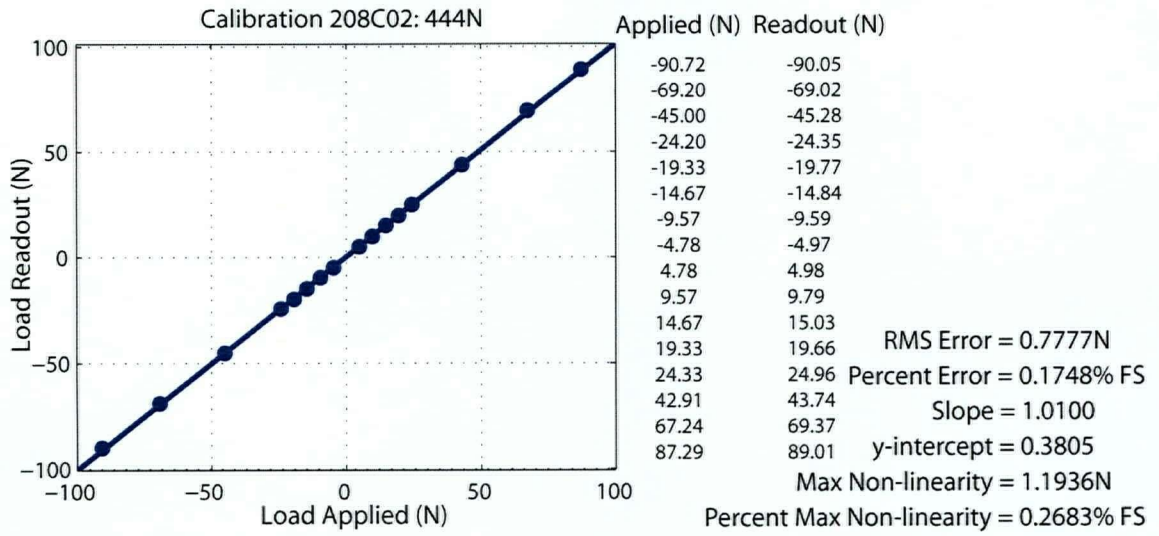


Figure A.6: Load cell calibration model 208C02: 444N

Appendix B

IMAGE ANALYSIS

5.14 Image Analysis Tools

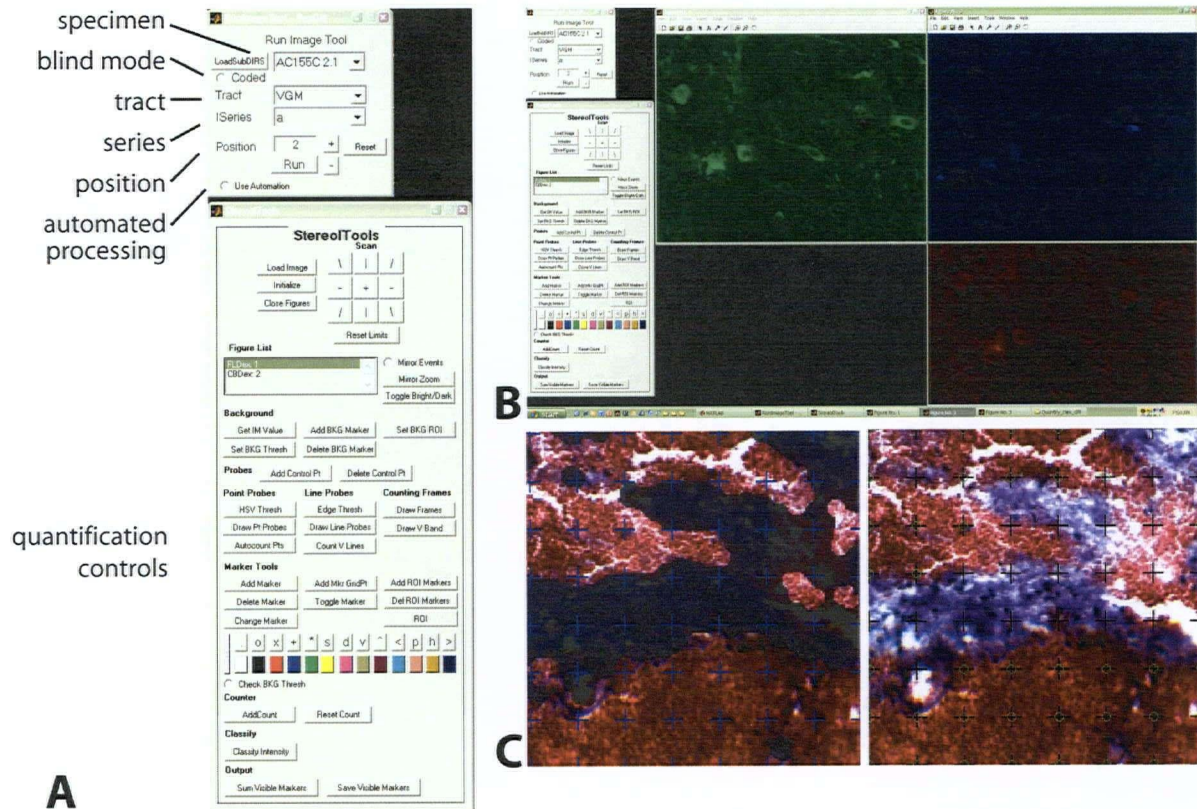


Figure B.1: StereolTools interface and screen images

A. StereolTools interface built in Matlab. Upper window is browser for selecting the image specimen, tract, series, and rostro-caudal position. Automated processing option runs software code to analyse the particular image series (e.g. detect neurons, detect axons, classify neurons, colocalize etc.). Blind mode codes the specimen number based on a cipher file that is opened after the completion of the analysis. Lower window shows quantification controls for laying down probes and counting objects. B. Representative screen shot showing gray matter immunostained for fluorescein-dextran, cascade-blue dextran, and 3-nitrotyrosine. C. Representative example of hemorrhage quantification using point probes. A high point density is necessary to achieve accurate area measurements, though accurate volume estimates can also be achieved with a low density of point probes and a greater number of sections. Simple automated algorithms such as colour segmentation and morphological feature detection accelerates quantification and is most efficient when combined with manual verification.

Appendix C

ANOVA TABLES

Table C.1: ANOVA summary – Acute dextran penetration into axons

Region	Effect	Sum of Squares	Degrees of Freedom	Mean Square	F	p
Dorsal Column	Mechanism ¹	181.399	2	90.699	7.309	0.003
	Error	297.821	24	12.409		
	Position	930.603	10	93.060	45.954	<0.001
	Mechanism × Position	221.739	20	11.087	5.475	<0.001
	Error	486.020	240	2.025		
Lateral Column	Mechanism ¹	6.239	2	3.119	0.542	0.589
	Error	138.045	24	5.752		
	Position	581.903	10	58.190	35.192	<0.001
	Mechanism × Position	240.671	20	12.034	7.278	<0.001
	Error	396.848	240	1.654		
Ventro-Medial	Mechanism ¹	207.496	2	103.748	5.955	0.008
	Error	418.103	24	17.421		
	Position ²	989.799	9	109.978	53.095	<0.001
	Mechanism × Position	342.007	18	19.000	9.173	<0.001
	Error	447.410	216	2.071		
Ventro-Lateral	Mechanism ¹	147.421	2	73.710	4.281	0.026
	Error	413.222	24	17.218		
	Position ²	956.825	9	106.314	54.014	<0.001
	Mechanism × Position	388.397	18	21.578	10.963	<0.001
	Error	425.147	216	1.968		

Square root transforms were applied to data prior to statistical testing because counts (axons/mm) exhibit a Poisson distribution.

¹ Sham surgical controls were not included in the ANOVA because dextran penetration was not detected in the white matter.

² The position at 5mm caudal was excluded as there was no variance on which to perform an analysis.

Table C.2: ANOVA summary – Acute dextran penetration into neuronal somata

Region	Effect	Sum of Squares	Degrees of Freedom	Mean Square	F	p
Ventral Gray Matter	Mechanism	6.653	3	2.217	11.324	<0.001
	Error	6.071	31	0.196		
	Position	12.249	10	1.224	31.341	<0.001
	Mechanism × Position	9.737	30	0.324	8.305	<0.001
	Error	12.116	310	0.039		

Arcsine transforms were applied to data prior to statistical testing because proportional data (% of cells) exhibit a binomial distribution.

Table C.3: ANOVA summary – Evolution of dextran penetration at 3 hours post-trauma

Region	Effect	Sum of Squares	Degrees of Freedom	Mean Square	F	p
Ventral Gray Matter	Mechanism	28.121	3	9.374	2.29	0.104
	Error	98.273	24	4.095		
	Dextran	2.255	1	2.255	6.08	0.021
	Dextran × Mechanism	2.682	3	0.894	2.41	0.092
	Error	8.897	24	0.371		
	Position	62.560	8	7.820	9.74	<0.001
	Position × Mechanism	42.226	24	1.759	2.19	0.002
	Error	154.137	192	0.803		
	Dextran × Position	0.316	8	0.040	0.429	0.903
	Dextran × Position × Mechanism	1.555	24	0.065	0.703	0.845
	Error	17.693	192	0.092		
	Ventro-Medial White Matter	Mechanism	35.495	3	11.832	1.056
Error		268.951	24	11.206		
Dextran		46.909	1	46.909	18.217	<0.001
Dextran × Mechanism		48.777	3	16.259	6.314	0.003
Error		61.800	24	2.575		
Position		16.527	8	2.066	1.390	0.203
Position × Mechanism		72.815	24	3.034	2.041	0.004
Error		285.445	192	1.487		
Dextran × Position		31.705	8	3.963	10.194	<0.001
Dextran × Position × Mechanism		13.754	24	0.573	1.474	0.080
Error		74.644	192	0.389		

Dextran denotes comparison between tracers that were infused before and after injury.

Table C.4: ANOVA summary – 3NT-positive cells

Region	Effect	Sum of Squares	Degrees of Freedom	Mean Square	F	p
Ventral Gray Matter	Mechanism	178.203	3	59.401	2.562	0.072
	Error	765.195	33	23.188		
	Position	133.800	8	16.725	4.114	<0.001
	Mechanism × Position	187.901	24	7.829	1.926	0.007
	Error	1073.400	264	4.066		

Square root transforms were used because count data (cells/mm²) exhibit a Poisson distribution.

Table C.5: ANOVA summary – Neurofilament degradation in ventro-medial white matter

Region	Effect	Sum of Squares	Degrees of Freedom	Mean Square	F	p
Ventro-Medial White Matter	Mechanism	207.991	3	69.330	3.563	0.024
	Error	642.148	33	19.459		
	Position	45.042	8	5.630	4.949	<0.001
	Mechanism × Position	65.582	24	2.733	2.402	<0.001
	Error	300.342	264	1.138		

Table C.6: ANOVA summary – β APP accumulation in axons

Region	Effect	Sum of Squares	Degrees of Freedom	Mean Square	F	p
Corticospinal Tract	Mechanism ¹	534810	2	267405	34.938	<0.001
	Error	160730	21	7654		
Dorsal Column	Mechanism ¹	31561.3	2	15780	17.114	<0.001
	Error	19363.9	21	922.1		
Lateral Column	Mechanism ¹	78156.1	2	39078.0	10.359	<0.001
	Error	79217.6	21	3772.3		
Ventral Column	Mechanism ¹	94527.2	2	47263.6	14.908	<0.001
	Error	66577.7	21	3170.4		

Square root transforms were used to ensure homoscedasticity prior to statistical testing.

¹ Sham surgical controls were not included in the ANOVA because sections from these animals did not exhibit any positive staining for β APP.

Table C.7: ANOVA summary – Reactive astrocytes

Region	Effect	Sum of Squares	Degrees of Freedom	Mean Square	F	p
Gray Matter	Mechanism	0.035	3	0.012	3.5	0.038
	Error	0.056	17	0.003		

Arcsine transforms were used to ensure homoscedasticity of proportional data (% area) prior to statistical testing.

Table C.8: ANOVA summary – Microglial activation

Region	Effect	Sum of Squares	Degrees of Freedom	Mean Square	F	p
Ventral Gray Matter	Mechanism	0.310	3	0.103	34.864	<0.001
	Error	0.098	33	0.003		
	Position	0.114	8	0.014	43.759	<0.001
	Mechanism × Position	0.076	24	0.003	9.759	<0.001
	Error	0.086	264	0.0003		
Lateral Column	Mechanism	0.081	3	0.027	9.436	<0.001
	Error	0.094	33	0.003		
	Position	0.011	8	0.001	5.475	<0.001
	Mechanism × Position	0.020	24	0.0008	3.356	<0.001
	Error	0.065	264	0.0002		
Dorsal Column	Mechanism	0.253	3	0.084	30.124	<0.001
	Error	0.092	33	0.003		
	Position	0.029	8	0.004	9.911	<0.001
	Mechanism × Position	0.048	24	0.002	5.573	<0.001
	Error	0.095	264	0.0004		
Ventral Column	Mechanism	0.038	3	0.013	4.207	0.013
	Error	0.098	33	0.003		
	Position	0.025	8	0.003	17.369	<0.001
	Mechanism × Position	0.019	24	0.0008	4.318	<0.001
	Error	0.047	264	0.0002		

Appendix D

ETHICS BOARD CERTIFICATES OF APPROVAL



THE UNIVERSITY OF BRITISH COLUMBIA

ANIMAL CARE CERTIFICATE

Application Number: A04-0186

Investigator or Course Director: Tom.R.Oxland

Department: Orthopaedics

Animals:

Rats Sprague-Dawley 180

Start Date: January 1, 2003 **Approval Date:** March 6, 2007

Funding Sources:

Funding Agency: BC Neurotrauma
Funding Title: Spinal cord injury mechanisms

Funding Agency: Natural Science Engineering Research Council
Funding Title: Injury mechanisms of the spinal cord

Funding Agency: Rick Hansen Man In Motion Foundation
Funding Title: Spinal cord injury mechanisms

Funding Agency: Canadian Institutes of Health Research
Funding Title: The effect of distinct modes of spinal column failure on spinal cord injury

Funding Agency: BC Neurotrauma
Funding Title: Spinal Cord Injury Mechanisms

Unfunded title: N/A

The Animal Care Committee has examined and approved the use of animals for the above experimental project.

This certificate is valid for one year from the above start or approval date (whichever is later) provided there is no change in the experimental procedures. Annual review is required by the CCAC and some granting agencies.

A copy of this certificate must be displayed in your animal facility.

Office of Research Services and Administration
102, 6190 Agronomy Road, Vancouver, BC V6T 1Z3
Phone: 604-827-5111 Fax: 604-822-5093